ISSN 1606-9277
Frequency: Annually
Vol. 16, No. 01 (2024)

TECHNICAL JOURNAL

River Research Institute

RIVER RESEARCH INSTITUTE

MINISTRY OF WATER RESOURCES

GOVT. OF THE PEOPLE'S REPUBLIC OF BANGLADESH

ISSN 1606-9277

TECHNICAL JOURNAL

Vol. 16 No. 01 JUNE 2024

RIVER RESEARCH INSTITUTE
MINISTRY OF WATER RESOURCES
GOVT. OF THE PEOPLE'S REPUBLIC OF BANGLADESH

EDITORIAL BOARD

Chairman

S M Abu Horayra
Director General
River Research Institute

Executive Editor

Dr. Fatima Rukshana
Principal Scientific Officer
Geotechnical Research Directorate, River Research Institute

Member

Engr. Pintu Kanungoe
Director
Administration and Finance Directorate, River Research Institute

Physicist Uma Saha
Director (In-charge)
Geotechnical Research Directorate, River Research Institute

Engr. A K M Ashrafuzzaman
Director (In-charge)
Hydraulic Research Directorate, River Research Institute

Dr. Moniruzzaman Khan Eusufzai
Principal Scientific Officer
Dhaka Office, River Research Institute

Physicist Nayan Chandra Ghosh
Senior Scientific Officer
Dhaka Office, River Research Institute

Md. Moniruzzaman
Senior Scientific Officer
Geotechnical Research Directorate, River Research Institute

Engr. Sajia Afrin
Senior Scientific Officer
Dhaka Office, River Research Institute

Azmal Fakir
Librarian
River Research Institute

Engr. Md. Masuduzzaman
Assistant Programmer
River Research Institute

Reviewer Panel of Technical Journal - River Research Institute

Dr. Md. Munsur Rahman
Professor
Institute of Water and Flood Management
Bangladesh University of Engineering and Technology, Dhaka

Dr. Mehedi Ahmed Ansary
Professor
Department of Civil Engineering
Bangladesh University of Engineering and Technology, Dhaka

Dr. Md. Shahidul Islam
Professor and Chairman
Department of Geography and Environment
University of Dhaka, Dhaka

Dr. Nasreen Jahan
Professor and Head
Department of Water Resources Engineering
Bangladesh University of Engineering and Technology, Dhaka

Dr. Sajal Kumar Adhikary
Professor
Department of Civil Engineering
Khulna University of Engineering and Technology, Khulna

Dr. Aysha Akter
Professor and Head
Department of Civil Engineering
Chittagong University of Engineering and Technology, Chittagong

Dr. Mohammed Mizanur Rahman
Professor and Head
Department of Irrigation and Water Management
Bangladesh Agricultural University, Mymensingh

Dr. Md. Rokonuzzaman
Professor
Department of Civil Engineering
Khulna University of Engineering and Technology, Khulna

Dr. G. M. Sadiqul Islam
Professor and head
Department of Water Resources Engineering
Chittagong University of Engineering and Technology, Chittagong

Dr. Mohammad Amir Hossain Bhuiyan
Professor
Department of Environmental Sciences
Jahangirnagar University, Dhaka

TECHNICAL JOURNAL
River Research Institute
Vol. 16, No. 01, June 2024

Table of Contents

Technical Journal
River Research Institute ISSN: 1606-9277

ASSESSMENT OF EROSION RISK POTENTIAL IN TERMS OF BANK MATERIAL PARTICLE SIZES AROUND 3KM UPSTREAM AND 3KM DOWNSTREAM OF HAJI SHARIATULLA BRIDGE ALONG ARIAL KHAN RIVER IN BANGLADESH

B. Roy[1*], S. Ferdhous[2], M. Moniruzzaman[2,3], F. Rukshana[2], S. M. A. Horayra[4], M. K. Eusufzai[5], K. R. Ahmed[2] and U. Saha[2]

Abstract

River bank erosion is a recurring issue at monsoon in Bangladesh. Erosion expedites the river bank failure occurring among many of the river bank failure criteria. So, it is very much important to assess bank erosion of the river prior to the planning of bank protection works. Here an attempt has been made to assess the erosion risk potential at the left and right banks around 6.0 km of Arial Khan River. In this study particle sizes are analyzed and percentage of Clay, Silt and Sand has been found out. From the particle size analysis, it has been seen that the left bank of the Arial Khan River predominantly consists of sand particles, except for Khas Char Bachamara, where silt particles dominate. On the other hand, right bank of Arial Khan River dominates the Silt and Sand particle. The erodibility index is determined through Bouyoucos erodibility index and EI_{ROM}. From the erodibility index result of EI_{ROM} the soil erosion of the bank is categorized and observed that the left bank of Arial Khan River is very high to critical position in risk of erosion except 3.0 m depth of Khas Char Bachamara which layer sometime protects the bank from erosion. On the other hand, the right bank of Arial Khan River is high to critical position in risk of erosion. From this study a design engineer can be aware of the bank materials and predict erosion risk. However, it is recommended that a full geotechnical investigation is needed to prevent river bank erosion.

Keywords: *Arial Khan River, Bank materials, Erosion risk potential, Particle sizes.*

Introduction

The major part of Bangladesh is on the delta formed by three significant rivers Brahmaputra, Ganges and Meghna. Originating beyond the country's borders, these rivers, along with numerous smaller ones, constitute the Ganges-Brahmaputra-Meghna River system. A wide delta has been formed over the past thousand years due to sediments from these rivers, which have shaped the vast area of Bangladesh and the submerged delta-plain in the Bay of Bengal. 80% of the country's soil is formed by these sedimentary deposits. The remaining 20% of soils, 12% are obtained from Tertiary and Quaternary sediments found in hills, while 8% are uplifted Pleistocene terraces. (Banglapedia, 2021). River bank erosion is a frequent occurrence during monsoon in Bangladesh. Almost every year river banks are facing problems like erosion and failure occurs due to erosion along with other river bank failure criteria (Alom *et al.*, 2020). By this way bank materials play an important role on river bank erosion as well as failure.

The Arial Khan river is a Prominent and highly active river in Bangladesh, creates significant bank erosion which is one of the main reasons for the suffering of the local people (Akter *et al*., 2013). This river serves as a significant branch of the Padma river's distributary network. It originates from the Padma river at 51.5 km downstream of Goalanda of Rajbari district. The river runs through Faridpur, Madaripur and Barishal districts and maintains meandering channel through its course and is erosion in nature. The river is navigable round the year and has tidal characteristics. Its normal tidal range at Madaripur is 0.32 m. This river covers a total length of 160.0 km (Hossain *et al*., 2007). Severe river bank erosion have caused destruction of number of settlements in vicinity of bank. Under such circumstances a study has been undertaken in order to assessment of the bank erosion in terms of particle sizes of bank material around 6.0 km of the left bank and right bank of Arial Khan River at Shibchar Upazilla under Madaripur district of Bangladesh. Watson *et al*. (2006) studied stream bank erosion with a review of processes of bank failure, measurement and assessment techniques and modelling approaches. They stated that stream bank erosion depends mainly on flow pattern, bank material composition, bank geometry, channel geometry, bank soil-moisture conditions, vegetation and man-induced factors. Talukdar (2006) studied the probable causes of erosion, river instability, soil erosion, sediment transport and deposition. He concluded that sediment gets into the river not only from the catchment area but is also contributed by erosion of its banks. He defined that causes of failure of river banks can be directed erosion of the river bank among other probable causes. Roslan *et al*. (2013) worked on river bank erosion erodibility of Langat river of Malaysia and found the Sheet, Rill and Gully three types of soil erosion features commonly seen along Langat river. They found that along the Langat river the soil classifications predominantly consist of sand and silt, commonly referred to as well-graded silty sand, sandy clay of low plasticity and very clayey sand. They stated that soils with a greater proportion of sand show a greater risk of failure which is substantiated and affirmed by the 'ROM' scale equation where most of the soil samples were categorized as very high and critical in the degree level of erosion risk and thus will lead to risk of river bank failure. 'ROM' scale (after the name of the researchers Roslan and Mazidah) is used to ascertain the degree of soil erodibility namely low, moderate, high, very high and critical along the river bank based on the percentage composition of sand, silt and clay. They concluded that the responsible authority could implement proactive measures to prevent adverse incidents along the Langat river at an early stage.

The soil scientist Bouyoucos invented Eq. (1) for determining the Bouyoucos erodibility index (BEI) on the basis of composition of soil

[1] Hydraulic Research Directorate, River Research Institute, Faridpur-7800, Bangladesh.
[*] Corresponding Author: (E-mail: bikashduet60@gmail.com)
[2] Geotechnical Research Directorate, River Research Institute, Faridpur-7800, Bangladesh.
[3] Institute of Water and Flood Management, Bangladesh University of Engineering and Technology, Dhaka-1000, Bangladesh.
[4] Office of the Director General, River Research Institute, Faridpur-7800, Bangladesh.
[5] Dhaka Laboratory, River Research Institute, Dhaka-1205, Bangladesh.

$$\text{BEI} = \frac{\%\ \text{Sand} + \%\ \text{Silt}}{\%\ \text{Clay}} \qquad \text{Eq. (1)}$$

This lack of versatility has led to the development of an advanced and new improved soil erodibility index in the name of EI_{ROM} or 'ROM' Scale as in Eq. (2).

$$EI_{ROM}\ \text{equation} = \frac{\%\ \text{Sand} + \%\ \text{Silt}}{2 \times (\%\ \text{Clay})} \qquad \text{Eq. (2)}$$

This new equation still uses the original principle of Bouyoucos, which is to analyze the soil textural composition of sand, silt and clay. The new equation has effectively demonstrated both the significant value and the threshold for delineating soil erodibility, while also indicating the anticipated erosion characteristics. With the new EI_{ROM} equation outlined in Eq. (2), the more realistic and significant value of soil erodibility index can be used concurrently considering its corresponding risk category as illustrated in **Table 1** to denote the extent of soil erodibility.

Table 1. 'ROM' scale with regards to soil erodibility category.

'ROM' scale	Soil erodibility category
< 1.5 Low	Low
1.5 -4.0	Moderate
4.0 -8.0	High
8.0 -12.0	Very High
> 12.0 Critical	Critical

(Source: Roslan and Mazidah, 2012)

EI_{ROM} = (% sand + % silt) / 2(% clay) The 'ROM' scale was developed solely on the grading characteristics of soil, utilizing the EI_{ROM} equation to derive the soil erodibility index and ascertain the configuration of erosion features. In other words, the 'ROM' scale quantifies the degree of soil erodibility by applying the EI_{ROM} equation. This pioneering scale represents the first endeavor to categorize erosion severity based on both the soil erodibility index and erosion features. During the early stages of developing the 'ROM' scale, various areas and locations across Peninsular Malaysia experiencing erosion-induced landslides were pinpointed. Physical reconnaissance and observation of soil erosion features, coupled with basic soil classification information, were documented during surveys conducted in the identified areas. The impact of the soil erosion process on the affected areas recognized from the erosion features commonly known as sheet, rill, and gully were critically observed. The identification of the soil textural composition namely sand, silt and clay are crucial in determining the risk of landslides caused by erosion. The EI_{ROM} equation as stated in advance was created to gain an acceptable sound erodibility value relative to other scale of measurements. Duong *et al.* (2019) studied the processes of river bank failure along the red river bank using three distinct bank soil and by modeling both mass failure and undercutting erosion. They found that there was a close relationship between the content of fine-grained particles and soil erosion. The rate of erosion is lowered by an increase in fineness. Majumdar and Mandal (2021) studied on the estimation of river bank erosion risk potential using mechanical and erodibility analysis of soil on the left bank of the Ganga river near Malda district in West Bengal, India. Their results reveal that the erodibility levels increase from high to moderate along an extended left bank line (middle to lower) and fall relatively low along another line on the upper branch of the line according to the 'ROM' scale. They concluded that the nature of soil along left bank is dominantly sandy in which promotes vulnerable condition of river bank sites. They also conclude that basic parameters of soil and its mechanical analysis also reveals that unstable condition exists along river bank line but instability condition is increasing from upper to lower segment of bank line. They recommended that the risk of river bank failure can be measured by determining textural composition of soil. Das and Deka (2020) studied on estimating bank erosion vulnerable areas in Kamrup district, Assam, India using 'ROM' scale. They observed that most of the soil categories in the study area have soils that have a higher proportion of sand and thus have greater risk of bank collapse. They found sandy soil is recognized as minimal cohesive force and thus more susceptible to erosion and transportation by stream. They established by the 'ROM' scale calculation where maximum number of the soil samples was sorted as very high and critical in the degree level of erosion vulnerability and is susceptible to bank failure. They recommended that suitable mitigating methods can be planned for prevention of bank erosion.

The main objective of this study is to categorize the erosion risk potential in terms of particle sizes of bank material.

Methodology

A total of 30 soil samples data has been collected from 6 holes within 6.0 km reach of the left and right bank of Arial Khan River of Bangladesh. The coordinates of the holes of the left bank and right bank have been shown in **Table 2**. The study area and boring layout have been shown in **Fig. 1** and **Fig. 2** respectively. The soil samples have been collected along the holes up to the depth 7.50 m. Here the soil data have been considered up to the depth 7.50 m as the lowest water level near the depth of soil layer. The lowest water level in Arial khan river is (0.13-1.16) mPWD. Particle sizes are analyzed through Laser Diffraction Particle Size Analyzer (Mastersizer 3000). In this study erodibility index has been determined using the BEI $= \frac{\%\ \text{Sand} + \%\ \text{Silt}}{\%\ \text{Clay}}$ and EI_{ROM} equation $= \frac{\%\ \text{Sand} + \%\ \text{Silt}}{2 \times (\%\ \text{Clay})}$. Soil erodibility has been categorized using 'ROM' scale.

Table 2. Showing the coordinates of boring points along the left and right bank of Arial Khan River.

Left bank	Coordinate (UTM Zone 45N)		Right bank	Coordinate (UTM Zone 45N)	
	Easting(m)	Northing(m)		Easting(m)	Northing(m)
Khas Char Bachamara	204966.44	2589225.30	Sannyasir Char	204142.34	2590445.94
Char Arial Khan	203086.31	2591543.68	Khankandi	205064.15	2587333.27
Bajehar Char	205717.15	2585987.13	UttarcharTajpur	205419.62	2584340.73

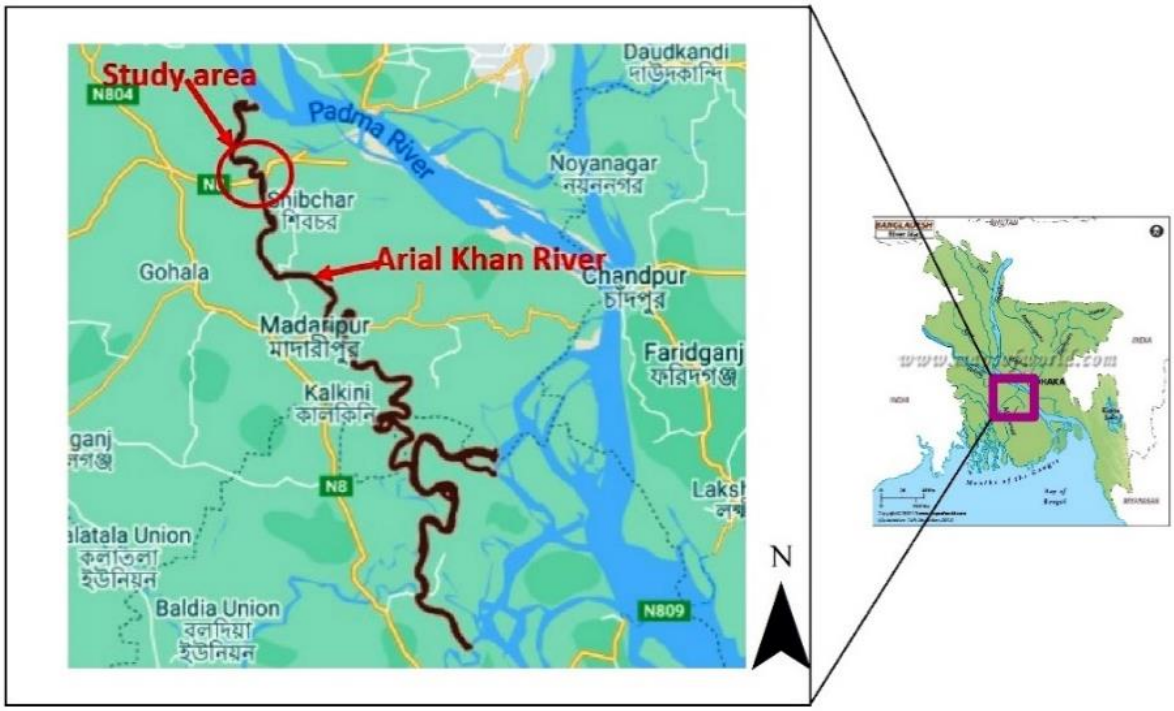

Fig. 1. Study area at and around the Haji Shariotullah bridge.

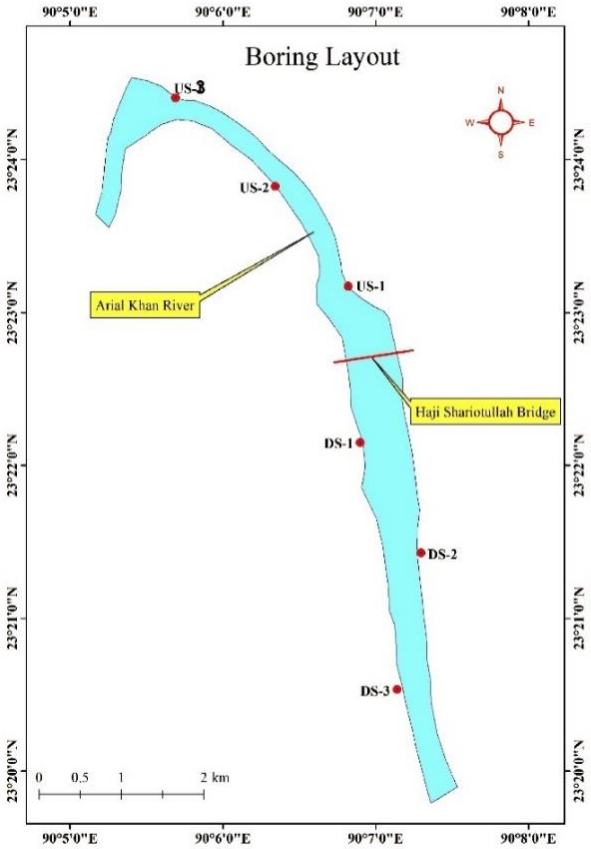

Fig. 2. Boring Layout of the study area.

Results and Discussions

The particle sizes of the soil samples, Bouyoucos erodibility index (BEI) and EI_{ROM} of the left bank of Arial Khan River have been shown in **Table 3**.

Table 3. Showing the percentage of Particle sizes, BEI and EI_{ROM} of the left bank of Arial Khan River.

Left bank of Arial Khan River	Coordinate (UTM Zone 45N)		Depth in m	Particle sizes Analysis			Bouyoucos Erodibility Index (BEI)	EI_{ROM}
	Easting	Northing		Clay in (%)	Silt in (%)	Sand in (%)		
Khas Char Bachamara	204966.44	2589225.30	1.50	5	65	30	19.00	9.50
			3.00	16	82	2	5.25	2.63
			4.50	4	87	9	24.00	12.00
			6.00	4	84	12	24.00	12.00
			7.50	1	27	72	99.00	49.50
Char Arial Khan	203086.31	2591543.68	1.50	4	66	30	24.00	12.00
			3.00	0	26	74	infinity	infinity
			4.50	0	23	77	infinity	infinity
			6.00	0	24	76	infinity	infinity
			7.50	1	35	64	99.00	49.50
Bajehar Char	205717.15	2585987.13	1.50	2	61	37	49.00	24.50
			3.00	1	30	69	9900	49.50
			4.50	0	9	91	infinity	infinity
			6.00	0	24	76	infinity	infinity
			7.50	0	21	79	infinity	infinity

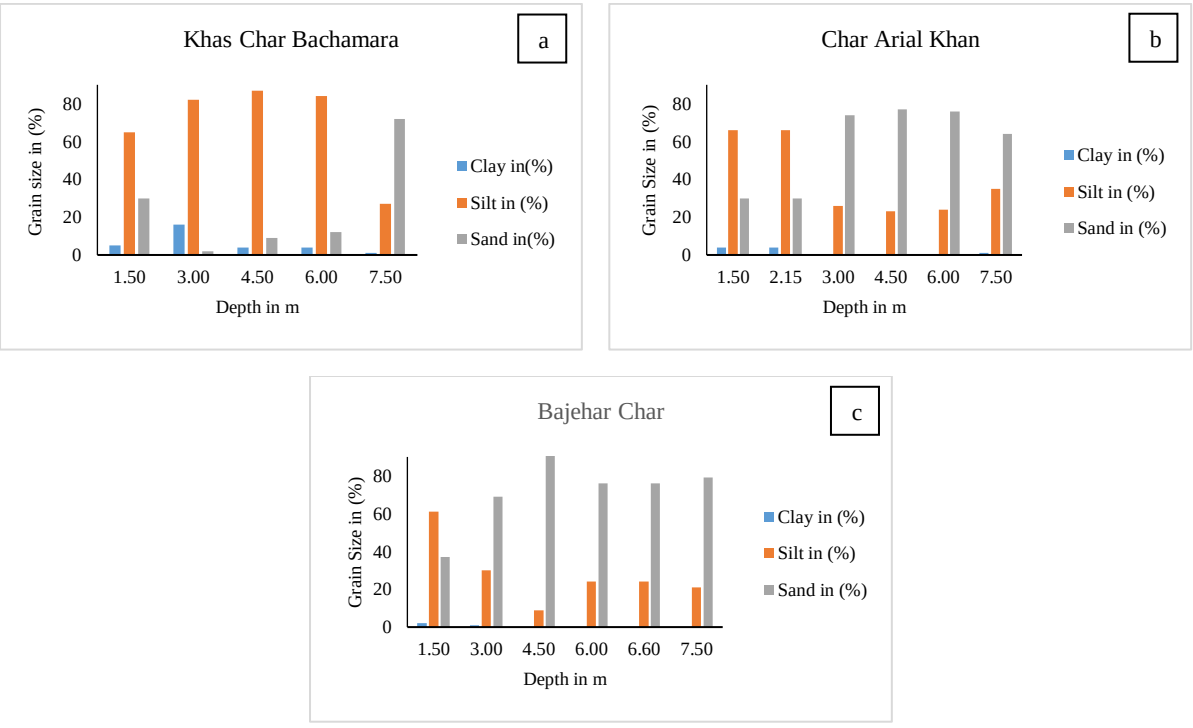

Fig. 3. Showing the Particle Size analysis (a) at Khas Char Bachamara (b) at Char Arial Khan (c) at Bajehar Char.

From **Table 3** and **Fig. 3**, it has been observed that Silt particles dominate at Khas Char Bachamara up to the depth of about 6.0 m and then it consists of Sand layer. On the other hand the layer up to the depth 1.5 m of Char Arial Khan consists of silt layer and then it consists of Sand layer. However, sand particles dominate at Bajehar Char up to the depth of about 7.5 m except upper layer of depth 1.5 m.

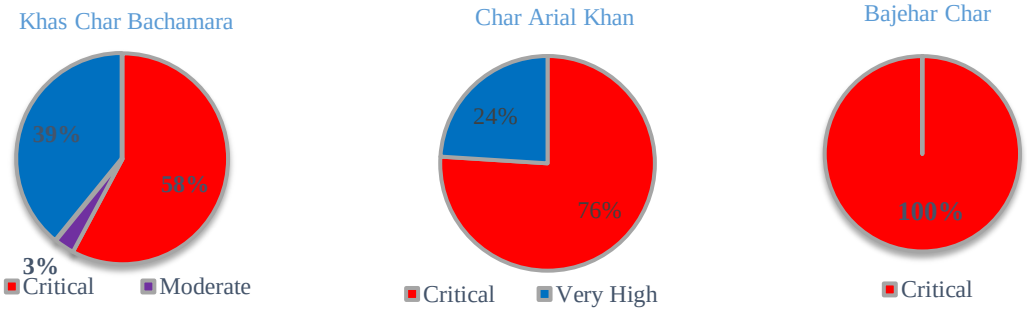

Fig. 4. Illustration of soil erodibility category at Khas Char Bachamara, Char Arial Khan and Bajehar Char.

From **Table 3** and **Fig. 4**, it has been observed that the erodibility index at the bank of Khas Char Bachamara at depth 1.5 m is 9.5 is very high and moderate at depth 3.0 m. However, the erodibility index is moderate to critical at the left bank of Arial Khan River along the bore hole. The erodibility index at the bank of Char Arial Khan is very high to critical at the left bank of Arial Khan River along the bore hole and the erodibility index at the bank of Bajehar Char is critical along the bore hole. In brief, the left bank of Arial Khan River is very high to critical position in risk of erosion except 3.0 m depth of Khas Char Bachamara which protects the bank from failure for little time. The soil erodibility category in terms of particle sizes has been shown in pie graph in **Fig. 4**. The particle sizes of the soil samples, Bouyoucos erodibility index and EI_{ROM} of the right bank of Arial Khan River have been shown in **Table 4**.

Table 4. Showing the percentage of Particle sizes, Bouyoucos erodibility index and EI_{ROM} of the right bank of Arial Khan River.

Right bank of Arial Khan River	Coordinate (UTM Zone 45N)		Depth in m	Particle Sizes Analysis			Bouyoucos Erodibility Index (BEI)	EI_{ROM}
	Easting	Northing		Clay in (%)	Silt in (%)	Sand in (%)		
Sannyasir Char	204142.34	2590445.94	1.50	4	74	22	24.00	12.00
			3.00	5	65	30	19.00	9.50
			4.50	0	37	63	infinity	infinity
			6.00	0	40	60	infinity	infinity
			7.50	0	34	66	infinity	infinity
Khankandi	205064.15	2587333.27	1.50	0	11	89	infinity	infinity
			3.00	1	70	29	99.00	49.00
			4.50	0	39	61	infinity	infinity
			6.00	0	46	54	infinity	infinity
			7.50	0	30	70	infinity	infinity
Uttarchar Tajpur	205419.62	2584340.74	1.50	1	44	55	99.00	49.50
			3.00	6	86	8	15.67	7.83
			4.50	5	81	14	19.50	9.50
			6.00	3	84	13	32.33	16.17
			7.50	5	81	14	19.00	9.50

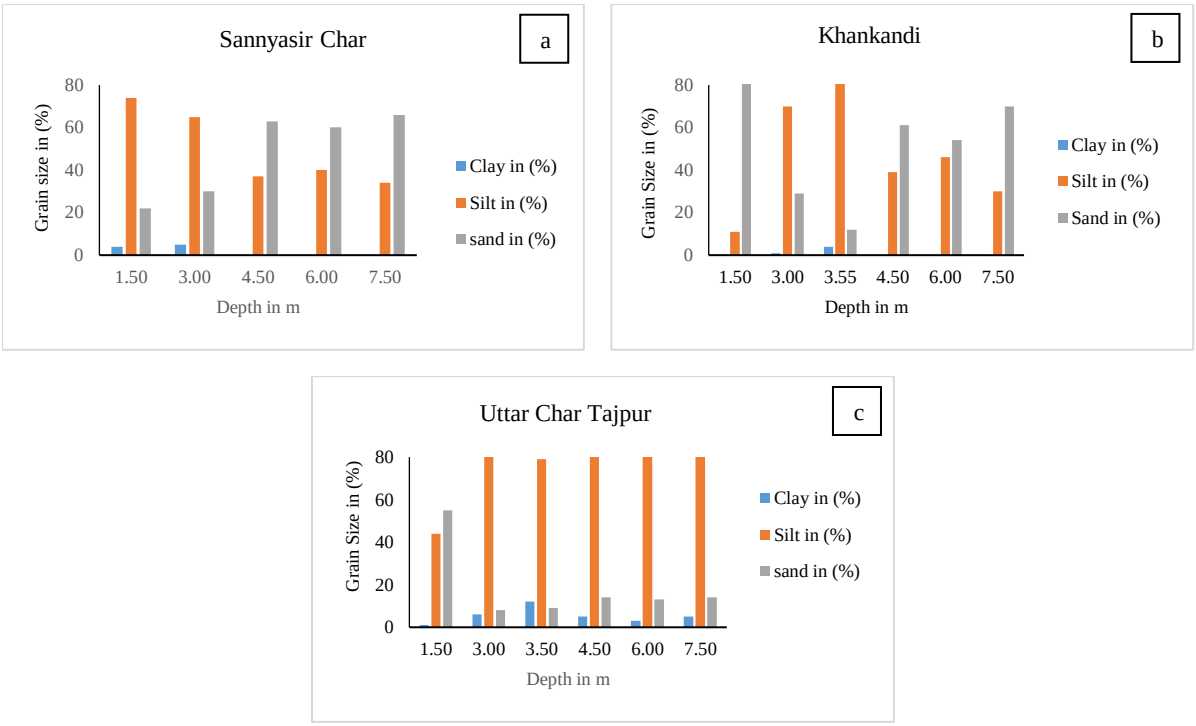

Fig. 5. Showing the Particle Size Analysis (a) at Sannyasir Char (b) at Khankandi (c) at Uttar Char Tajpur.

From **Table 4** and **Fig. 5**, it has been observed that Silt and Sand particles dominate at Sannyasir Char and Khankandi up to the depth of exploration. whereas Silt particle dominates at Uttar Char Tajpur except the upper layer of about 1.5 m which consists of Silt and Sand layer.

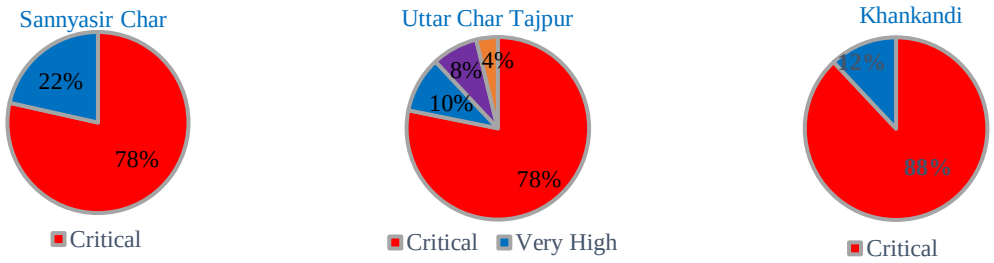

Fig. 6. Illustration of soil erodibility category at Sannyasir Char, Khankandi & Uttar Char Tajpur.

From **Table 4** and **Fig. 6**, it has been observed that the erodibility index at the bank of Sannyasir Char is very high to critical at the right bank of Arial Khan River along the bore hole. The erodibility index at the bank of Khankandi is critical at the right bank of Arial Khan River along the bore hole and the erodibility index at the bank of Uttar Char Tajpur is high to critical along the bore hole. In brief, the right bank of Arial Khan River is high to critical position in risk of erosion.

Conclusions

It has been observed from the left bank of Arial Khan River that Silt particle dominates at Khas Char Bachamara up to the depth of about 6.0 m and then it consists of Sand layer. On the other hand the layer up to the depth 1.5 m of Char Arial Khan consists of Silt layer and then it consists of Sand layer. However, Sand particle dominates at Bajehar Char up to the depth of about 7.5 m except upper layer of depth 1.5 m. The erodibility index has been observed at the bank of Khas Char Bachamara at depth 7.5 m is critical and moderate at depth 3.0 m. However, the erodibility index is moderate to critical at the left bank of Arial Khan River along the bore hole. The erodibility index at the bank of Char Arial Khan very high to critical at the left bank of Arial Khan River along the bore hole and the erodibility index at the bank of Bajehar Char is critical along the bore hole. In brief, the left bank of Arial Khan River is very high to critical position in risk of erosion except 3.0 m depth of Khas Char Bachamara which protects the bank from failure for little time.

It has been observed from the right bank of Arial Khan River that Silt and Sand particle dominate at Sannyasir Char and Khankandi up to the depth of exploration whereas Silt particle dominates at Uttar Char Tajpur except the upper layer of about 1.5 m which consists of Silt and Sand layer. The erodibility index has been observed at the bank of Sannyasir Char is very high to critical at the right bank of

Arial Khan River along the bore hole. The erodibility index at the bank of Khankandi is critical at the right bank of Arial Khan River along the bore hole and the erodibility index at the bank of Uttar Char Tajpur is high to critical along the bore hole. In brief, the right bank of Arial Khan River is high to critical position in risk of erosion. The study result can help a design Engineer. However, it is recommended here that full geotechnical investigation is needed to prevent the erosion of the river banks.

References

Alom, M. M., Rahman, Dr. M. M. and Rahman, M. M. (2020). Assessing riverbank erosion at upstream and downstream side of Padma bridge by using satellite images. *Tech. J. River Res. Inst.* 15(1): 1-7.

Akter, J., Sarker, M. H. and Haque, P. (2013). Morphological Processes and Effective River Erosion Management: A Case Study of the Arial Khan River in Bangladesh. 4th International Conference on Water & Flood Management (ICWFM-2013). Dhaka, Bangladesh.

Banglapedia (2021). Bangladesh Soil, National Encyclopedia of Bangladesh [online]. https://en.banglapedia.org/index.php/Bangladesh_Soil (Accessed 03 April 2023).

Das, I. and Deka, S. (2020). Application of 'ROM' scale for estimating bank erosion vulnerable areas in Kamrup district, Assam. *International Journal of Management (IJM)*, 11(12): 1652-1656. http://iaeme. com/Home/issue/IJM

Duong, T. T. and Duc D. M. (2019). Riverbank Stability Assessment under River Water Level Changes and Hydraulic Erosion. *Water* 11(12): 2598. https://doi.org/10.3390/w11122598

Hossain, M. M., Islam, M. Z., Ferdousi, S., Kabir, M. A. and Rahman, K. M. Morphological Characteristics of Arial Khan River in the vicinity of Arial Khan Bridge in Bangladesh. International conference on water and flood management (ICWFM-2007), 12-14 March 2007, Dhaka, Bangladesh.

Majumdar, S. and Mandal, S. (2021). River bank erosion risk potential estimation through mechanical and erodibility analysis of soil: A study on left bank of Ganga river near Malda district in West Bengal, India. *International Research Journal of Social Sciences*. 10(3): 23-34.

RRI (2023). Characterization of soils around the Arial Khan River of Bangladesh. River Research Institute, Faridpur, Bangladesh.

Roslan, Z. A., Naimah. Y and Roseli. Z. A. (2013). River bank erosion risk potential with regards to soil erodibility. *WIT Transactions on Ecology and The Environment.* 172: 289 – 297. https://doi.org/10.2495/RBM130241

Talukdar, B. (2006). River bank erosion-A perspective Assam engineering college. Email :bipulaec@gmail.com.

Watson, A. J. and Basher, L. R. Landcare (2006). Stream bank erosion: a review of processes of bank failure, measurement and assessment techniques, and modeling approaches. Motueka Integrated Catchment Management Programme Report Series: Bank erosion review, Motueka Integrated Catchment Management (Motueka ICM), Programme Report Series by ICM Report No. 2005-2006/01(June 2006).

Technical Journal
River Research Institute ISSN: 1606-9277

QUANTIFICATION AND SPATIOTEMPORAL EVOLUTION OF TIDAL ASYMMETRY IN THE SIBSA-PUSSUR ESTUARY: A HARMONIC ANALYSIS APPROACH

M. N. Kadir[1*] and T. Naher[2]

Abstract

Tidal asymmetry in deltas, resulting from the interaction between astronomical tides and nonlinear tidal processes in shallow water, plays a crucial role in sediment transport within estuaries. Quantifying tidal asymmetry is vital for understanding the factors contributing to long-term morphological changes. This study applies the harmonic analysis method (T_tide) to examine the spatiotemporal evolution of tidal asymmetry in the Sibsa-Pussur (SP) estuary of the GBM delta, considering strongly variable river discharge conditions. Data required for analysis is collected from the results of a hydrodynamic model for 1978, 1988, 2000, and 2011. The study focuses on eight main tidal constituents (M2, M4, M6, K1, S2, O1, MS4, MSf). Tidal duration asymmetry and peak current asymmetry are determined, quantifying tidal asymmetry based on amplitude ratios and phase differences. The findings reveal that the SP estuary becomes increasingly flood dominant over time, with the Pussur River exhibiting greater flood dominance in tidal asymmetry compared to the Sibsa River. Incorporating morphological changes into the model could enhance results and provide a more accurate understanding of the sedimentation issues in the SP estuary.

Keywords: *Harmonic analysis, Morphological changes, Sibsa-Pussur Estuary, Spatiotemporal evolution, Tidal asymmetry, Tidal constituent.*

Introduction

Deltas have become desirable to inhabit due to their fertile land, abundant fisheries, and ecological and economic value (Guo *et al*., 2016). The high population density in these regions necessitates the implementation of various infrastructural projects for flood protection and land reclamation for agricultural and other purposes. Typical measures include polderization and the construction of dams and barrages for the diversion of river water for irrigation. Unfortunately, such reclamation projects often lead to a host of environmental problems, including the loss of biodiversity, deterioration of coastal water quality, and depletion of fishery resources (Son and Wang, 2009). The direct consequences of these human interventions are the prevention of natural land elevation and the onset of subsidence (Li *et al*., 2010). Additionally, embankments alter the planform shape and cross-sectional geometry of tidal rivers, resulting in strongly convergent estuaries and a reduction in intertidal area (Stark *et al*., 2017).

Like other deltas, the Ganges-Brahmaputra-Meghna (GBM) delta, a thriving ecosystem at the interface of vast rivers and the Bay of Bengal, also faces significant challenges due to its densely populated nature. Understanding these complex interactions necessitates a multifaceted approach, examining the interplay between freshwater discharge variations, tidal dynamics, and their combined influence on sediment transport. This delta exhibits a distinct spatial variation in its governing processes. The eastern part is dominated by freshwater input from the mighty Ganges and Brahmaputra rivers, resulting in a significant sediment load discharged into the Bay of Bengal (Elahi *et al*., 2020; Rahman *et al*., 2014). In contrast, the western part, comprised of the Sibsa and Pussur rivers, experiences a tide-dominated regime, allowing for importing tidal sediments (Rahman *et al*., 2018; Bomer *et al*., 2019). This inherent spatial variability underscores the need for a nuanced investigation into the specific factors shaping sediment transport within each river system.

Further complicating the scenario are anthropogenic interventions like the Farakka Barrage, constructed in 1975 to divert water from the Ganges to the Hooghly River. This has significantly reduced freshwater inflow into the Gorai River, the primary source of freshwater for the western delta (Rahman and Rahaman, 2018). The combined effects of reduced freshwater discharge and other human activities have led to many problems, including channel siltation, subsidence, and even channel abandonment (Angamuthu *et al*., 2018; Wilson *et al*., 2017).

One under-investigated aspect with potentially significant ramifications is the role of tidal asymmetry. Tidal asymmetry is one of the critical factors influencing sediment transport within estuaries (McLachlan *et al*., 2020; Yang *et al*., 2023). Unlike perfectly balanced tides, estuaries often experience flood currents with greater strength or duration compared to ebb currents. This asymmetry plays a significant role in determining the net direction and volume of sediment transport (Dronkers, 1986; Friedrichs and Aubrey, 1988; Jiang *et al*., 2011; Speer and Aubrey, 1985). In flood-dominant systems, stronger flood currents act like an import mechanism, bringing in more sediment than the ebb flow can remove. This can lead to a gradual infilling of estuaries over time. Conversely, ebb-dominant systems, with stronger ebb currents, tend to promote erosion and can deepen channels within the estuary. Understanding the type of tidal asymmetry present within a specific estuary is crucial for predicting its morphological evolution and the potential consequences for human infrastructure and coastal stability.

This research aims to elucidate the role of tidal asymmetry in shaping the contrasting behavior of the Sibsa and Pussur rivers. We hypothesize that historical changes in river discharge patterns and anthropogenic interventions may have altered the degree of tidal asymmetry within each system, influencing the direction and volume of sediment transport. By employing a hydrodynamic model and analyzing historical data, we will assess how changes in tidal asymmetry can explain the observed contrasting behavior of these rivers. This investigation will improve our understanding of the complex interplay between tides, freshwater discharge, and sediment transport in the GBM delta and provide valuable insights for sustainable management strategies to ensure the future navigability of these vital waterways. Through this research, the following questions will be answered.

[1] Department of Agricultural Engineering, Sher-e-Bangla Agricultural University, Dhaka, Bangladesh.
[*] Corresponding Author (E-mail: mnkadir@sau.edu.bd)
[2] Hydraulic Research Directorate, River Research Institute, Faridpur-7800, Bangladesh.

- How has tidal asymmetry developed in the Sibsa-Pussur estuary?
- What are the differences in tidal asymmetry between the Sibsa and Pussur rivers?

Methodology

Study Site

The western part of the lower GBM delta is considered for this study. This part is characterized as an extensive system of tide-dominated rivers (distributaries of the Ganges). The two main rivers in this part are Sibsa and Pussur Rivers. These are connected to the Ganges by the Gorai and partly by the Madhumoti and the Arial Kha rivers (**Fig. 1**). So, the flow in these systems directly depends on the Ganges River flow. The second-largest seaport of Bangladesh, known as Mongla seaport (approximately 132 km upstream from the sea), is located on the east bank of the Pussur River (**Fig. 1**). Since its establishment in 1950, this port has been playing an important role in international trade, national defense, and commerce of the country (Islam and Haider, 2016). Maintaining the navigability (at least 7.5 m navigable draft) of these rivers is necessary to keep this port active throughout the year. Because of that, several dredging efforts have been made to restore the navigability of the Pussur River (Rahman and Ali, 2018). The construction of polders is also present in this system. In 1960, the East Pakistan Water and Power Development Authority (called EP-WAPDA at that time, now known as BWDB) constructed over 139 polders (4000 km of embankments) across the entire coastal belt of Bangladesh (BWDB, 2013). These polders were built to protect the land from coastal flooding and storm surges and help achieve food security through better water control. In the southwestern part alone, about 1566 km of embankments (polders) were constructed (BWDB, 2013). Therefore, many anthropogenic interventions have affected the natural system of this area over the past five decades. This system is also crucial for the presence of the mangrove forest "Sundarbans" (**Fig. 1**). A significant part of the system runs through this forest. These extensive vegetated areas also have an enormous influence on tidal propagation.

Data processing approach

Data used in this study were obtained from secondary sources, primarily from the Bangladesh Inland Water Transport Authority (BIWTA) and the Bangladesh Water Development Board (BWDB). The BIWTA collects water level (WL) data through an automated gauge at 30-minute intervals, while the BWDB manually records high and low tide WL readings daily. Within the study area, there are two BIWTA WL measuring stations: Hiron Point, with data available from 1977 to 2015, and Mongla, with data available from 2000 to 2015 but with some missing values. The BWDB-operated Rupsha station inland has data from 1981 to 2012. However, it should be noted that the available data needed to be more sufficient for conducting a tidal analysis. Therefore, a calibrated hydrodynamic model developed by Deltares (Deltares, 2014) has been used to generate the required data for the analysis.

Tidal Analysis

Tidal analysis is necessary to determine the tidal asymmetry of a system. Harmonic analysis is the most common tidal analysis method, which provides quantitative metrics to analyze the tides. A least-squares tidal analysis (T_tide) (Pawlowicz *et al*., 2002) separates the main tidal constituents' amplitudes and phases. Before using the model output in tidal analysis, removing the high-frequency signal from the time-series data is required to get a more accurate tidal analysis result. The Godin filter was used to remove the high-frequency signal (Godin, 1972) for both the WL time-series data (**Fig. 2a**) and the velocity (both "u" and "v" components) time-series data (**Fig. 2b**).

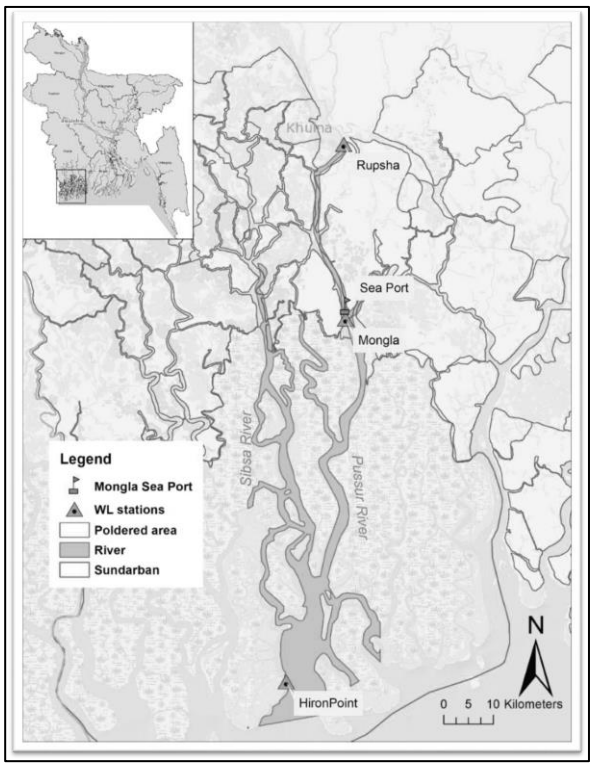

Fig. 1. Location map of the study area.

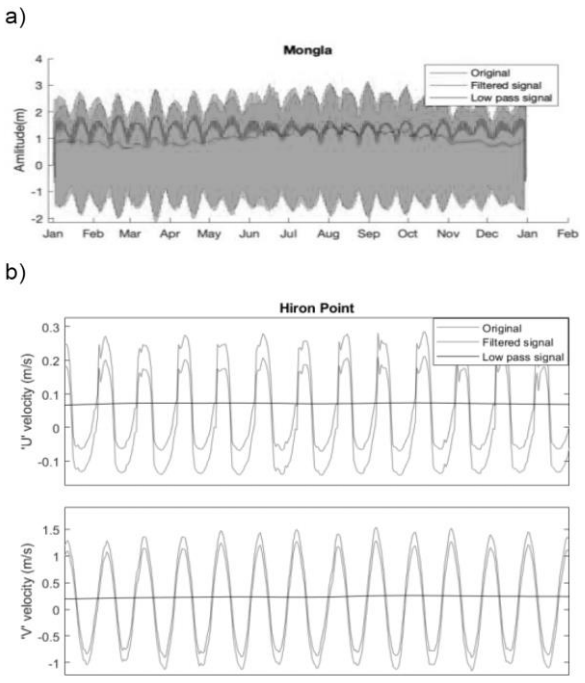

Fig. 2. Godin-filtered time series a) water level at Mongla, b) Expanded velocity time series at Hiron Point station.

a)

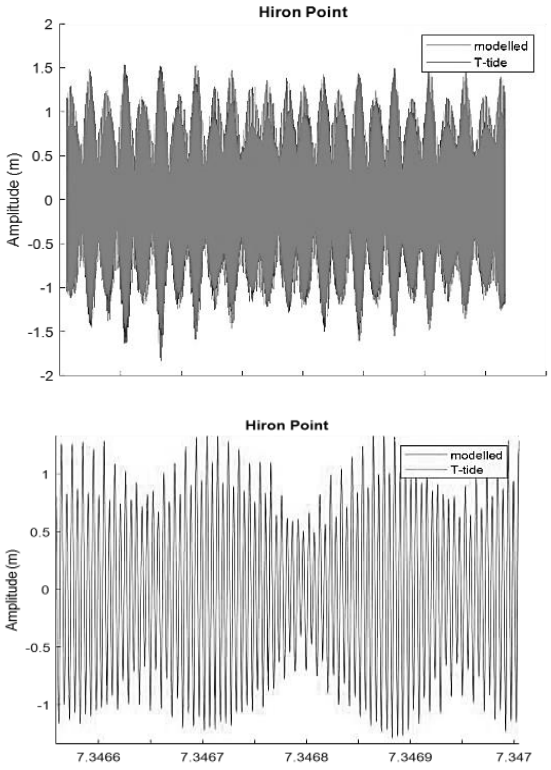

b)

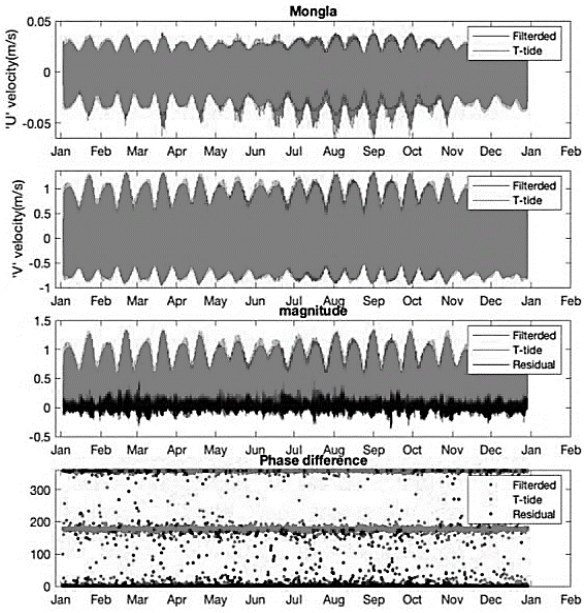

Fig. 3. Outputs of T_tide a) water level series at Hiron Point, and b) velocity time series data at Mongla station for the analysis period 2011.

According to Godin (1972), this function applies a three-step low-pass filter to a time series to remove the higher-frequency signals and obtain the residual signal. After getting the filtered time series value, the T_tide function was used for the Harmonic analysis. T_tide uses an equilibrium tide model to obtain frequencies of tidal constituents, then fits each of these constituents to the provided time series and finds each constituent's best-fit phase.

T_tide models the tidal heights ζ as

$$\zeta(t) = f_{0,0} + \sum_{i=1}^{n} [f_{1,i}\cos(\omega_i t) + f_{2,i}\sin(\omega_i t)]$$

Where t is time, ω_i is the frequency of an individual tidal constituent, and $f_{0,0}$, $f_{1,i,}$ & $f_{2,i}$ are unknown coefficients to be determined by regression analysis using observations (Pawlowicz *et al*., 2002).

The T_tide function is a powerful tool for analyzing scalar data, such as heights (**Fig. 3a**), and complex data, such as velocity (**Fig. 3b**). This model makes it possible to generate the depth-averaged velocity at a specific observation point, represented by complex data with "U" and "V" components. As all observation points are situated on the thalweg of the river, the depth-averaged velocity of the corresponding observation point is a reliable indicator of the entire cross-section. During harmonic analysis, the T_tide function calculates the magnitude of the complex data as "U" plus the square root of negative one time "V" (where "U" refers to eastward velocity and "V" refers to northward velocity) (Pawlowicz *et al*., 2002). **Fig. 3** showcases the output obtained from T_tide for the analysis period of 2011, with the model prediction fitting well with the filtered data (**Fig. 3a**).

Results

River Characteristics

A total of 21 observation points (OPs) have been selected for the Sibsa and Pussur River models, with 12 OPs located in the Pussur system and 8 OPs in the Sibsa system. The Hiron Point OP is common to both rivers and all OPs are situated on the thalweg of the river. Fig. 4 depicts the model bathymetry of the respective OPs, providing a clear illustration of the river depth and width.

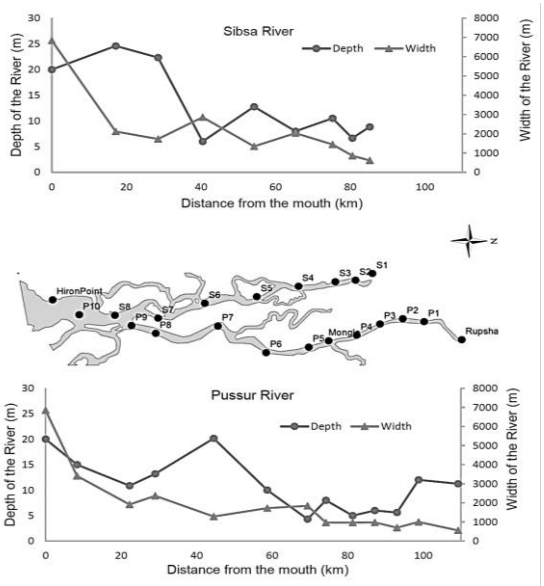

Fig. 4. River characteristics (Width and Depth) against distance from the mouth of the sea.

The rivers appear to be converging as their width decreases towards the landward direction. Upon analyzing their depths, it is evident that Sibsa holds a slightly deeper channel than Pussur. However, both rivers exhibit a decrease in depth, with Sibsa experiencing a drop at the 40km mark, and Pussur showing a sudden rise at 45km. Interestingly, the depth of Pussur begins to increase again after approximately 93km.

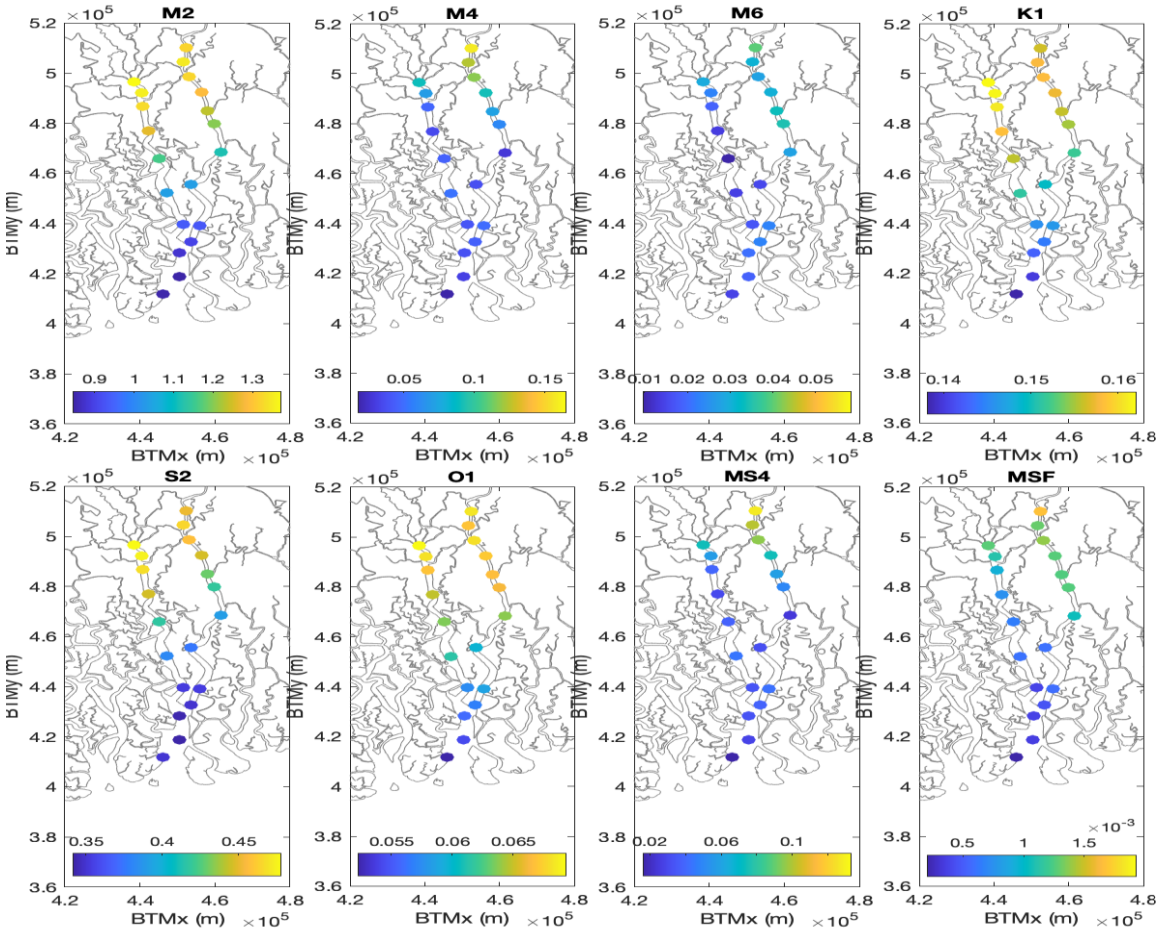

Fig. 5. Spatial variation of the vertical tidal amplitudes (M2, M4, M6, K1, S2, O1, MS4, and MSf) for the 2011 tidal analysis.

Asymmetry of the vertical tide

Spatial variation of tidal amplitudes: Like other semi-diurnal estuaries, tidal asymmetry in the Sibsa-Pussur (SP) estuary can be related to M2, S2, K1, O1, M4, M6, MS4, MSf, which are further analyzed here. M2 is the most dominant tidal constituent in the SP system, followed by S2, K1, and MS4 (**Fig. 5** and **Fig. 6**). Besides that, M4 is also considered because it is the first harmonic of M2 and dominates in many estuaries. The tidal asymmetry can also be affected by the sixth-diurnal tide M6 in some, mainly semi-diurnal estuaries. Near the coast, the effects of the fortnightly tide MSf are limited compared with those of the main diurnal and semi-diurnal tides. **Fig. 5** shows how the amplitudes of these eight constituents enlarge in the landward direction. However, the enlargement rate differs in these two rivers (**Fig. 6a** and **Fig. 6b**). The geometric convergence and decreasing depth of the Sibsa and Pussur rivers (**Fig. 5**) may gradually increase tidal amplitudes towards the estuary's landward direction.

Focusing on the main diurnal constituents K1 and O1, the T_tide results show that the variations of the mean amplitudes are in the range of 0.19–0.23 m and 0.05–0.08 m, respectively, among the different stations. The mean amplitudes of the main semi-diurnal constituents M2 and S2 range between 0.8–1.35 m and 0.28–0.4 m, respectively (**Fig. 6**). The largest amplitudes are found at the stations around the rivers' landward direction, where the poldered areas start (**Fig. 1**). The S2 amplitude is about one-third of the M2 amplitude. The narrowing of the rivers also enhances the overtides and compound tides, such as M4, MS4, and M6. The peak values of M4, MS4, and M6 amplitudes are 0.17 m, 0.12 m, and 0.06 m, respectively (**Fig. 6**). There is also a landward increase of the MSf amplitude throughout the estuary. However, compared to other constituents, the contribution from the MSf is relatively small to the tide. Two main channels are identified within the SP estuary: the Sibsa and Pussur channels. For these two channels, the along-channel variations of the mean tidal amplitudes of eight main constituents are shown in **Fig. 6a** and **Fig. 6b**.

M2 is the most dominant tide in both cases, followed by the S2, K1, MS4, M4, O1, M6, and MSf. M2 has a similar amplitude until the bifurcation point (about 13 km from the mouth of the ocean) of the two rivers; from that point onward, the trends increase. At around 93km of the Pussur channel, there was a downward trend for the M2 and S1 amplitudes. The possible reason for this change is probably the presence of interconnected channels at that point (**Fig. 1**). This may cause scouring and increase the depth (**Fig. 4**), leading to a decrease in M2 and an increase in M4.

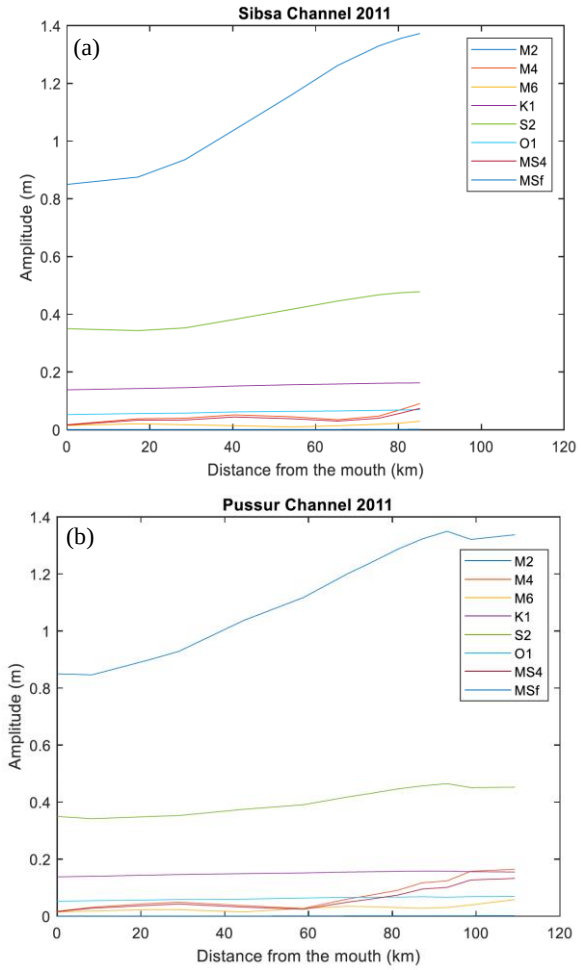

Fig. 6. Longitudinal profiles of mean tidal amplitudes of main constituents (M2, M4, M6, K1, S2, O1, MS4, MSf) along the a) Sibsa channel and b) Pussur channel in the SP estuary during 2011.

Temporal Variation of Tidal Amplitude: From 1978 to 2011, four different years (1978, 1988, 2000, and 2011) chose to run the model to mimic the temporal variation of over 33 years. The choice of the year depends on data availability and hydrological characteristics. 1978 is the earliest available data year, 1988 is the most flooded year, 2000 is the driest year, and 2011 is the latest available data and model-validating year. **Fig. 7** shows the model predictions of amplitude ratios along the Sibsa and Pussur channels between 1978 and 2011. **Fig. 7a** and **Fig. 7b** show that the Pussur channel's tidal asymmetry is more robust than the Sibsa channel. There is a slight drop at 65km for the Sibsa channel and around 60 km for the Pussur channel. Among the years, 1988 shows the strongest tidal asymmetry, followed by 2000, 1978, and 2011 for the Sibsa channel and 1978, 1988, and 2011 for the Pussur channel.

Nature of the Tidal Asymmetry

The phase difference calculations can determine whether the system is flood-dominant or ebb-dominant (2φ2- φ4). In the case of asymmetry of the horizontal tide, a system is called flood dominant when the phase difference lies between 0°-90° & 270°- 360°. From 90°-270°, represent the system as ebb dominant. The system is known as the symmetric tide if the phase difference is close to 90° or 270° (-90°). So farther from these two points will represent a more asymmetric tide. For the SP estuary, phase differences are calculated from the tidal analysis of horizontal tide (**Fig. 8**) and vertical tide (**Fig. 9**) for the years 1978, 1988, 2000, and 2011.

Peak current asymmetry:

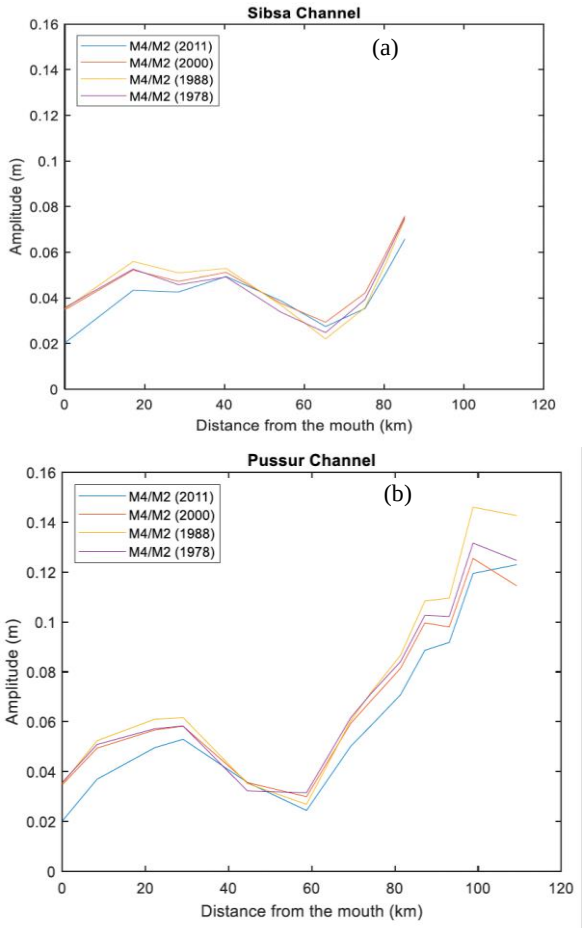

Fig. 7. The evolution of the amplitude ratio of the M2 and M4 (a & b) tidal constituent for the asymmetry of the vertical tide, derived from the model, along the Sibsa-Pussur channel between 1978 and 2011.

Fig. 8 shows the peak current asymmetry of the Sibsa (dotted line) and Pussur (solid line) rivers, along with the longitudinal profile and four different years of temporal variation. In the Sibsa channel, the temporal variations of the tidal asymmetry are not that much, except for the first point and at 30km (**Fig. 8**). However, the spatial variations are significant. Initially, it seems to be ebb dominant till 30 km, then goes close to the flood dominant to symmetric. After 80 km, the asymmetry becomes maximum flood dominant.

On the other hand, in the Pussur channel, there are some temporal variations along the river at 23 km, 45 km, and 93 km (**Fig. 8**). From 0 to 40km, recent years show close to ebb dominance. However, the rest of the river shows flood dominance. The asymmetry towards the longitudinal profile of the Sibsa River also shows flood dominance in most of the points (**Fig. 8**).

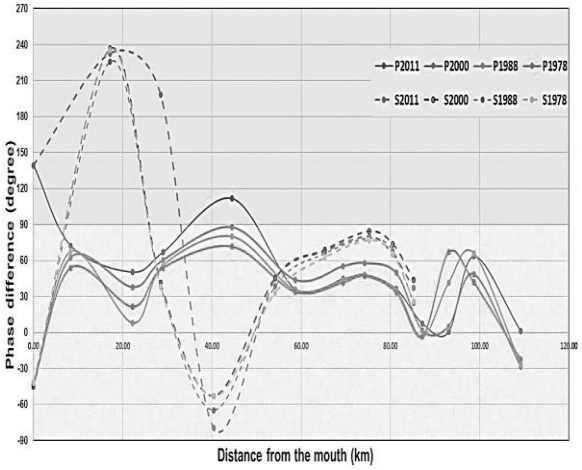

Fig. 8. Comparison of asymmetry of the horizontal tide between the Sibsa and the Pussur channel.

Tidal duration asymmetry:

Fig. 9 shows that the Sibsa channel shows more symmetrical behavior considering the tidal duration asymmetry.

In contrast, the Pussur has become more flood-dominant over time and is moving toward the landward direction. The central part of the Sibsa River (from 30 to 60 km) is symmetric or slightly ebb-dominant; afterward, it becomes flood-dominant. Whereas the Pussur behaves differently, it shows maximum flood dominant asymmetry in the central (around 60km). Afterward, it stayed at maximum flood dominance almost throughout the rest of the channel. From 0 to around 40km, Pussur behaves the same as Sibsa, becoming symmetric from the flood dominance asymmetry.

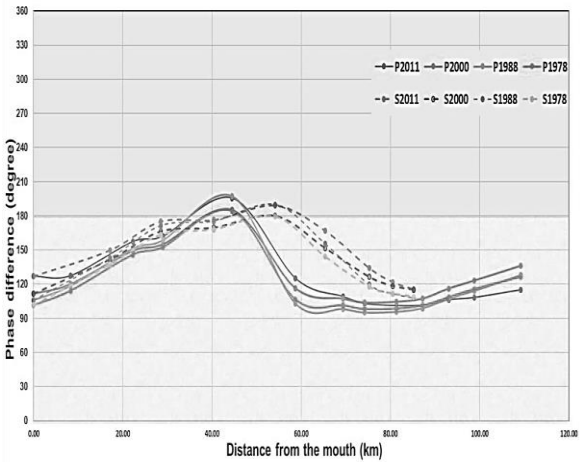

Fig. 9. Comparison of asymmetry of the vertical tide between the Sibsa and the Pussur channel.

Discussion

As stated in the introductory section, the GBM delta encounters a significant obstacle due to continuous sedimentation in the Sibsa-Pussur (SP) estuary system. This predicament is exacerbated by the sediment filling and decreased navigability of the adjacent peripheral rivers. Although human interventions may contribute, our emphasis is only on the dynamic relationship between tidal asymmetry and natural geomorphological processes.

Hoitink *et al*., (2017) suggest in their study that flood-dominant tidal asymmetry in tide-dominated deltas like the western GBM delta can lead to a dominance of inland sediment transport over river discharge and seaward sediment transport. This phenomenon essentially traps sediment within the estuary, causing aggradation (accumulation). Our findings also support this notion. The SP estuary exhibits characteristics of increasing flood dominance over time. The stronger flood currents compared to ebb currents precisely match the conditions described by Hoitink *et al.* (2017) for flood-dominant sediment transport and accumulation.

However, an exciting anomaly exists within the SP system. While the overall trend suggests flood dominance and sedimentation, a specific 20 km stretch of the Sibsa River exhibits ebb dominance (**Fig. 8**). This localized ebb dominance explains the observed erosion in this section, highlighting the erosive potential of ebb-dominant currents. The interplay between flood dominance and sedimentation creates a positive feedback loop within the SP estuary. Sedimentation alters the estuary's morphology, potentially further amplifying flood dominance. This, in turn, exacerbates the sedimentation problem, creating a self-perpetuating cycle. Understanding this feedback loop between tidal asymmetry and sedimentation is crucial for developing sustainable management strategies for the SP estuary. Numerical models and analyses of historical data can offer valuable insights into the historical evolution of tidal asymmetry and its link to morphological changes. This knowledge can then be used to devise strategies to mitigate sedimentation and ensure the long-term navigability of these vital waterways.

Future research should explore the combined effects of anthropogenic interventions and natural processes on tidal asymmetry within the SP estuary. Additionally, investigating the role of sediment grain size and channel bathymetry in influencing sediment transport dynamics can provide a more comprehensive understanding of this complex system.

Conclusion

A harmonic analysis method is applied to examine the spatiotemporal evolution of tidal asymmetry in the Sibsa-Pussur (SP) estuary of the GBM delta. The required data is generated using a hydrodynamic model (Delft-3D) for 1978, 1988, 2000, and 2011. The eight main tidal constituents (M2, M4, M6, K1, S2, O1, MS4, MSf) are considered for data analysis. The tidal duration asymmetry (as the tidal asymmetry of the vertical tide) and peak current asymmetry (as the tidal asymmetry of the horizontal tide) are determined here. The results quantify the tidal asymmetry based on the amplitude ratio and phase difference. The morphological effects are assessed based on the response of tidal asymmetry

to varying river discharge and downstream boundary conditions (changing WL), with the following main findings:

- Despite some anomalies in the peak current asymmetry, most parts of the Sibsa-Pussur system are flood-dominant. Tidal asymmetry changes are slightly symmetric, followed by maximum flood dominant asymmetry towards the delta's landward direction under the substantial effect of nonlinear interactions. The M2 and M4 amplitudes are more dominant among the other semidiurnal tides and overtides, respectively. Temporal variation in the tidal asymmetry is found very little, considering the hydrodynamical changes only.
- The Pussur channel is more flood-dominant than the Sibsa. The Sibsa channel shows more symmetrical behaviors, whereas the Pussur channel mostly shows maximum flood-dominant asymmetry. The influence of anthropogenic activities on the Pussur system is more significant than that on the Sibsa system.

Acknowledgment

This article is a rendition of the master's thesis authored by the corresponding author. The author expresses heartfelt gratitude to all the advisors involved in this project for their unwavering support and guidance throughout. Additionally, the authors sincerely thank Deltares for generously granting permission to utilize their model. Furthermore, the author acknowledges the constructive reviewer, which positively impacted the quality of this article.

References

Angamuthu, B., Darby, S. E. and Nicholls, R. J. (2018). Impacts of natural and human drivers on the multi-decadal morphological evolution of tidally-influenced deltas. *Proc. R. Soc. A.* 474(2219): 20180396. https://doi.org/10.1098/rspa.2018.0396

Bomer, E. J., Wilson, C. A. and Datta, D. K. (2019). An integrated approach for constraining depositional zones in a tide-influenced river: Insights from the Gorai River, Southwest Bangladesh. *Water*. 11(10): 2047. https://doi.org/10.3390/w11102047

BWDB. (2013). Final Report on Environmental Impact Assessment (EIA) CEIP-I. Bangladesh Water Development Board (BWDB). *(Issue January)*. https://www.bwdb.gov.bd/archive/pdf/284.pdf

Deltares. (2014). 3D/2D modeling suite for integral water solutions: Hydro-Morphodynamics. 710.

Dronkers, J. (1986). Tidal asymmetry and estuarine morphology. *Neth. J. Sea Res.* 20(2–3): 117–131.

Elahi, M. W. E., Jalón-Rojas, I., Wang, X. H. and Ritchie, E. A. (2020). Influence of seasonal river discharge on tidal propagation in the Ganges-Brahmaputra-Meghna Delta, Bangladesh. *J. Geophys. Res. Oceans.* 125(11): e2020JC016417.

Friedrichs, C. T. and Aubrey, D. G. (1988). Non-linear tidal distortion in shallow well-mixed estuaries: a synthesis. *Estuar. Coast Shelf Sci. 27(5)*: 521–545. https://doi.org/10.1016/0272-7714(88)90082-0

Godin, G. (1972). The analysis of tides. *Univ. of Toronto Press*. https://doi.org/10.1016/0025-3227(73)90070-4

Guo, S., Sun, J., Zhao, Q., Feng, Y., Huang, D. and Liu, S. (2016). Sinking rates of phytoplankton in the Changjiang (Yangtze River) estuary: A comparative study between Prorocentrum dentatum and Skeletonema dorhnii bloom. *J. Mar. Syst.* 154 (Part A): 5–14. https://doi.org/10.1016/j.jmarsys.2015.07.003

Hoitink, A. J. F., Wang, Z. B., Vermeulen, B., Huismans, Y. and Kästner, K. (2017). Tidal controls on river delta morphology. *Nat. Geosci.* 10(9): 637–645. https://doi.org/10.1038/ngeo3000

Islam, M. A. and Haider, M. Z. (2016). Performance assessment of Mongla seaport in Bangladesh. *Int. J. Transp. Eng. Tech.* 2(2): 15-21. https://doi.org/10.11648/j.ijtet.20160202.11

Jiang, A. W., Ranasinghe, R., Cowell, P. and Savioli, J. C. (2011). Tidal asymmetry of a shallow, well-mixed estuary and the implications on net sediment transport: A numerical modelling study. *Aust. J. Civ. Eng.* 9(1): 1–18.

Li, K., Liu, X., Zhao, X. and Guo, W. (2010). Effects of reclamation projects on marine ecological environment in Tianjin Harbor Industrial Zone. *Procedia Environ. Sci.* 2: 792–799. https://doi.org/10.1016/j.proenv.2010.10.090

McLachlan, R. L., Ogston, A. S., Asp, N. E., Fricke, A. T., Nittrouer, C. A. and Gomes, V. J. C. (2020). Impacts of tidal-channel connectivity on transport asymmetry and sediment exchange with mangrove forests. *Estuar. Coast Shelf Sci.* 233: 106524.

Pawlowicz, R., Beardsley, B. and Lentz, S. (2002). Classical tidal harmonic analysis including error estimates in MATLAB using TDE. *Comput. Geosci.* 28(8): 929–937. https://doi.org/10.1016/S0098-3004(02)00013-4

Rahman, M., Dustegir, M., Karim, R., Haque, A., Nicholls, R. J., Darby, S. E., Nakagawa, H., Hossain, M., Dunn, F. E. and Akter, M. (2018). Recent sediment flux to the Ganges-Brahmaputra-Meghna delta system. *Sci. Total Environ.* 643: 1054–1064.

Rahman, M. Z., Beg, M. N. A. and Khan, Z. H. (2014). Sediment budget of Meghna Estuary. *Tech. J. River Res. Inst.* 12(1): 106–118. https://doi.org/10.5281/ZENODO.3351639

Rahman, Md. M. and Rahaman, M. M. (2018). Impacts of Farakka barrage on hydrological flow of Ganges river and environment in Bangladesh. *Sustain. Water Resour. Manag.* 4(4): 767–780.

Rahman, M. M. and Ali, M. S. (2018). Potential causes of navigation problem in Pussur river and interventions for navigation enhancement. *4th Int. Conf. Civil Eng. Sust. Dev.* (ICCESD-2018).

Son, S. and Wang, M. (2009). Environmental responses to a land reclamation project in South Korea. *Eos*, 90(44): 398–399. https://doi.org/10.1029/2009EO440002

Speer, P. E. and Aubrey, D. G. (1985). A study of non-linear tidal propagation in shallow inlet/estuarine systems Part II: Theory. *Estuar. Coast Shelf Sci.* 21(2): 207–224. https://doi.org/10.1016/0272-7714(85)90097-6

Stark, J., Smolders, S., Meire, P. and Temmerman, S. (2017). Impact of intertidal area characteristics on estuarine tidal hydrodynamics: A modelling study for the Scheldt Estuary. *Estuar. Coast Shelf Sci.* 198: 138–155. https://doi.org/10.1016/j.ecss.2017.09.004

Yang, Z., Liang, Z., Ren, Y., Ji, D., Luan, H., Li, C., Cui, Y. and Lorke, A. (2023). Influence of asymmetric tidal mixing on sediment dynamics in a partially mixed estuary. *Acta Oceanologica Sinica*, 42(9): 1-15.

Wilson, C., Goodbred, S., Small, C., Gilligan, J., Sams, S., Mallick, B. and Hale, R. (2017). Widespread infilling of tidal channels and navigable waterways in the human-modified tidal delta plain of southwest Bangladesh. *Elem. Sci. Anth.* 5: 78. https://doi.org/10.1525/elementa.263

Technical Journal
River Research Institute ISSN: 1606-9277

A STUDY ON THE OPTIMIZATION OF DREDGING ALIGNMENT AND PERFORMANCE OF BANK PROTECTION WORKS ALONG TETULIA RIVER AT BAKERGANJ AND BAUPHAL UPAZILLAS

M. Shahabuddin[1*], A. K. M. Ashrafuzzaman[1], O. A. Maimun[1], B. Roy[1], M. A. H. Podder[1], M. Tofiquzzaman[1], M. K. Eusufzai[2] and P. Kanungoe[1]

Abstract

This paper presents the results for finalization of the proposed dredging alignment & its design and performance of the revetment for bank protection work in the Tetulia River at Bakerganj and Bauphal upazillas using scale modeling. The model is an overall distorted morphological model having horizontal scale 1:600 and vertical scale 1:80. The main purpose of this model is to provide decision support for determining of suitable and optimal dredging alignment and to investigate the efficacy of the proposed bank protection work to ensure a stable river course facilitating smooth navigation. The river reaches of about 50 km of Tetulia River and about 10 km of Karkhana River have been reproduced in this study. Different application test runs were conducted with different test scenarios (introducing revetment & dredged channel) using different discharges (ebb & flood) conditions. A 7 km revetment is proposed at the right bank of Tetulia River and 0.5 km at the left bank of Karkhana River. Model study shows it works well and is recommended. Dredged channel alignment is optimized along the left side channel of Char Durgapasha at a shallow depth. The longitudinal bed slope of the dredged channel is 4 cm km^{-1}. The bottom width of the dredged channel is considered as 120 m. Total volume of material to be dredged under this test condition is around 10,26,685 m^3. The recommended length of dredged channel is 2.534 km having bottom width 120 m, bottom level -9.0 mPWD, longitudinal bottom slope 4.0 cm km^{-1} and side slope 1:3. The volume of dredged material is 10,26,685 m^3 for dredged channel section of recommended dredging option. About 56% of the dredged volume, or approximately 574,944 m3, was used to fill up the dredged channel. To maintain the channel's usability, maintenance dredging once a year for two years is recommended.

Keywords: *Application, Bank Protection Work, Discharge, Dredging, Dumping, Maintenance, Offtake, Performance, Revetment, Scenarios.*

Introduction

At present the vast area from Dhulia Launch ghat area in Bauphal upazilla of Patuakhali district to Durgapasha area in Bakerganj upazilla of Barisal district are facing severe bank erosion. In fact, unabated right bank erosion at this river stretch has been taking place over the last four decades as can be seen from the available historical satellite images. In the seventies of the 20th century, the river at the erosion prone area used to be a single-channel river with a few small sized chars in the middle of the channel. However, with the passage of time these small sized chars grew in size causing changes in flow pattern and consequent braid-dominance with anabranches. A number of consequences have been visible including reduced flow depths, over-flow of banks and bank erosion. Such issues are constituted by sediment transport and deposition characteristics along the river bed (RRI, 2021). This study is done for the protection of area about 7.5 km from Dhulia Launch ghat area under Bauphal upazilla of Patuakhali district to Durgapasha area under Bakerganj upazilla of Barishal district from the erosion of Tetulia River with provision of dredging in the Tetulia River. It aims to divert the flow from the eroding bank to the center of the channel thus reducing bank erosion. It is very important to select a suitable dredging alignment that would be sustainable and would bring benefit in terms of reduction of near bank flow velocity. The overall objective of the physical model study is to fix suitable alignment of dredging of the Tetulia River at Dhulia-Durgapasha and determine suitable location for dredged material disposal and type, dimension and orientation of river training works for stabilizing the river bank (RRI, 2022b). The location map of the study area is shown in **Fig.1.**

Physical model is employed to investigate the performance of different options and strategies of dredging and dredged material disposal, sustainability of dredged channel and hydraulic and morphological impacts of dredging. As such, present initiative is taken in order to obtain necessary physical modeling support for effective and sustainable dredging of the Tetulia River at the project site where the river has been experiencing large right bank erosion. The model can be used as a decision support tool for fixation of dredging alignment and design of bank protection work.

Tetulia River is a channel in the Meghna Estuary region of Bangladesh where the constant process of erosion and deposition takes place due to the complex interactions between large river discharge and sediment load, tidal forces, waves, storm surges etc. In fact, interactions among these factors together with their seasonal occurrence, variation and dominance over one another shape the morphology of the Meghna estuary. The distribution of discharge, sediment and water level in the different channels of the Meghna estuary including the Tetulia River are governed by river discharge, the tide and the wind speed. Karkhana River, on the other hand, is a distributary of the Tetulia River. The flow and sediment distribution in the Karkhana River as a percentage of discharge and sediment load of the Telulia River is influenced by the hydraulic and morphological developments of the parent river at its off-take.

Due to unabated bank erosion in the study area many people have lost their homesteads and cultivable lands. Damaged properties include educational institutions, religious places, private and public infrastructures, communication systems etc. In fact, river erosion has changed the life pattern of many people of the study area. Losing livelihood many people were compelled to look for alternative sources of income. People are taking shelter in nearby rural areas, khashlands etc. losing homesteads and most of the affected people are being migrated to urban and sub-urban areas. Enough initiatives are not taken for the resettlement of the displaced people. Only small percentage of displaced population has been resettled in the char land. The char land of the Tetulia River is also

[1] Hydraulic Research Directorate, River Research Institute, Faridpur-7800, Bangladesh.
[*] Corresponding Author (E-mail: mshahabuddin@rri.gov.bd)
[2] Dhaka Laboratory, River Research Institute, Dhaka-1205, Bangladesh.

susceptible to erosion. Since most of the people in the study area are dependent on agriculture loss of homesteads and cultivable lands due to bank erosion takes a heavy toll on these people's livelihoods forcing internal migration.

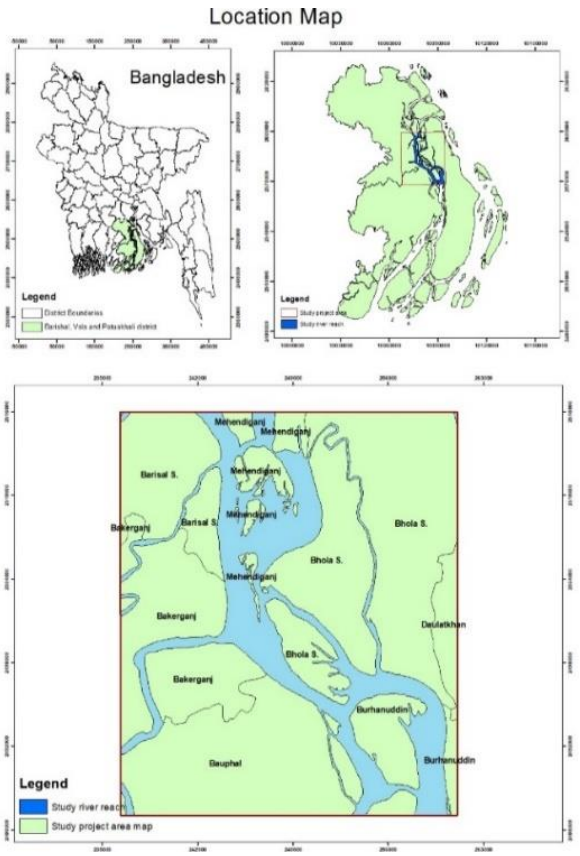

Fig.1. Location map of the study area.

The present bank erosion situation in the study area is visible from **Fig. 2**. At present there is no planned bank protection work in the erosion prone area of the Tetulia and Karkhana Rivers. Along the erosion prone stretch of the Tetulia River from Durgapasha to Dhulia only a small stretch of the bank has been stabilized by implementing hard material protection using cement concrete blocks in order to protect the Dighirpar Launch Terminal (**Fig. 3**). Geobag protection measure has also been implemented up to a certain extent beyond this hard material protection works both upstream and downstream (**Fig. 4**). Scattered and piecemeal geobag protection works are also noticeable elsewhere along the erosion prone bank (RRI, 2023).

Dredging has been proven as an effective process to control the deposited sediment to prevent flooding and make a pathway for the main channel flow (Gob *et al.*, 2005; *Zinger et al.*, 2011). The process also allows us to further solve engineering problems related to sedimentation and erosion in rivers, estuaries, and coastal seas (Van Rijn, 2005). A better prediction of erosion-sedimentation scenarios is inevitable to justify the long-term effectiveness of dredging, which could further promote the design strategies based on qualitative and quantitative analysis. Prediction of accurate scour depth and deposition of the braided river is methodologically very challenging because of the variation in simple path-length distribution resulting in over-scouring (Kasprak *et al.*, 2019).

Fig. 2. Present right bank erosion situation of the Tetulia River in the upstream of Dhulia Launch Ghat area.

Fig. 3. Existing hard material protection (CC block) works at Dighirpar Launch Terminal.

Fig. 4. Existing geobag protection works in the upstream of Dighirpar Launch Terminal.

The principal estuarine channels, proceeding from west to east are the Raymangal, Malancha, Bara Panga, Marjhata, Bangara, Haringhata or Baleswar, Ramnabad-Tetulia, Shahbazpur of Lower Meghna (Rob, 2012). Tetulia River originates from the Lower Meghna River at north of Bhola district. The river flows through Tetulia, Nimdi, Kalaiya and Purbamunia and ends up to the Bay of Bengal as the Buragouranga channel at Rangopaldi of Galachipa upazilla under Patuakhali district. It used to flow with a strong or rapid current. However, hydrodynamics of flow has been changed in recent years due to formation of many sand bars. The river separates Bhola island from the

main land. The Ramnabad Island is located at the west bank of the river. An offshoot of the Meghna River from Shahbajpur meets the Tetulia River. The total length of the river is about 84 km and the average width is 6 km (Chowdhury, 2012).

Methodology

An overall distorted morphological model was constructed which included a river stretch covering around 40 km of Tetulia River and also another river stretch covering around 10km of Karkhana River from its offtake with Tetulia River. The overall objective of the physical model study was to fix a suitable alignment for dredging of the Tetulia River at Dhulia-Durgapasha and determine a suitable location for dredged material disposal and the type, dimension, and orientation of river training works for stabilizing the river bank. The specific objectives of the overall distorted morphological model were to quantify the optimum dredging alignment and section of the dredged channel in the Tetulia River, the hydraulic performance of the dredged channel, to investigate the hydraulic and morphological effects of dredging, the impact on flow pattern, bank erosion phenomena, and other associated features, and to devise suitable types, placement, dimensions, and orientation of river training works to ensure a stable river course. The initial bathymetry of the model in prototype value is shown in **Fig. 5.**

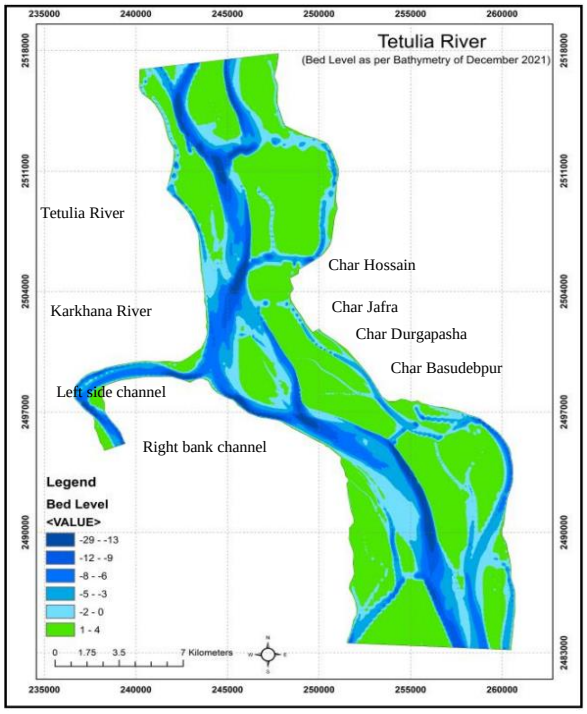

Fig. 5. Initial bathymetry of the model in prototype value.

The sustainability and effectiveness of any river dredging project depended on how intelligently it was planned and designed. Back-filling of the dredged channel was a natural tendency. However, it was important to quantify the best-suited alignment for maximizing the benefit and lengthening the sustainability of the initiative. Therefore, morphological physical modeling was a useful tool to be employed before dredging activities. This allowed observation of the overall morphological developments in response to dredging, leading to a more informed approach.

The effect of dredging on river morphology could be predicted by this model, and potentially effective dredging strategies could have been devised. It was showed that in some cases, dredged channel silted up with sediment within a single monsoon season. Therefore, successful and sustainable river dredging involved a number of issues that needed to be well-understood and addressed during the dredge planning and design phases (RRI, 2022a)

These issues involved various morphological changes, such as the formation of shoals, islands, and chars, the meandering tendency of the river, the effect of construction hydraulic structures, damages to the banks, the effect of afforestation/deforestation, and even tectonic occurrences. Prior to preparing a dredge plan and design, some of these issues could have been addressed through modeling. Additionally, post-dredge monitoring of these issues could have been supplemented by model studies, as required, to allow for timely corrective measures to maintain the river's morphology and check for local erosion damage. Suitable river training works would have also been necessary to ensure the long-term sustainability and cost-effectiveness of the protection efforts.

Physical modeling could have been used as an important tool to assist in developing an optimal dredge plan. Additionally, it could have been employed for post-dredge monitoring and the design of optimal bank protection works to combat riverbank erosion. This model would have allowed prediction of the dredging's effects on surrounding areas, both upstream and downstream, facilitating the development of effective dredging strategies.

The RRI open air model bed with dimensions of 100m × 80m had been used to reproduce the overall distorted morphological model. The model itself was a sand bed morphological model. It had been constructed based on selected geometric scales. Because it was a distorted model, vertical and horizontal scales of the model had been selected as 80 and 600 respectively for construction. The construction of the model involved a series of tasks. In addition to selecting the geometric scale ratios, the model bed had been prepared through several steps. These included uprooting the grass, dismantling any previous structures in the selected area, and disposing of any debris. The old sand from the model bed had been removed and replaced with new fine sand with the required median size. Additionally, the necessary model construction materials had been procured, and bathymetric and bank line data had been collected.

The model design adhered to established scale laws and conditions for river scale models. In this regard, recent development in the theories of the physical processes of the large alluvial rivers was considered during scaling and design of the models. The model was investigated on a mobile bed. The hydraulic similarity was established in the model to a distorted scale. The design ensured that the model fulfilled both flow and sediment transport criteria simultaneously. This meant the water velocity in the model exceeded the critical velocity required to initiate sediment movement. This design choice was made because, for velocities exceeding the critical point, the dimensions of any resulting scour (erosion) are primarily determined by the flow direction and the geometry of any structures present.

In this physical model, various types of instrument and facilities was needed such as, sharp-crested weir for measuring flow, point gauge for measuring water level, 3-D

current meter for measuring velocity, high resolution camera for taking video and photographic view of model, stopwatch for taking instant time and plastic-coloured balls (floats) for tracing flow path of flowing water. The discharge in the model was measured using sharp-crested weir at the inflow section using Rebock's formula. Model velocity was quantified by current meter.

Water slope was determined by analyzing water level measurements from various point gauges installed in the model. Flow lines of the stream were identified by dropping colored balls from a calibration section and observing their path to the end of the model. A stopwatch was used to calculate the surface velocity of the flow. Data from the physical model was then analyzed to interpret the test results. The initial bathymetry (December 2011) of the model was reproduced based on field survey data collected for this study. Calibration of the model was achieved using prototype water levels, flow velocities, and sediment transport data. Sediment feeding in the model was done artificially to maintain sediment balance. This process was conducted manually by observing the formation of bed forms. Continuous monitoring of the model bed was performed by taking soundings (depth measurements) (RRI, 2023).

The rate of sediment feeding for a particular model discharge was typically determined first using sediment transport formulas or relationships proposed by various researchers. In this specific model, the formula developed by Engelund and Hansen (1967) was initially used to establish the sediment feeding rate. However, this initial rate required calibration. Calibration involved taking measurements of bed levels along several cross-sections located at different points in the model at regular time intervals. The goal of calibration was to achieve a condition where the bed level remained relatively constant. This meant that the amount of sediment fed into the model should equal the amount transported out, achieving a state of sediment equilibrium.

Model Calibration

Model calibration is done in existing condition of the river to ensure that the model is able to reproduce the flow condition, morphological behavior and sediment transport in the field. The model is calibrated for single discharge (estimated) and verified with another single discharge (measured). The model layout is shown in **Fig. 6.**

Velocity distribution in the model at the sections where discharge has been measured in the field is compared with the field measurements at the same sections. In this regard, depth averaged flow velocities are measured in the model and compared with prototype measurements. Discharge distribution into the Karkhana River in the model and prototype as a percentage of the total discharge (upstream of the off-take) of the Tetulia River has also been compared.

The measurements during the calibration include water levels, bed levels, point velocities, float tracks and discharges. Calibration of water surface slope aims to achieve a dynamic equilibrium in water surface slope in the model. Calibration of discharge distribution aims to achieve a more or less constant discharge through the Karkhana River as a percentage of total discharge of the Tetulia upstream. At the end of the calibration test the discharge through the Karkhana River is found to be as about 25% of the Tetulia River. It is to be noted here that variable discharges in the Karkhana River have been measured at different times during the calibration test. This variation in the Karkhana discharge has been occurred with the developments in the Tetulia bed in response to the imposed conditions for sediment transport similar to that in the prototype.Calibration of sediment transport depends on the reliable field data of the same.

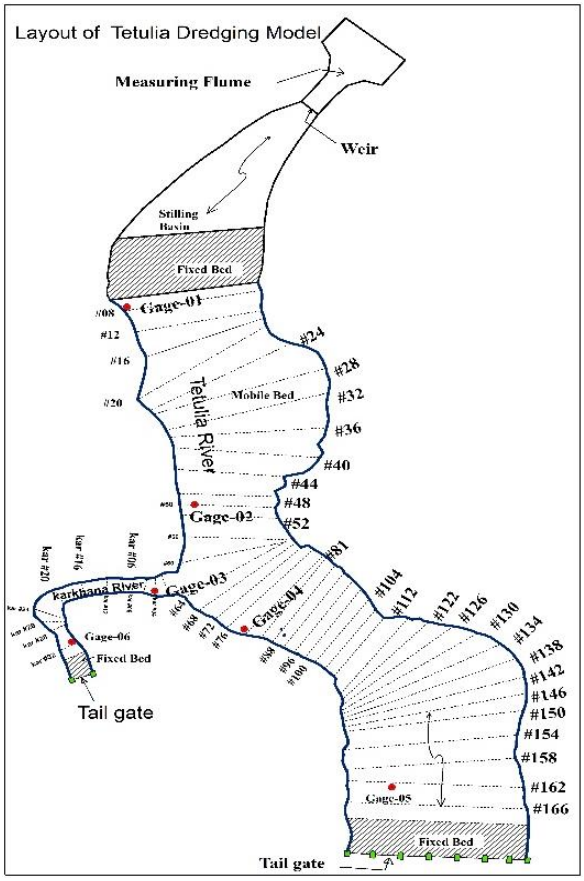

Fig. 6. Layout of the Model.

During calibration test sediment was fed manually at the inflow section of the model. Initially the rate of sediment feeding has been determined using Engelund and Hansen model. However, at the end of the test the calculated rate has been verified and it is found that equilibrium sediment transport rate in the model is 0.054 $m^3 h^{-1}$ for estimated channel forming discharge. It is to be noted here that some deviations around this value is caused by bed forms that migrate through the model. The sediment transport could not be compared as the sediment transport measurements in the prototype for the considered discharge is not available. Moreover, the sediment transport in the model is very difficult to compare with the prototype measurements as the model has some scale effects in reproduction of the magnitude and direction of sediment transport. The necessary measurements taken during the calibration test have been processed and analyzed. The scales of the different basic and derived parameters have been determined based on the calibration test results. **Table 1** presents the characteristics parameters of the dominating processes for the overall morphological model after calibration. It is to be noted here that scales of water depth and velocity vary at different locations of the model signifying the presence of scale effects. However, the range of variation is less. The scale factors presented in this table correspond to a representative section somewhat upstream of the Karkhana River off-take.

During the calibration test the model is allowed to adjust its water surface slope and bed slope. Water levels at six prefixed gauge stations have been recorded at certain time interval and plotted to see the development of water level slope with time. The water level slope is found to vary within 0.0010 - 0.0020 and the equilibrium water level slope is 0.0015. However, still water surface slope may vary from stretch to stretch and there is a control of daily tidal water level fluctuation on slope. Calibration of morphology requires historical bathymetric data, which is not available with RRI. Calibration of morphology has, therefore, been concentrated on achieving an equilibrium condition in the model bed configuration similar to the initial bathymetry of the model.

Table 1. Characteristic hydraulic and morphological parameters of the calibrated model (At upstream cross-section CS50 of the Tetulia River).

Basic and Derived Parameters	Prototype Data	Model Data	Scale Factor
Cross-sectional area (A) in m^2	20800	0.43	48372
Average depth (h) in m	7.30	0.089	82
Water Width (W) in m	2850	4.75	600
Slope (i)	0.000015	0.0015	0.01
Median diameter (D_{50}) in m	0.00008	0.000108	0.74
Relative density (Δ)	1.65000	1.6500	1
Shields parameter (θ)	0.83	0.75	1.11
Average Velocity (V) in m s^{-1}	0.93	0.19	4.9
Chezy (C) in $m^{1/2}$ s^{-1}	88	25	3.55
Froude number (Fr)	0.11	0.20	0.55
Discharge (Q) in m^3 s^{-1}	19200	0.82	235006
Friction velocity (U*) in m s^{-1}	0.0328	0.0362	0.91
Non-dimensional particle parameter (D*)	2.02	2.73	0.74
Critical Shields parameter for motion (θ_{crm})	0.094	0.077	1.22
Fall velocity (w_s) in m s^{-1}	0.00576	0.0105	0.549
Critical friction velocity (U^*_c) in m s^{-1}	0.0184	0.0209	0.8789
Critical Shields parameter for suspension (θ_{crs})	0.10884	0.0932	1.1684
Critical velocity for motion (U_{cm}) in m s^{-1}	0.33300	0.2136	1.5587415
Critical velocity for suspension (U_{crs}) in m s^{-1}	0.35828	0.2353	1.52295701
Critical depth (h_{cr}) in m	0.958	0.0111	86.55
Rouse parameter (w_s/kU*)	0.439	0.725	0.606
U*/w_s	5.695	3.45	1.65
Reynolds number (Re)	6789000	16910	401
Reynolds particle parameter (R*)	2.622	3.91	0.671
Reynolds critical particle parameter (R^*_c)	1.472	2.26	0.66
Sediment Transport, s (m^2 s^{-1})	0.00007	0.000003	23.33
Sediment Transport, S (m^3 s^{-1})	0.2	0.0000143	14000
1D celerity (m s^{-1})	0.00005	0.0002	0.28
1D time scale (days)	8932	4.6	1941
Aspect ratio	390.41	53.37	7.32
Flow adaptation length (λ_w) in m	2938.84	2.84	1036.6
f(θ)	0.266	1.04	0.256
Mode of oscillation	1.0	1.0	1.0
Adaptation length for sediment transport (λ_s) in m	30068	26.72	1125.18
Interaction parameter (I_P)	10.23	9.426	1.08

Application Tests

After calibration of the model, tests are carried out for different discharges in base and intervention conditions. Calibration of the model is considered as test T0. Besides 9 (nine) tests including base run have been anticipated. The discharge measurement in the river was carried out in the second week of September, 2021 when the Tetulia River was

in spate. There is no discharge gauge station anywhere on the Tetulia river to have the historical discharge record and carry out flood frequency analysis for determining probable discharges and compare the measured discharge with probable discharges. However, it appears from the information obtained through the available literature review that the measured discharge of the Tetulia River (25,513 m^3 s^{-1} in the upstream of the Karkhana River off-take) is a high discharge for the Tetulia River and is not one that may be termed as channel forming discharge. Therefore, based on available cross-section data and water surface slope a discharge of 19,200 m^3 s^{-1} has been estimated and is considered as channel forming discharge. Base run is considered for measured discharge as well as estimated channel forming discharge.

Six application tests (T2, T3, T4, T5, T7 & T9) have been conducted with six different alignments of the dredged channel both in the left and right-side channels of the Tetulia River. These two channels are divided by char land (Char Laxmipur and Char Durgapasha). Same design section has been considered for four alternative alignments of the dredged channel (T2, T3, T4 & T5) where the design bed level is considered to be -9.0mPWD at the start and -10.0mPWD at the end of the dredged channel, bottom width 150m (for test T5, bottom width 175m) with a side slope of 1:3.

Recommended Test

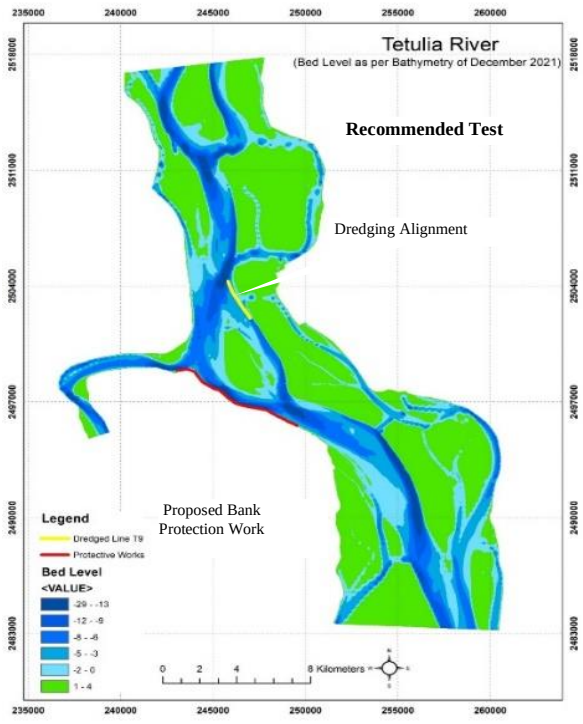

Fig. 7. The alignment of the proposed short dredged channel and bank protection work.

Test T9 is the recommended application test, which is conducted for dominant discharge of 19200 $m^3 s^{-1}$ as for other application tests. In this test the length of dredging is reduced to 2.534 km. Besides, the location and alignment of the dredged channel are also changed. The length of proposed bank protection works is kept the same (7.5 km). Out of 7.5 km, 7 km is for the protection of right bank of Tetulia River and 0.5 km is for the protection of left bank of Karkhana River from its offtake.

The alignment of the recommended dredged channel has been fixed along the left side channel of Char Durgapasha at a relatively shallow depth (**Fig. 7**). The bottom elevation of dredged channel at the starting point, middle point and end point is -8.946 mPWD, -9.000 mPWD and -9.047 mPWD respectively. The side slope of the dredged channel is 1:3. The longitudinal bed slope of the dredged channel is 4 $cm.km^{-1}$ as per suggestion by Field Engineer of BWDB. The bottom width of the dredged channel is considered as 120m. Total volume of material to be dredged under this test condition is around 10,26,685 m^3.

The bank protective works consists of geobag bags and CC blocks. The geobags are placed in the bottom layer of protective work and CC blocks in the top layer. The length of launching apron is 45 m. The volume of geobag dumping is 35 $m^3 m^{-1}$ and also the CC block dumping over geobag is 35 $m^3 m^{-1}$. Since the model is distorted the reproduction of CC blocks and geo bags in the model is qualitative to some extent.

Results and Discussion

The near right bank velocity along the erosion prone bank (Durgapasha-Dhulia-Mathbaria) stretch of the river) is measured and it is found that at the end of the test the velocity is found to vary from 0.33 m s^{-1} to 0.96 m s^{-1}. The flow velocity along the end of launching apron of protective works has been measured starting from the off-take mouth and is found to vary between 0.54 m s^{-1} and 1.59 m s^{-1}. The maximum velocity occurs at cross-section number CS 86 of the Tetulia River.

The measured model discharge at the end of the test indicates that about 22% of the total discharge of the Tetulia River in the upstream of the Karkhana River off-take finds its way into the Karkhana River. Of the remaining 78% of the total discharge about 61% passes through the right bank channel in the erosion prone area, 35% through the left side channel adjacent to the Char Durgapasha and 4% through the relatively smaller left bank channel.

Change in bed level with time within the dredged channel has been measured at some preselected sections. In the upstream part the dredged channel the rate of filling up is found to be higher compared to its downstream part. At the end of the test final bed level at some preselected points along the dredged channel have been recorded. The initial bed elevation at these points over the dredged bed is known. Based on initial and final bed level data the thickness of deposition at each point has been estimated. On the other hand, percentage of filling up dredged channel has been eatimated based on final bed level and initial bed level in pre dredged condition. The variation in the thickness of deposition along the dredged channel has been measured. It is noticeable that maximum thickness of deposition is 3.66 m. However, for the entire dredged channel the average thickness of deposition is estimated to be approximately 1.81 m.

Disposal or dumping of dredged material at a suitable location with minimal adverse environmental impacts is a very important issue to be addressed. For the proposed dredging in test T9 there is scope for dumping the dredged material on the charlands (Char Hossain and Char Jafra) situated on left side of the dredged channel. There are

vegetation (trees), sparse human settlements (guchhagram) and other infrastructures (cyclone center, road, etc.) on these charlands. The dredged material may be dumped on these charlands for raising land elevation and reclaiming land without causing any negative environmental impact or social conflict. Details of the dumping areas are given in **Table 2.** The scour/deposition around the end of the launching apron of proposed bank protection works is measured and the net maximum scour is found 8.40 m at cross-section number CS 72 in the Tetulia River. The bed level in the left side channel where the dredging is considered under test T9 has undergone change with time compared to the initial condition. The same happened in other locations too where the flow pattern is changed due to dredging. The bed level for the cross-sections situated within the proposed bank protection work under test T9 at the right bank of Tetulia River has undergone somewhat change with time compared to the initial condition.

Table 2. Details of the likely dumping areas of dredged material.

Areas where dredged material to be dumped				
Dumping areas	Length (m)	Width (m)	Height (m)	Approximate distance from CL of dredging alignment, m
1 (Char Hossain)	600	300	3	1200
2 (Char Jafra)	600	267	3	650

Conclusions

From Dhulia to Durgapasha, the near right bank velocity is high enough to cause bank erosion when tested with flood discharge condition. Bank erosion may continue at this area if appropriate bank protection measures are not taken immediately. Maximum velocity in the left side channel of Char Durgapasha remains below 1.5 m s^{-1} and the same in the left bank channel is found to be below 1.0 m s^{-1} under flood discharge. For dominant discharge the percentage of flow through the Karkhana River is 23%. Of the remaining 77% flow 68% passes through the right bank channel, 28% through the left side (of Char Durgapasha) channel and 4% through the left bank channel. Under different test conditions (with dredging and bank protection works) and for dominant discharge the percentage of flow through the left side channel (of Char Durgapasha) is increased by 2%, 9%, 12%, 11% and7% in tests T3, T4, T5, T7 and T9 respectively compared to base condition.

Sustainability of the dredged channel in the right bank channel is less due to relatively quick filling up of the upstream part of the dredged channel. Complex flow pattern in the immediate upstream of the off-take is responsible for such quick filling up of the dredged channel. Such complex flow pattern is caused by occurrence of flow separation near the off-take. Dredging in the left side channel of Char Durgapasha could be a relatively better solution although it may also involve substantial maintenance dredging. As a result of dredging in the left side channel the overall average bed level of this channel may decrease to some extent although a large percentage of the dredged channel (56% in test T9) may get filled up within a year.

For all test conditions with dredging noticeable flow velocity along the dredged channel occurs in the beginning. However, with the passage of time the dredged channel gets gradually silted up with a corresponding fall in the magnitude of flow velocity. The upstream portion of dredged channel gets silted up earlier than the downstream portion. The proposed bank protection works introduced at the right bank is found to work well as found from the model study. Special care should be taken at CS72 where bed level is -29.16mPWD, 138m away from right bank. In this case, geo-bags/CC blocks should be kept ready for emergency dumping. The protective structures (combination of CC blocks over geo-bags) are effective to protect the erosion prone area from Dhulia to Durgapasha.

recommended test for dredging alignment where length of the dredged channel is 2534 m. If the proposed dredging along the left side channel is intended it will ensure the stability of the bank protection work by reducing the flow through the right bank channel and thereby, reducing the near bank flow velocity. But the dredged channel is mostly found to be silted up. The model results indicate that the average percentage of filling up of the dredged channel is about 56% in one year. However, the cross-sectional area of the left side channel where dredging will be carried out is likely to be increased as a whole due to dredging.

Total volume of material to be dredged for recommended dredging alignment and dredged channel section is 10,26,685 m^3. The volume of filling up of the dredged channel is found about 5,74,944 m^3. For test T9 conditions the maximum thickness of deposition is 3.66m and the average thickness of deposition after one year is 1.81m. The maximum scour around the end of launching apron in test T9 is about 8.4 m at the end of test and it occurs at cross-section number 72 (CS72) about 2.53km downstream of the Karkhana off-take mouth along the Tetulia River. The suitable locations for dumping the dredged material are Char Hossain and Char Jafra situated on the left side of the dredged channel.

Recommendations

The bank protection work (7.0 km is for the protection of right bank of Tetulia River and 0.5 km is for the protection of left bank of Karkhana River from its offtake) proposed by BWDB tested in different tests work well and it is recommended to implement in the field. There should be provision for keeping adequate geo-bags/CC blocks ready for emergency dumping.

Bank protection work and dredging considered under test T9 are the recommended interventions to achieve the project objectives in terms of erosion protection as it provides better results from technical and economical point of view. The recommended length of dredged channel is 2.534 km in the left side channel having bottom width 120m, bottom level -9.0 mPWD, longitudinal bottom slope 4 cm km^{-1} and side slope 1:3. The position (Easting, Northing) of centreline of the recommended dredged channel is given in the report.

The implementation of the recommended bank protection works and dredging in the field may be carried out immediately for the protection of the erosion prone Dhulia-Durgapasha area and to prevent further bank erosion in the coming year. Substantial left bank erosion in the Karkhana River beyond the termination of the proposed bank protection

work has been observed during model tests. Based on the model results it is suggested to provide bank protection work on the left bank of the Karkhana River for a length of about 1.5km from its off-take.

Some right bank erosion in the Tetulia River beyond the termination of the proposed bank protection work has also been observed during model tests. Based on the model results it is suggested to provide bank protection work on the right bank of the Tetulia River for a length of about 1.0 km from its termination. The depth of suggested dredged channel may get reduced considerably after one year despite the fact that overall cross-sectional area of the left side channel where the dredging is suggested will be increased. In order to keep the dredged channel active maintenance dredging is suggested for two years with frequency of once in a year.

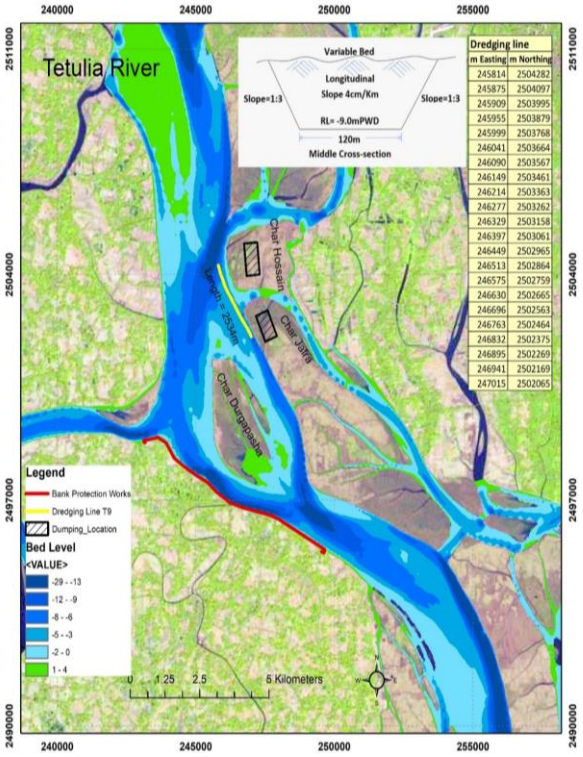

Fig. 8. Detailed layout of the recommended dredged channel section and bank protection work and potential suitable locations for dumping the dredged material.

Monitoring of the developments in the dredged channel is suggested for taking decision as to maintenance dredging. Cross-section survey along the dredged channel at some preselected locations before dredging, after dredging and during post monsoon period is needed for this purpose. Bank protection work alignment, dredging alignment, dredged channel section and dredged material dumping locations as shown in **Fig. 8** may be considered.

References

Chowdhury, M. H. (2012). Tentulia River, Banglapedia: National Encyclopedia of Bangladesh (Second ed.). Asiatic Society of Bangladesh.

Engelund, F. and Hansen, E. (1967). A Monograph on Sediment Transport in Alluvial Streams. *Teknish Forlag*, Copenhagen, 62 p.

Gob, F., Houbrechts, G., Hiver, J. and Petit, F. (2005). River Dredging, Channel Dynamics and Bedload Transport in an Incised Meandering River (the River Semois, Belgium). *River Res. Appl.* 21, 791-804. https://doi.org/10.1002/rra.883

Kasprak, A., Brasington, J., Hafen, K., Williams, R. D. and Wheaton, J. M. (2019). Modelling Braided River Morphodynamics Using a Particle Travel Length Framework. *Earth Surf. Dyn.* 7, 247-274. https://doi.org/10.5194/esurf-7-247-2019

Rob, M. A. (2012). Ganges-Padma River System. Banglapedia: National Encyclopedia of Bangladesh (Second ed.). Asiatic Society of Bangladesh.

RRI (2021). Physical Modeling Study for Dredging and Bank Protection Works along Tetulia River at Bakerganj and Bauphal Upazillas under Barishal and Patuakhali Districts, Inception Report, October 2021.

RRI (2022a), Annual Report of River Research Institute, July 2021- June 2022, River Research Institute, Ministry of Water Resources Government of the People's Republic of Bangladesh.

RRI (2022b). Physical Modeling Study for Dredging and Bank Protection Works along Tetulia River at Bakerganj and Bauphal Upazillas under Barishal and Patuakhali Districts, Revised Interim Report, May 2022.

RRI (2023). Physical Modeling Study for Dredging and Bank Protection Works along Tetulia River at Bakerganj and Bauphal Upazillas under Barishal and Patuakhali Districts, Final Report, February 2023.

Van Rijn, L. C. (2005). Principles of Sedimentation and Erosion Engineering in Rivers, Estuaries and Coastal Seas Including Mathematical Modelling Package (Toolkit on CD-ROM). Aqua Publications.

Technical Journal
River Research Institute ISSN: 1606-9277

SLOPE STABILITY ANALYSIS OF THE LEFT BANK OF ARIAL KHAN RIVER OF BANGLADESH

U. Saha[1*], M. Moniruzzaman[1,2], N. C. Ghosh[3,4], B. Roy[5], S. Ferdhous[1], M. E. A. Mondal[6], M. K. Eusufzai[3], K. R. Karim[1] and S. M. A. Horayra[7]

Abstract

Slope instability is one of the major problems in geotechnical engineering where loss of life and property are in hazardous situation. Therefore, it is essential to check the stability of slope. Such an important earthen structure is river bank slope. Here an attempt has been made to analyze the slope stability of the left bank of Arial Khan River at Khas Char Bachamara. Slope stability has been analyzed through geotechnical investigation with parameters cohesion, angle of internal friction, unit weight, slope angle and slope height etc. Geo05 software has been used for slope stability analysis. For slope stability analysis the two methods such as Bishop simplified and Janbu methods have been used for finding safety factor. Here safety factor of Bishop simplified has been considered as it gives low value of safety factor. Accordingly, from the slope stability analysis it has been observed that left bank of Arial Khan River at Khas Char Bachamara is stable at the coordinates (204966.442E & 2589225.303N) and (204765.552E & 2589425.425N) however, at the coordinate (204864.521E & 2589699.255N) the bank is not stable of the study area according to safety factor 1.50 of slip circle. Safety factor less than 1.50 recognize the river bank is unstable and a design engineer may reconstruct with reinforcement through injecting cement.

Keywords: *Arial Khan River, Geotechnical Investigation, Left bank, Slope stability.*

Introduction

Bangladesh is a broad deltaic plain and it has complex river system. The plain is largely formed by the Ganges, the Brahmaputra and the Meghna. Different rivers bring sediments from areas of different geology. There is active bank erosion almost in all major rivers in the country. The failure of riverbank is a common problem in Bangladesh. Erosion expedites the river bank failure occurring among many of the river bank failure criteria. Riverbank erosion occurs both for hydraulic and geotechnical instability. River bank slope instability is one of the major issues in geotechnical engineering. Therefore, it is utmost important to check the stability of slope of the river bank.

Seepage induced slope instability is a complex phenomenon which has not been quantified and not even fully understood as a wide range of factors affect a slope's ability to resist seepage induced instability (Terzaghi and Peck, 1948) They concluded that this work provides a possible solution to describe seepage-induced slope instability utilizing critical state soil mechanics. They also concluded that further work will be required to determine stability for natural slopes. Watson *et al.* (2006) studied on stream bank erosion with a review of processes of bank failure, measurement and assessment techniques and modelling approaches. They stated that stream bank erosion depends mainly on flow pattern, bank material composition, bank geometry, channel geometry, bank soil-moisture conditions, vegetation, and man-induced factors. Inamul (2010) explains that the river bank can collapse depends on a number of factors predominating the geotechnical characteristics. He also expressed that river bank failure can be caused when the gravitational forces acting on a bank exceed the forces hold the sediment together.

Failure depends on sediment type, layering and moisture content. Fatema and Ansary (2014) studied on an embankment at Basuria in Sirajganj near the bank of Jamuna River. They observed that grain size of the soil contains 63% sand, 35% silt and 2% clay. They found the maximum safety factor 2.255 for soil at dry condition with a slope 1:2 while the minimum factor is 0.66 at rapid drawdown condition with 1:1 slope. Islam *et al.* (2014) worked on dry and wet in-situ soil sample in the laboratory for showing the major cause of bank erosion. They found that the soil samples are silty clay with friction angles of 40° and 24° at dry and wet condition respectively. The factor of safety (FS) is similar and are more than 1 at dry condition while it is ~0.7 at wet condition. Harabinova and Panulinova (2019) studied on the influence of change in shear strength parameters on the factor of safety. They observed that the factor of safety of the slope changes with varying cohesion c and internal friction angle ϕ. They recommended that the factor of safety can be correctly obtained only if the critical failure surface of the slope is accurately identified, and shear strength parameters are correctly measured.

Islam *et al.* (2023) studied on the riverbank erosion of the Surma River due to slope failure using both liquid equilibrium and finite element method and showed that the river banks are eroding mainly due to slope failure in the wet condition. The factor of safety (FS) and shear reduction factor (SRF) values are similar and are more than 1 at dry condition while it is ~0.7 at wet condition. They recommend that the steep slope of the Surma River should training with support like cement concrete (CC) block. Aryanti *et al.* (2018) studied on slope stability analysis in Lusi River, Kedungrejo through characteristics of soil mass using limit equilibrium method with comparing Bishop, Janbu and Spencer method using Slide 6.0 Program. They found that study area is composed of clay with the firm to stiff structure. They analyzed the result of slope stability using Bishop simplified method and obtained the factor of safety is 1.680 and 1.14 based on Slide 6.0 program, the smallest factor of safety 1.130 is obtained using Janbu simplified method (Slide 6.0 Program Software). They classified the slope stability is unstable in condition according to the Terzaghi and Peck

[1] Geotechnical Research Directorate, River Research Institute, Faridpur-7800, Bangladesh.
[*] Corresponding Author (E-mail: umasaharri@gmail.com)
[2] Institute of Water and Flood Management, Bangladesh University of Engineering and Technology, Dhaka-1000, Bangladesh.
[3] Dhaka Laboratory, River Research Institute, Dhaka-1205, Bangladesh.
[4] Department of Physics, Bangladesh University of Engineering and Technology, Dhaka-1000, Bangladesh.
[5] Hydraulic Research Directorate, River Research Institute, Faridpur-7800, Bangladesh.
[6] Administration and Finance Directorate, River Research Institute, Faridpur-7800, Bangladesh.
[7] Office of the Director General, River Research Institute, Faridpur-7800, Bangladesh.

(1976) factor of safety criteria. They conclude that reinforcement is required for improving the slope stability. Oo *et al.* (2013) studied on numerical analysis of river bank slope stability during rapid drawdown of water level. The results of computation showed that rapid drawdown of river water level most easily leads to the slipping of the slope of the river bank and the stability of the slope of the river bank gradually increases with the dissipation of the excess pore-water pressure. The contribution of the matrix suction to shearing strength increases with the enlargement of unsaturated soil region, which has remarkable action on raising the stability of the slope of the river bank. They concluded that the monitoring of the river bank soil body should be intensified during rapid drawdown of river water level so as to avoid the occurrence of slipping of the slope of the river bank.

Tseng (1975) conducted a review study of river bank stability and slope movements in the Winnipeg area of Manitoba in Canada. In this study, residual strength parameters were used in effective stress analysis, using the simplified Bishop's Method of Slices for a circular slip surface and a modified rigorous Janbu solution for a non-circular failure surface. It has been observed that factor of safety has been improved and safety factors for the given pore water pressure conditions were more reasonable. It has also been observed that the rate of slope movement varied according to the groundwater conditions and reflected the state of riverbank stability.

Fig. 1. Bank of Arial Khan River.

Arial Khan Riveris one of the biggest distributaries on the right bank of the Padma River at Sadarpurthana in Faridpur district and Shibcharthana in Madaripur district. The river maintains a meander channel through its course and is erosion in nature and very difficult to identify its left and right bank (Ashrafuzzaman *et al*., 2020). The river bank is somewhere very steep and somewhere is plain to flood plain. The bank scenario of Arial Khan River has been shown in **Fig. 1**.

A number of settlements have already been destroyed due to severe river bank erosion and the process is ongoing. Therefore, bank protection is one of the prime necessities for poverty alleviation and national growth. Before that stability analysis is an utmost important work for the bank protection. Over the last few decades, many numbers of river bank are protected through many engineering ways. In this regard, it is often noticed that conventional designs are adapted to protecting the river bank. Such protecting works are failed before the return period. As a results, the government is compelled to fund a significantly larger amount than the actual budget. So, it needs appropriate measure through proper investigation and engineering implication. Here an attempt has been made to analyze the slope stability of the left bank of Arial Khan River at Khas Char Bachamara of Shibcharthana of Madaripur district of Bangladesh through geotechnical investigation.

The objective of this study is to analyze the stability of the slope of the left bank of Arial Khan River located at Khas Char Bachamara of Shibchar thana through geotechnical investigation.

Methodology

The data have been collected from River Research Institute (RRI) report (2023). The study area is located at Khas Char Bachamara of Shibcharthana of Madaripur district. The coordinate of the boreholes are at #BH-1 (204966.442E & 2589225.303N), #BH-2 (204765.552E & 2589425.425N), #BH-3 (204864.521E & 2589699.255N) at the left bank of Arial Khan River from where soil samples have been collected. The study area has been shown in the river map in **Fig. 2**.

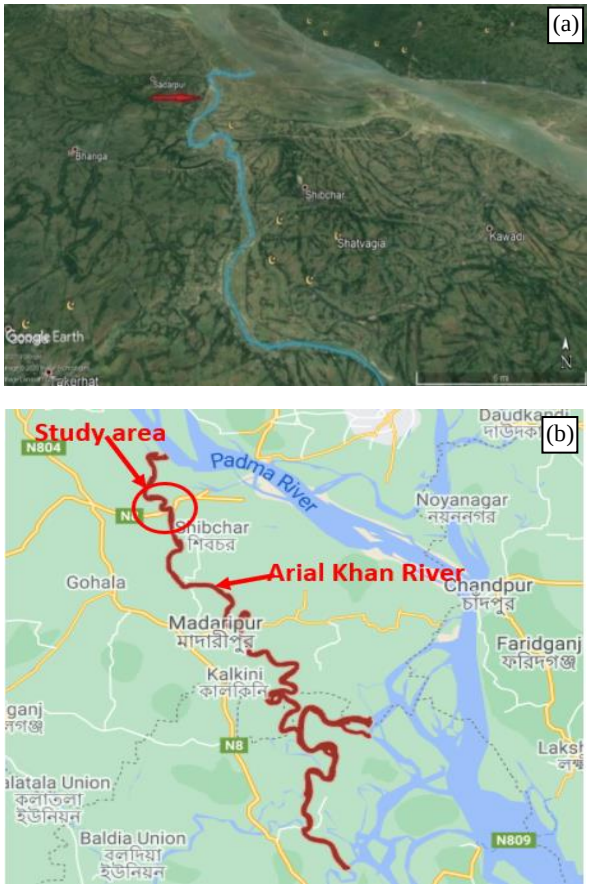

Fig. 2. (a) Image map of Arial Khan River (Source: Google Earth) and (b) Study area.

Field and laboratory investigation have been conducted for geotechnical investigation. Field investigation includes standard penetration resistance for test SPT-N values, soil strata depth wise, ground level, ground and surface water level etc. For slope stability analysis the soil parameters such as unit weight, cohesion, angle of internal friction are usually used. These parameters have been collected from direct shear

test and which have been tested in the soil mechanics division of RRI. Field parameters such as slope angle slope height, ground water level etc. have been collected from the study area. In this study, Bishop's Simplified Method has been used for slope stability analysis compare it with and Janbu method. Numerical Geo05 Software has been used for slope stability analysis. In the Bishop method the safety factor is defined 1.50 for circular slip surface according to Terzaghi and Peck (1948).

Direct Shear Measurement

The test is carried out on remolded samples prepared by three layers of soils by tamping according to soil density index in the laboratory of soil mechanics division of geotechnical research directorate of RRI using direct shear apparatus. The specimen was prepared for the direct shear test within the direct shear mold. A normal load was applied to the specimen sample and the specimen was shared across the pre-determined horizontal plane between the two halves of the shear box. This procedure was repeated for three remolded samples. Measurements of shear load, shear displacement and normal displacement were recorded. From the results, internal angle of friction and cohesive strength were measured using Coulomb's shear strength equation.

$$\tau_f = c + \sigma_f \tan \emptyset \qquad \text{Eq. (1)}$$

Where τ_f= shearing resistance of soil at failure, c =apparent cohesion of soil, σ_f = total normal stress on failure plane, ϕ = angle of shearing resistance of soil (angle of internal friction). The values of these parameters such as cohesion, angle of internal friction and unit weight were used to determine factor of safety.

Limit Equilibrium Method

The conventional limit equilibrium methods for investigating the equilibrium of soil mass tending to slide down under the influence of gravity are used. Transitional or rotational movement is considered on assumed or known potential slip surface below soil or rock mass. All methods are based on comparison of forces (moments or stresses) resisting instability of the mass and those that causing instability (disturbing forces). Limit equilibrium methods are still currently mostly used for slope stability analysis. These methods consist in cutting the slope into fine slices so that their base can be compared with a straight line, then to write the equilibrium equations (the equilibrium of the forces and/or moments). According to the assumptions made in the efforts between the slices and the equilibrium equations considered. The Bishop's simplified method is also applicable to non-homogeneous slopes and cohesive soils where slip surface can be approximated by a circle. It is more accurate than the Ordinary Method of slices, especially for analyses with high pore water pressures. Moreover, the Junbo generalized procedure is applicable to non-circular slip surface. Here it is mentioned that Bishop's simplified method and Janbu's simplified method are in limit equilibrium method.

Bishop's simplified method

Arora (2010) explained that a simplified method of analysis gave Bishop (1955) which considers the forces on the slides of each slice. Bishop's simplified method is a primary slope stability method where the inter slice shear forces are neglected and regardless of whether the slip surface is circular or composite that is based on the equation. The requirement of equilibrium is applied to each slice. The factor of safety of the assumed failure surface determined by the equation.

$$F_s = \frac{\Sigma \frac{1}{m\alpha}[c'b+(W-ub)\tan\emptyset']}{W\sin\alpha} \qquad \text{Eq. (2)}$$

Where, $m_\alpha = (1+\tan \text{ø'} \tan \alpha/F_s) \cos\alpha$, b is the width of the slice c' and ϕ' is the shear strength parameters for the center of the base of the slice, W is the weight of the slice, is the inclination of the bottom of the slice, u is the pore water pressure at the center of the base of the slice.

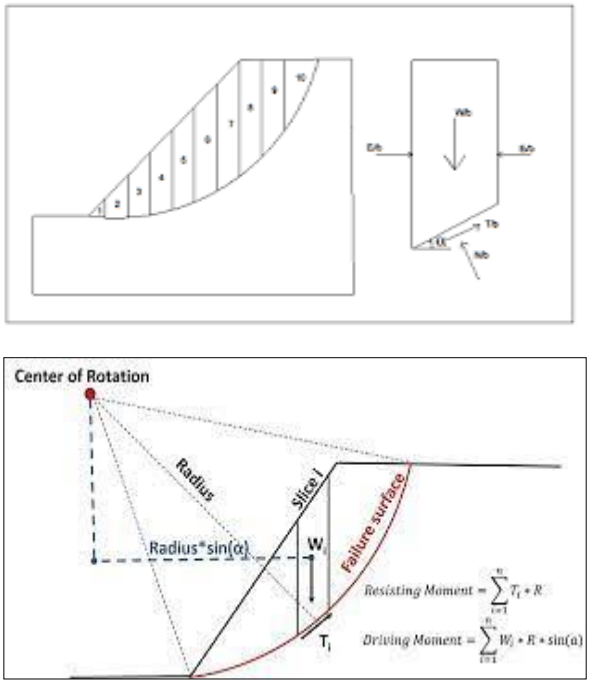

Fig. 3. a) Ordinary method of slices b) Slope stability-The Bishop Method of Slices (Source: Salunkhe, *et. al.*, 2017).

Janbu's Simplified Method

The Janbu's simplified (1956) method is similar to the Bishop's simplified method except that the Janbu's simplified method satisfies only overall horizontal force equilibrium but not overall moment equilibrium. The Janbu's simplified factor of safety is too low, even though the slices are in force equilibrium. Since force equilibrium is sensitive to the assumed inter slice shear, as in the Junbu's simplified method, makes the resulting factor of safety too low for circular slip surfaces.

$$F = c'\mathrm{l} + \mathrm{P} - \mathrm{ul}\tan\phi'\cos\alpha P\sin\alpha \pm A \qquad \text{Eq. (3)}$$

Where, c' is effective cohesion intercept, ϕ' is effective angle of internal friction, l is the length of the failure surface at the base of each slice, P is the total normal force on the base of the slice, A is the resultant external water forces, α is the angle between the tangent to the center of the base of each slice and the horizontal.

The assumptions made by Janbu's method are that the inter slice forces acting on a single slice.

where, W = the weight of the soil above the failure surface, Xi-1, Xi+1, Vi-1, Vi+1= the inter slice reactions from the adjacent slices, N′=normal effective force, T= Shear component force, U= the boundary water force.

Janbu's method suggests that the normal interslice forces are equal and can be neglected.

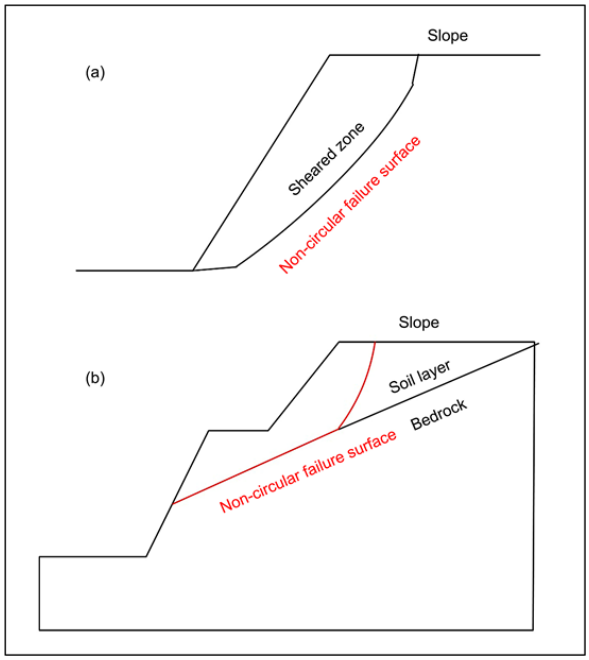

Fig. 4. (a) Failure surface that passes through a sheared zone, and *(b)* a failure surface that begins as circular but is then interrupted by a stronger geological formation (bedrock).

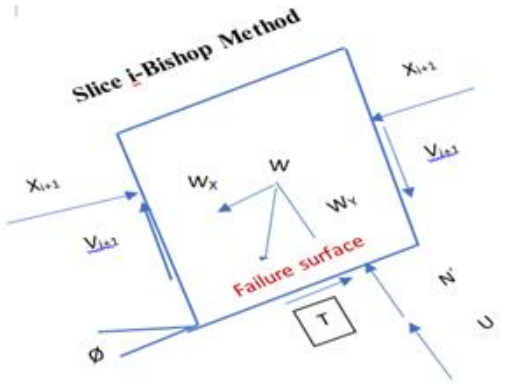

Fig. 5. Showing inter-slice forces acting on a single slice at Janbu method (Salunkhe *et.al.*, 2017).

Results and Discussions

Field and laboratory investigation results of soil density, particle sizes, specific gravity, cohesion, angle of internal friction, etc. have been presented in the tabular form in **Table 1** and the stability analysis results have been shown in **Table 2**.

Table 1. Showing the test results of cohesive and non-cohesive soils of different boring holes of Khas Char Bachamara of Shibcharthana of Madaripur district.

Name of the parameters	Khas Char Bachamara	
	Cohesive Soil	Non-cohesive Soil
Soil Density	Very soft to stiff	very loose to dense
Sand in %	1-48	42-92
Silt in %	52-91	8-55
Clay in %	3-35	0-3
Specific Gravity, Gs	2.678-2.682	2.670-2.671
Unit Weight in kNm^{-3}	18.22-18.44	17.58-18.22
Plasticity in %	25-26	-
Cohesion, c in kNm^{-2}	22-30	0-3
Angle of internal friction, ø in degree	2-20	24-32
Permeability in cm s^{-1}	10^{-6}-10^{-4}	10^{-4}-10^{-2}
Compression index, Cc	0.168-0.336	-
Colour	Light brown to grey	
Height of the slope in m	3-6	
Slope angle in degree	22-85	

Table 2. Slope Stability Analysis of the different coordinates of the left bank of Arial Khan River.

Location	Easting	Northing	Factor of Safety by Bishop Method	Factor of Safety by Janbu Method
Khas Char Bachamara	204966.442	2589225.303	3.10	4.67
	204765.552	2589425.425	7.42	7.79
	204864.521	2589699.255	1.37	1.90

Slope Stability Analysis by Bishop Method

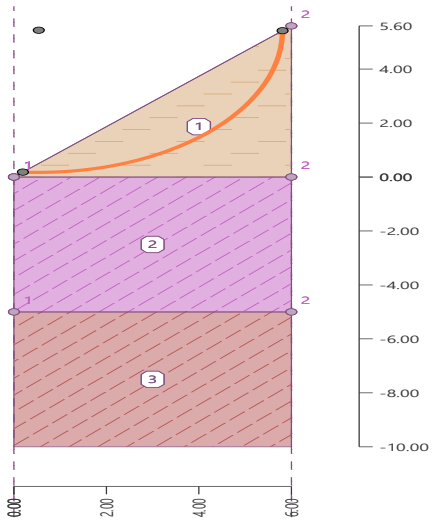

Slope stability Analysis (Bishop Method)

Sum of active forces, F_a = 72.00 kN.m^{-1}

Sum of passive forces, F_p = 222.86 kN.m^{-1}

Sliding moment, M_a = 379.44 kNm.m^{-1}

Resisting moment, M_p = 1174.48 kNm.m^{-1}

Factor of safety = 3.10 > 1.50

Slope stability ACCEPTABLE

Fig. 6. Slope Stability Analysis at the coordinate (204966.442E &2589225.303N).

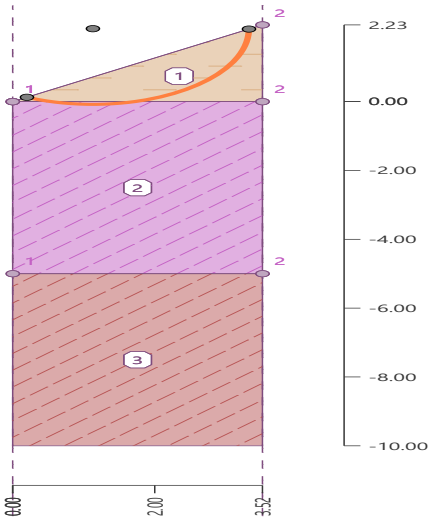

Slope stability Analysis (Bishop Method)

Sum of active forces, F_a = 15.11 kN.m^{-1}

Sum of passive forces, F_p = 112.11 kN.m^{-1}

Sliding moment, M_a = 33.25 kNm.m^{-1}

Resisting moment, M_p = 246.64 kNm.m^{-1}

Factor of safety = 7.42 > 1.50

Slope stability ACCEPTABLE

Fig. 7. Slope Stability Analysis at the coordinate (204765.552E & 2589425.425N).

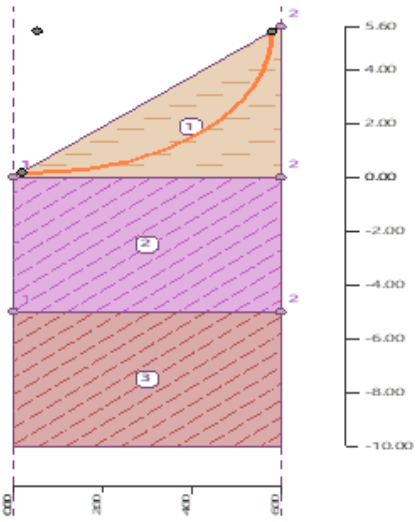

Slope stability Analysis (Bishop Method)

Sum of active forces, F_a = 38.45 kN.m^{-1}

Sum of passive forces, F_p = 52.85 kN.m^{-1}

Sliding moment, M_a = 145.71 kNm.m^{-1}

Resisting moment, M_p = 200.30 kNm.m^{-1}

Factor of safety = 1.37 < 1.50

Slope stability NOT ACCEPTABL

Fig. 8. Slope Stability Analysis at the coordinate (204864.521E &2589699.255N).

Slope Stability Analysis by Janbu Method

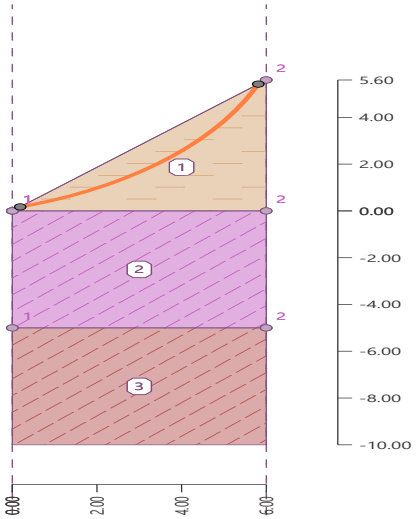

Slope stability analysis Janbu Method

Factor of safety = 4.67 > 1.50

Slope stability ACCEPTABLE

Fig. 9. Slope Stability Analysis at the coordinate (204966.442E & 2589225.303N).

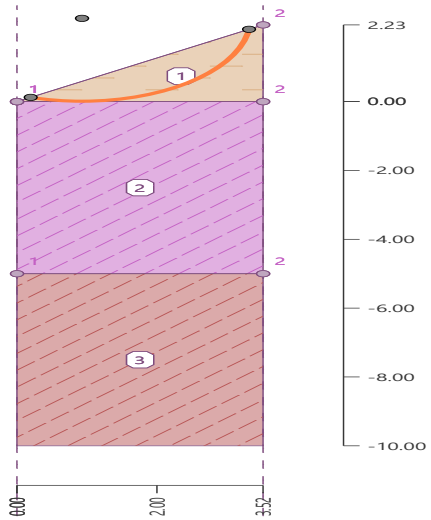

Slope stability analysis Janbu Method

Factor of safety = 7.79 > 1.50

Slope stability ACCEPTABLE

Fig. 10. Slope Stability Analysis at the coordinate (204765.552E & 2589425.425N).

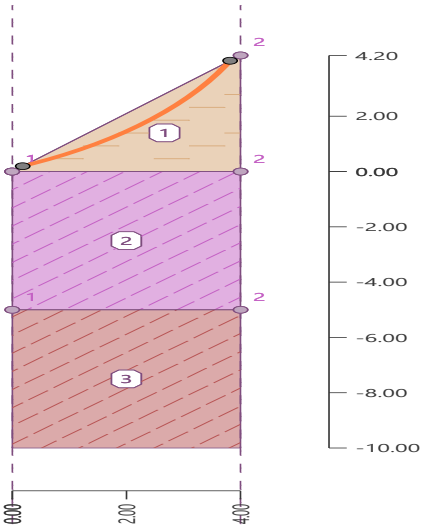

Slope stability analysis Janbu Method

Factor of safety = 1.90 > 1.50

Slope stability ACCEPTABLE

Fig. 11. Slope Stability Analysis at the coordinate (204864.521E &2589699.255N).

Aryanti *et al.* (2018) studied on slope stability analysis in Lusi River, Kedungrejo and mentioned the ranges of minimum total factors of safety defined by Terzaghi and Peck (1976) and the Canadian Geotechnical Society (1992) in the tabular form in **Table 3**.

Table 3. Showing the value of minimum total safety factors.

Failure Type	Category	Safety Factor
Shearing	Earthworks	1.3-1.5
	Earth retaining structures, excavations	1.5-2.0
	Foundations	2.0-3.0

Garg (2009) expressed that the overall factor of safety should be 1.50 for stability of the foundation against shear. Arora (2010) stated that the factor of safety determined by Bishop's simplified method is on the safe side as its error is generally less than 2% and not more than 7% even in extreme case.

From the slope stability analysis of Bishop Method, it has been observed that left bank of Arial Khan river at Khas Char Bachamara is stable at the coordinates (204966.442E & 2589225.303N) and (204765.552E & 2589425.425N) as their safety factors are 3.10 & 7.42 whereas the safety factor of the coordinate (204864.521E & 2589699.255N) is 1.37 which is unstable. Because the stable safety factor less than 1.50 of slip circle of slope stability analysis considered unstable according to Terzaghi & Peck (1976), Canadian Geotechnical Society (1992) and Garg (2009). On the other hand, the slope stability analysis of Janbu Method provides the left bank of Arial Khan River at Khas Char Bachamara is stable at all the three coordinates as their safety factors are 4.67, 7.79& 1.90. In comparison of Bishop and Janbu method it is observed that the three coordinates are stable according to Janbu method. However, the bank is stable at the two coordinates which are mentioned according to the analysis of Bishop method as there are less error in this method (Arora, 2010). Consequently, the coordinate (204864.521E & 2589699.255N) of the bank of Arial Khan River may be reconstructed.

Conclusion

From the slope stability analysis, it has been observed that left bank of Arial Khan River at Khas Char Bachamara is stable at the coordinates (204966.442E & 2589225.303N) and (204765.552E & 2589425.425N). However, at the coordinate (204864.521E & 2589699.255N) of the study area is not stable according to stable safety factor 1.50 of slip circle of slope stability analysis. Therefore, it is recommended that the coordinate (204864.521E & 2589699.255N) of the study area is unstable and a design engineer may reconstruct with reinforcement through injecting cement which can enhance the stability of the riverbank of Arial Khan River.

Acknowledgement

The authors are gratefully acknowledging the Ministry of Water Resources and GoB for financial assistance to conduct the study RRI (2023) of Arial Khan River of Bangladesh.

References

Arora, K. R. (2010). *Soil Mechanics and Foundation Engineering*. Reprint Edition, Standard Publishers Distributors, Delhi-110006, p-463,465,466.

Aryanti, D. E., Eveny, O. N., Tulus. A. and Saptono, S. (2018). Slope Stability Analysis in Lusi River, Kedungrejo Using Limit Equilibrium Method. *IOP Conf. Ser.: Earth Environ. Sci.*, Volume 212, International Conference on Earth Science, Mineral, and Energy 11–12 October 2018, Yogyakarta, Indonesia Citation.

Ashrafuzzaman, A. K. M., Das, S. K., Ghosh, S. K., Eusufzai, M. K., Rahman, M. N., Mondal, E. A. (2020). A Case Study on Performance of Concrete Block Mat for River Bank Protection using Scale Modeling. *Tech. J. River Res. Inst.* 15(1): 38-47.

Fatema, N and Ansary, M. A. (2014). Slope Stability Analysis of a Jamuna River Embankment. *J. Civ. Eng.* (IEB), 42 (1):119-136.

Garg, S.K. (2009). *Soil Mechanics and Foundation Engineering*. Khanna Publishers, Delhi-110006. p-437.

Harabinova, S. and Panulinova, E. (2019). Impact of Shear Strength Parameters on Slope Stability. *MATEC Web of Conferences*, 310, 00040, (2020). 4th International Scientific Conference Structural and Physical Aspects of Construction Engineering (SPACE 2019). https://doi.org/10.1051/matecconf/202031000040

Inamul, M.H. (2010). Water Resources Management in Bangladesh. Anushilon, Chuadanga.

Islam, M. S. and Hoque, F. (2014). River Bank Erosion of the Surma River due to Slope Failure. *International Journal of Research and Innovations in Earth Science*, 1(2): 2394-1375.

Oo, H. Z., Ai, L. Z. and Qiu, Z. (2013). Numerical analysis of river bank slope stability during rapid drawdown of water level. *SCEA*, 2(4): 98-103.

Padma River, Banglapedia, National Encyclopedia of Bangladesh.

RRI (2023). Characterization of Soils around the Arial Khan River of Bangladesh. River Research Institute, Bangladesh.

Salunkhe, D. P., Bartakke, R. N., Chvan, G. and Kothavale, P. R. (2017). An overview on Methods for slope stability analysis. *Int. J. Eng. Res. Tech.* 6(3): 528-535.

Terzaghi and Peck (1948). Soil Mechanics in Engineering Practice. John Wiley & Sons, Inc. & CHAPMAN & HALL, Ltd.

Tseng, Ling-Wai. (1975). A review study of river bank stability and slope movements in the Winnipeg area. http://hdl.handle.net/1993/3486.

Watson, A. J. and Basher, L. R. Landcare. (2006). Stream bank erosion: a review of processes of bank failure, measurement and assessment techniques, and modeling approaches. Motueka Integrated Catchment Management Programme Report Series: Bank erosion review, Motueka Integrated Catchment Management (Motueka ICM), Programme Report Series by ICM Report No.2005-2006/01 (June2006).

Technical Journal
River Research Institute ISSN: 1606-9277

IMPACT OF GEOTECHNICAL PROPERTIES ON BANK FAILURE MECHANISM AT DAULATDIA FERRY GHAT OF PADMA RIVER OF BANGLADESH

U. Saha[1*], N. C. Ghosh[2,3], M. Moniruzzaman[1,4], S. Ferdhous[1], F. Rukshana[1], M. D. Bawali[1], B. Roy[5] and K. R. Karim[1]

Abstract

The river bank of Bangladesh is generally established of alluvial deposit which contains sand, silt and clay particles. Char Bahirdia is one of the vulnerable bank sides of the Padma River adjacent to Daulatdia ferry ghat of Goalanda upazilla of Rajbari district. Bank failure mechanism depends on different hydraulic properties of the river and the geotechnical properties of the river bank. The study area is selected for investigation of the geotechnical properties and its impact on the bank failure of Daulatdia ferry ghat of Padma River. The study findings indicate that the cohesive soil strata are soft to hard which are less permeable and challenge surface erosion due to their permeability. This reduces the effects of seepage and piping. However, because of their permeability soil water pressure increases which are subjected to failure during rapid drawdown of water levels as well as soil erosion from toe zone. As a result, the river bank fails as toe failure due to tension crack. On the other hand, the non-cohesive soil strata are very loose to medium dense and dense and there is no bonding between the soil particles as clay particles are almost absent. Pore pressure increases with the increases of saturation and shear strength decreases with the increases of pore pressure. The results show the river bank tends toward the failure disposition. In addition, it is observed that the standard penetration resistance–N values have been changed along all the holes as bored where the soil layers are sometimes very loose and sometime medium dense to dense. As a result, rising of water level intensifies water pressure and increased velocity contributes to the bank failure over there due to liquefaction.

Keywords: *Bank failure, Daulatdia ferry ghat, Geotechnical properties, Padma River.*

Introduction

Bangladesh is formed on the delta by three major rivers named Brahmaputra, Ganges, and Meghna. These rivers and other rivers of the country originate from outside of the national boundary of the country and make up the Ganges-Brahmaputra-Meghna River system. The sediments carried by the huge discharges of these rivers have built a broad delta over millennia. Eventually the large area of Bangladesh is formed by the sediments and the submerged delta-plain in the Bay of Bengal (Haque, 2023). The 80% soils formation of Bangladesh is the sources of these sediments. The remaining 20% of soils have been formed in Tertiary and Quaternary sediments of hills (12%) and in uplifted Pleistocene terrace (8%) (Banglapedia, 2021). Brammer (1996) expressed that Bangladesh soil contains the different amounts of sand mixed with silt and clay in different areas of the country as the rivers deposit various amounts of these particles in different parts of their floodplains when they flood and over flood the land. He also stated that sandy material is deposited near the river banks and silty material further away from the banks whereas clay to the furthest away from the river. When rivers change their course, the pattern of sandy and silty materials are seen on the slightly higher ridges of the rivers and clay materials are seen left behind of the adjoining basins. Talukdar (2006) defined the causes of erosion are river instability, soil erosion, sediment transport and deposition. Inamul (2010) explains that the river bank can collapse depending on a number of factors predominating the geotechnical characteristics. He expresses that river bank fails when the gravitational forces acting on a bank and exceed the forces hold the sediment together. He also expresses that failure depends on sediment type, layering, and moisture content. Stream bank failure is closely related to the composition of the stream bank material with various categories of materials. It is mentioned here that geotechnical failures occur when the river bank resistance exceeds the forces created by moisture condition of the river bank. It is also explained that human actions are often responsible. It is also mentioned here that any unnatural destruction of bank vegetation promotes erosion by hydraulic forces (Wikipedia, 2019). Arora (2010) stated that river bank fail due to liquefaction occurs when the soil is cohesion less, loose, saturated and there is a shaking of ground of the required intensity and duration where the undrained conditions develop in the soil due to its permeability. He also expressed that liquefaction could occur in the soil deposit at any depth where these above conditions are satisfied. He stated that liquefaction normally occurs in Indian Standard Classifications type SP where the SPT number N is less than 15. However, sometimes liquefaction occurs in the well graded Sands (SW), Silty Sands (SM) and low plastic Silts (ML) classified soil. He also stated that fine grained soils do not compress under dynamic loadings due to high dynamic pore water pressure. Moreover, they hold the shear strength due to cohesion. Dapporto *et al.* (2003) investigated the riverbanks on the Arno River to identify the main mechanisms of failure and observed that the most common mechanism is the slab-type failure on fine grained banks while cantilever failures prevail on composite banks. They also observed that the role of the river stage and its pore water pressure distributions triggering the main mechanisms of failure. Chiang *et al.* (2010) mentioned with reference to other researchers that bank failure generally occurred particularly during the recession of hydrographs when the riverbank material is under nearly or totally saturated conditions. They recommended that the effect of matric suction has significant impact on riverbank stability and concluded that it should be taken into consideration under lower groundwater level conditions. Nasermoaddeli and Pasche (2010) stated regarding bank failure that when river banks are weakened due to piping of cohesion less soil than capillary action temporarily decreases the angle of repose of the river bank material which is less than existing bank slope. It also stated that when pore pressure increases during rapid drawdown then fluid like failures occur because of liquefaction of fine-grained materials. Nasermoaddeli and Pasche (2010) mentioned that tension cracks are occurred due to shrinking and swelling of clay soils during wetting and

[1] Geotechnical Research Directorate, River Research Institute, Faridpur-7800, Bangladesh.
[*] Corresponding Author (E-mail: umasaharri@gmail.com)
[2] Dhaka Laboratory, River Research Institute, Dhaka-1205, Bangladesh.
[3] Department of Physics, Bangladesh University of Engineering and Technology, Dhaka-1000, Bangladesh.
[4] Institute of Water and Flood Management, Bangladesh University of Engineering and Technology, Dhaka-1000, Bangladesh.
[5] Hydraulic Research Directorate, River Research Institute, Faridpur-7800, Bangladesh.

drying cycles. It also explained that subsurface moisture changes weaken the internal shear strength of the soil mass at the interface of soil types of river bank. In cases of wave action (Nasermoaddeli and Pasche, 2010) expressed that waves directly hits on exposed soil as waves vary with wind speeds and duration, water depth, and the continuous length of water over which winds blow in one direction. Fox *et al.* (2007) synthesized the research on seepage flow and erosion occurring at two stream banks in northern Mississippi and investigated the impact of seepage undercutting on stream bank stability and observed that the loss of supporting material brought by seepage undercutting is a major cause of slope instability. Rinaldi *et al.* (2004) studied on investigating pore pressure changes in response to flow events and their effects on bank stability and observed that positive pore pressures reduced the effective stress. They also observed that destroyed shear strength due to the matric suction and the sudden loss of confining pressure of the river during the initial drawdown were responsible for triggering the mass failure. Watson et al (2006) reviewed on river bank failure factors such as flow properties, bank material composition, bank geometry, bank moisture conditions, channel geometry, vegetation and man-induced factors. They found that these factors have influenced river bank failure. They expressed that soil which contains large quantities of clay particles creates a higher level of bonding between the particles. They also stated that cohesive soils are more resistant to surface erosion because they are less permeable, and it reduces the effects of seepage and piping. Due to low permeabilities these soils are more susceptible to failure during rapid drawdown of water levels due to the increase in soil water pressure. Terzaghi (1948) stated on the sign of river bank failure and explained that slide is the failure of a soil mass which is located beneath a slope. He stated that it involves a downward and outward movement of the entire soil mass which participates in the failure.

River bank failure is a common phenomenon in Bangladesh. The failure process due to devastating flood and excessive rainfall accelerating the failure process resulting in immense damage of agriculture and infrastructures every year. The people suffered unbearable miseries wherever the river bank failure occurred. Daulatdia ferry ghat of Goalonda upazila in Rajbari district is such a bank failure prone river bank which has been shown in **Fig. 1**.

Fig.1: Daulatdia ferry ghat of Goalonda upazilla in Rajbari district

In this context it is required to pay attention to how to control river bank from erosion through proper planning and design. Under such circumstances, it is needed to identify the mechanism of river bank failure prior the river bank protection. Although there have been many factors influencing the bank failure activities even it is necessary to specify the prioritization of bank failure mechanism. In this regard an attempt has been made to predict the bank failure mechanism of Daulatdia ferry ghat of Padma River in Bangladesh through investigation of influential factors such as bank material composition, bank moisture conditions with the help of a flow property such as water level. From this point of view the location Char Bahirdia of Daulatdia ferry ghat of Goalonda upazilla of Padma River in Rajbari district has been selected.

The main objectives of the study are to investigate the geotechnical properties of Char Bahirdia of Daulatdia ferry Ghat of Padma River of Rajbari district of Bangladesh and its impact on bank failure mechanism.

Methodology

A location of Daulatdia ferry ghat of Padma River in Bangladesh has been considered as a bank failure prone area. The coordinates of the study area have been shown in **Table 1** as well as **Fig. 2** respectively. The boring is conducted by wash boring method. The boring layout for sub-surface soil collection has been shown in **Fig. 3**. Holes are bored perpendicular to the bank line and the distance first, second and third bore hole were kept 10m, 50m and 300m to 500m respectively from the bank line.

Table 1. Coordinates of the bore holes.

Location	Hole No.	Coordinate	
		Northing	Easting
Char Bahirdia	1	N-2631241	E-784402
	2	N-2631237	E-784349
	3	N-2631205	E-784152

During the boring process samples are collected from each boring hole maintaining a depth of initial of 1.5 m from ground level up to 22 m with count of SPT-N value. After the completion of the boring river, the water level and ground water level had been collected. The locations of the bore holes are BH-1 (N-2631241 & E-784402), BH-2 (N-2631237

& E-784349) & BH-3 (N-2631205 & E-784152) from where soil samples were collected. The laboratory tests were conducted following ASTM procedure for different geotechnical properties. Saturation, pore pressure and shear strength are the most important parameters for evaluating the river bank failure incident. Permeability, which has a relation to grain size of soil particle is also an important parameter for bank failure investigation. Saturation and pore pressure are determined from consolidation test as well as specific gravity consideration and field depth of their respective pressure. Saturation has been considered here 100% as the soils are submerged. Grain size has been analyzed according to ASTM-D421-58 and D422-63 (Bowles, 1978) and the grain sizes have been accounted from the graph following Unified Soil Classification System.

The grain size analysis is determined by three general procedures such as i) sieve analysis ii) hydrometer analysis iii) combined analysis.

Particle sizes are determined from Grain size distribution curve which has been shown in **Fig. 4**.

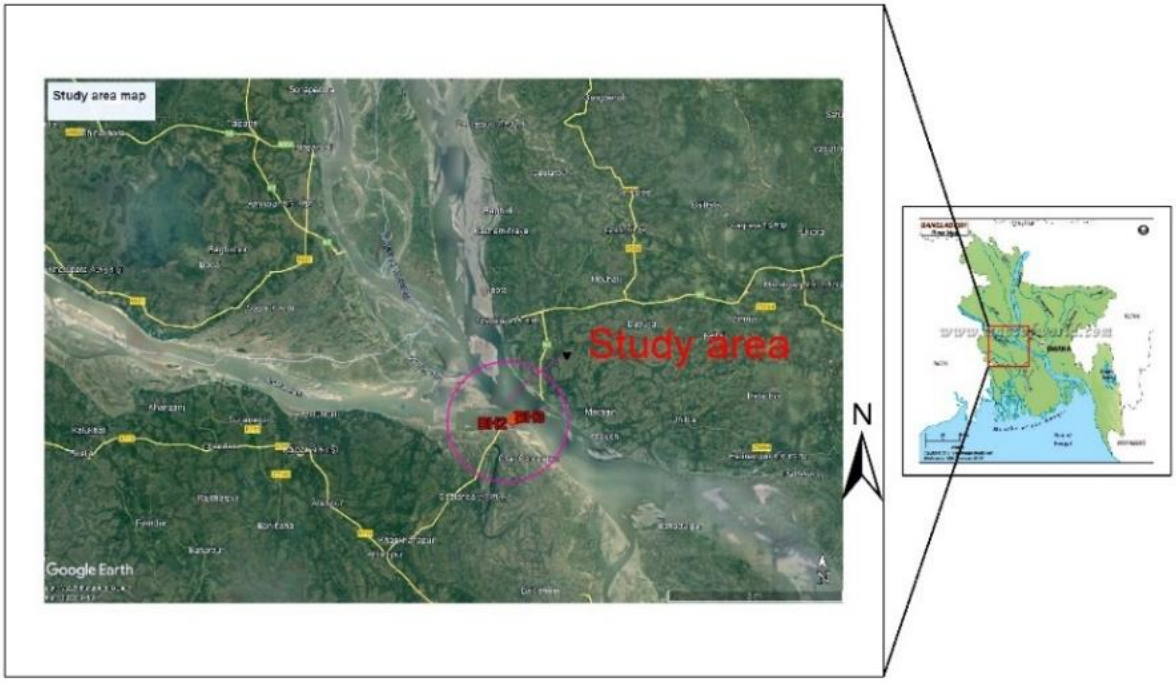

Fig. 2. Study area map.

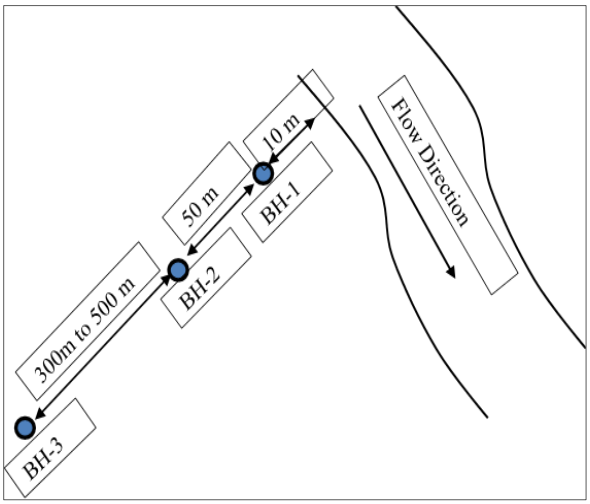

Fig. 3. Boring layout of study area.

Terzaghi & Peck (1948) stated that there is relation of consistency of cohesive soils and density index of non-cohesive soils with number of blows i.e. standard penetration resistance-N value which have been shown in **Table 2** & **Table 3** respectively.

Arora (2010) explained that coefficient of permeability depends upon the particle size and many other factors. The typical values of the coefficient of permeability have been shown in **Table 4**.

Table 2. Showing the relation of consistency of clay, number of blows N on sampling spoon and unconfined compressive strength, q_u in tons per ft^2.

Consistency	Very soft	Soft	Medium Stiff	Stiff	Very stiff	Hard
Unconfined Compressive Strength, q_u (TSF)	0-0.25	0.25-0.50	0.50-1.00	1.00-2.00	2.00-4.00	>4.00
Compressive Strength ($kN.m^{-2}$)	0-23.94	23.94-47.88	47.88-95.76	95.76-191.52	191.52-383.04	>383.04
Standard Penetration Resistance- 'N'	0-2	2-4	4-8	8-16	16-32	>32

Table 3. Showing the tabular form of density Index (I_D) of sand.

Number of blows	Density Index (ID)
0-4	Very loose
4-10	Loose
10-30	Medium Dense
30-50	Dense
Over 50	Very dense

(Source: Terzaghi & Peck, 1948**)**

Table 4. Showing the values of the coefficient of permeability in terms of soil type.

Sl. No.	Soil Type	Coefficient of permeability (mm. s^{-1})	Drainage properties
1	Clean gravel	10^{+1} to 10^{+2}	Very good
2	Coarse and medium sands	10^{-2} to 10^{+1}	Good
3	Fine sands, loose silt	10^{-4} to 10^{-2}	Fair
4	Dense silt, clayey silts	10^{-5} to 10^{-4}	Poor
5	Silty clay, clay	10^{-8} to 10^{-5}	Very poor

(Source: Arora, 2010)

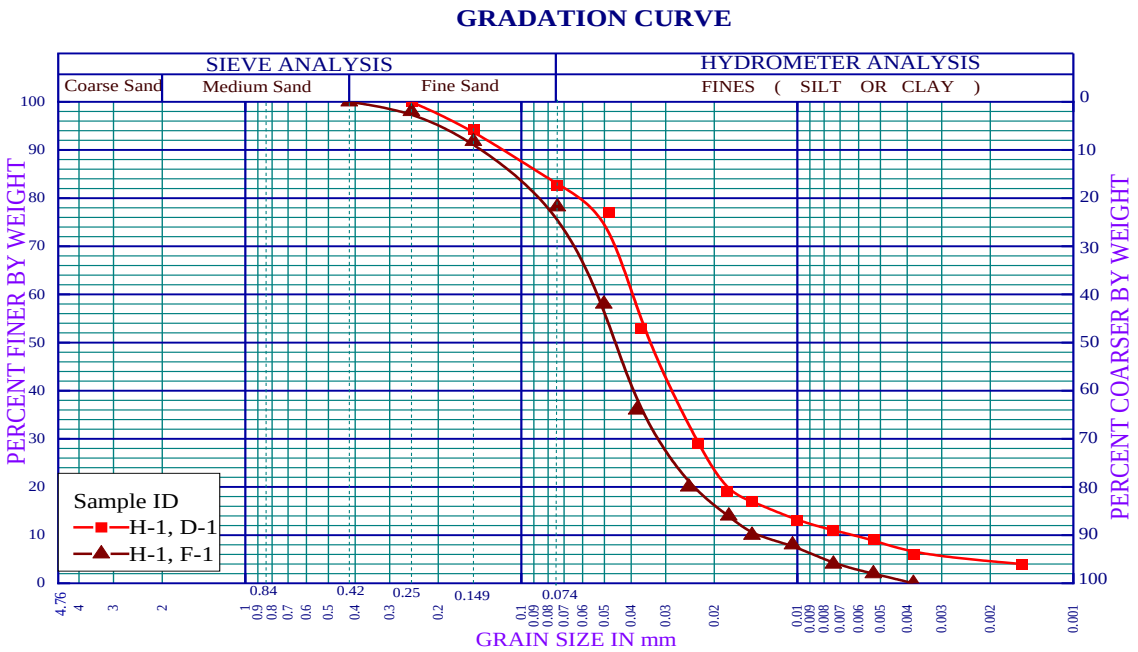

Fig. 4. Showing the grain size distribution curve.

Table 5. Sand, Silt and Clay according to their range

Name of the grain	Range of Values in mm
Gravel	<76.2-4.76>
Sand	<4.76-0.074>
Silt	<0.074-0.002>
Clay	<0.002

(Source: Garg, 2010)

Results and Discussions

Geotechnical properties of Char Bahirdia of Goalonda upazilla of Rajbari district in Bangladesh have been collected from the River Research Institute report (RRI, 2020) and presented in **Table 6**. Geotechnical properties with depth have been presented graphically in **Fig. 5** and **Fig. 6** respectively.

From the graph it has been observed that cohesive soil layer is occasionally observed along the whole 22 m depth of exploration were non-cohesive layer. The SPT values are 3 to 38 for cohesive soils where the SPT values are 3 to 39 for non-cohesive soils. The consistency of cohesive soils varies from soft to hard and the plasticity is medium. The clay particle varies (4 to 9) %, silt particle varies (69 to 88) % and sand particle varies (5 to 27) % for cohesive soils. In the case of non-cohesive soils, it is observed that the clay particle varies (0 to 1) %, silt particle varies (8 to 83) % and sand particle varies (49 to 92) %. It was found that the soil layers were dominating the site through its non-cohesive characters. The density index of non-cohesive soils varied from very loose to dense and the plasticity is non-plastic. The cohesion varies from (3 to 6) $kN.m^{-2}$ and the angle of internal friction varies from (5 to 20) degree. The permeability varies from (10^{-5} to 10^{-4}) $mm.s^{-1}$ for cohesive soils and (10^{-3} to 10^{-2}) $mm.s^{-1}$ for non-cohesive soils. The specific gravity varies from 2.646 to 2.770 for cohesive soils and 2.623 to 2.670 for non-cohesive soils.

Table 6. Showing the geotechnical properties of Char Bahirdia of Goalonda ferry ghat of Padma River.

Name of the parameter	CharBahirdia					
	BH # 01		BH # 02		BH # 03	
	N-2631241 & E-784402		N-2631237 & E-784349		N-2631205 & E-784152	
	Cohesive	Non-cohesive	Cohesive	Non-cohesive	Cohesive	Non-cohesive
N.M.C in %	29-33	24-37	25-40	27-31	31-37	12-36
SPT value	3-38	6-19	2-7	7-39	3	3-27
Unit Weight in $kN.m^{-3}$	Wet-17.29 Dry-13.02	Wet-18.62 Dry-17.29	Wet-18.43-19.37 Dry-14.80-14.81		Wet-17.41 Dry-13.32	Wet-17.4 Dry-13.36
Specific Gravity, Gs	2.668-2.707	2.623-2.67	2.66-2.77	2.66	2.646-2.692	2.65-2.67
Cohesion, c in $kN.m^{-2}$	3-6				4	
Angle of internal friction in degree	5-16				20	
Sand in (%)	11-27	49-92	5-20	49-91	6	50-92
Silt in (%)	69-83	8-50	73-88	45-83	85	8-50
Clay in (%)	4-7	0-1	6-9	0-1	9	0
Permeability in $mm.s^{-1}$	10^{-5} to 10^{-4}	10^{-3} to 10^{-2}	10^{-5} to 10^{-4}	10^{-3} to 10^{-2}	10^{-5} to 10^{-4}	10^{-3} to 10^{-2}
Mica in (%)	-	8	-	-	-	10
Colour	Grey		Grey		Grey	

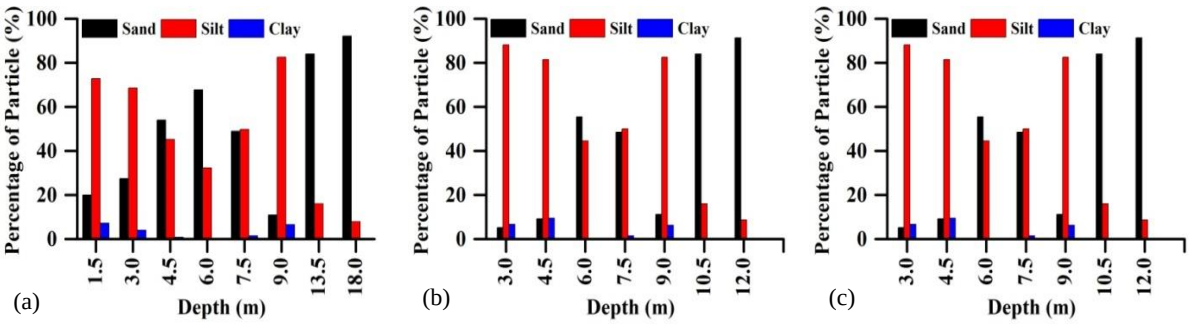

Fig. 5. Percentages of Particle of soil vs. depth graph of a) BH#1 and location (N-2631241 & E-784402), b) BH#2 and location (N-2631237 & E-784349), c) BH#3 and location (N-2631205 & E-784152) of Char Bahirdia at Daulatdia side.

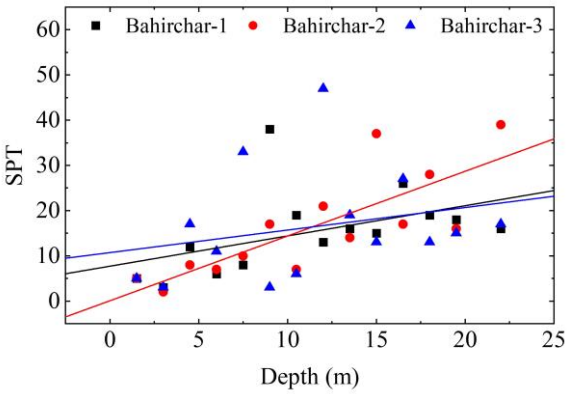

Fig. 6. SPT-N value vs. depth graph for BH#1 to BH#3 of Char Bahirdia at Daulatdia side.

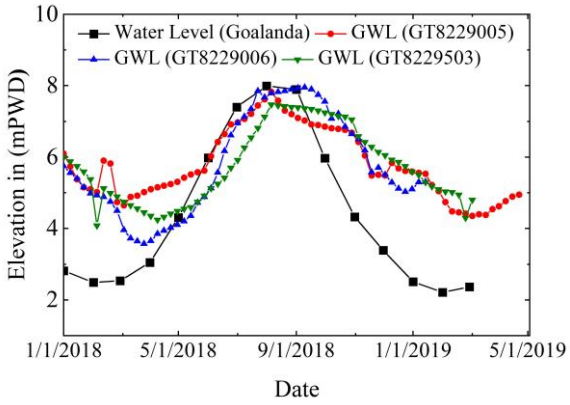

Fig. 7. Graph showing the surface water level (SWL) of Goalanda ghat and ground water level (GWL) of 3 stations of Goalanda ghat, Rajbari with period.

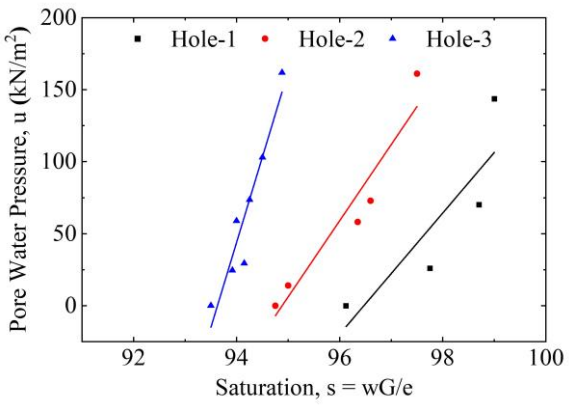

Fig. 8. Graph showing the saturation and pore pressure at Char Bahirdia of Daulatdia side of Padma River.

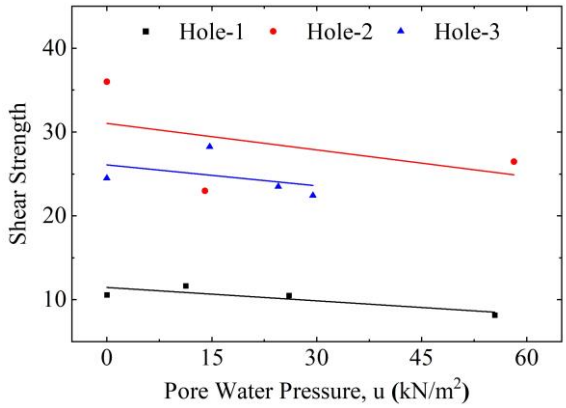

Fig. 9. Graph showing the effect of pore pressure on shear strength at Char Bahirdia of Daulatdia side of Padma River.

Variation of Ground Water Level and Surface Water level at Daulatdia side and their adjust Soil Strata

Ground water level and surface water level of one year period has been shown in **Fig. 7**.

From **Fig. 7** it has been observed that the low flood level at Daulatdia side has generally been varied from 2.5 mPWD to 3.0 mPWD and high flood level varied from 8 mPWD to above in 2018-19. The elevation at Daulatdia side is adjacent to the bank line is 7.0 mPWD, 6.0 mPWD. It would become submerged at monsoon. From the low flood level, the bank slope height from bank line remains 5.0 mPWD and 4.0 mPWD. In these bank lines, the layering of the bank material is non-cohesive sand mixed with silt particles.

On the other hand, the stratification of the materials from the bank line 5.0 mPWD to the ground surface consists of cohesive layer wherever SILT particles are dominant. The soil strata from the bank line 4.0 mPWD to the ground surface consist of variation of cohesive and non-cohesive soil layer. Where cohesive soil layers dominate SILT particles together with CLAY and SAND particles.

Effect of Saturation on Pore Pressure and effect of Pore Pressure on Shear strength

The pore water pressure has been plotted with its respective saturation in **Fig. 8**. The data have been considered here on the month of February 2018. From the figure it is observed that the pore water pressure has been increased with the increases of saturation. It is mentioned that the data would be changed monthly as the location is situated on the river bank and the distance of the holes adjacent to the bank line. The saturation becomes full when the soil is submerged. The saturation has been increased here from 93% to 99% in accordance with its soil properties as it depends on specific gravity as well as void ratio of the soils and its density. Their corresponding pore water pressures have been increased from 0 to 177 $kN.m^{-2}$ accordingly. Here the small variation of saturation has occurred due to its soil layers and properties and its ground water level as well as location.

Shear strength has been plotted with corresponding pore pressure in **Fig. 9**. From the graph it is observed that shear strength has been decreased with the increases of pore water pressure in all the holes. The shear strength of the soils of BH#1 is less than that of BH#2 and BH#3. The shear strength of the BH#3 has been varied to a certain limit and the strength is more in hole no. 2. Here it is noticed that reduced level was not existed at the alike coordinate and ground water level varies due to water surface water level. That's why the soil strength is not homogeneous, however, the location was identical. It is also observed that waves are created by ferry, launch and trawler boat traffic near the two bank lines at Daulatdia side.

Conclusion

The stratification of the materials from the bank line to the ground surface consists of non-cohesive layer wherever clay particles are zero except upper and some other layers which are cohesive soil layers. On another bank lines SILT particles together with CLAY and SAND particles make cohesive soils so, according to Watson *et al.* (2006) a medium to poor level of bonding makes among the particles. Consequently, these soils are medium to poor resistant to surface erosion because they are poorly permeable. As a result, seepage and piping have fewer negative impacts. But because these soils have low permeability, they can fail quickly when water levels drop because of the rise in pore water pressure in the soil and soil erosion from the toe zone. As a result, the river bank fails as toe failure due to tension crack. In the low flood level soil layer contains SAND particles together with little amount of silt particles make non-cohesive soils layer. So, there is no bonding between the particles as CLAY particles are absent. The standard penetration resistance–N values have been altered which make the soil layers sometime very loose and sometime medium dense to dense. Consequently, rising water level intensifies water pressure resultant the loose layer bank failure due to liquefaction according to Arora (2010). As a result, the river bank as well as the homogeneous soil zone as long liquefies due to water pressure. According to Nasermoaddeli and Pasche (2010) wave action is the impact of waves hitting directly on exposed soil as well as trafficking ferry and launch. So, it expedites the bank failure action in addition with the remaining pore water pressures of cohesive soil at the Daulatdia side.

Recommendations

Geotechnical information is always very important for any type of construction work on it. Therefore, it is very much essential and recommended to investigate the geotechnical properties of the river bank prior to any bank protection works. The soil properties at the study area indicate that soil strengthening is required for bank protection works. The findings of the present study are expected to help a lot to the concerned authorities in undertaking any construction work at the study area. It needs special attention as the water level has become varied in this river. It is also recommended that wave action is to be considered at the design of the ferry ghat protection works.

References

Arora, K. R. (2010). *Soil Mechanics and Foundation Engineering*. Reprint Edition. Standard Publishers Distributors, Delhi-110006, p-136,442,852.

Banglapedia (2021). Bangladesh Soil, National Encyclopedia of Bangladesh [online]. https://en.banglapedia.org/index.php/Bangladesh_Soil (Accessed 09 April 2023).

Chiew, Y. M., Narasimhan, N. & Chu, J. (2010). Effect of Seepage on River bank Stability. School of Civil and Environmental Engineering, Nanyang Technological University, Nanyang Avenue, Singapore 639798, Conference Paper, Published Version, Hydraulic Engineering Repository (HENR). https://doi.org/10.1061/41147(392)34.

Dapporto, S., Rinaldi, M., Casagli, N. & Vannocci, P. (2003). Mechanisms of river bank failure along the Arno river. *Earth Surf. Process.* 28(12): 1303-1323. https://doi.org/10.1002/esp.550.

Fox, G., Wilson, G. V., Simon, A., Langendoen, E. J., Akay, O. & Fuchs, J. W. (2007). Measuring stream bank erosion due to ground water seepage: correlation to bank pore water pressure, precipitation and stream stage. *Earth Surf. Process.* 32(10): 1558-1573. https://doi.org/10.1002/esp.1490.

Fox, G. A., Chu-Agor, M. L., & Wilson, G. V. (2007). Seepage Erosion: A Significant Mechanism of Stream Bank Failure. Proceedings of the American Society of Civil Engineers (ASCE) World Environmental and Water Resources Congress, May 15-19, 2007, Tampa, FL, 14 pages (CD-ROM).

Garg, S. K. (2010), *Soil Mechanics and Foundation Engineering*. First Reprint: 2010, Khanna Publishers, Delhi. Page-17, 53.

Brammer, H. (1996). The Geography of the soils of Bangladesh. *University Press Limited*. 1996, Page-4.

Haque, M. I. (2010). Water Resources Management in Bangladesh. *Anushilan publisher*, Chuadanga.

Haque, C.E. and Jakariya, M. (2023). Bengal Delta, Charland Formation, and Riparian Hazards: Why Is a Flexible Planning Approach Needed for Deltaic Systems?. *Water*, 15(13): 2373. https://doi.org/10.3390/w15132373.

Nasermoaddeli, M. H. and Pasche, E. (2010). Modelling of undercutting and failure of non-cohesive river banks. Proceeding of River Flow 2010 International Conference on Fluvial Hydraulic. 1323-1330.

Rinaldi, M., Casagli, N., Dapporto. S. & Gargini, A. (2004). Monitoring and modelling of pore water pressure changes and riverbank stability during flow events. *Earth Surf. Process.* 29(2): 237–254. https://doi.org/10.1002/esp.1042.

RRI (2020). Investigation of Geotechnical Reasons for Bank Failure on Daulatdia and Paturia Side of Padma River of Bangladesh. River Research Institute, Faridpur, Bangladesh.

Talukdar, B. (2012). River bank Erosion-A Perspective. Assam Engineering College, Email: bipulaec@gmail.com.

Terzaghi, K., Peck, R. B. & Mesri, G. (1948). Soil Mechanics in Engineering Practice. John Wiley & Sons, Inc. & Chapman & Hall, Ltd.

Watson, A. J. and Basher, L. R. (2006). Stream bank erosion: a review of processes of bank failure, measurement and assessment techniques, and modelling approaches. Motueka ICM Programme Report Series: Bank erosion review, Motueka Integrated Catchment Management Programme Report Series. Landcare ICM Report No. 2005-2006/0.

Technical Journal
River Research Institute ISSN: 1606-9277

CORRELATION BETWEEN MAXIMUM DRY DENSITY AND SOIL PARTICLES' SIZE USING MODIFIED PROCTOR TEST: A CASE STUDY

K. R. Ahmed[1*], F. Rukshana[1], M. M. R. Mondol[1,2], M. D. Bawali[1] and M. E. A Mondal[3]

Abstract

Soils are aggregates of mineral particles, along with air and water in the voids. Soil compaction is the most vital factor in any earthwork's construction. Compaction improves the engineering properties of the soil. Experience and experimentation have shown us that compacting the soils we use makes the infrastructure more sustainable, along with some other advantages. In this study, a particular amount of soil samples was collected in a large bag to find out the maximum dry density of the soil specimen, and several numbers of soil samples were collected from various point locations. The dry density of the soil samples was determined by calculating the moist density and moisture of the specific soil samples. Then, the performance of soil compaction work was determined by calculating the degree of compaction. There were four locations on the site in Kushtia. The average degree of compaction at each of the four locations was above ninety percent, which was in the acceptance range. From the regression graph of the maximum dry density and percentage of particle size, it is clear that the maximum dry density will increase with the increase of the clay and silt portion. With the expansion of the smaller particles, the value of maximum dry density will rise. There were a very small numbers of research work on correlating the dry density with the soil particle characteristics. In this work, the variation of the dry density of soil samples with the types and sizes of the particles is described vividly.

Keywords: *Compaction test, Dry density, Modified Proctor test, Moisture, Soil particles, Strength.*

Introduction

In order to get a high density, filling material for road embankments, railway subgrade, earth-dams must be compacted. Compaction reduces the soil's permeability and water-absorbing propensity while increasing the soil's shear strength and decreasing its tendency to settle (Spagnoli, 2020). Soil compaction works against the undesirable soil subsidence of an embankment (Anggraini *et al.*, 2023). The aim of every compaction specification is to attain a certain value of dry unit weight. The first and foremost benefit of soil compaction is to increase the bearing capacity of the soil and decrease the chance of settlement. The effect of compaction effort is represented by the soil's moisture content and dry density in reference to optimum moisture content and maximum dry density. Sufficient time and effort are needed in laboratory experiments in order to obtain compaction properties (Ng *et al.*, 2015). The main objective of soil compaction is to create a soil material that can meet three essential requirements. First, reduce the subsequent settlement of the soil mass under live loads. Second, the reduction in permeability will gradually prevent the development of enormous water stresses, causing liquefaction issues, and containing water in the case of earth dams. Finally, the soil material's shear resistance is enhanced (Fondjo *et al.*, 2021).

A systematic approach to examining the compaction ability of disturbed soils over a range of soil water contents is provided by the Proctor test. (Aragon, *et al.*, 2000). In 1933, Ralph R. Proctor started a research work that effectively identifies the practical highest density of a soil sample along with the optimum moist situation needed to achieve that density. That idea is referred to in the present time as the moisture content-density kinship test, laboratory compaction qualities of soils, or just the standard Proctor test, and is point by point in ASTM D698 and AASHTO T 99 test procedure. The modified Proctor test was established in 1958 as ASTM D1557 and AASHTO T 180 to accelerate the testing procedure at higher loads effects of soil types (Benjamin, 2023). During construction, the geotechnical engineers assess the unit weight of compacted soil in the field to verify the relative soil compaction percentage. The Proctor test is the most usual laboratory soil test and the basis for compacted soil placements for embankments, pavements, and structural fills. The process of compaction involves rearranging the particle locations to reach a higher density by figuring out the maximum dry density (MDD) and optimum moisture content (OMC) (ASTM, 2012). The process of compaction takes a lot of time and effort. To reduce time and effort for getting desired MDD, many studies were conducted to correlate the MDD with different index of soil properties. Six parameters such as, liquid limit, plastic limit, specific gravity, fine content, gravel content and sand content are correlated to the MDD (Gunaydin, 2009). Typically, all compaction specifications depend on gaining a certain value of dry unit weight. During construction, the geotechnical experts measure the in situ dry unit weight of compacted soil in the field to verify the results with the requirements (Rahman *et al.*, 2011). Soil compaction involves the mechanical process of bringing soil grains closer together, decreasing soil volume and pore space. However, the volume occupied by the soil grains remains the same. Engineers often consider soil compaction when designing construction projects, utilizing techniques such as grinding or compression. By controlling the dry soil density and moisture content within specific limits, essential soil properties can be determined, including density, California Bearing Ratio (CBR), consolidation, permeability, shear strength, and more. Soil compaction plays a vital role in the construction of many structures, such as roads, airports, embankments, and other infrastructural projects (Analysis of Soil Compaction using Proctor Standards in Highway Construction Design, 2021). From several reviews, it is confirmed that a certainly viable correlation exists between maximum dry density versus optimum water content. The kinship between an optimum degree of saturation and optimum moisture content (OMC) shows that OMC is lower for soils with higher maximum dry density, because the rising value of OMC results in increasing porosity, and there exists a negative relationship between porosity and MDD (Udom, 2018). The soil type concerning the grain-size distribution, the shape of the soil grains, the specific gravity of soil solids, and the presence of fine particles offer a great effect on the maximum dry unit weight

[1] Geotechnical Research Directorate, River Research Institute, Faridpur-7800, Bangladesh.
[*] Corresponding Author: (E-mail: krahmed147@gmail.com)
[2] Department of Civil Engineering, Bangladesh University of Engineering and Technology, Dhaka-1000, Bangladesh.
[3] Administration and Finance Directorate, River Research Institute, Faridpur-7800, Bangladesh.

and optimum moisture content (Guerrero, 2004). For certain moisture contents, when soil compaction is greatest, clay achieves theoretical saturation, whereas sand does not (Ren *et al.*, 2015). Testing methods for the standard and modified Proctor test procedures are the American Association of State Highway and Transportation Officials (AASHTO) T99 and T180 respectively. The proportionate American Society for Testing and Materials (ASTM) testing procedures are D 698 and D 1557 respectively (Connelly, 2008).

Table 1. Difference between standard and modified Proctor tests.

Test procedure	Standard Proctor test (AASHTO T99)	Modified Proctor test (AASHTO T180)
Hammer weight (lb)	5.5	10
Falling distance of the hammer (inch)	12	18
Numbers of layer	3	5
Energy (ft-lb.ft^{-3})	12375	56250

(Note: There are fundamental differences between standard and modified proctor tests (**Table 1**)).

To verify the degree of compaction, the in-place field density of fillings and maximum dry density is determined. Besides compaction, consolidation is also important to increase dry density. Compaction is a dynamic application of load, whereas consolidation is a static process of loading. Compaction is to be done for the exclusion of air, and consolidation is done for the expulsion of water. The aim of compaction is to attain the maximum dry density of the soil sample. Maximum dry density depends on different factors, especially on types and sizes of soil particles. This paper presents a case study about the determination of field density of earth filling works and the effect of some properties of soil sample on its maximum dry density. This will help experts to predict the soil properties requirements for earth filling works requiring a particular maximum dry density.

Methodology

Study area

The study area is located at the bank of River Gorai in Kustia. As a part of bank protective work, an embankment has been constructed on the right bank of Gorai River. This embankment was constructed by holding layers of soils and other fills, one above another, and compacting them using a heavy rolling plant until adequate strength has been achieved. To verify the degree of compaction, the in-place field density of fillings and maximum dry density was determined. The execution and supervision works of this embankment was done by Jaduboyra O & M Sub-division, Kushtia O & M Division, Bangladesh Water Development Board, Kushtia. A team from Geo-technical Research Directorate, River Research Institute, Faridpur was directed to measure the relative compaction of that earth filling works and particle analysis of soil sample of this embankment. In the project area there were four regions, these four regions covered different chainage sections. (**Table 2**).

Table 2: Location and chainage of the study area.

Region no.	Chainage	Length covered along the bank (m)	Location
01	Km 15.50 to km 16.25	750	Right bank of the Gorai River, Khoksha, Kushtia.
02	Km 16.25 to km 17.00	750	
03	Km 25.00 to km 26.00	1000	
04	Km 26.00 to km 27.00	1000	

Test for determination of maximum dry density

This work was divided in two stages. The first one was to determine the maximum dry density of soil sample from selected region, and the second one was to find field density of different spots from same region. In order to determine the degree of compaction of the earthen embankment, firstly, 12 kg of moist soil samples from each region were collected. Four regions were selected in the project area to find out the degree of compaction. Then the collected samples were carried to the laboratory. In the lab, samples were air-dried to the desired moisture, usually around 10% or more below the anticipated optimum moisture. For soil having more moisture, quick moisture can be achieved by using a heater. This can be accelerated for cohesive and high plastic soils by breaking down clumps and spreading the sample out on open trays. The breakdown may be continued more thoroughly when the soil was friable enough. For the standard and modified Proctor test, the finer materials to pass through either a 4.75mm (#4) sieve were taken for the compaction test. From 12kg soil sample, a minimum of four specimens of 2000g soils were prepared for the compaction with increasing moisture content that will cover the realized optimum water content. Then each of the five specimens were placed in a mould. The diameter and height of the mould were 4 inches and 4.6 inches respectively. Then water was added to each of four specimens and mixed thoroughly with it. The amount of added water to the next specimen was increased by 2% than that of previous one. Here 2% of the weight of soil samples was 40gm that means 40ml water. The prepared specimens were stored in closed containers for curing for 16 hours for proper moisture conditioning. Next, the prepared samples were compacted in a mould of 1/30 ft^3 by a hammer of 10lb falling from 18inch, the number of blows was 25, and the mould was vertically divided into five parts, and the mould was filled by the soil sample in five layers and compacted each layer cumulatively (Reddy, 2023). So, the compaction effort in the modified proctor test was 56,250 ft-lbft^{-3}. After compaction, the collar was removed carefully, and the compacted soil was trimmed off so that the surface was completely flat with the top of the mould. Replace small bits of a soil sample to fill the little shortage created during the trimming process.

Fig. 1. Water added soil sample, mold, and hammer.

Fig. 2. Automatic soil compaction machine.

Then the weight of the compacted soil including mould (with base and without collar) was recorded. The weight of the mould was known. Next the wet weight of the compacted soil sample was calculated, and the wet density of the soil samples was determined, and a small portion of this sample was taken to a pot, and the weight of the soil plus pot was measured. Next, the can with soil was placed in an oven for the next 24 hours. After 24 hours, the weight of the soil plus the container was taken. Thus, the percentage of the water content in the compacted soil sample was determined. Then, the process was repeated for the rest of the four previously prepared and cured specimens. From the wet density and moisture content of compacted soil specimens, dry density of every specimen was calculated, and the values of the dry density of soil and perspective water content (%) were plotted on a simple graph (**Fig. 3, 4, 5, and 6**).

Test for determination of field dry density

Then, calculation of the field density of various points in one the four particular regions of the embankment was taken into account. For that reason, a small amount, approximately 200g of soil samples were taken. The weight of each moist sample was recorded, and the wet unit weight of these samples was determined [Eq. (1)].

$$\gamma moist = W/V \qquad \text{Eq. (1)}$$

The samples were dried in an oven for 24 hours at 110°C (Rasti et al., 2020). From the difference between the two results percentage of moisture was calculated and the dry densities of the soil samples were determined [Eq. (2)].

$$\gamma d = \gamma moist/(1 + \frac{w\%}{100}) \qquad \text{Eq. (2)}$$

By dividing the dry density of each soil sample by the maximum dry density of the soil specimen of the same region, the degree of compaction was derived [Eq. (3)].

$$Relative\ Compaction = \left(\frac{Field\ dry\ density}{Maximum\ dry\ density}\right) \times 100\%) \qquad \text{Eq. (3)}$$

The higher value of degree of compaction means the better performance of the compaction work.

For determining particle sizes of soil sample a Particle Size Analyser (Mastersizer 3000) was used. Using this analyser, percentages of soil particles and the values of D_{50}, D_{90}, D_{10}, etc were found directly. In this study, soil particles from 4.76 mm to 0.074mm are treated as sand portion and soil particles from 0.074mm to 0.002mm are taken as silt and particles less than 0.002mm are treated as clay portion.

Results and discussions

Using modified Proctor test, maximum dry density was determined for the soil samples of each region. For determining the relative compaction of the embankment, field density has determined. For each location various number of sites were selected for collecting a few gram of soil samples for determining field density. The inner volume of the mould used for modified Proctor test was 947.59 cm^3. Applying the test procedure of determining the maximum dry density using modified Proctor test, the values of maximum dry density of the soil samples of the four regions were determined, and the corresponding points of the optimum moisture content were found out by plotting the values of dry density verses corresponding values of moisture content in a plain graph (**Fig. 3, 4, 5, and 6**).

After determining the maximum dry density, the dry densities of soil samples taken from different points of the same region were calculated from the moist density of in-situ soil sample and the moisture content, the field dry density was derived [Eq. (2)]. After finding the dry density, using the [Eq. (3)], the relative compactions of earth filling works of different points of all four regions were derived (**Table 3, 4, 5, and 6**).

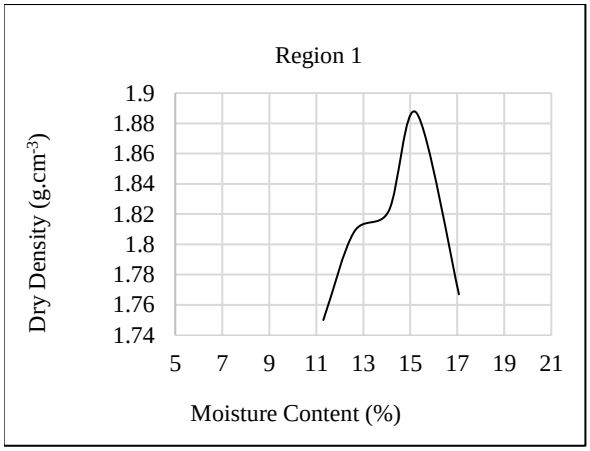

Fig. 3. Dry density vs moisture content curve.

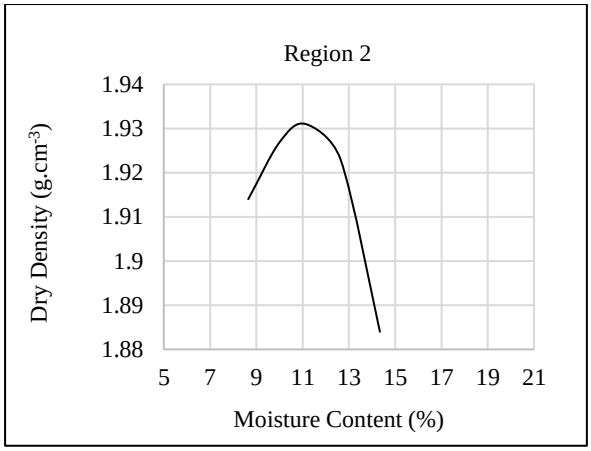

Fig. 4. Dry density vs moisture content curve.

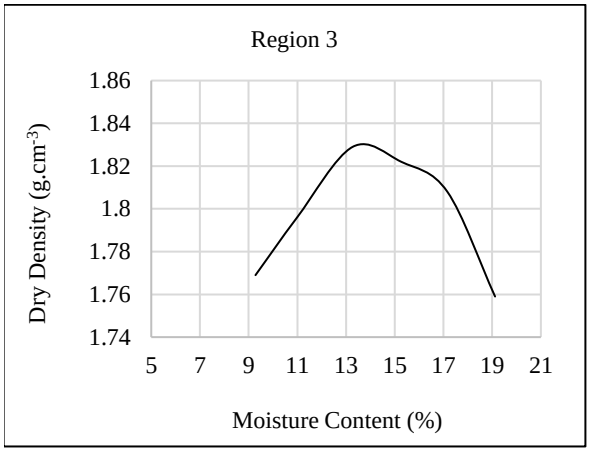

Fig. 5. Dry density vs moisture content curve.

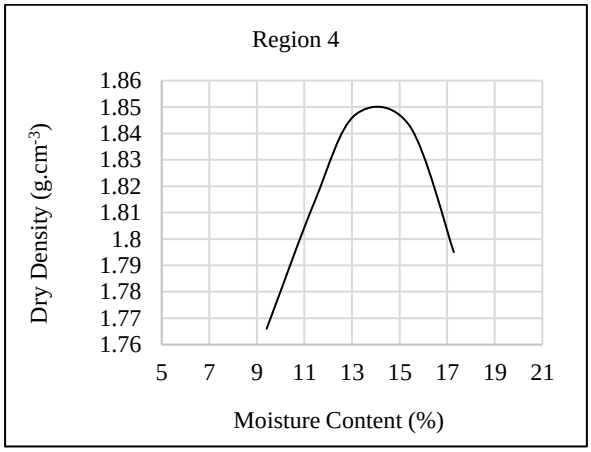

Fig. 6. Dry density vs moisture content curve.

After determining the maximum dry density, the dry densities of soil samples taken from different points of the same region were calculated from the moist density of in-situ soil sample and the moisture content, the field dry density was derived [Eq. (2)]. After finding the dry density, using the [Eq. (3)], the relative compactions of earth filling works of different points of all four regions were derived (**Table 3, 4, 5, and 6**).

Table 3. Relative compaction of earth filling work of region no. 01 (MDD 1.883 g.cm^{-3}).

Chainage	15.500 km	15.550 km	15.600 km	15.700 km	15.750 km	15.800 km	16.050 km	16.100 km
MDD (g.cm^{-3})				1.883				
Dry Density (g.cm^{-3})	1.83	1.74	1.66	1.69	1.78	1.78	1.88	1.85
Relative Compaction in %	97.19	92.41	88.16	89.75	94.53	94.53	99.84	98.25

Table 4. Relative compaction of earth filling work of region no. 02 (MDD 1.934 g.cm^{-3}).

Chainage	16.330 km	16.350 km	16.710 km	16.715 km	16.720 km	16.800 km	16.850 km	16.900 km
MDD (g.cm^{-3})				1.934				
Dry Density (g.cm^{-3})	1.86	1.83	1.78	1.66	1.77	1.57	1.65	1.74
Relative Compaction in %	96.17	94.62	92.04	85.83	91.52	81.18	85.32	89.97

Table 5. Relative compaction of earth filling work of region no. 03 (MDD 1.829 $g.cm^{-3}$).

Chainage	25.500 km	25.570 km	25.685 km	25.810 km	25.990 km
MDD ($g.cm^{-3}$)			1.829		
Dry Density ($g.cm^{-3}$)	1.48	1.42	1.55	1.43	1.53
Relative Compaction in %	80.92	77.64	84.75	78.18	83.65

Table 6. Relative compaction of earth filling work of region no. 04 (MDD 1.848 $g.cm^{-3}$).

Chainage	26.300 km	26.500 km	26.700 km	26.825 km	27.000 km
MDD ($g.cm^{-3}$)			1.848		
Dry Density ($g.cm^{-3}$)	1.21	1.76	1.29	1.38	1.47
Relative Compaction in %	65.48	95.24	69.81	74.68	79.55

With the rising of clay and silt content of soil particles, the maximum dry density of soil is increasing and vice versa. Sensitivity analyses showed that while the gravel content is a major factor in predicting maximum dry density, the plastic limit has a significant impact on the optimum moisture content. Similar observation has found by Ali *et al*, 2024. As the plastic limit depends on the types of soil particles, both MDD and OMC depend on soil particles.

The percentage of soil particles and maximum dry density of the selected four locations soil samples are given below (**Table 7**).

Table 7: Relationship between MDD and soil properties.

Location	Region 1	Region 2	Region 3	Region 4
% of clay	2.85	3.15	2.37	2.67
% of silt	89.0	90.99	84.16	87.24
% of sand	8.05	5.86	13.47	10.09
D_{50} (µm)	13.62	9.73	20.06	19.01
Maximum dry density ($g.cm^{-3}$)	1.883	1.934	1.829	1.848
Optimum moisture content	15.26	11.14	13.2	14.8

Dry density of compacted soil samples depends on moisture content, compaction energy and soil particles' sizes. As the maximum dry density is obtained by applying a certain compaction energy, so the maximum dry density depends on moisture content of soil sample and particle size of sample. Since moisture content also depends on particle size of soil, so the maximum dry density for a constant compaction energy depends on soil particle size. Finer particles have less voids and compacted soil will be denser, so the maximum dry density will be more (Alshameri, 2020). By plotting the values of the maximum dry density with the variations of soil particles the coefficients of determination were found **(Fig. 7, 8 and 9).**

From **Fig. 7, 8 and 9**, it can be decided that the maximum dry density of soil specimens is directly proportional to the percentage of clay and silt particles and inversely proportional to the percentage of sand particles. So, using that soil for subgrade, which has minimum sand content to achieve the maximum dry density, will be wise. Soil with a large amount of sand content should be avoided as much as possible. Now, the values of the maximum dry density of soil specimens were plotted against the sizes of the soil particles below which 50% soil particles were finer (**Fig. 10**).

Regression analysis is a statistical apparatus that is for defining the functions between independent and independent variables. The power of dependence between variables is determined by using correlation research. If, $R \leq 0.3$, no significant correlation exists, if $0.5<R<0.7$, then significant correlation, and if $0.7<R<0.9$, then a strong correlation sustains (Djokovic, 2013). So, there is a strong relation between the maximum dry density of soil samples and the percentage of soil particles. Moreover, in the case of a number of soil specimens, there remains a significant correlation between the maximum dry density and optimum moisture content of the specific soil samples. Furthermore, the maximum dry density is also directly proportional to D_{50} of the soil samples (**Fig. 10**). In the Proctor test the two

parameters such as the maximum dry density and optimum moisture content depend on hammer weight, the height of the hammer drop, and the number of blows. With the increase of hammer weight and the height of the hammer drop, the compaction effort will rise. As a result, maximum dry density will rise. Although, the number of blows on the soil and the dry density of the soil is directly proportional (Hussein, 2018).

So, it can be stated that, as the number of blows increases, the maximum dry density of that particular soil sample is increasing and vice versa. The method of compaction plays a vital role in determining maximum dry density. The highest dry density gained by the modified Proctor test will be more than that of the standard Proctor test. Not only that, the maximum dry density varies more than 5% from the result of the standard compaction test (Lvovska, 2018, pp. 636-641).

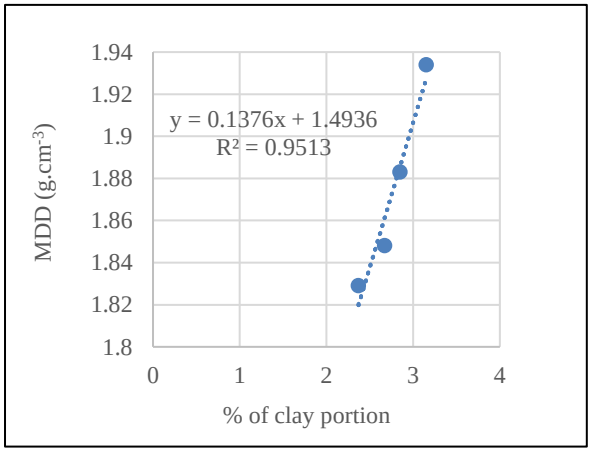

Fig. 7. Clay quantity and dry density relationship.

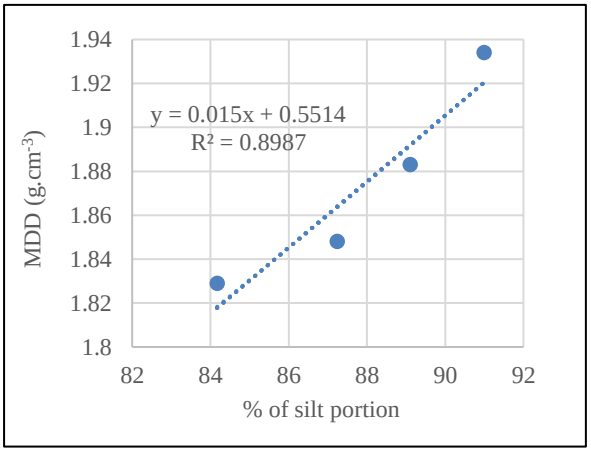

Fig. 8. Silt quantity and dry density relationship.

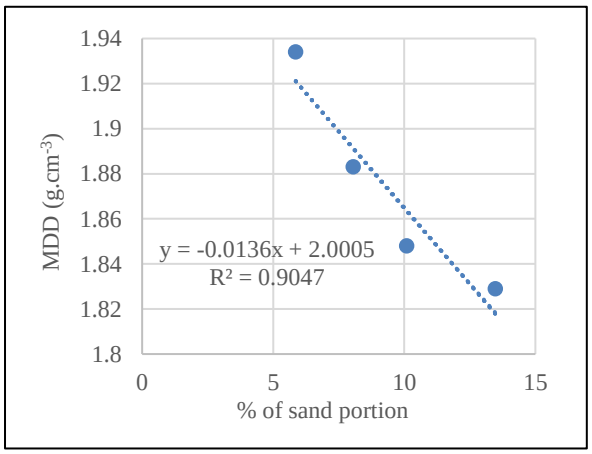

Fig. 9. Sand quantity and dry density relationship.

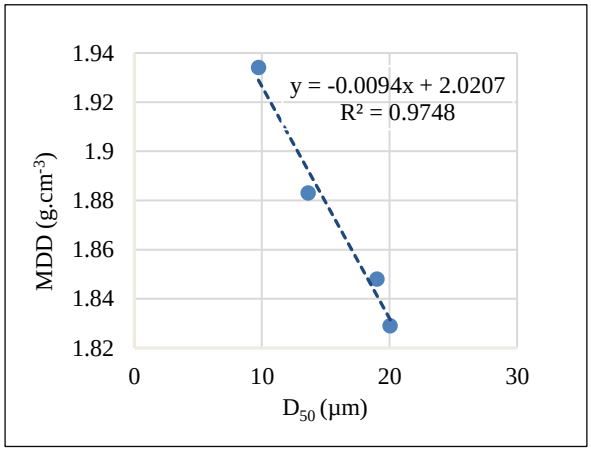

Fig. 10. Relationship between MDD and D_{50}.

Conclusions

From the study, the moisture content and size of the soil particles are significant for the density of a compacted soil sample. The linear relationships showed excellent coefficient of determination values, presenting the magnitudes of the correlation between MDD and sand, silt and clay percentages of compacted soil samples. The values of R^2 for clay, silt and sand portion are 0.9513, 0.8987 and 0.9047 respectively. The soil sample of the four regions of the study area contains sand percentage from 5.86% to 13.47%, and the MDD of the soil sample of these four compacted regions varies from 1.829 to 1.934 gcm^{-3}. For the presence of more voids in the sand portion, with the increase of sand particles, the value of MDD decreased. Engineers must choose a well-graded soil sample to construct a barrier to fill all the pores with finer particles. In the same way as the Proctor test, the embankment's compaction work should be done layer by layer, and the experts should design the compactor's load and the compaction work's duration. Even though variables like soil type, moisture content, compaction energy, and compaction technique are essential, a whole picture can require more than just these. Because soil behaviour is complex, engineers must have a sophisticated grasp of it and use a variety of approaches to guarantee the best possible embankment performance. A comprehensive strategy and cutting-edge technologies will make more resilient and sustainable infrastructure possible.

Acknowledgement

We want to express our deep gratitude to Kushtia O & M Division, Bangladesh Water Development Board, Kushtia, for giving us a significant opportunity to be a part of the construction of an embankment along the right bank of Gorai River, Khoksha, Kushtia.

References

Ali, H, F, H., Omer, B., Mohammed, A, S. and Faraj, R, H. (2024). Predicting the maximum dry density and optimum moisture content from soil index properties using efficient soft computing techniques. Neural Computing and Applications. https://www.doi.org/10.1007/s00521-024-09734-7

Alshameri, B. (2020). Maximum dry density of sand–kaolin mixtures predicted by using fine content and specific gravity. *SN Appl. Sci.* 2: 1693. https://doi.org/10.1007/s42452-020-03481-9

Anggraini, M., Haris, V, T. and Saleh, A. (2023). Characteristics of Embankment Soil as Subgrade in Road Pavement Structure. Proceedings of the International Conference on Advance Transportation, Engineering, and Applied Science (ICATEAS 2022) (pp.120-127). https://doi.org/10.2991/978-94-6463-092-3_11

Aragon, A. M., Garcia, M. G., Filgueira, R.R. and Pachepsky, Ya. A. (2000). Maximum Compaction ability of Argentine soils from the Proctor Test. The relationship with organic carbon and water content. *Soil and Tillage Research.* 56 (3-4): 197-204.

ASTM (2012). ASTM-D698, Standard test methods for laboratory compaction characteristics of soil using standard effort (12400 ft-lbf/ft3 (600 kN-m/m3)). West Conshohocken, PA.

Benjamin, E. B. https://www.globalgilson.com/blog/proctor-compaction-test-a-basic-guide (accessed 12 June 2023).

Connelly, J. (2008). Proctor Compaction Testing. Nebraska Department of Transportation: Research Reports, USA.

Djokovic, K., Rakic, D. and Ljubojev, M., (2013). Estimation compaction parameters of soil based on Atterberg limits. Mining and Metallurgy Institute BOR. Vol. 4.

Fodjo, A. A., Theron, E. and Ray, R, P., (2021). Estimation of Optimum Moisture Content and Maximum Dry Unit Weight of Fine-Grained Soils using Numerical Methods. *Walailak Journal of Science and Technology (WJST)*. 18(16): Article 22792. https://doi.org/10.48048/wjst.2021.22792

Guerrero, A. (2004). Effects of the soil properties on the maximum dry density obtained from the standard proctor test. Electronic Theses and Dissertations. 161. https://civiljungle.com/modified-proctor-test/ (Accessed 01 June 2023)

Hussein, I. S. (2018). Influence of Number of Blows and Water Content on Engineering Properties of Compacted Gypseous Soil. *AL-Bahir Quarterly Adjudicated Journal for Natural and Engineering Research and Studies.* 7(13-14): 83-93.

Kitch, W. A., www.geoengineer.org/education/laboratory-testing/compaction-test. (Accessed 29 May 2023).

Lvovska, T. (2018). Soil Compaction Methods Development. *International Journal of Engineering & Technology.* 7: 636-641.

Ng, K. S., Osman, M. H., Chew, Y. M. and Ghazali, M, S. K. (2015). Estimating Maximum Dry Density And Optimum Moisture Content Of Compacted Soils. International Conference on Advances in Civil and Environmental Engineering 2015. Faculty of Civil Engineering, Universiti Teknologi MARA Pulau Pinang.

Rahman, M. G. F., Talukdar, M. and Rahman, A. (2011). *MIST International Journal of Science and Technology*. Vol. 13.

Rasti, A., Pineda, M. and Razavi, M. (2020). Assessment of Soil Moisture Content Measurement Methods: Conventional Laboratory Oven versus Halogen Moisture Analyzer. *Journal of Soil and Water Science.* 4(1). 151-160. https://doi.org/10.36959/624/440

Reddy, K. R. https://cemmlab.webhost.uic.edu/Experiment%209-Compaction.pdf. (Accessed 31 May 2023).

Ren, X, C., Lai, Y, M., Zhang, F, Y. and Hu, K. (2015). Test method for determination of optimum moisture content of soil and maximum dry density. KSCE *Journal of Civil Engineering.* 19: 2061-2066.

Spagnoli, G., and Shimobe, S. (2020). An overview on the compaction characteristics of soils by laboratory tests. *Engineering Geology.* Vol. 278: 105830. https://doi.org/10.1016/j.enggeo.2020.105830

Udom, B, E. and Ehilegbu, J. (2018). Critical Moisture Content, Bulk Density Relationships and Compaction of Cultivated and Uncultivated Soils in the Humid Tropics. *Asian Soil Research Journal*. 1(2): 1-9; Article no. ASRJ.43180.

Technical Journal
River Research Institute ISSN: 1606-9277

DESIGN SCOUR DEPTH AROUND THE PIER OF THE RAILWAY BRIDGE ACROSS THE JAMUNA RIVER IN BANGLADESH: A PHYSICAL MODEL BASED APPROACH

A. K. M. Ashrafuzzaman[1*], M. J. Islam[1], M. Shahabuddin[1], S. K. Ghosh[1], M. Tofiquzzaman[1], M. K. Eusufzai[2], M. Moniruzzaman[3,4] and M. E. A. Mondal[5]

Abstract

For further enhancement of the capacity and to overcome the loading restriction of existing Bangabandhu Sheikh Mujib Multipurpose Bridge, it would be essential to construct a parallel railway bridge, dedicated to railway, while the existing bridge could carry road traffic only. In this context, Bangladesh Railway has decided to construct the proposed Bangabandhu Sheikh Mujib Railway Bridge over the Jamuna River which will be located 300 m upstream of the existing bridge. Therefore, a study was undertaken by River Research Institute (RRI) to support the design required for the proposed railway bridge using scale modelling having scale 1:100. The study shows that maximum scour occurred around the bridge piers is 27.5 m (-21.0 mPWD) at pier-3 (of existing Bangabandhu Sheikh Mujib Multipurpose Bridge) & 39.4 m (-31.9 mPWD) at pier -3 (of proposed Bangabandhu Sheikh Mujib Railway Bridge) when a barrier is provided to impinge the flow on the revetment and bridge piers. The study also shows that maximum velocity around the bridge piers is 3.68 ms^{-1} & 4.52 ms^{-1} at existing bridge pier-2 & proposed bridge pier-2 respectively under 60-degree oblique flow attack at the bridge corridor guide bund. In addition, maximum scour around the revetment of west guide bund (WGB) is 29.5 m (-23.5mPWD) when the approach flow condition has been changed by providing a barrier to concentrate the flow around the upstream tip of revetment. Moreover, maximum velocity found around the revetment of WGB is 5.3 ms^{-1} (at the upstream tip of WGB) when the launching portion of revetment is strengthened as per design under 200-yr water level (WL) 14.49 mPWD and discharge (Q) 111,000 m^3s^{-1}.

Keywords: *Bangabandhu bridge, calibration, guide bunds, Jamuna River, River Training Work (RTW), Scour depth, Undistorted model and West Guide Bund (WGB).*

Introduction

Bangladesh is a riverine country having three major rivers namely the Ganges, the Meghna and the Jamuna. The Jamuna River, which is the mightiest of the three and which ranks as the fifth largest river in the world in terms of volumetric discharge and highest silt carrying river in the world. The construction work of Bangabandhu Bridge Project started in October 1994 and opened to traffic on 23 June 1998. The length of the bridge is 4.8 km and lengths of west & east guide bunds are 3.26 km and 3.07 km respectively. The guide bunds direct the river into a single channel under the bridge. A west channel closure has also been constructed to close the western channel of the Jamuna, thereby reducing the width of the river at the bridge site from about 10 km to 4.8 km. The main objective of the construction of the Bangabandhu Bridge was to establish a strategic link between the east and the west region of Bangladesh and to integrate the country by generating multifaceted benefits for the people, promoting better inter-regional trade and economic and social development. It enables quick movement of goods and passenger traffic by road and by rail across the Jamuna River.

In addition, its facility promotes transmission of electricity, transfer of natural gas and integration of telecommunication links. For further enhancement of the capacity and to overcome the loading restriction of Bangabandhu Bridge, it would be necessary to go for construction of a parallel Bangabandhu railway Bridge, dedicated to railway, while the existing the Bangabandhu Bridge could carry road traffic only. The proposed railway bridge is under construction. The model study was done before starting of the bridge construction in the field. The model boundary of West Guide Bund (WGB) is shown in **Fig.1.** The bridge will be located on the strategic Asian Highway and the Trans-Asian Railway which, when fully developed, will provide an interrupted international road and railway link from S.E. Asia to N.W. Europe. The roadway bridge is quite capable to connect the Asian Highway. But the existing Rail Track Bed over the Bangabandhu Bridge is not enough to link to the Trans-Asian Railway. The construction of Railway Bridge over the river Jamuna would also be helpful to ensure safe and less costly movement of passenger and goods between East and West region of Bangladesh as well as to promote the interconnectivity from S.E. Asia to N.W. Europe.

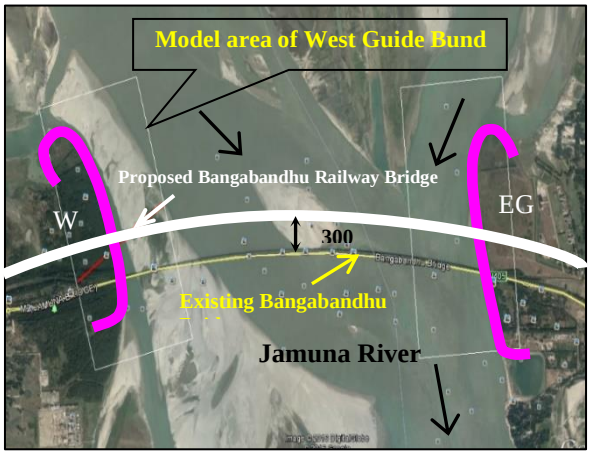

Fig. 1. Boundary of West Guide Bund (WGB) Model.

Scouring Process around Bridge Piers

Local scour involves the removal of material from around piers, abutments, spurs, and embankments. It is caused by an acceleration of the flow and resulting vortices induced by the flow obstructions. Local scour occurred at bridge piers are caused by the interference of the piers with flowing water. This interference will result in a considerable increase in the mean velocity of the flowing water in the channel section.

[1] Hydraulic Research Directorate, River Research Institute, Faridpur-7800, Bangladesh.
[*] Corresponding Author: (E-mail: ashrafcebuet89@gmail.com)
[2] Dhaka Laboratory, River Research Institute, Dhaka-1205, Bangladesh.
[3] Geotechnical Research Directorate, River Research Institute, Faridpur-7800, Bangladesh.
[4] Institute of Water and Flood Management, Bangladesh University of Engineering and Technology, Dhaka-1000, Bangladesh.
[5] Administration and Finance Directorate, River Research Institute, Faridpur-7800, Bangladesh.

Scouring vortex will be developed when the fast moving flow near the water surface (at the location of the maximum velocity in the channel section) strikes the blunt nose of the pier and deflected towards the bed where the flow velocity is low. Portion of the deflected surface flow will dive downwards and outwards. This will act as a vacuum cleaner and suck the soil particles at the pier site and result in a considerable increase in the scouring depth at this location. Local scour can occur as either 'clear-water scour' or 'live-bed scour'. In clear-water scour, bed materials are removed from the scour hole, but not replenished by the approach flow while in live-bed scour the scour hole is continually supplied with sediment by the approach flow and an equilibrium is attained when, over a period of time, the average amount of sediment transport into the scour hole by the approach flow is equal to the average amount of sediment removed from the scour hole. Under these conditions, the local scour depth fluctuates periodically about a mean value. The interaction between the flow around a bridge pier and the erodible sediment bed surrounding it is very complex (Cheremisinoff, 1998). In fact, the phenomenon is so involved that only very limited success has been achieved by the attempts to model scour computationally, and physical model remains the principal tool employed for estimating the expected depths of scour. In this paper, a physical model was used to investigate the effect of the variables affecting the clear-water local scour around piers.

Scour Depth Prediction

Scour around bridge piers has been the subject of many investigations throughout the world, and numerous scour prediction formulas have been published. Selected scour formulas related to the studied topic are described below. Shen (1971) suggested the following equation:

$$\frac{d_s}{b} = k_1 k_2 \frac{v}{2g} - \frac{30d}{b} \qquad \text{Eq. (1)}$$

where k_1 is a coefficient depending on pier dimensions, k_2 is a coefficient depending on the ratio of flowing depth to pier width and pier's Froude number, d_s is scour depth, v is the mean velocity of flow, b is pier width, g is acceleration due to gravity, and d is bed particle size. The unit of d in Eq. (1) is in centimetres, while the units of the rest of the parameters are in meters and seconds.

The scour depth is related to the Pier Reynolds number which is defined as the flow velocity multiplied by pier width divided by the kinematic viscosity of the flowing water, since the horseshoe vortex system is a function of the Pier Reynolds number. Shen *et al*. (1969) used laboratory data and limited field data to develop the following clear-water scour equation:

$$d_s = 0.00022R^{0.619} \qquad \text{Eq. (2)}$$

where R is Pier Reynolds number. Eq. (2) is valid only for a bed of particle size of 0.52 mm or less. The following linear equation was given by Shen (1971) to estimate the scour depth:

$$d_s = 1.4b \qquad \text{Eq. (3)}$$

Also, there were several non-linear formulas proposed by many researchers for the purpose of estimating the local scour depth, but the following formulas are famous and given by Cheremisinoff (1988):

$$d_s = 1.05kb^{0.75} \qquad \text{Eq. (4)}$$

$$d_s = 3b^{0.8} \qquad \text{Eq. (5)}$$

where k is a coefficient depending on pier shape and the value of k is equal to 1

for cylindrical pier and 1.4 for rectangular pier.

Equations (4) and (5) are applicable for a pier which is aligned with the flow direction. For piers which are inclined by an angle 0 from the flow direction (called the angle of attack), the value of this coefficient k_θ is equal to 1.1 as given by Melville and Sutherland (1988). They developed a scour model based on extensive laboratory experiments.

$$d_s = K_i K_d K_y K_\alpha K_s b \qquad \text{Eq. (6)}$$

where K_i is flowing intensity factor, K_d is sediment size factor, K_y is flowing depth factor, K_α is pier alignment factor, and K_s is pier shape factor.

Qadar (1981) studied the mechanism of the local scour around the bridge pier using physical model. The local scour depth is related to some of the basic characteristics of the scouring vortex as described by the following formula:

$$d_s = 538\ (C_0)^{128} \qquad \text{Eq. (7)}$$

where C_0 is the initial strength of the vortex. Equation (7) is applicable for sediments with a diameter up to 0.5 mm. Colorado State University's pier scour equation is commonly used within the United States and this equation is described by the following equation (USDT, 1993):

$$d_s = 2.0K_1K_2K_3\left(\frac{b}{y}\right)^{0.65} F^{0.43} \qquad \text{Eq. (8)}$$

where y is the flow depth directly upstream of the pier, K_1 is the shape factor for pier, K_2 is the factor for the angle of attack for the flow, K_3 factor for bed condition, and F is Froude number. The HIRE (2024) equation is based on field data of scour at the end of spurs in the Mississippi River (obtained by the USACE). The HIRE equation is:

$$y_s = 4y_1\left(\frac{K_1}{0.55}\right)K_2 Fr_1{}^{0.33} \qquad \text{Eq. (9)}$$

Table 1. Description of Symbols.

Symbol	Description	Units
ys	Scour depth	m
$Fr1$	Froude number based on velocity and depth adjacent and just upstream of the abutment toe	
$y1$	Depth of flow at the toe of the abutment on the overbank or in the main channel, taken at the cross section just upstream of the bridge.	m
$K2$	Correction factor for angle of attack (θ) of flow with abutment. θ = 90 when abutments are perpendicular to the flow, θ < 90 if embankment points downstream, and θ > 90 if embankment points upstream. $K2=(\theta/90)0.13$	
$K1$	Correction factor for abutment shape (see table below)	

Table 2. Correction Factor for Abutment Shape, K1.

Description	K1
Vertical-wall Abutment with wing walls	0.82
Vertical-wall Abutment	1.00
Spill-through Abutment	0.55

The correction factor, $K2$, for angle of attack can be taken from the figure below.

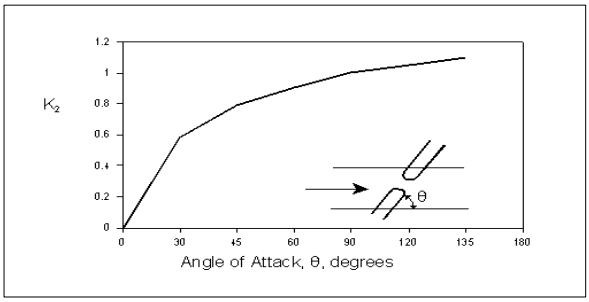

Fig. 2. Correction Factor for Abutment Skew, K2.

The scour depth calculated by Hire method is 33 m at WGB & 20 m at proposed rail bridge pier. But the maximum scour depth found from physical model study around WGB is 29.5 m, which is less than the Hire method and proposed rail bridge pier 39.4 m (around two times the Hire method).

Methodology

About 3.0 km river length and a part width of about 1.0 (one) km of the Jamuna River including existing roadway bridge and proposed rail bridge have been reproduced in the WGB model. Model bed and bank are composed of fine sand having d_{50} about 0.085mm. Maximum flood discharge of 100-year, 200-year & 500-year return period is taken into account to investigate the model with two different discharge conditions. One is Froudian discharge, and the other is scouring discharge for scour development. Froudian discharge provides the flow pattern and velocity field as a whole and the scour discharge focuses on the scour simulation and sediment transport. Each test of the model continues about 16-20 hours until a dynamic equilibrium scour is reached. The need for reliable field data on the flow and sediment transport processes is of immense importance in the scaling process. The previous information and present surveyed data were taken into consideration for calculating different parameters. The WGB model has been designed so that the scale conditions for simulation of flow field, sediment transport and local scour are satisfied. The scale conditions are described below:

a) Geometric Condition

The detail models should be undistorted *i.e.*, $L_r = h_r$, where L_r= horizontal scale and h_r = vertical scale.

b) Roughness Condition

In the model the following roughness condition is required in order to reproduce the flow field properly. But in this model some deviation is occurred as the model is rougher.

$C_r^2 = L_r/ h_r = 1$, where, Cr = roughness scale

In the movable bed model following scale condition for sediment transport should be satisfied:

$V_m > V_{cr}$, V_{cr} in the model will be calculated using the following formula:

$V_{cr} = 0.19(d_{50})^{0.1} \log(12h/3d_{90})$ for $0.0001m \leq d_{50} \leq 0.0005m$

Where, d_{50} = Median particle diameter (m), d_{90} = 90% particle diameter (m)

The critical velocity for sediment transport can also be calculated from the critical Shields value. The critical velocity in the model has been calculated from the following equations.

$D_* = d_{50}\{(s-1)\, g/v^2\}^{1/3}$

$\theta_{cr} = 0.14D^{*\wedge(-0.64)}$ for $4<D^*<=10$

$\theta_{cr} = 0.24D^{*\wedge(-1)}$ for $1<D^*<=4$

$L_r/ h_r = 1$ Where, Cr = roughness scale

c) Froude Condition

The Froude condition is fulfilled which holds when: $V_r = h_r^{0.5}$

d) Sediment Transport Condition

$$V_{cr} = \{\theta_{cr} (s\text{-}1)\, d_{50} C^2\}^{1/2}$$

In which, D_* = Particle parameter, d_{50} = Median grain size, s = Relative density of the sediment,

v = Kinematic viscosity, C = Chezy co-efficient and θ_{cr} = Critical shields parameters.

The critical flow velocity for median particle diameter of model bed sand (0.085mm) has been determined from the above equations. The investigation is aimed at the equilibrium scour depth with continuous sediment transport. A requirement in this type of model is that in the model sediment transport has to be occurred at all locations as it occurs in prototype. In order to fulfil this condition an increase in the model velocity has been considered to ensure the sediment transport upstream and downstream of the proposed bridge. In this situation the scour hole characteristics are not influenced by the size of the bed material or approach flow velocity.

Test Scenarios

In the WGB model, two calibration tests (T0-1 & T0-2) and seven application tests (T1-T7) have been conducted.

The test scenarios of these test run along with various discharge / WL conditions are mentioned in **Table 3.**

Table 3. Test Scenarios of the WGB Model.

Test Scenarios	Discharge & Water Level Conditions
T0-1: Calibration test with existing structure (Bangabandhu Roadway Bridge) using bathymetry of July 2017 and measured field velocity.	Observed Water Level 13.72 mPWD and discharge 89,600 m^3s^{-1}.
T0-2: Calibration test with existing structure (Bangabandhu Roadway Bridge) using simulated velocity corresponding to 100-yr discharge.	100-year Water Level 14.14 mPWD and discharge 101,506 m^3s^{-1}
Application Test-T1 With piers and revetment of Bangabandhu bridge. Flow alignment near the bank/in line with pier.	100-year Water Level 14.41 mPWD and discharge 105,552 m^3s^{-1} 500-year Water Level 14.62 mPWD and discharge 118,668 m^3s^{-1}
Application Test-T2 Test to assess bridge-to-bridge pier & bridge-to-revetment interaction with proposed bridge and Bangabandhu bridge and piers of Bangladesh Railway (BR) bridge. Flow in-line with the existing and proposed bridge pier.	100-year Water Level 14.38 mPWD and discharge 105,552 m^3s^{-1}
Application Test-T3 Test to assess bridge-to-bridge pier & bridge-to-revetment interaction with proposed bridge and Bangabandhu bridge having modified revetment and piers of BR bridge. Flow alignment is at the tip in bridge corridor away from the guide bund. The proposed bridge piers are tested with an angle of 53-degree with the approach flow/revetment alignment.	200-year Water Level 14.49 mPWD and discharge 111,000 m^3s^{-1}
Application Test-T4 Test to assess bridge-to-bridge pier & bridge-to-revetment interaction with proposed and existing bridge piers and revetment. The proposed bridge piers are tested with an angle of 45-degree with the approach flow/revetment alignment. The pile cap of proposed SPSP bridge piers is raised to a level of 14.2mPWD.	500-year Water Level 14.53 mPWD and discharge 118,668 m^3s^{-1}
Application Test-T5 Test to assess bridge-to-bridge pier & bridge-to-revetment interaction with proposed &existing bridge piers and existing revetment only. The proposed bridge piers are tested with an angle of 45-degree with the approach flow/revetment alignment. The pile cap of proposed SPSP bridge piers is kept at a level of 8mPWD. Here the approach flow condition has been changed by providing a temporary brick wall as lateral boundary to concentrate the flow around the u/s tip of revetment. The objective of this test to produce additional local scour around the u/s tip of revetment by concentrating flow around it.	100-year discharge 105,552 m^3s^{-1} and corresponding Water Level of 14.41mPWD.

Test Scenarios	Discharge & Water Level Conditions
Application Test-T6 Test to assess the scour around the bridge corridor. A char was developed at the u/s of bridge corridor so that an oblique flow attack of about 60-degree is reproduced at the WGB corridor.	100-year, 200-year and 500-year The corresponding Water Level 14.38, 14.49 and 14.53 mPWD and discharge 105,552, 118,668 and 137036 m^3s^{-1}
Application Test-T7 The proposed bridge piers are tested with an angle of 45-degree with the approach flow/revetment alignment. The objective of this test is to impinge the flow at the middle portion of WGB by introducing some interventions.	500-year Water Level 14.62 mPWD.

Model Setup

The WGB model is setup in the indoor model bed (100mX25m) of RRI using the available facilities. On the basis of topographic, bankline and bathymetric survey of July 2017 the model bed is constructed. The model setup consists of model bed preparation, water circulation system, construction of stilling pond, installation of point gauges and measurement of water level, discharge, velocity and outflow condition. The model setup for this model is done using the available indoor facilities of RRI. After calibration of the model the application tests are conducted with 100-year, 200-year & 500-year Return Period discharges. These data are used to measure the flow velocity, scour depth and float tracking. Existing bridge piers of the Bangabandhu Bridge is composed of racking piles. On the other hand, the proposed Bangabandhu Rail bridge pile groups are SPSP type with larger diameter as a whole. The model is tested with present bathymetry as well as assumed bathymetry which might occur in severe situation. The layout of the WGB model is shown in **Fig. 3.**

The scour hole around the structure is almost independent of bed material when the average velocity in the model is about 2-2.5 times the critical velocity for sand movement. But, like on the prototype, it is influenced only by the flow pattern, the geometry of the structure and cross-section. However, field observation as well as available formulae for scour estimation can also be taken into account during the design of the piers. Thus, live bed scour condition is ensured in the model at which equilibrium scour depth is reached when, over a period of time, the eroded material equals the supplied material from upstream. Sediment is fed into the model manually. Generally, the rate of sediment feeding for a particular model discharge is determined first by using sediment transport formulae/relation proposed by different researchers. For this model the sediment transport formulae proposed by Engelund and Hansen (1967) has been used to determine the initial sediment feeding rate. The sediment feeding rate, however, has been calibrated. The calibration of sediment feeding rate has been done by taking measurements of bed levels along a few cross-sections located at different parts of the model at a regular interval of time. Calibration of sediment feeding rate involves a condition where bed level remains more or less unchanged. It means whatever sediment is fed into the model is transported out of the model.

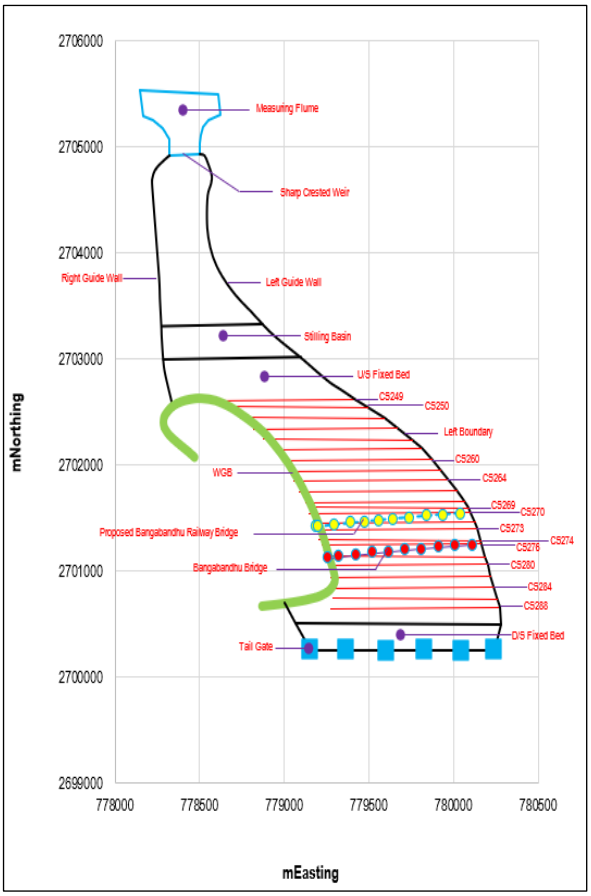

Fig. 3. Layout of the WGB Model.

As per selected scale it is found that the maximum equilibrium scour around the structure reaches within 10-15 hours in the model. One hour in the model corresponds to about 48 hours in the prototype which is computed based on Meyer-Peter and Muller Formulae that used in FAP study. That means the maximum scour which reaches in equilibrium within one day in the model is expected to happen in the prototype/in the field within 48 days. However, these are estimation. For more information, field measurement is more appropriate.

Table 5. Hydro-morphological Parameters for WGB Model

Description	Unit	Prototype	Model	Scale
Sectional length, L	m	3000	30	100
Sectional width at CS-Calibration (CS-280)	m	950	9.50	100
Sectional average water depth, h	m	4.64	0.046	100
Water surface slope, i	-	0.000075	0.000450	0.1667
Sectional average velocity, v	ms^{-1}	2.06	0.206	10
Sectional cross-sectional area, A	m^2	4178	0.4178	10000
Roughness height (K_s)	m	-	0.02500	-
Critical velocity by van Rijn, v_{cr}	ms^{-1}	-	0.100	-
Chezy roughness co-efficient, C	$m^{1/2}s^{-1}$	80	30	-
Sectional discharge, Q	m^3s^{-1}	8627	0.086	100000
Scour discharge, Q_s	m^3s^{-1}	-	0.126	82350
Median particle diameter, D_{50}	m	0.00016	0.000085	-
Dimensionless particle diameter, D*	-	3.584	1.904	-
Shields parameter, Θ	-	1.318	0.149	-
Critical Shields parameter, Θ_{cr}	-	0.067	0.126	-
Froude number, Fr	-	0.306	0.306	1
Shear velocity, v*	ms^{-1}	0.058	0.014	-
Critical shear velocity, v^*_{cr}	ms^{-1}	0.01317	0.01317	-
Particle Reynolds number, Re*	-	1.756	0.933	-
Reynolds number, Re	-	7984431	7984	-
Sediment Transport by Enguland-Hansen	m^3hr^{-1}	9190.80	0.22	42638
Critical velocity by Sheilds, v_{cr}	ms^{-1}	0.336	0.126	-
Fall velocity, w	ms^{-1}	0.01918	0.00541	-
Shear velocity/fall velocity, v*/w	-	3.046	2.643	-
Drag force co-efficient, C_d	-	0.47	0.49	-

Results and Discussion

Test T0-1 is done with existing bridge structure using bathymetry of July 2017 and measured field velocity. Test T0-2 is conducted with existing structure using simulated velocity corresponding to 100-yr discharge. Test T1-a is carried out with Bangabandhu bridge and 100-yr WL 14.41 mPWD & discharge 105,552 m^3s^{-1}. Maximum scour in this test is found about 13.2m (-8.9 mPWD) at pier P2 (existing). Test T1-b is carried out with existing bridge structure and 500-yr WL 14.62 mPWD & discharge 118,668 m^3s^{-1}. Maximum scour is 13.3m (-9.0 mPWD) at pier P2 (existing). This value is little bit more than that of test T1-a because of slightly more discharge & WL. To assess bridge-to-bridge pier & bridge-to-revetment interaction with existing & proposed bridge structure, test T2 is conducted with 100-yr WL 14.38 mPWD & discharge 105,552 m^3s^{-1}. In this test, maximum scour is 11.8m (-8.5 mPWD) at existing pier P2 and 13.3m (-6.70 mPWD) at proposed pier P3. Here scour is more around proposed pier as it experienced more obstruction and turbulence compared to the existing pier. In test T3, flow impinges at an angle of 53-degree with the proposed bridge piers having strengthened revetment of WGB using 200-yr WL 14.49 mPWD and discharge 111,000 m^3s^{-1}. In this case, maximum scour is 4.4 m (-15.1 mPWD) at existing pier P4 and 13.8m (-7.40 mPWD) at proposed pier P5.

Table 6. Maximum Scour and Velocity around Piers of WGB Model**.**

Test No.	Maximum scour (m) around existing bridge piers		Maximum scour (m) around proposed bridge piers		Maximum velocity (ms^{-1}) around existing bridge piers		Maximum velocity (ms^{-1}) around proposed bridge piers		Test conditions
	u/s	d/s	u/s	d/s	u/s	d/s	u/s	d/s	
T1-a	13.20 m (P2) (-8.9mPWD)	11.40 m (P3) (-3.8mPWD)	No pier Final bed level (-1.69mPWD)	No pier Final bed level (-1.69mPWD)	3.03 ms^{-1} (P1)	3.12 ms^{-1} (P1)	-	-	(a) With piers and revetment of Bangabandhu bridge. 100-yr WL 14.41 mPWD and discharge 105,552 m^3s^{-1}.
T1-b	13.30m (P2) (-9.0mPWD)	11.60m (P3) (-4.0mPWD)	No pier Final bed level (-1.70mPWD)	No pier Final bed level (-1.70mPWD)	3.54 ms^{-1} (P1)	3.65 ms^{-1} (P1)	-	-	(b) With piers and revetment of Bangabandhu bridge. 500-yr WL 14.62 mPWD and discharge 118,668 m^3s^{-1}.
T2	11.80m (P2) (-8.50mPWD)	11.80m (P2) (-8.60mPWD)	13.30m (P3) (-6.70mPWD)	10.30m (P3) (-4.0mPWD)	3.15 ms^{-1} (P1)	3.15 ms^{-1} (P2)	3.25 ms^{-1} (P2)	3.57 ms^{-1} (P2)	Test to assess bridge-to-bridge pier & bridge-to-revetment interaction with proposed bridge and Bangabandhu bridge and piers of proposed bridge. 100-yr WL 14.38 mPWD and discharge 105,552 m^3s^{-1}.
T3	3.70m(P4&P5) (-15.1mPWD & -14.9mPWD)	4.40m (P4) (-15.1mPWD)	13.80m (P5) (-7.40mPWD)	12.30m (P6) (-25.8mPWD)	3.36 ms^{-1} (P3)	3.36 ms^{-1} (P2)	3.04 ms^{-1} (P5,6)	3.36 ms^{-1} (P4)	Test to assess bridge-to-bridge pier & bridge-to-revetment interaction with proposed bridge and Bangabandhu bridge having modified revetment and piers of BR bridge. 200-yr WL 14.49 mPWD and discharge 111,000 m^3s^{-1}. Flow impinging at an angle of 53-degree with the proposed bridge piers. The model bed is prepared (-13.99 mPWD around the tip of WGB and -10.86 mPWD at other portion) as per design.
T4-a	-	-	-	-	2.41 ms^{-1} (P2)	2.51 ms^{-1} (P2,3)	2.51 ms^{-1} (P3)	3.25 ms^{-1} (P3)	(a) Test to assess bridge-to-bridge pier & bridge-to-revetment interaction with proposed and existing bridge piers and revetment. This test is conducted with 500-yr WL 14.53mPWD and discharge 118,668 m^3s^{-1}. The pile cap of proposed SPSP bridge piers is raised to a level of 14.2mPWD from 1.2mPWD. Flow impinging at an angle of 45-degree with the proposed bridge piers.

Test No.	Maximum scour (m) around existing bridge piers		Maximum scour (m) around proposed bridge piers		Maximum velocity (ms^{-1}) around existing bridge piers		Maximum velocity (ms^{-1}) around proposed bridge piers		Test conditions
	u/s	d/s	u/s	d/s	u/s	d/s	u/s	d/s	
T4-b	27.5m (P3) (-21.0mPWD)	25.80m (P3) (-19.8mPWD)	39.4m (P3) (-31.9mPWD)	38.6m (P3) (-28.1mPWD)	-	-	-	-	(b) This test is same as test T4.a but additionally a temporary brick wall is provided to impinge the flow on the revetment and bridge piers.
T5	15.6m (P3) (-7.8mPWD)	14m (P3) (-6.5mPWD)	22m (P3) (-14.5mPWD)	21 (P3) (-13.3mPWD)	2.41 ms^{-1} (P3)	2.62 ms^{-1} (P3)	2.09 ms^{-1} (P2,3)	2.93 ms^{-1} (P2)	Test to assess bridge-to-bridge pier & bridge-to-revetment interaction with proposed & existing bridge piers and existing revetment only. This test is conducted with 100-yr discharge 105552 m^3s^{-1} and corresponding WL of 14.41mPWD. The pile cap of proposed SPSP bridge piers is kept at a level of 8mPWD. Flow impinging at an angle of 45-degree with the proposed bridge piers. Here the approach flow condition has been changed by providing a temporary brick wall to concentrate the flow around the u/s tip of revetment.
T6	14m (P2) (-10mPWD)	13.6m (P3) (-6.0mPWD)	31.7m (P3) (-23.6mPWD)	26.3m (P3) (-18.2mPWD)	0-3.68 ms^{-1} (P2)	3.57 ms^{-1} (P2)	3.36 ms^{-1} (P2)	4.52 ms^{-1} (P2)	This test is done with about 60-degree oblique flow angle of attack at the bridge corridor guide bund. To achieve this a char is developed in the model u/s of the proposed bridge. Flow impinging at an angle of 45-degree with the proposed bridge piers. This test is conducted with 100-yr, 200-yr & 500-yr WL which is respectively 14.38, 14.49 & 14.53 mPWD. The corresponding discharge is 105,552, 118,668 & 137036 m^3s^{-1}.
T7	3.5m (P4) (1.9mPWD)	1.5m (P3) (-7.5mPWD)	18.6m (P3) (-20.2mPWD)	11.3m (P3) (-18.8mPWD)	0.6-1.13 ms^{-1} (P4-P2)	1.35 ms^{-1} (P2)	1.35 ms^{-1} (P2)	1.77 ms^{-1} (P2)	This test is conducted using the bed level of test T6 after run but there are some changed in the bed level. The proposed bridge piers are tested with an angle of 45-degree with the approach flow/revetment alignment. The test is conducted with 500-yr WL 14.62 mPWD. The objective of this test is to impinge the flow at the middle portion of WGB by introducing some interventions.

Test T4.a is done with 500-yr WL 14.53 mPWD & discharge 118,668 m^3s^{-1} where the pile cap of proposed SPSP bridge piers is raised to a level of 14.2 mPWD from 1.2 mPWD. Test T4.b is same as test T4.a but here a barrier is provided to impinge the flow on the revetment and bridge piers. Maximum scour among the proposed & existing bridge piers occurred in test T4.b [39.4 m (-31.9 mPWD)] at u/s of proposed pier P3. This is due to the provision of barrier for impinging flow. In this test, maximum total scour around the existing bridge piers is 27.5m (-21.0 mPWD) at u/s of pier P3. The WGB model during running condition (T4.b) is shown in **Fig. 4.** The scour in the vicinity of proposed & existing bridge pies in WGB model (Test T4.b) is shown in **Fig. 5.** Test T5 is conducted with 100-year discharge of 105552 m^3s^{-1} and corresponding WL of 14.41 mPWD. The pile cap of proposed SPSP bridge piers is kept at a level of 8.0 mPWD instead of 14.2 mPWD. Here the approach flow condition has been changed by providing a temporary barrier as lateral boundary to concentrate the flow around the u/s tip of revetment. Maximum scour is 22 m (-14.50 mPWD) at proposed pier P3. Maximum total scour at the proposed pier P3 is 31.7m (-23.6 mPWD) of which about 20 m is general scour & confluence scour in test T6 which is conducted with 60-degree oblique flow attack at the bridge corridor guide bund. To achieve this, a char is developed in the model u/s of the proposed bridge. The objective of test T7 is to impinge the flow at the middle portion of WGB by introducing some interventions. Here maximum scour is found 18.6 m (-20.2 mPWD) at pier P3 (proposed). Maximum velocity among the proposed & existing bridge piers is found in test T6 (4.52 ms^{-1} at proposed pier P2). Maximum scour around the WGB occurred in test T5 [29.5 m (-23.5 mPWD) around the u/s tip of revetment of WGB]. Maximum velocity around the WGB occurred in test T3 which is 5.3 ms^{-1} at the u/s tip of WGB. Maximum scour and velocity found around the existing and proposed bridge piers under different test scenarios can be seen in **Table 6.** Maximum scour and velocity around the revetment of WGB is shown in **Table 7.**

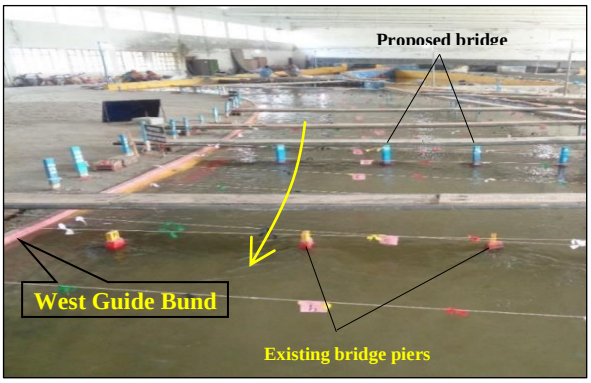

Fig. 4. WGB model during running condition (T4.b).

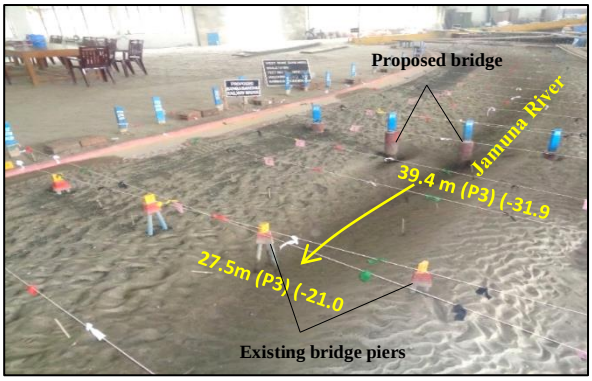

Fig. 5. Scour in the vicinity of proposed & existing bridge pies in WGB model (Test T4.b).

Table 7. Maximum Scour and Velocity around Revetment of WGB Model

Test No.	Maximum scour (m) around WGB	Maximum velocity (m/s) around WGB
T1-a	-	3.49m/s (90m away from R/B along CS-273)
T1-b	10.2m (-4.9mPWD) (160m away from R/B, CS-284)	3.76m/s (90m away from R/B along CS-273)
T2	9.3m (-4.7mPWD) (119m away from R/B, CS-282)	3.57m/s (80m away from R/B along CS-273)
T3	6.3m (-16.6mPWD) (5:778504mE, 2702818mN)	**5.3m/s (tip of WGB)** **(778605mE, 2702812mN)**
T4-a	-	4.21m/s (180m away from R/B along CS-250)
T4-b	19.1m (-9.9mPWD) (208m away from R/B along CS-250)	-
T5	**29.5m (-23.5mPWD)** **(778504mE, 2702818mN)**	3.46m/s (95m away from R/B along CS-250)
T6	12.6m (-8.6mPWD) (140m away from R/B along CS-278)	3.89m/s (95m away from R/B along CS-250)
T7	6.2m (-6.7mPWD) (165m away from R/B along CS-254)	1.88m/s (120m away from R/B along CS-254)

Conclusion

In the WGB model, 2 (two) calibration and 7 (seven) application tests are completed. The maximum scour occurred around proposed & existing bridge piers in test T4.b. This test is conducted with 500-yr WL 14.53 mPWD and discharge 118,668 m^3s^{-1}. The pile cap of proposed SPSP bridge piers is raised to a level of 14.2 mPWD from 1.2 mPWD. Here a temporary brick wall is provided to impinge the flow on the revetment and bridge piers. The maximum total scour around the proposed bridge piers is 39.4m (-31.9 mPWD) at u/s of pier P3 and 38.6m (-28.1 mPWD) at d/s of pier P3. The maximum velocity is 3.25 ms^{-1} at d/s of pier P3. The maximum total scour around the existing bridge piers is

27.5m (-21mPWD) at u/s of pier P3 and 25.8m (-19.8 mPWD) at d/s of pier P3. The maximum velocity is 2.51 ms^{-1} at d/s of pier P2, P3.

The maximum scour around the guide bund occurred in test T5 which is conducted with 100-yr discharge 105,552 cumec and corresponding WL of 14.41 mPWD. The pile cap of proposed SPSP bridge piers is kept at a level of 8mPWD instead of 14.2 mPWD. Here the approach flow condition has been changed by providing a temporary brick wall as lateral boundary to concentrate the flow around the u/s tip of revetment. The maximum scour is 29.5m (-22.60 mPWD) at the u/s tip of WGB [at point 5 (778504mE, 2702818mN)]. The maximum velocity around the guide bund occurred in test T3 which is conducted with 200-yr WL of 14.49 mPWD and discharge of 111,000 m^3s^{-1}. The proposed bridge piers are tested with an angle of 53 degree with the approach flow/modified revetment alignment. The maximum velocity is 5.3 ms^{-1} at the u/s tip of WGB [at point 7 (778605mE, 2702812mN)].

Maximum total scour at the proposed bridge piers is 30.6m (-22.5 mPWD) (u/s of pier P3) of which about 20m is general scour & confluence scour in test T6 which is done with about 60 degree oblique flow angle of attack at the bridge corridor guide bund. To achieve this a char is developed in the model u/s of the proposed bridge. This test scenario is selected as per guidelines of RRI's outsourcing Senior Design Engineer and discussing with the RTW specialist of the BRBP. Maximum total scour at the existing bridge piers is 14m (-10 mPWD) (u/s of pier P2). Maximum velocity around the proposed bridge piers is 4.54 ms^{-1} (d/s of pier P2) and around the existing bridge piers is 3.68 ms^{-1} (u/s of pier P2). The maximum scour depth found in the physical model conducted at RRI is 29.5m around the WGB and 39.4m around the proposed rail bridge pier. The maximum scour depth calculated by Hire method is 33m at the WGB & 20m at the proposed rail bridge pier. The scour depths obtained by physical model testing differs to some extent from Hire method.

The assessment of the bridge-to-bridge and bridge to RTW interactions are given below:

Existing Bridge- Scour

It is observed in general that with the same bathymetry and approach flow condition, the proposed rail bridge piers experienced more scour than the existing bridge piers since the proposed rail bridge experienced more obstruction and turbulence due its location, shape and size compared to the existing piers.

Existing Bridge- Velocity

The change in velocity to the existing bridge due to the proposed bridge is not noticeable under the tested planforms and flow conditions although the two bridges are only 300 m away from each other.

Existing Bridge- Deposition

Deposition tendency is observed between the two bridges in the model study due to the obstruction of flow.

WGB- Velocity

The change in velocity at the WGB due to the proposed bridge is not noticeable under the tested planforms and flow conditions although the same guide bund will be used for two bridges.

WGB- Scour/Deposition

The WGB model is constructed with sectional width. Moreover, different modelling techniques are adopted to create severe condition in the model. So, aggradation and degradation tendency as a whole is not possible to report. Scour & deposition both observed irregularly in WGB model and it was due to the different tested flow conditions and planforms.

Performance of Modified Design of Revetment

The modified design of the revetment is found to work effectively.

References

Cheremisinoff, P. N. (1988). Civil Engineering Practice, Technomics Publishing Company, Lancaster (1988), Vol. 2.

Engelund, F. and Hansen, E. (1967). A Monograph on Sediment Transport in Alluvial Streams. Teknish Forlag, Copenhagen, p. 62.

HIRE Equation (2024). HEC-RAS River Analysis System, Version 6.5, Exported - April 2024.

Melville, B. W. and Sutherland, A. J. (1988). Design Method for Local Scour at Bridge Piers, *Journal of Hydraulic Engineering*. 114(10): 1210-1226.

Qadar, A. (1981). The Vortex Scour Mechanism at Bridge Piers, Proceedings of the Institution of Civil Engineers, 71(8443): 739-757, Part 2.

Shen, H. W. (1971). River Mechanics, Colorado State University, Ft. Collins, Colorado. USA, Vol. 2.

Shen, H. W., Schneider, V.R. and Karaki, S. (1969). Local Scour around Bridge Piers, Proceedings of ASCE, 95(6): 1919-1940.

USDT (1993). Evaluation Scour at Bridges, Hydraulic Engineering, Circular No. 18, Rep. No. FHWA-IP-90-017, U. S. Department of Transportation, Federal Highway, Washington, D. C.

Technical Journal
River Research Institute ISSN: 1606-9277

A STUDY ON OPTIMIZATION OF RIVER TRAINING AND BANK PROTECTION WORK FOR PAIRA BRIDGE PROTECTION

A. K. M. Ashrafuzzaman[1*], M. J. Islam[1], M. Shahabuddin[1], S. K. Ghosh[1], M. Tofiquzzaman[1], M. K. Eusufzai[2], M. Moniruzzaman[3,4] and M. E. A. Mondal[5]

Abstract

A study was undertaken to optimize the river training and bank protection work for the safeguard of the bridge on the Paira River on Barisal-Patuakhali Road using scale modelling. About 3.0 km river reach including the bridge was reproduced in this study. The study shows that the length of the revetment required along the Paira river bank is 921 m & 554 m respectively at the upstream & downstream of the Varani khal mouth. The curved length of the upstream & downstream termination of revetment in the Paira river at the crest (top) of embankment is 41.9 m, at the inner side (end of slope pitching) 60.2 m and at the outer side (end of launching apron) 206.8 m. The research also reveals that maximum local scour near the revetment is 19 m (-52.5 mPWD), Pier No.18 experiences maximum local scour around it which is 8m (-30.5 mPWD). It is found that maximum velocity around the revetment and bridge piers is 3.04 ms^{-1} and 2.88 ms^{-1} respectively. Maximum velocity of 2.2 ms^{-1} is found around the pier no. P18 and maximum velocity is 3.1 ms^{-1} at the downstream termination of revetment with 100-year return period discharge. The maximum velocity along the left bank at upstream of bank revetment is found 2.62 $ms^{-1}$and at downstream of it is 3.04 ms^{-1}. Severe flow concentration at the left bank of Paira River adjacent to the Varani khal and Paira bridge is observed with present planform and ebb flow condition.

Keywords: *Bridge, Bank protection, Optimization, Pier, Revetment, River training, Scour, Velocity.*

Introduction

At present, Paira Bridge is constructed over the Paira River. But the model study was done at RRI before its construction in the real field. The bridge is constructed as per recommendations based on model study conducted at RRI. The objectives of the model study were to find out the maximum scour around the bridge piers, sheet piles, abutments etc. with detail analysis and give necessary recommendations with priorities after installing sand on river bed, to find out the maximum scour around the river training structures with detail analysis and give necessary recommendations, to find out the maximum velocity around the structures and river behaviour around the bridge during peak flooding condition, to find out the flow field around the structures and to find out the scour and sedimentation around the structures and also to suggest the dredging area sedimentation phenomenon occurred by bed loads. The bridge should be protected in a manner to guarantee the stability of the bridge for its intended design life. Under the above circumstances, it was mandatory to carry out research through scale modelling at RRI to address the present and future existing problems. The river width at the ferry terminal is about 450m (as per survey) and the river is a tidal one with reported tidal variation of (+/-) 2m. The Paira River originates from Pandab River in Koloskati union of Bakerganj upazilla of Barisal district. The river flowing down southwards by the side of Lebukhali, meets the Patuakhali River just at the upstream of the ferry terminal and the combined flow moves further down as Paira River and crosses Amtoli of Barguna district. The river is about 90km long. Its recorded depth at Amtoli was 20m in monsoon and 12.5m in winter. Its catchment area is reported to be 557 km^2. The normal direction of flow is from north to south. The existing ferry ghat is located just below the confluence of the Paira and Patuakhali rivers. At proposed bridge location the maximum depth from water surface was about 43.4 m. Deepest elevation of river bed at bridge location was (-) 42.4 mPWD. It moves further southwards and falls in the Bay of Bengal as Burisshawr River. (RRI, 2016)

Design discharge at HFL 3.24 mPWD was 12,697.94 m^3s-1 at proposed bridge location and the corresponding average velocity 1.57 ms^{-1} were mainly considered in the model study (Volume I, Hydraulic and Morphological Study Report, 2014, Paira Bridge in Bangladesh). But other WL and discharge were also used for 25, 50 & 100-year return period as advised and supplied by Mr. Tapas Das, Senior Hydraulic/River Training Engineer of ICT Ltd. India. The slope was 8.27cm.km^{-1} within the study area, which was considered to estimate the water level at the proposed bridge location. As per requirement, RRI conducted test runs to determine the maximum scour and velocity around the bridge piers & bank protection works and to optimize the bank protection works. It is required to make proper Environmental Management Plan (EMP) and Environmental Impact Assessment (EIA) due to construction of Paira bridge at Lebukhali area under Patuakhali district. Md. Hamidul Islam et al, 2014 studied the EMP due to industrialization at Lebukhali area under Patuakhali district. According to them, enhancement of tree plantation programs, dredging of river, waste management and use of environmentally friendly technology ensures proper EMP. Islam *et al*. (2017) studied the EIA due to Paira bridge at Lebukhali area under Patuakhali district. According to them, the major environmental impact would be air pollution, water pollution and waste siltation, river erosion, migration, loss of agricultural land etc. They designed an EIA on the basis of ecological, physio-chemical and human interest for construction of bridge. They also prepared EMP to minimize and control of negative impacts during pre-construction, construction and operation/management stages for its sustainability. The study found that there were no significantly sensitive ecological, physicochemical socio-cultural impact in the area. The environmental impact value was estimated +2 (Positive two) shows the acceptance of this project. This bridge will help to mitigate the transportation

[1] Hydraulic Research Directorate, River Research Institute, Faridpur-7800, Bangladesh.
[*] Corresponding Author: (E-mail: ashrafcebuet89@gmail.com)
[2] Dhaka Laboratory, River Research Institute, Dhaka-1205, Bangladesh.
[3] Geotechnical Research Directorate, River Research Institute, Faridpur-7800, Bangladesh.
[4] Institute of Water and Flood Management, Bangladesh University of Engineering and Technology, Dhaka-1000, Bangladesh.
[5] Administration and Finance Directorate, River Research Institute, Faridpur-7800, Bangladesh.

problem as well as increase the socio-economic development of southern coastal region of Bangladesh.

Alam *et al.* (2020), studied the use of high strength concrete (C-60) in Paira bridge (Lebukhali bridge), Bangladesh. They observed high cement content, low water cement ratio, high quality materials, chemical admixtures and mineral admixtures such as silica fume, fly ash and slag with appropriate proportion would result in a high strength concrete. Proper curing of concrete is also necessary in this regard. Selection of mix proportion for concrete grade-60 was finalized in Paira bridge after doing many trial mixes with low water cement ratio and higher cementitious material since these two are the key way to obtain high strength concrete. High strength concrete like C-60 can be used in large infrastructure for its added advantages.

Paira Bridge is one of the first bridges in Bangladesh to have a bridge health monitoring system. The length of the bridge is 1.48 km. The bridge has been constructed at a height of 18.3 meters above the water level to facilitate navigation. Not more than one pillar of this bridge has been placed in the river. N. Alam *et al*. (2020) also studied the Bridge Health Monitoring System (BHMS) of Paira bridge. They concluded that life span of structures needs to be increased to ensure sustainable development. With proper health monitoring life of structure could be increased. BHMS give us opportunity to know about any structural damage in real time. So, it is possible to repair quickly and protect structure from greater damage. Proper use of BHMS would increase bridge sustainability. Beg and Beg (2013) tried to reduce the depth of scour by placing the riprap around the pier, providing an array of piles in front of the pier, a collar around the pier, submerged vanes, a delta-wing-like fin in front of the pier, a slot through the pier and partial pier-groups and tetrahedron frames placed around the pier. He also presented a detailed review of the up-to-date work on scour reduction around bridge piers including all possible aspects, such as flow field, scouring process, parameters affecting scour depth, time-variation of scour. Shunyi *et al.* (2019) presented the protective effect of one active countermeasure named an "anti-scour collar" on local scour around the commonly used cylindrical bridge pier. According to the experimental results, it can be concluded the application of an anti-scour collar alleviates the local scour at the pier effectively and the protection effect decreases with an increase in the collar installation height, but increases with an increase in the collar external diameter and the protection range.

Methodology

About 3.0 km length of the river including tentatively 1.5 km upstream and 1.5 km downstream of the proposed bridge was reproduced in the movable bed model. It was an undistorted model having horizontal and vertical scale 1: 100. Model bed and bank were composed of fine sand having d_{50} about 0.085mm. Maximum flood discharge (50-year return period) of about 12698 m^3s^{-1} was taken to investigate the model with two different velocity scales. One was Froudian discharge, and the other was scouring discharge for scour development. Froudian discharge provided the flow pattern and velocity field as a whole and the scour discharge focused on the scour simulation and sediment transport. The water level and velocity during spring tide and ebb tide were taken into account. This model was run with severe flow condition (flood discharge) in one direction only since the proper development of the local scour around the structure was concerned. Each test of the model continued about 16-20 hours until a dynamic equilibrium scour was reached.

Table 1. Hydro-morphological Parameters for the Paira Bridge Model.

Description	Unit	Prototype	Model	Scale
Length, L	m	4000	40	100
Top width at CSU27	m	956	9.56	100
Avg. water depth, h	m	10	0.10	100
Water surface slope, i	-	0.00008	0.00008	1
Average velocity, v	ms^{-1}	1.40	0.14	10
Cross-sectional area, A	m^2	9892	0.99	10000
Roughness height (K_s)	m	-	0.025	-
Critical velocity by van Rijn, v_{cr}	ms^{-1}	-	0.125	-
Chezy roughness co-efficient, C	$m^{1/2}s^{-1}$	60	30	-
50-yr discharge, Q	m^3s^{-1}	13861	0.139	100000
Scour discharge, Q_s	m^3s^{-1}	-	0.248	-
Median particle diameter, D_{50}	m	0.00008	0.000085	-
Dimensionless particle diameter, D*	-	1.79	1.90	-
Shields parameter, Θ	-	6.33	0.06	-
Critical Shields parameter, $Θ_{cr}$	-	0.13	0.13	-
Froude number, Fr	-	0.14	0.14	1
Shear velocity, v*	ms^{-1}	0.091	0.009	-
Critical shear velocity, v^*_{cr}	ms^{-1}	0.013	0.013	-
Particle Reynolds number, Re*	-	0.88	0.93	-
Reynolds number, Re	-	11798935	11799	-
Sediment Transport by Enguland-Hansen	m^3hr^{-1}	6307	0.09	72130
Critical velocity by Sheilds, v_{cr}	ms^{-1}	0.252	0.126	-
Fall velocity, w	ms^{-1}	0.0048	0.0054	-
Shear velocity/fall velocity, v*/w	-	18.88	1.67	-

There was a close water circulation system in the model controlled by discharge measurement weirs, tail gates for water level control, gate valve for water flow etc. The performance of each model test runs was analysed and evaluated and accordingly the next test run had been planned/finalized after discussing with the client to achieve a concluding recommendation. he model was calibrated on the basis of prototype water levels, flow velocities and sediment transport data. The sediment feeding in the model was done artificially for sediment balance in the model and it was done manually looking at the formation of the bed forms. Continuous monitoring of the model bed was done by taking soundings of the model bed. Generally, the rate of sediment feeding for a particular model discharge was determined first by using sediment transport formulae/ relation proposed by different researchers. For this model the sediment transport formulae proposed by Engelund and Hansen (1967) had been used to determine the initial sediment feeding rate. The sediment feeding rate, however, had been calibrated. The calibration of sediment feeding rate had been done by taking measurements of bed levels along a few cross-sections located at different parts of the model at a regular interval of time. Calibration of sediment feeding rate involved a condition where bed level remained more or less unchanged. It means whatever sediment is fed into the model is transported out of the model. In **Table 1**, the scale factors for the prototype and model have been obtained for different parameters (RRI, 2017).

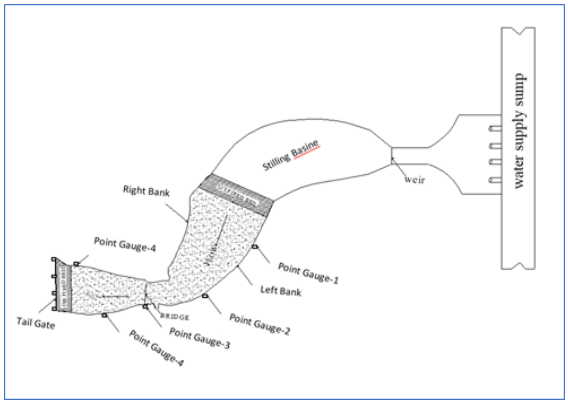

Fig. 1. Layout of the model**.**

The model was setup in the indoor model bed (100m X 30m) of RRI. The length of river reproduced in the model was about 3.0 km (1.5 km upstream and 1.5 km downstream of the proposed bridge and full width of the river). The model bed was constructed on the basis of topographic, bank and bathymetric survey of September 2016. After calibration of the model the application tests were conducted with 50-year return period discharge of 12,698 m^3s^{-1} at the bridge section and corresponding water level of 3.24 mPWD. These data were used to measure the flow velocity, scour depth and float tracking. The model setup consisted of model bed preparation, water circulation system, construction of stilling pond, installation of point gauges and measurement of water level, discharge, velocity and outflow condition. The model setup for this model was done using the available indoor facilities of RRI. The model layout is shown in **Fig. 1**.

Results and Discussion

Bank erosion is found in all the tests at the left bank, upstream of the Paira bridge. However, the proposed upstream termination for bank protection work is sufficient to protect the embayment of the bank protection works from bank erosion with present flow condition and planform **(Fig 2).** Bank erosion at the left bank downstream of protection works is also observed but it will not be harmful for the bank protection works. Maximum local scour measured near the bank protection works varies about 5.9m (-23.2 mPWD) to 19m (-52.5 mPWD) around the cross sections CS-16US (T5) and CS-06DS (T2) respectively **(Table 3).** Local scour is measured at bridge piers P17, P18 and P19 and in front of the bank protection structure in the region of cross section CS-20US to CS-10DS **(Table 4).** A typical cross- section showing the local scour near the bridge is shown in **Fig. 3** (T4).

Fig. 2. U/S termination of revetment prevents the embayment due to river bank erosion (T5).

Table 3. Summary of maximum local scour near the revetment in different tests.

Test No.	C/S No.	Dist. from L/B (m)	Final bed level (mPWD)	Initial bed level (mPWD)	Net scour (-) / deposition (+) (m)
T2	CS-06DS	110	-52.5	-33.5	-19
T3	CS-08DS	88	-44	-29.5	-14.5
T4	CS-06DS	82	-50.8	-34	-16.8
T5	CS-16US	71	-23.2	-17.3	-5.9

Table 4. Summary of maximum local scour around piers in different tests.

Test No.	Maximum scour, (m)	Initial bed level (mPWD)	Final bed level (mPWD)	Remarks
T2	-3.40	-20.3	-23.7	No protection works around P18
T3	-6.50	-22.50	-29.00	Mild protection works around P18
T4	-8.00	-22.5	-30.5	Mild protection works around P18
T5	-2.00	-27	-29	More protection works around P18

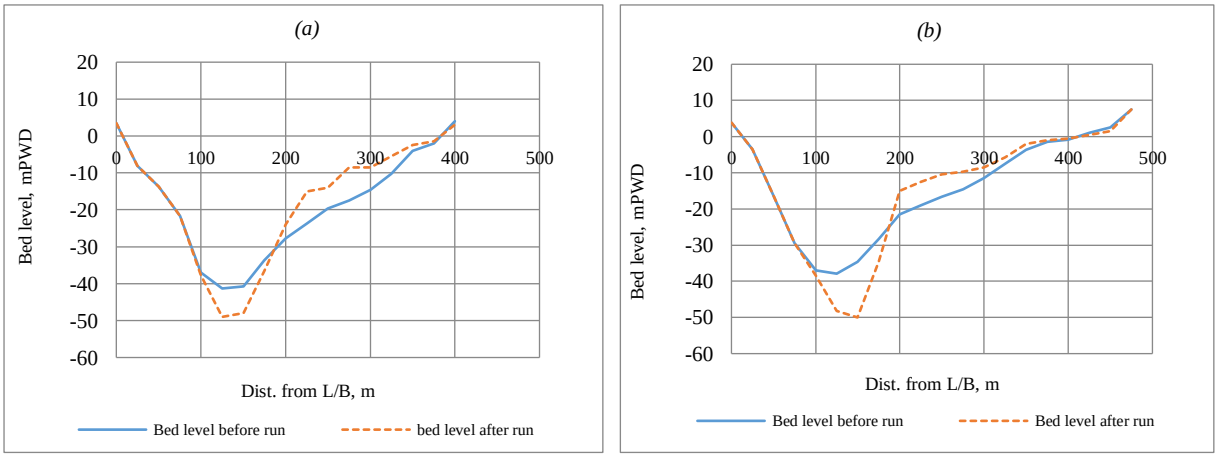

Fig. 3. Local scour at (a) u/s (CS-02) and (b) d/s (CS-02) of bridge in test run (T4).

There is sedimentation tendency at the right bank (CS-00 to CS-26DS) just opposite to the Paira bridge and also at Pier-19 for the present approach flow condition. The existing working jetty is also restricting the bank erosion at this location and accelerating sedimentation along the right bank (**Fig. 4**). This influences more flow concentration between the left bank protection works and the pier P18 after inclusion of the proposed structures. A typical cross section showing the local scour near the bridge is shown in **Fig. 5** (T5).

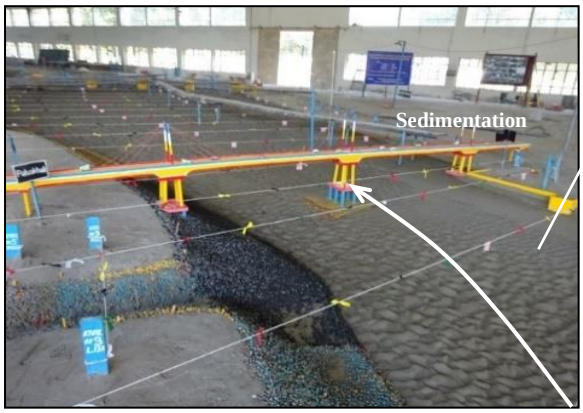

Fig. 4. A view of model bed showing the sedimentation at the right bank.

Scour depths have been found by using scale model tests and empirical formula as shown in **Table 5**. There are a lot of empirical formula to determine the scour around bridge piers. These empirical formulas have been selected randomly. The scour depths obtained from the model study are less than that of from empirical formula. There may be several reasons. The empirical formulas have some limitations where the values of some parameters are assumed. Scale modelling has also some limitations such as scale effects. As a result, sour depths did not match. Scale modelling can provide better results than empirical formula if scale effects are carefully assessed. For this reason, scale modelling is recommended for the vital water resources projects of the world. The project will not be economically viable if more scour depth than the required is considered for design. On the other hand, if the less scour depth is considered, the structure will be unsafe. Sometimes, it is necessary to visit the field condition by the designer. So, optimum scour depth will be considered from design point of view. In this case, the designer should carefully select the required scour depth around bridge pier considering the above factors. **Table 6** shows the comparison of scour, velocity and protective materials among different tests.

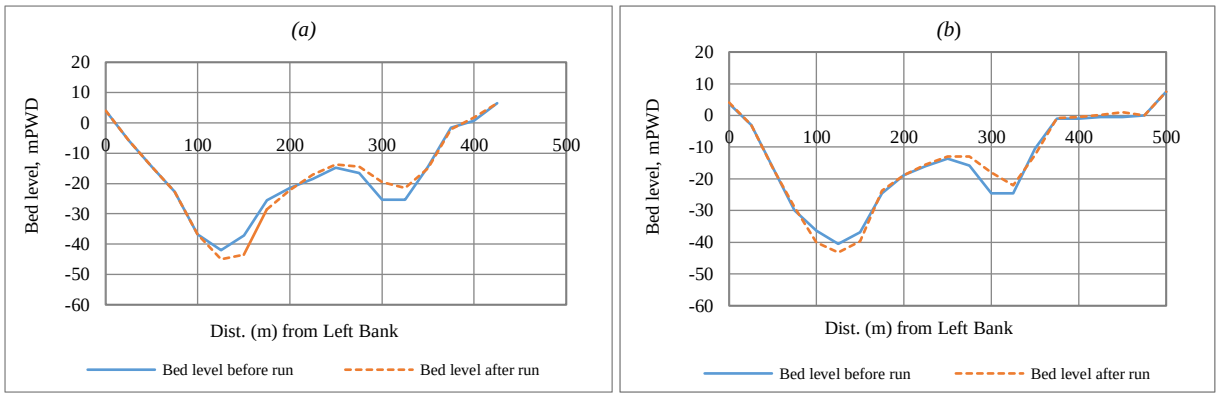

Fig. 5. Local scour at (a) u/s (CS-02) and (b) d/s (CS-02) of the bridge and the corresponding initial & final bed level in test T5.

Table 5. Comparison of Scour Depth by Using Scale Modelling and Empirical Formula.

*Scour determination by Empirical Formula around pier P18			Scour measured from model tests around pier P18		
Using Empirical Formula	Scour, m	Tests	Scour, m	Remarks
1) C.S.U. Formula $\frac{d_s}{y}=2\times k_1\times k_2\times k_3\times k_4\times(\frac{b}{y})^{0.65}\times(Fr)^{0.43}$ Here k_1 : Following pier shapes correction factor 1 k_2 : About the angle of incidence flowing correction factor 1 k_3 : About river bed condition correction factor 1.1 k_4 : About size of river bed material correction factor 1	6.73	T1	1.30	No pier protection
2) Neill Formula $\frac{d_s}{b}=1.5\times(\frac{y}{b})^{0.3}$	9.95	T2	3.40	No pier protection
3) Laursen Formula $\frac{b}{y}=5.5\times\frac{d_s}{y}\times[(\frac{d_s}{11.5\times y}+1)^{1.7}-1]$	11.2	T3	6.50	• Pier protected by cc blocks (top) and geo-bags (bottom) Unprotected space is more between toes of pier protection and revetment protection
4) Melville Formula $\Rightarrow Fr < 0.5$ $11.5\times y=\frac{d_s}{(1+\frac{0.182}{\frac{d_s}{b}})^{0.589}-1}$	11.22	T4	8.00	▪ Pier protected by cc blocks (top) and geo-bags (bottom) • Unprotected space is more between toes of pier protection and revetment protection
5) Froehlich Formula $\frac{d_s}{b}=0.32\times\Phi\times(\frac{b'}{b})^{0.62}\times(\frac{y}{b})^{0.46}\times Fr^{0.2}\times(\frac{b}{D_{50}})^{0.08}+1$ Here, Quadrangular pier : 1.3 Circular pier : 1.0 Sharp pier : 0.7	8.16	T5.3	2.00	▪ Pier protected by hard rocks (top) and geo-bags (bottom) ▪ Revetment and pier protection have been increased in test T5 relative to test T4. ▪ Unprotected space is more between toes of pier protection and revetment protection

Table 6. Comparison of Scour, Velocity and Protective Materials among Different Tests.

Test No.	Discharge and Water Level	Maximum scour around pier, m	Maximum scour around revetment, m	Maximum velocity around pier, ms^{-1}	Maximum velocity around revetment, ms^{-1}	Protective materials
T1	Q=13861 m^3s^{-1} WL=3.24 mPWD	-	-	1.84 (P17)	2.31	Only Sheet pile
T2	Q=13861 m^3s^{-1} WL=3.24 mPWD	-3.40 (P18)	-19 (-52.5 mPWD)	2.52 (P17)	2.35	Sheet pile + revetment (cc block + geo-bag).
T3	Q=13861 m^3s^{-1} WL=3.24 mPWD	-6.50 (P18)	-14.5 (-44.0 mPWD)	2.88 (P17)	2.94	Revetment (cc block + geo-bag) modified by RRI
T4	Q=13861 m^3s^{-1} WL=3.24 mPWD	-8.00 (P18)	-16.8 (-50.8 mPWD)	2.74 (P17)	2.64	Revetment [hard rock (200m u/s and200m d/s of pier P17 along left bank) + rest portion cc blocks] + geo-bag
T5.3	Q=15266 m^3s^{-1} (100-year RP) WL=2.50 mPWD	-2.00 (P18)	-5.9 (-23.2 mPWD)	2.20 (P18)	3.10	Revised design of revetment (hard rock + geo-bag) and dredged channel

Conclusion

The following conclusions can be drawn based on the scale model investigation.

Maximum local scour near the bank protection works is measured from 5.9 m (-23.2 mPWD) to 19 m (-52.5 mPWD). Pier no.17, 18 and 19 are in the river. Pier no.17 is located on the left bank which is protected by the hard materials, so no scour is occurred around it. Pier no.18 experiences local scour around its protection and its magnitude is within 2 m (-29 mPWD) to 8 m (-30.5 mPWD) at different locations. Pier no.19 is on the right bank side of the river, where maximum deposition of 1.9 m (-0.6 mPWD) is measured. So, with the present planform and flow condition, there is no possibility of scour around it in near future (within 2-5 years).

Maximum velocity measured around the bank protection works is within 2.35 ms^{-1} to 3.04 ms^{-1}. Maximum velocity around the piers is found to vary from 1.84 ms^{-1} to 2.88 ms^{-1}. Maximum velocity of 2.2 ms^{-1} is found around the pier no. P18. Maximum velocity of 3.1 ms^{-1} is measured at the d/s termination of revetment with 100-year return period discharge. Maximum velocity at different tests along the left bank upstream of the bank revetment is found from 1.81 ms^{-1} to 2.62 ms^{-1} and at the downstream it is 1.92 ms^{-1} to 3.04 ms^{-1}. Severe flow concentration at the left bank adjacent to the Varani khal and Paira bridge is observed with present planform and ebb flow condition. So, this location requires special attention.

The findings of model test in T5.3 (WL 2.50 mPWD and discharge 15266 m^3s^{-1} can be followed for river training works of 100-year return period which produces more severe condition and more representative than Test T4. River training/bank revetment is optimized based on the performance/effectiveness of various design in different tests and also considering the local scour value.

Recommendation

The following recommendations can be drawn based on the scale model investigation.

The length of the upstream bank revetment along the Paira River should be 921m from the centre of Varani khal mouth. The length of the downstream bank revetment along the Paira River is 554m from the centre of Varani khal mouth. The length of the upstream termination in the Paira River at the crest (top) of embankment is 41.9m, at the inner side (end of slope pitching) 60.2m and at the outer side (end of launching apron) 206.8m. The length of the downstream termination in the Paira River is same as upstream termination.

References

BUET and IWM (2008). Manual on Hydrologic and Hydraulic Design of Bridges, Bangladesh University of Engineering & Technology, Dhaka 1000 and Institute of Water Modelling, Mohakhali, Dhaka 1206.

BWDB (1993). Guide to planning and design of river training and bank protection works, design manual. Bangladesh Water Development Board, Ministry of Water Resources, Government of the People's Republic of Bangladesh, Dhaka.

Engelund, F. and Hansen, E. (1967). A Monograph on Sediment Transport in Alluvial Streams. Teknish Forlag, Copenhagen, p. 62.

Hydraulic and Morphological Study Report, Volume I, 2014, Paira Bridge in Bangladesh.

Islam, M. H., Rani, C. and Jahan, R. (2014). Study on environmental management plan (EMP) of proposed leather industry in Lebukhali, Patuakhali, published in the International Journal of Renewable Energy and Environmental Engineering, Vol. 02, No. 04, October.

Islam, M. S., Majumder, M. S. I., Hasan, I., Yeasmin, T., Islam, M. K., Rahman, M. M., Hawlader, N. H. and Sultana, I. (2017). Environmental Impact Assessment of Lebukhali Bridge Construction Project over the River of Paira, Bangladesh. *Journal of Energy, Environmental & Chemical Engineering.* 2(1): 10-15. https://www.doi.org/10.11648/j.jeece.20170201.13

Beg, M. and Beg, S. (2013). Scour Reduction around Bridge Piers: A Review. *International Journal of Engineering Inventions.* 2(7): 07-15.

Alam, N., Shajib, A. S., Hasan, K. and Elahi, M. N. (2020). Use of high strength concrete (C-60) in Paira bridge (Lebukhali bridge), Bangladesh. IABSE-JSCE Joint Conference on Advances in Bridge Engineering-IV, August 26-27, 2020, Dhaka, Bangladesh ISBN: 978-984-34-8313-3.

Alam, N., Shajib, A. S., Hasan, K. and Mamun, M. A. (2020). Bridge health monitoring system. IABSE-JSCE Joint Conference on Advances in Bridge Engineering-IV, August 26-27, 2020, Dhaka, Bangladesh ISBN: 978-984-34-8313-3.

RRI (2017). Physical model investigation for the protection of Paira Bridge over the river Paira under Patuakhali district, Final Report.

RRI (2016). Physical model study for the protection of Paira Bridge over the river Paira under Patuakhali district, Interim Report.

Wang, S., Wei, K., Shen, Z. and Xiang, Q. (2019). Experimental Investigation of Local Scour Protection for Cylindrical Bridge Piers Using Anti-Scour Collars. Department of Bridge Engineering, Southwest Jiaotong University, Chengdu 610031, China, published in the MDPI (Multidisciplinary Digital Publishing Institute).

Viaduct drawings (excluding foundations), vol. 4 of 5, March 2015 for consultancy services for design and construction supervision of Paira Bridge (Lebukhali Bridge) over the river Paira on Barisal-Patuakhali Road (N8), Bangladesh. (KFAED-841).

Technical Journal
River Research Institute ISSN: 1606-9277

IRON REMOVAL PERFORMANCE OF MULTI STAGE FILTRATION UNITS FROM GROUND WATER OF BANGLADESH

M. M. R. Mondol[1,2*]

Abstract

Iron is found widely distributed in both surface and ground waters in nearly all geographic areas. Dissolution of iron occurs by various processes and results in a variety of conditions regarding the concentration and chemical forms in which they are found in water. Iron in concentrations greater than 0.3 ppm stains plumbing fixtures and laundered clothes. Although discoloration from precipitates is the most serious problem associated with water supplies having excessive iron, foul tastes and odors can be produced by the growth of iron bacteria in water distribution mains. The iron problem has long been recognized in Bangladesh and many technologies have been developed for iron removal at municipal, community and household levels adopting the techniques of oxidation, sedimentation, precipitation and filtration process. To conduct this study six individual filtration units treating tube well water having iron concentrations ranging from 4.6 to 16 ppm installed at Sirajgonj, Cumilla and Jashore districts of Bangladesh have been selected. Crushed brick chips have been used as adsorptive media for the filtration units. Collected raw water samples and treated water samples from different chamber of the filtration units were tested in the laboratory for determining the concentration of residual iron and other relevant water quality parameters. The result reveals that higher the initial tube well water iron concentration, greater is the iron removal performance. Depending on raw water iron concentrations around 89.13 to 98.25 % iron removal performance have been achieved.

Keywords: *Concentration, DRF, Effluent, Iron, MSFU, Removal Performance, URF.*

Introduction

The presence of Fe and Mn in groundwater could confer colour, poor bitter taste, staining of laundry and plumbing fixtures (Mondol, 2020). Arsenic, on the other hand, is potential health hazard if its concentration is in excess of guideline value (Ahmed, 2005). Many arsenic containing ground water also contain significant level of iron and manganese due to natural geochemistry. The presence of iron in ground water is now considered to be a major problem throughout the world and produce numerous adverse effects. These problems are severe in the context of Bangladesh as groundwater is a vital source for the safe drinking water supply. In some places of Bangladesh the concentration of iron in ground water is at a much higher level than the limit acceptable to the rural people. People of those areas generally refuse to use tube well water and inclined to use pond and river waters (ITN-BUET, 2011).The national hydro-chemical quality surveys conducted by the British Geological Survey (BGS) and the Department of Public Health Engineering (DPHE) have shown that in Bangladesh, large numbers of wells also exceed permissible limits for iron (Fe) and manganese (Mn) (Habib, 2013). In this survey, a total of 3534 groundwater samples from throughout Bangladesh, excluding the Chittagong Hill Tracts, were analyzed for arsenic, manganese, iron and a wide range of other water quality parameters (BGS and DPHE, 2001). About half of the wells surveyed exceeded the Bangladesh drinking water standard for iron (1 mgl^{-1}), and about three quarters exceeded the permissible limit for Mn (0.1 mgl^{-1}). Above these levels, people may be unwilling to drink the water, and turn instead to a better-tasting, but microbiologically less safe, water sources (Hasan and Ali, 2010). Iron in concentrations greater than 0.3mgl^{-1} stains plumbing fixtures and laundered clothes. Although discoloration from precipitates is the most serious problem associated with water supplies having excessive iron, foul tastes and odors can be produced by the growth of iron bacteria in water distribution mains. These filamentous bacteria, using reduce iron as an energy source, precipitate it, causing pipe encrustations. Decay of the accumulated bacterial slimes creates offensive tastes and odors (Steel, 1960). Dissolved irons are often found in ground water from wells located in shale, sandstone and alluvial deposits. Impounded surface water supplies may also have troubles with iron (Mondol, 2009).

This full research work has been taken for investigating the performance of simultaneous removal iron, arsenic and manganese under different conditions using multiple up-flow and down-flow gravel bed. The present study is a part of the full research and will be confined only in analyzing iron removal performance.

Iron (II) (Fe^{2+}) and Manganese (II) (Mn^{2+}) are chemically reduced, soluble, invisible in ferrous form (Abanda, 2021) and may exist in tubewell waters or anaerobic reservoir bottom water in absence of DO, at high CO_2 concentration (>100 mgl^{-1}), at lower pH (<6.5), lower alkalinity (<130 mgl^{-1} as $CaCO_3$) and complex with organic materials. On the other hand, Iron (III) (Fe^{3+}) and Manganese (IV) (Mn^{4+}) are oxidized, insoluble, visible in presence of DO, at higher pH value (>7.5) due to release of CO_2 concentration (<10 - 15 mgl^{-1}), higher alkalinity and in absence of organic materials (ITN-BUET, 2011).To remove soluble iron it is generally accepted that an oxidation process followed by a suspended solids removal process is most effective. Usually, oxidation of soluble iron is accomplished by simple aeration or chlorination/potassium permanganate application. Coagulation - flocculation with sedimentation and filtration are employed as solid removal processes (Ahmed, 2005).

During 1990 a study was conducted by WHO, UNICEF and DPHE on improved iron plants which showed that iron removal was satisfactory (WHO *et al.*, 1990). The iron concentration was reduced to around 1.5 ppm from 15 ppm with average cleaning period of 12 days (with minimum of 5 days). With the same interval of cleaning it has been observed that the higher the concentration in raw water the higher the concentration in treated water but it was not exceeded 2.5 ppm (Mondol, 2009). For the elimination of iron from hand pump tubewell water, In 1981, Aowal (1981) proposed to introduce a spray aeration, a settling tank and a plain sand filter, all housed in a single chamber. Although an effective removal was achieved the length of run between cleaning was very short, less than 24 hours. The top layer of fine sand was

[1] Geotechnical Research Directorate, River Research Institute (RRI), Faridpur-7800, Bangladesh.
[2] Department of Civil Engineering, Bangladesh University of Engineering and Technology, Dhaka-1000, Bangladesh.
[*] Corresponding Author (E-mail: mrmondol68@gmail.com)

needed to be removed, washed and dried for the next use, which is laborious and time consuming (ITN-BUET, 2011). In 1985-86 over hundred iron removal units, which were originally designed by BUET under a research programme, were built at Sirajgonj and Comilla (Hasan, 2003). These units are reported to fail due to lack of community participation in all activities of the project, faulty construction of the unit, difficulty in cleaning the filter due to short filter runs, complicated design of the unit. In 1988, DPHE with the help of UNICEF, Dhaka Bangladesh, designed and constructed iron removal plant for hand pump tube wells in different parts of Bangladesh (ITN-BUET, 2011). Those plants were also failed due to faulty design of sedimentation chamber, where flocs were gradually settled and mixed with treated water (Hasan, 2003). Removal of iron is generally hastened and made more efficient by letting water trickle downward or rise upward through gravel or other relatively coarse heavy materials (Mondol and Ahmed, 2014).

The iron problem has long been recognized in Bangladesh, and many technologies have been developed for iron removal at municipal, community and household levels. Municipal Iron Removal Plants (IRPs) were first installed in Bangladesh during the early 1980s (BRTC, 2006). After the detection of arsenic in ground water, many municipal IRPs are now being designed and used for removal of both iron and arsenic (Mondol, 2020). In the backdrop of the discovery of arsenic in many areas of the country, community treatment units designed for removal of both arsenic and iron are becoming popular. Many NGOs are now installing different types of such community-based iron/ arsenic removal plants. However, most of the plants have been constructed without following any technical design parameters (BRTC, 2006). It would be interesting to see whether Mn is removed significantly in the currently operational iron and/or Fe-As removal plants, which have been designed primarily for removal of iron and/or arsenic. Therefore, more research works are needed to find out suitable technologies for simultaneous removal of iron, arsenic and manganese from ground water.

Methodology

To conduct the study six spots were selected in 3 zones on the basis of different hydro-geological condition and iron, manganese and arsenic concentration present in ground water as shown in **Fig.1**. These spots are located in Sirajgonj,Cumilla and Jashore district of Bangladesh. In each spot one Multi Stage Filtration Unit (MSFU) was constructed.

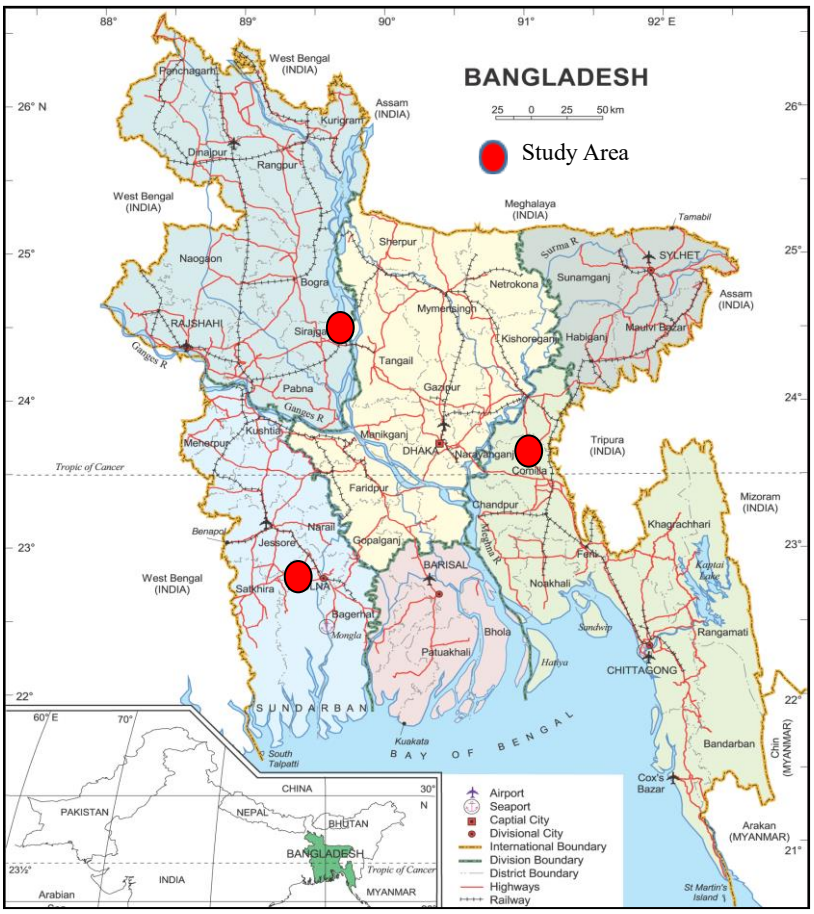

Fig.1. Location map of the study area.

The raw water and treated water from different locations of each MSFU were collected at suitable interval for subsequent analysis of iron, manganese, arsenic and other selected water quality parameters in the laboratory. Iron, manganese, arsenic concentrations were analyzed using Atomic Absorption Spectrophotometer (AAS). A number of samples were analyzed by HACH spectrophotometer for iron and manganese contents. Samples were collected in pre-washed

500 ml plastic bottles. Water samples in pre-washed bottles were acidified with 1 ml concentration Nitric acid, which were later used for analysis of dissolved arsenic, manganese and iron in the laboratory. The present study is a part of the full research and will be confined only in analyzing iron removal performance.

In the Construction of Multistage Filtration Units,a combination of down-flow at the beginning, an up-flow at the middle and a down-flow at the end have been incorporated. The MSFU is connected to the spout of tube well with a short piece of 75 mm PVC / flexible pipe as shown in **Fig. 2**.

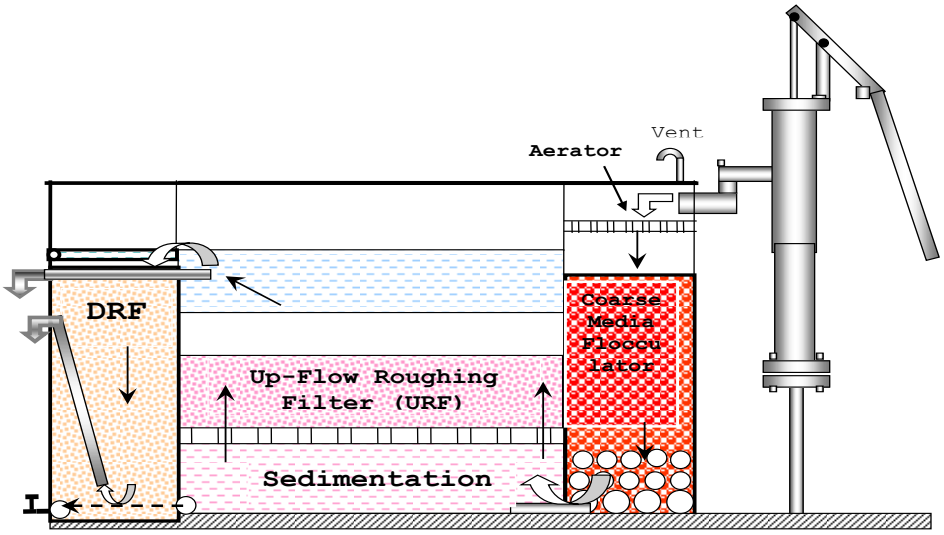

Fig. 2. Schematic diagram of the MSFU.

Table 1. Construction cost of MSFU.

Sl.No.	Item	Sub-item	Quantity	Unit price (TK.)	Estimated cost (TK.)
1	Bricks	Brick Flat Soling (BFS) for 5" brick wall	800 nos.	4.50	3600.00
2	Cement	Brick works, RCC works, CC works, etc.	9 bag	360.00	3240.00
3	Sand	Brick works, RCC works, CC works, BFS, etc.	80 cft	7.00	560.00
4	Khoa (#1 bricks)	RCC works, CC works,	40 cft	60.00	2400.00
5	M.S. Rod	RCC works	20 kg	45.00	900.00
6	Plumbing	3" PVC pipe, GI pipe, GI gate valve, GI socket, 3" Flexible inlet pipe, Strainer, Delivery pipe fittings, etc.	L.S.	-	2000.00
7	Burned bricks chips (khoa)	Flocculator, URF, DRF	40 cft	60.00	2400.00
8	Labour	Mason and Helper	6 days	(250+150)	2400.00
9	Local carriage		L.S.	-	1000.00
10	Miscellaneous		L.S.	-	500.00
Total TK./UNIT=					19000.00

Water entering the first chamber is distributed uniformly over the whole bed of course media through a porous thin ferro-cement plate placed on the top, resulting strip out of CO_2 and increase of pH value for the oxidation of soluble iron. Oxidation and subsequent precipitation of iron oxy-hydroxides occurs respectively on the top and within the interstices of coarse media which adsorbs arsenic oxyanions. Sinusoidal flow across the coarse media enhance collisions for the flocculation of precipitated particles. Comparatively larger flocculated precipitates settle at the bottom of the 2nd chamber. Maximum removal of precipitated particles occurs by sorption on to iron oxy hydroxides and mechanical straining during up-flow through the comparatively finer coarse media bed in the 2nd chamber, Up-flow Roughing Filter (URF). Final removal of precipitated particles occurs through sorption on to iron oxy hydroxides and mechanical

straining during down-flow through the comparatively finer coarse media bed in the 3rd chamber, Down-flow Roughing Filter (DRF). Crushed brick chips have been used as adsorptive media for the filtration units.

Construction Cost of MSFU

On the basis of considering the materials and others market value as on 2008-2009 Financial Year the construction cost of MSFU have been furnished for each unit (**Table 1**).

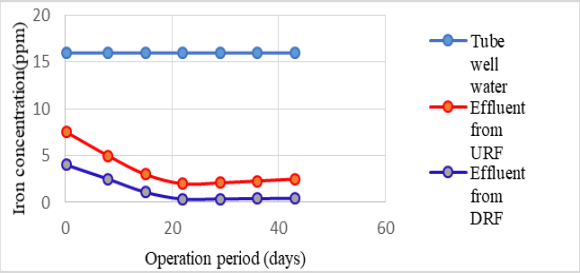

Fig. 3. Variation of average iron concentration in different treatment unit process of MSFU-1.

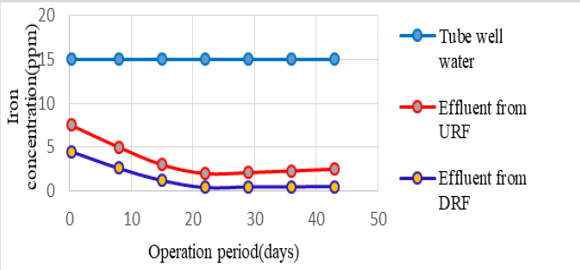

Fig. 4. Variation of average iron concentration in different treatment unit process of MSFU-2.

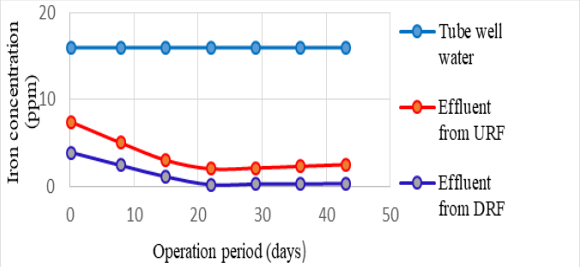

Fig. 5. Variation of average iron concentration in different treatment unit process of MSFU-3.

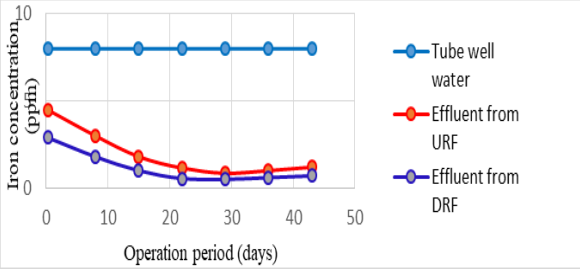

Fig. 6. Variation of average iron concentration in different treatment unit process of MSFU-4.

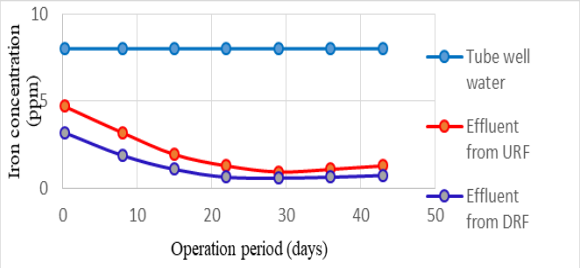

Fig. 7. Variation of average iron concentration in different treatment unit process of MSFU-5.

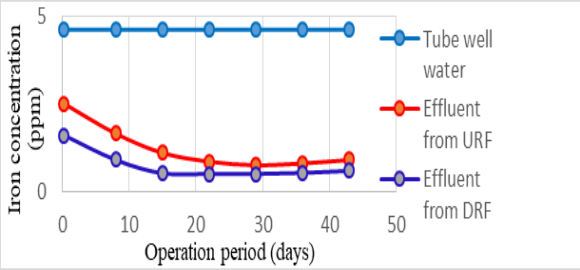

Fig. 8. Variation of average iron concentration in different treatment unit of MSFU-6.

Results and Discussion

i). Variation of Iron Concentration:

The variation of residual Fe concentration with length of filter run for MSFU-1, MSFU-2, MSFU-3, MSFU-4, MSFU-5 and MSFU-6 are presented in **Fig. 3-8** respectively.

Iron (II) (Fe^{2+}) and Manganese (II) (Mn^{2+}) are chemically reduced, soluble, invisible in ferrous form (Abanda, 2021) and may exist in tubewell waters or anaerobic reservoir bottom water in absence of DO, at high CO_2 concentration (>100 mgl^{-1}), at lower pH (<6.5), lower alkalinity (<130 mgl^{-1} as $CaCO_3$) and complex with organic materials. On the other hand, Iron (III) (Fe^{3+}) and Manganese (IV) (Mn^{4+}) are oxidized, insoluble, visible in presence of DO, at higher pH value (>7.5) due to release of CO_2 concentration (<10 - 15 mgl^{-1}), higher alkalinity and in absence of organic materials (ITN-BUET, 2011). The rate of ferrous iron oxidation is of the first order with respect to ferrous iron concentration present and partial pressure of oxygen. Aeration is sufficiently rapid only if it is catalyzed by accumulation of oxidation products (Fe_2O_3 and MnO_2) on a porous bed. Previously precipitated iron (Fe_2O_3) serves to catalyze the oxidation of iron. Moreover, hydrous oxides of metal, e.g. ferric oxide, Fe (III) and manganic oxide, Mn (IV) have high sorption capacities for un-oxidized metal ions including Fe^{++} ion (Mondol, 2009).

Fig.3 represents the variation of average iron concentration in the effluent of different treatment unit processes of the MSFU-1 (at Kodda, Sirajgonj). The raw water Fe content was 16 ppm and it decreased progressively in each chamber with time. With the passage of time the iron concentration in the effluent of URF and DRF decreased up to 2 and 0.36 ppm indicating iron removal performance of 87.5 % and 97.75 %, respectively with a influent flow rate of 12 $l.min^{-1}$. This was due to gradually adsorption of precipitated iron flocs on the

coarse media surfaces and gradually deposition of the flocs in the interstices. The removal was significant during the initial days with gradually less removal with time and then the reduction was slow in general.

Fig.4 represents the variation of average iron concentration in the effluent of different treatment unit processes of the MSFU-2 (at Chala, Sirajgonj). The raw water Fe content was 15 ppm and it decreased progressively in each chamber with time. With the passage of time the iron concentration in the effluent of URF and DRF decreased up to 2 and 0.41 ppm indicating iron removal performance of 86.67 % and 97.27 %, respectively with a influent flow rate of 12 l.min $^{-1}$.

Fig.5 represents the variation of average iron concentration in the effluent of different treatment unit processes of the MSFU-3 (at Homna, Cumilla). The raw water Fe content was 16 ppm and it decreased progressively in each chamber with time. With the passage of time the iron concentration in the effluent of URF and DRF decreased up to 2 and 0.28 ppm indicating iron removal performance of 87.5 % and 98.25 %, respectively with a influent flow rate of 12 l.min $^{-1}$.

Fig.6 represents the variation of average iron concentration in the effluent of different treatment unit processes of the MSFU-4 (at Polua, Jashore). The raw water Fe content was 8 ppm and it decreased progressively in each chamber with time. With the passage of time the iron concentration in the effluent of URF and DRF decreased up to 0.85 and 0.5 ppm indicating iron removal performance of 89.38 % and 93.75%, respectively with a influent flow rate of 12 l.min^{-1}.

Fig.7 represents the variation of average iron concentration in the effluent of different treatment unit processes of the MSFU-5 (at Sadipur, Jashore). The raw water Fe content was 8 ppm and it decreased progressively in each chamber with time. With the passage of time the iron concentration in the effluent of URF and DRF decreased up to 0.95 and 0.6 ppm indicating iron removal performance of 88.13 % and 92.5%, respectively with a influent flow rate of 12 l.min $^{-1}$.

Fig.8 represents the variation of average iron concentration in the effluent of different treatment unit processes of the MSFU-6 (at Sonakur, Jashore). The raw water Fe content was 4.6 ppm and it decreased progressively in each chamber with time. With the passage of time the iron concentration in the effluent of URF and DRF decreased up to 0.73 and 0.5 ppm indicating iron removal performance of 84.13 % and 89.13%, respectively with a influent flow rate of 12 l.min $^{-1}$.

As the rate of ferrous iron oxidation is of the first order with respect to ferrous iron concentration present and raw water iron concentration of MSFU-1, MSFU-2 and MSFU-3 are approximately same so the iron removal performance of these three plants are almost same. The iron removal performance of MSFU-4 was not observed as efficient as of MSFU-1, MSFU-2 and MSFU-3. Because the tube well water iron concentration of MSFU-4 was less than of MSFU-1, MSFU-2 and MSFU-3. Again as the tube well water iron concentration of MSFU-4 and MSFU-5 were same, so the iron removal performance of both plants were observed almost same. It is mentionable here that as the tube well water iron concentration of Sonakur (MSFU-6) was less than those of Kodda, Chalaj, Homna, Polua and Sadipur, so the iron removal performance of this plant was less than the others.

ii). Level of Performance:

On the basis of the above results and discussion the effect of raw water Iron concentration on Fe removal performance have been summarized (**Table 2**).

Table 2. Summary of the test results evaluating the effect raw water Iron concentration on Fe removal performance.

MSFU identification	Raw water Iron concentration (ppm)	Iron Removal %
MSFU-1	16	97.75
MSFU-2	15	97.27
MSFU-3	16	98.25
MSFU-4	8	93.75
MSFU-5	8	92.5
MSFU-6	4.6	89.13

The result reveals that higher the initial tube well water iron concentration, greater is the iron removal performance. Because the rate of ferrous iron oxidation is a function of ferrous iron concentration present in water. The level of performance have been presented in **Fig. 9**.

The trend of the iron removal performance with respect to initial iron concentration of tube well water achieved through the MSFU have been expressed through the equation,

$$y = 7.0146 \ln(x) + 78.48 \quad \text{Eq. (1)}$$

Where, y = percentage of iron removal, x = tube well water iron concentration (ppm).

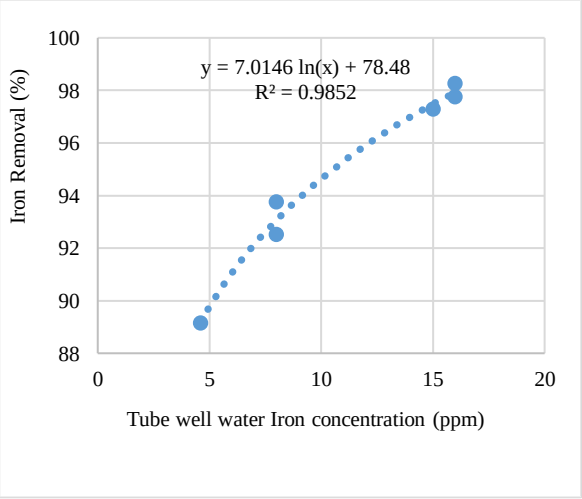

Fig.9. Effect of tube well water iron concentration on iron removal performance.

iii). Social Impact:

Presence of high concentration iron, arsenic and manganese in the tube well water discouraged the beneficiaries to use it for all domestic purposes. It was reported that before the construction of the MSFU(s) the tube wells were used only for toilet and cleaning purposes. After the construction of the

MSFU(s), the local people were attracted by the treated water quality and consequently the number of users were increased. The concentration of iron, manganese and arsenic in the treated water well below the acceptable limit of WHO guideline Value and Bangladesh Drinking Water Standard Value. As a result, people from the vicinity were inclined to use the treated water from the MSFUs and day by day number users were increasing since peoples from distant places started to use the treated water.

Conclusion

Through this study iron removal performance of Multi Stage Filtration Units (MSFU) treating tube well water having iron concentrations ranging from 4.6 to 16 ppm have been investigated. Investigation reveals that MSFU can be used effectively in removing iron from groundwater of Bangladesh. Depending on presence of raw water iron concentration around 89.13 to 98.25% iron removal performance was observed during the investigation. Iron removal performance was observed to be a function of initial iron concentration.

References

Abanda, V. (2021). Removal of Iron from Industrial Ground Water. *Trends Journal of Sciences Research.* 10.31586. 1-5. 10.31586/wastewater101005.

Ahmed, F. (2005). Development of community based arsenic & iron removal unit for rural water supply system, ITN Research Series 06, ITN-BUET, Dhaka, Bangladesh.

Aowal, A. F. S. A. (1981). Design of an iron eliminator for hand tube wells. *J. Indian W.W.A.* 13(1):65.

BGS and DPHE (2001). Arsenic Contamination of Groundwater in Bangladesh. Final Report, British Geological Survey and Department of Public Health Engineering, Government of the people's republic of Bangladesh.

BRTC (2006). Assessment of iron and manganese removal technologies for drinking water supplies in Bangladesh, Final Report, BRTC, BUET, Dhaka, Bangladesh.

Habib, M. E. (2013). Removal of manganese and arsenic from groundwater using manganese oxide coated sand. PhD Thesis, Department of Civil Engineering, Bangladesh University of Engineering and Technology (BUET), Dhaka, Bangladesh.

Hasan, S. and Ali, M. A. (2010). Occurrence of manganese in groundwater of Bangladesh and its implications on safe water supply. *Journal of Civil Engineering (IEB).* 38(2): 121-128.

Hasan, K. M. (2003). Development of a community based arsenic - iron removal unit, M.Sc. Eng. Thesis, Dept. of Civil Engg. BUET, Dhaka.

ITN-BUET (2011). Assessment of the performance of modified AIRU under different hydro-goelogical conditions, International Training Network (ITN) and Bangladesh University of Engineering and Technology (BUET), Dhaka, Bangladesh.

Mondol, M. M. R. (2020). Manganese removal from drinking water using roughing filtration. *Tech. J. River Res. Inst.*15(1):31-37.

Mondol, M. M. R. and Ahmed, F. (2014). Effect of tubewell water iron concentration on arsenic removal performance. *Tech. J. River Res. Inst.*12(2):127-135.

Mondol, M. R. (2009). Effectiveness of multistage filtration in removing iron, manganese and arsenic from ground water of Bangladesh, M.Sc. Engg. Thesis, Department of Civil Engineering. BUET, Dhaka, Bangladesh.

Steel, E. W. (1960). Water supply and sewerage. Fourth edition, Mc Graw-Hill Kogakusha, p. 217.

WHO, UNICEF, DPHE (1990). A report on study of improved iron plants.

Technical Journal
River Research Institute ISSN: 1606-9277

A STUDY ON THE IMPROVEMENT OF WATER RETENTION CAPACITY OF THE LOWER KARATOA RIVER UNDER BOGURA DISTRICT THROUGH DREDGING AND SETTING UP OF A PROPOSED REGULATOR

M. J. Islam[1*], A. K. M. Ashrafuzzaman[1], M. E. A. Mondal[2], S. M. A. Horayra[3], S. K. Ghosh[1], K. R. Ahmed[4], M. K. Eusufzai[5] and P. Kanungoe[1]

Abstract

The Lower Karatoa River originates from the Jamuneshwari-Karatoa (Upper Karatoa) River at Gobindogonj upazila under Gaibandha district and flows towards the west. From Gobindogonj upazila, the Lower Karatoa flows through Bagura district and finally falls into Bangali River under Sherpur upazila. At present, the Lower Karatoa River is fully silted up and dried up due to lack of water flowing through it. Therefore, a study is undertaken by River Research Institute (RRI) to support the design of proposed dredging and new regulator in the Lower Karatoa River using scale modelling. There is an existing regulator at its offtake whose sill level is around 3.0 meter above the water level of Upper Karatoa during dry season. A new regulator is proposed in addition to the existing regulator whose sill level is below the sill level of existing regulator to pass more flow in the Lower Karatoa River. The model is an undistorted model having horizontal and vertical scale 1:50. The study reach covers around 3.0 km of Upper Karatoa River and 1.5 km of Lower Karatoa River. The study reveals that one 4-vent regulator (each vent width 3.0 m) having sill level 14.50 mPWD is recommended to construct in the field just downstream of existing regulator. The recommended dredged channel has bottom width 15 m, side slope 1:2 and longitudinal slope 5.5 cmkm^{-1}. Maintenance dredging for two successive years as suggested is recommended.

Keywords: *Karatoa River, Maintenance dredging, Regulator, Scale model, Sill level, Silted up, Undistorted.*

Introduction

The Jamuneshwari-Karatoa is one of the oldest branches of the Teesta River. It flows towards South-East direction and is divided into two branches at Gobindogonj upazila of Gaibandha district. One-part flows towards the east through Katakhali River and falls into Bangali River. Another branch flows towards the west as Lower Karatoa. From Gobindogonj upazila, the lower Karatoa flows through Shibgonj, Bagura Sadar, Shahjahanpur & Sherpur of Bagura district and finally falls into Bangali River at Khanpur area of Sherpur upazila. This combined flow is called Karatoa and enters Sirajgonj District. **Fig.1** shows the satellite image around the study area. The flow path of the river Karatoa is of meandering type and its flow path has changed several times in the past and so its name. As a result, it has become difficult to identify the main branch of this river. At present it is considered as a part of the Deonai-Choralkatha-Jamuneshwari-Karatoa river system (RRI, 2022).

Karatoa River is an intriguing river, formerly the main channel of the Teesta, and perhaps a distributary of the Brahmaputra. In the Siyar-al-Mutakhkhirin it is recorded that this river was three times the size of the Ganges when Bakhtiyar Khalji invaded the Northern Region (1115 AD). Tectonic disturbances had broken it up into four distinct parts. The northern part, called the Dinajpur-Karatoa, is the main source of the Atrai. It rises in a marsh in Baikanthapur in Jalpaiguri (India), but also receives water from underground streams. In Khansama upazila its name changes to Atrai. The Dinajpur-Karatoa was connected with the Rangpur-Karatoa north of Khansama, but very little water now passes down that channel. The upper part of Rangpur-Karatoa originates in the Jalpaiguri district of India and is known as the Deonai-Jamuneshwari up to Gobindagonj upazila.

The Jamuneshwari-Karatoa flows in slight meanders south-southeast to Gobindagonj upazila where the mainstream turns east through the Katakhali and falls into the Bangali. The portion of the former river passing through Shibganj upazila is dry most of the year. It effectively separates the Rangpur-Karatoa from the Bogura-Karatoa. The latter river flows south past Bogura town till it joins the Bangali to make Phuljhor River, which falls into the Hurasagar.

The maximum discharge of the Bogura-Karatoa is below 3,000 cusec and has declined rapidly since the construction of the Brahmaputra Right Embankment. The fourth part, the Pabna-Karatoa, is a moribund riverbed near Handial. Various other channels are also pointed out as parts of the Old Karatoa. The ancient Karatoa must have been a large river. In Ven den Brouck's map of Bengal, prepared in 1660, it is shown as a large channel, and in the map of Rennell, prepared in 1776, it is still a major river. As late as 1810, Buchanan-Hamilton writes of it as a very considerable river. The decline, however, came so rapidly after the 1820 flood that the old banks of the river are distinctly traceable. The river was formerly sacred to the Hindus, as the derivation of the name shows. Kar (hand) and Toa (water) signified that the river was formed by the water, which was poured on the hands of Siva, when he married the mountain goddess Parvati. The system formed by the rivers Karatoa, Atrai, Gur, Gumani and Hurasagar has a total length of about 597 km and is free from tidal influence. (RRI, 2023).

In another study done by Chowdhury *et al.* (2017) the bathymetry of the Karatoya River was obtained using both echo-sounding and field survey techniques. The study showed that the river bed was highly variable and complex, with depths fluctuating from 1 meter to about 30 meters. The study also recognized several submerged sand bars and channels, and a few areas of erosion and siltation. There is little literature available on the 100-year return period flood discharge of the Karatoya River. However, a study was done to find out the flood frequency analysis of the Karatoya River using the L-moment method. The study found that the

[1] Hydraulic Research Directorate, River Research Institute, Faridpur-7800, Bangladesh.
[*] Corresponding Author: (E-mail: johurul1999@yahoo.com)
[2] Administration and Finance Directorate, River Research Institute, Faridpur-7800, Bangladesh.
[3] Office of the Director General, River Research Institute, Faridpur-7800, Bangladesh.
[4] Geotechnical Research Directorate, River Research Institute, Faridpur-7800, Bangladesh.
[5] Dhaka Laboratory, River Research Institute, Dhaka-1205, Bangladesh.

Generalized Extreme Value (GEV) distribution provided the best fit for the yearly highest flood data. The estimated 100-year return period flood discharge was found to be 3,438 m^3s^{-1}, which is a very important element for the design of hydraulic structures and flood control measures along the river.

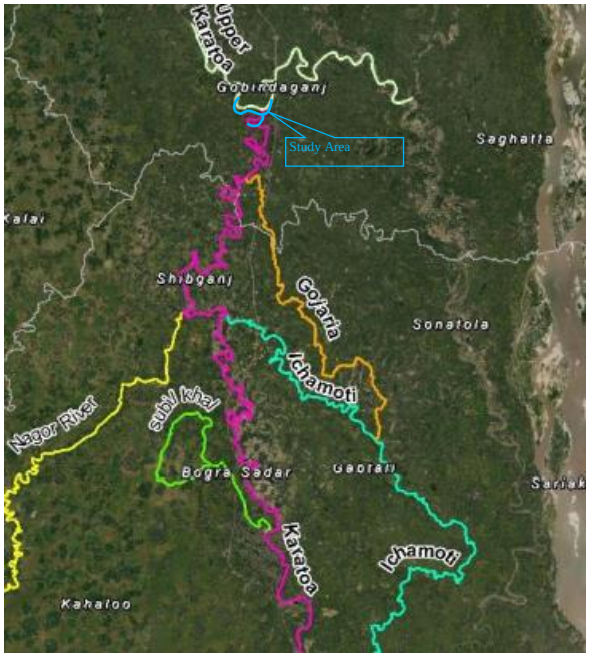

Fig.1. Satellite image around the study area (IWM, 2022).

The water quality of the Karatoya River is a subject of major concern due to man-made activities. The river is highly polluted, with high levels of faecal coliform bacteria, heavy metals, and organic pollutants. The poor water quality of the river has significant implications for human health, aquatic biodiversity, and ecosystem services. The Karatoya River has a rich biodiversity of aquatic plants and animals. Sarker *et al.* (2015) stated the river supports various commercially important fish species, such as the Rohu, Catla, and Mrigal. However, the biodiversity of the river is under threat due to habitat destruction, overfishing, and pollution. The Karatoya River is one of the important sources of livelihood for the local communities. Haque *et.al.* (2019) stated the river provides irrigation, fishing, and transportation water. The river also has cultural and religious significance, with several remarkable temples along its banks. However, the river is also a source of argument due to the sharing of water resources between all stakeholders, including farmers, fishermen, and industries. In short, the river faces versatile challenges, including pollution, habitat disintegration, and water resource issues, which require collaborative efforts from all stakeholders to address. Further analysis is also necessary to understand the dynamics of the river and develop effective management strategies to conserve and sustainably and fruitfully utilize its resources (RRI, 2023).

Methodology

An overall morphological model is constructed which includes a river stretch covering around 3km of Upper Karatoa River and 1.5 km of Lower Karatoa River. The model bed is prepared according to the bathymetric survey of December, 2022 as shown in **Fig.2.** In order to meet the scale conditions for reproducing the flow and sediment transport processes simultaneously as well as to meet the roughness condition of the model, an undistorted model with suitable geometric scales has been planned. The model layout is shown in **Fig.3**. The main purpose of this model is to provide support to the design of the dredging as well as suitable & optimal dredging alignment through the Lower Karatoa River. Moreover, the model will help to optimize the design of proposed regulator and fix up the sill level of the same.

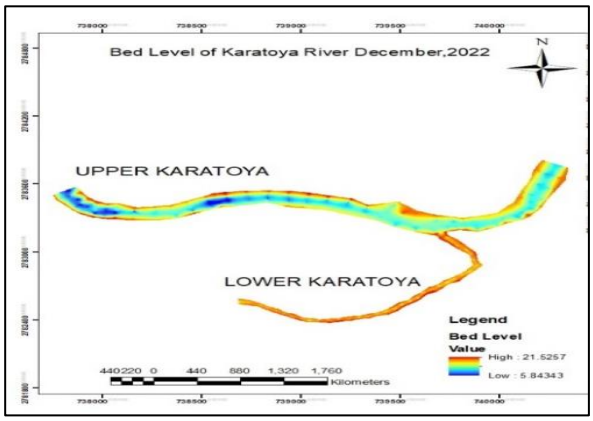

Fig. 2. Initial bathymetry of Karatoa River (Surveyed on December 2022).

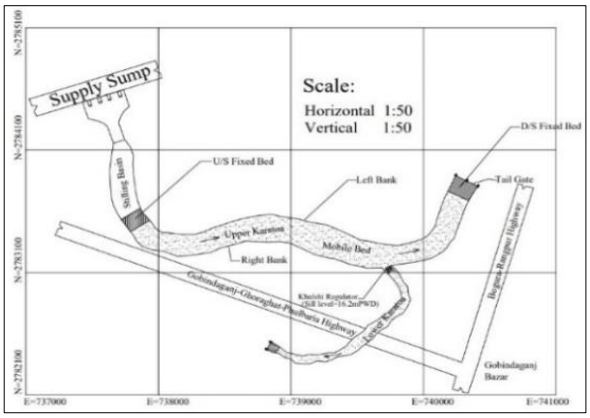

Fig. 3. The layout of the model.

Dredging has been proven as an effective process to control the deposited sediment to prevent flooding and make a pathway for the main channel flow (Gob *et al.*, 2005; Zinger *et al.*, 2011). The process also allows us to further solve engineering problems related to sedimentation and erosion in rivers, estuaries, and coastal seas (Van Rijn, 2005). A better prediction of erosion-sedimentation scenarios is inevitable to justify the long-term effectiveness of dredging, which could further promote the design strategies based on qualitative and quantitative analysis. Prediction of accurate scour depth and deposition of the braided river is methodologically very challenging because of the variation in simple path-length distribution resulting in over-scouring (Kasprak *et al.*, 2019).

The sustainability of any river dredging depends on the intelligent/well planned dredging. There is always a tendency of silting up of the dredged channel by sediment which comes from the adjacent region and acts as a kind of sheet that accelerates the silting process of the channel. It is found in some cases that the dredged channel has gotten silted up within one monsoon. Therefore, successful and sustainable river dredging involves a number of issues that must be understood and addressed well in dredge plan and design.

These issues involve various morphological changes such as formation of shoals, islands and chars, meandering tendency of the river, effect of construction of hydraulic structures, damages to the bank, effect of afforestation/deforestation and tectonic occurrences. Some of the issues may be addressed by modeling prior to preparation of dredge plan and design.

Post dredge monitoring of these issues may also be supplemented by model studies, as per requirements, to take timely corrective measures to maintain its morphology and to check local erosion damages. Physical modeling may be used as an important tool to assist in optimal dredge plan as well as to assist in post dredge monitoring. The effect of dredging around the surrounding areas and upstream and downstream of the same can be predicted by this model and effective dredging strategies may be devised.

Fig. 4. Installment of Khulshi regulator in the model.

Sediment is fed into the model manually. Generally, the rate of sediment feeding for a particular model discharge is determined first by using sediment transport formulae/relation proposed by different researchers. For this model the sediment transport formulae proposed by Engelund and Hansen (1967) has been used to determine the initial sediment feeding rate. The sediment feeding rate, however, has been calibrated. The calibration of sediment feeding rate has been done by taking measurements of bed levels along a few cross-sections located at different parts of the model at a regular interval of time. Calibration of sediment feeding rate involves a condition where bed level remains more or less unchanged. It means whatever sediment is fed into the model is transported out of the model. RRI open air model bed of dimension 100m × 80m is used for reproduction of the overall undistorted morphological model. The initial bathymetry of the model is reproduced based on the field survey data collected under the framework of this study. The model is a sand bed morphological model. The model has been constructed based on selected geometric scales. Khulsi regulator has been constructed in the model as per scale down and shown in **Fig. 4.** The construction of model involves a series of tasks. Besides selection of geometric scale ratios, the model bed has been prepared by uprooting the grass, dismantling of the previous works in the selected model bed and disposal of debris, removing the old sand from the model bed and filling the same with new fine sand having required median size, procurement of model construction materials, collection of bathymetric and bank line data etc.

Test Scenarios

The proposed test scenarios of the model along with various Test & flow conditions are mentioned in **Table 1.**

Table 1. Test Scenarios of the Model.

No.	Tests	Test conditions	Flow Conditions
1	Calibration test (T0)	Existing (without project) condition.	2.33 year return period discharge and corresponding water level.
2	Base run (T1)	Existing (without project) condition.	2.33 year return period discharge and corresponding water level.
3	Application test (T2)	Dredging in the Lower Karatoa River with bottom width 12m, side slope 1:1.5 and longitudinal slope 7 $cmkm^{-1}$ (as per DPP of BWDB).	2.33 year return period and other discharges and corresponding water levels .
4	Application test (T3)	Proposed regulator (4-vent, sill level 15.70 mPWD) in addition to existing regulator (3-vent, sill level 16.2 mPWD) and dredging in the Lower Karatoa River with bottom width 15 m, side slope 1:2 and longitudinal slope 7.0 $cmkm^{-1}$ proposed by IWM.	2.33 year return period and other discharges and corresponding water levels.
5	Application test (T4)	Proposed regulator (4-vent, sill level 15.7 mPWD) in addition to existing regulator (3-vent, sill level 16.2 mPWD) and dredging in the Lower Karatoa River with bottom width 15m, side slope 1:2 and longitudinal slope 7.0 $cmkm^{-1}$ proposed by IWM.	Design discharge (10 year return period) and corresponding water level.
6	Application test (T5)	Proposed regulator (4-vent, sill level 15 mPWD in addition to existing regulator (3-vent, sill level 16.2 mPWD) and dredging in the Lower Karatoa River with bottom width 15 m, side slope 1:2 and longitudinal slope 5.5 $cmkm^{-1}$ proposed by IWM.	2.33 year return period discharge, design discharge and other discharges and corresponding water levels.
7	Application test (T6)	Proposed regulator (4-vent, sill level 14.5 mPWD in addition to existing regulator (3-vent, sill level 16.2mPWD) and dredging in the Lower Karatoa River with bottom width 15m, side slope 1:2 and longitudinal slope 5.5 $cm.km^{-1}$. proposed by IWM.	2.33 year return period discharge, design discharge and other discharges and corresponding water levels.

Model Calibration

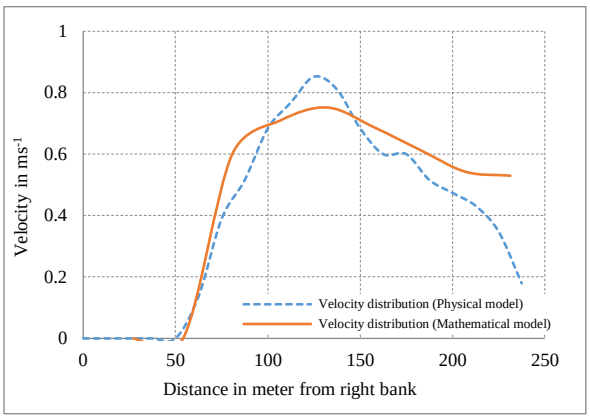

Fig. 5. Comparison of velocity distribution at 900m u/s of Khulshi Regulator for 2.33 year return period in test T0.

This test is carried out with existing (without project) condition. The purpose of calibration test is to calibrate the model i.e., to simulate the model with prototype conditions. Calibration test is done using peak discharge (Q=578 cumec) and corresponding water level. Model calibration is done to ensure that the model is able to reproduce the flow condition, morphological behavior and sediment transport in the field. The calibration of the model primarily aims to see whether the model is able to reproduce a more or less similar bathymetry as is measured during field survey under imposed conditions to bring about similarity between model and prototype in terms of flow and sediment transport simultaneously.

Base Run (T1)

Base run is conducted with existing regulator and model bathymetry obtained after calibration test has been used as initial bathymetry. **Table 2** shows discharge distribution between the Upper & Lower Karatoa River in Base Run T1. Some photographs of model before and during running conditions in base run (T1) are shown in **Fig. 6** & **Fig. 7** respectively.

Table 2. Discharge Distribution between the Upper and Lower Karatoa River in Base Run T1.

Discharge	Flow entered in to Upper Karatoa River upstream of confluence (cumec)	Flow passing through Lower Karatoa River (cumec)	% of flow passing through Lower Karatoa River
Peak flow from 2.33 year discharge	578	20	3.46%

Fig.6. A view of the model bed before test run in test T1.

Fig.7. Model under running in base condition (T1).

Application Test (T2)

This test has been conducted with existing regulator and having dredged channel of Lower Karatoa River. The dredged channel proposed in this test is shown in **Fig. 8.** A super-imposed cross-section between existing bed level and dredged channel proposed by DPP is shown in **Fig. 9** (near to the Khulshi regulator). **Table 3** shows discharge distribution between the Upper and Lower Karatoa River in test T2. Some photographs of model during & after running conditions in test T2 are shown in **Fig. 10** and **Fig. 11** respectively.

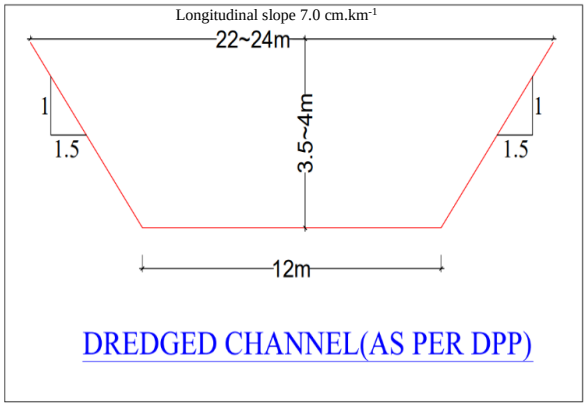

Fig. 8. Design of dredged channel for application test (T2).

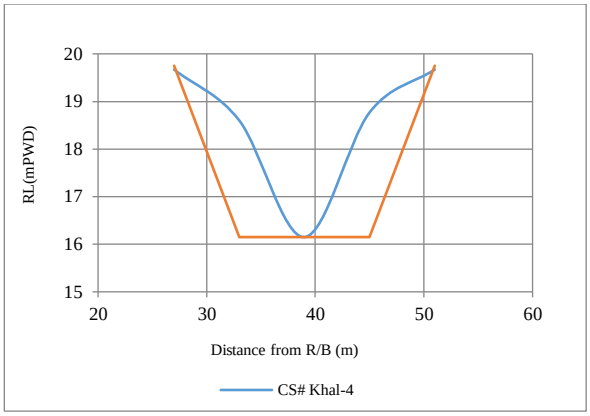

Fig. 9. Super-imposed cross-section between existing bed level and dredged channel (near to the Khulshi regulator) in test T2.

Fig. 10. Model under running condition (T2).

Fig. 11. Model bed after test run in the vicinity of existing regulator (T2).

Table 3. Discharge distribution between the Upper and Lower Karatoa River in test T2.

Name of Month	Flow entered in to the Upper Karatoa River upstream of confluence (cumec)	Flow passing through the Lower Karatoa River (cumec)	% of flow passing through the Lower Karatoa River
Jan	37.47	0	0.0
Feb	34.1	0	0.0
Mar	32.11	0	0.0
Apr	33.31	0	0.0
May	43.02	0	0.0
Jun	178.8	3.6	2.0
Jul	99.62	1.88	1.9
Aug	120.45	2.2	1.8
Sep	245.02	5.6	2.3
Oct	93.69	1.8	1.9
Nov	54.67	0	0.0
Dec	36.49	0	0.0

Application Test (T3)

This test has been conducted with proposed regulator (4-vent, sill level 15.7mPWD) in addition to the existing regulator using 2.33 year discharges. **Table 4** shows discharge distribution between the Upper and Lower Karatoa River in test T3. Some photographs of model during & after running conditions in test T3 are shown in **Fig. 12** and **Fig. 13** respectively.

Table 4. Discharge distribution between the Upper and Lower Karatoa River in test T3.

Name of Month	Flow entered in to the Upper Karatoa River upstream of confluence (cumec)	Flow passing through the Lower Karatoa River (cumec)	% of flow passing through the Lower Karatoa River
Jan	37.47	0	0.0
Feb	34.1	0	0.0
Mar	32.11	0	0.0
Apr	33.31	0	0.0
May	43.02	0	0.0
Jun	178.8	10.54	5.9
Jul	99.62	5.48	5.5
Aug	120.45	6.7	5.6
Sep	245.02	18.8	7.7
Oct	93.69	5.2	5.6
Nov	54.67	not measurable	-
Dec	36.49	0	0.0

Fig. 12. Flow through the Upper and Lower Karatoa River (T3).

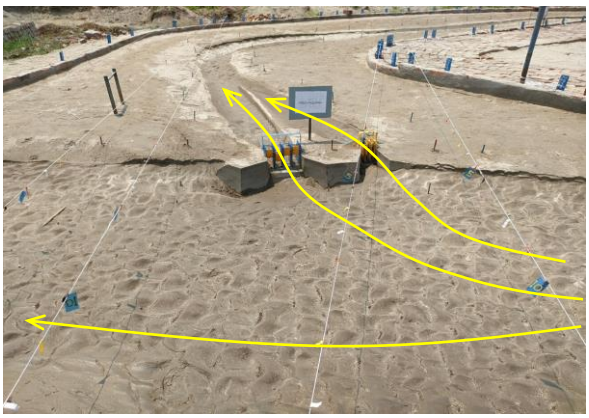

Fig. 13. Model bed after run in the vicinity of proposed & existing regulator (T3).

Application Test (T4)

This test is same as test T3 but caried out with design discharge only. **Table 5** shows discharge distribution between the Upper and Lower Karatoa River in test T4. Some photographs of model before & during running conditions in test T4 are shown in **Fig. 14** and **Fig. 15** respectively.

Table 5. Discharge distribution between the Upper and Lower Karatoa River in test T4.

Discharge	Flow entered in to the Upper Karatoa River upstream of confluence (cumec)	Flow passing through the Lower Karatoa River (cumec)	% of flow passing through the Lower Karatoa River
Design Discharge	1117	82	7.3

Fig. 14. Dry bed condition of before Test run (T4).

Fig. 15. Flow through the existing and proposed regulator (T5).

Application Test (T5)

This test has been conducted with proposed regulator (4-vent, sill level 15 mPWD) in addition to the existing regulator using 2.33 year discharges and design discharge.

Table 6 shows discharge distribution between the Upper and Lower Karatoa River in test T5. Some photographs of model before & during running conditions in test T5 are shown in **Fig. 16** and **Fig. 17** respectively.

Table 6. Discharge distribution between the Upper and Lower Karatoa River in test T5

Name of Month	Flow entered in to the Upper Karatoa River upstream of confluence (cumec)	Flow passing through the Lower Karatoa River (cumec)	% of flow passing through the Lower Karatoa River
Jan	37.47	1.89	5.04
Feb	34.1	not measurable	-
Mar	32.11	not measurable	-
Apr	33.31	not measurable	-
May	43.02	2.33	5.42
Jun	178.8	14.36	8.03
Jul	99.62	8.06	7.60
Aug	120.45	9.82	7.98
Sep	245.02	20.14	8.12
Oct	93.69	7.54	7.53
Nov	54.67	3.12	5.70
Dec	36.49	1.83	5.01
Design Discharge	1117	89.36	8.0

Fig. 16. Dry bed condition of before Test run (T5).

Fig. 17. Flow through the existing and proposed regulators in the model (T5).

Application Test (T6)

This test has been conducted with proposed regulator (4-vent, sill level 14.5 mPWD) in addition to the existing regulator using 2.33 year discharges and design discharge.

Table 7 shows discharge distribution between the Upper and Lower Karatoa River in test T6. Some photographs of model during & after running conditions in test T6 are shown in **Fig. 18** and **Fig. 19** respectively.

Table 7. Discharge distribution between the Upper and Lower Karatoa River in test T6.

Name of Month	Flow entered in to the Upper Karatoa River upstream of confluence (cumec)	Flow passing through the Lower Karatoa River (cumec)	% of flow passing through the Lower Karatoa River
Jan	37.47	2.11	5.63
Feb	34.1	1.92	5.62
Mar	32.11	1.80	5.60
Apr	33.31	1.87	5.60
May	43.02	2.45	5.69
Jun	178.8	14.61	8.17
Jul	99.62	7.60	7.63
Aug	120.45	9.76	8.10
Sep	245.02	20.70	8.45
Oct	93.69	7.08	7.56
Nov	54.67	3.19	5.84
Dec	36.49	2.03	5.57
Design Discharge	1117	92.15	8.25

Fig. 18. Dry bed condition at and around the existing and proposed regulators in the model (T6).

Fig. 19. Flow through the existing and proposed regulator in the model (T6).

Conclusion

The following conclusions have been drawn based on physical model study:From Kamarpara Bazar to Chandpur Arefia Govt. Primary School, the near right bank velocity of Upper Karatoa River is high enough to cause bank erosion when tested with design discharge condition. Bank erosion may continue at this area if appropriate bank protection measures are not taken. Float tracks reveal that the right bank of the Upper Karatoa River is under flow attack in the immediate upstream of its off-take mouth (Khulshi Regulator). Maximum velocity in the right bank of Upper Karatoa River remains about1.5 ms^{-1} and the same in the left bank of Lower Karatoa River is found to about 1.0 ms^{-1} under design discharge. Under different test conditions (with dredged channel and proposed intervention) and for monthly average discharge the flow through the Lower Karatoa River is increased by about 2, 2.5 and 3 times in tests T3, T5 and T6 respectively compared to base (existing) condition. For all test conditions with dredging noticeable flow velocity along the dredged channel occurs in the beginning. However, with the passage of time the dredged channel gets gradually filled up with a corresponding fall in the magnitude of flow velocity. The rate of filling is relatively faster in the upstream part of the dredged channel compared to that in the downstream portion of the same.

In the present physical model, a 3.0km stretch of the Upper Karatoa and 1.5km stretch of the Lower Karatoa River have been included. Therefore, morphological developments beyond the study reach under different discharge conditions remain unknown. Also, the rate of bank erosion varies spatially and temporarily and depends on several factors. The composition of bank materials in model and prototype are not

same. Therefore, it is not possible to predict the rate and extent of bank or char erosion quantitatively. The hydraulic performance of interventions (dredging and proposed regulator) under Test T6 appears to be satisfactory in terms of flow and sediment distribution into the Lower Karatoa River. The model results indicate that the average percentage of filling up of the dredged channel is about 15% in one year. The volume of filling up of the dredged channel is found about 15,00m^3 in the Lower Karatoa River in one year is found from T6 (1.5km length from offtake). For test T6 conditions the maximum thickness of deposition is 1.8m and the average thickness of deposition after one year is 0.65m.

Model results show that with the proposed dredging in place the dredged channel will get filled up by about 15,000m^3 within a year. Further filling up of the dredged channel may occur in the subsequent year reducing the flow capacity of the dredged channel if no maintenance dredging is carried out. Monitoring of the developments in the dredged channel is very important to assess the need, frequency and volume of maintenance dredging. Cross-section survey at some preselected locations covering the entire length of the dredged channel before dredging, after dredging and during post monsoon period is needed for monitoring purpose as well as to assess need for maintenance dredging and its volume. It appears from the model results that maintenance dredging is needed once in a year and may be carried out for two years following the capital dredging. The proposed maintenance dredging is needed to keep the dredged channel active and serve the intended purpose. It is suggested to dredge the entire length of the channel within one year period as partial dredging may induce large siltation during the monsoon period.

The percentage of discharge distribution between the Karatoa River Upper and Lower varies with the variation of oncoming flood discharge and sill level of regulator. The percentage of flow distribution into the Lower Karatoa River increases with the increase in the magnitude of oncoming flood discharge and with the decrease in the sill level of the proposed regulator. Maintenance dredging is required to ensure the flow in the Lower Karatoa River Lower all over the year. If a four vent regulator (each vent width 3m) having sill level 14.50 mPWD is constructed in the field just d/s of existing regulator; there will be some flow in the month of November to May.

Recommendation

The following recommendations have been drawn based on physical model study:

From Kamarpara Bazar to Chandpur Arefia Govt. Primary School, right bank of the Upper Karatoa River 850m bank protection measures should be taken. Proposed interventions (regulator and dredging) under test T6 are recommended to achieve the project objectives in terms of allowing more or less flow into the Lower Karatoa River in most of the months or time of a year with regular monitoring and maintenance dredging at the off-take and in the downstream of the same. The implementation of the recommended bank protection works may be carried out immediately for the protection of the erosion prone Kamarpara Bazar to Chandpur Arefia Govt. Primary School area and to prevent further bank erosion in the coming years.

The mean bed level of the dredged channel in the downstream of the off-take may go up due to morphological changes hampering its conveyance capacity. Therefore, maintenance dredging with frequency once in two years is suggested. Monitoring of the developments in the dredged channel is suggested for taking decision as to maintenance dredging. Cross-section survey along the dredged channel at some preselected locations before dredging, after dredging and during post monsoon period is needed for this purpose. The model bed has been reproduced based on bathymetric survey data of December, 2022. The bed configuration of the Karatoa river within the study reach might have undergone changes during monsoon period of 2023. Therefore, recommended dredging length and alignment may be adjusted according to the field condition during implementation.

A 4-vent regulator (each vent width 3m) having sill level 14.50 mPWD is recommended to construct in the field just downstream of existing regulator. Dredging is recommended in the Lower Karatoa River as it is fully silted up. The recommended length of dredged channel is 123 km. The recommended dredged channel has bottom width 15m, side slope 1:2 and longitudinal slope 5.5 cmkm^{-1}. Maintenance dredging for two successive years as suggested under test T6 is recommended. Without maintenance dredging the objective of the proposed capital dredging may not be fulfilled.

References

Chowdhury et. al. (2017). Karatoya River, Banglapedia: National Encyclopedia of Bangladesh (Second ed.). Asiatic Society of Bangladesh.

Engelund, F. and Hansen, E. (1967). A Monograph on Sediment Transport in Alluvial Streams. Teknish Forlag, Copenhagen, 62 p.

Gob, F., Houbrechts, G., Hiver, J. and Petit, F. (2005). River Dredging, Channel Dynamics and Bedload Transport in an Incised Meandering River (the River Semois, Belgium). *River Research and Applications*. 21: 791-804. https://doi.org/10.1002/rra.883

Haque et. al. (2019). Seasonal dynamics of phytoplankton community and functional groups in a tropical river, Springer, vol 193, article 704, 2021.

IWM (2022). Feasibility Study for the Management of Karatoa River System and Rehabilitation of FCD Projects on Both Banks of Nagar River in Bogura District, Inception Report, November 2022.

Kasprak, A., Brasington, J., Hafen, K., Williams, R. D. and Wheaton, J. M. (2019). Modelling Braided River Morphodynamics Using a Particle Travel Length Framework. *Earth Surface Dynamics*. 7: 247-274. https://doi.org/10.5194/esurf-7-247-2019

RRI (2023). Physical Modelling Study for Feasibility Study for the Management of Karatoya River System and Rehabilitation of FCD Projects on Both Bank of Nagar River in Bogura District, Final Report, Juny 2023.

RRI (2022). Physical Modelling Study for Feasibility Study for the Management of Karatoya River System and

Rehabilitation of FCD Projects on Both Bank of Nagar River in Bogura District, Inception Report, December 2022.

Sarker et. al. (2015). Fishing Gear and Diversity of Fishes of Karatoya River in Bangladesh.

Van Rijn, L. C. (2005). Principles of Sedimentation and Erosion Engineering in Rivers, Estuaries and Coastal Seas Including Mathematical Modelling Package (Toolkit on CD-ROM). Aqua Publications.

Technical Journal
River Research Institute ISSN: 1606-9277

A CASE STUDY OF MANAGING THE BRAHMAPUTRA-JAMUNA RIVER: A PHYSICAL MODEL BASED APPROACH

A. K. M. Ashrafuzzaman[1*], M. Shahabuddin[1], O. A. Maimun[1], S. M. A. Horayra[2], B. Roy[1], K. R. Ahmed[3], S. Ferdhous[3] and P. Kanungoe[1]

Abstract

Rowmari and Rajibpur are two upazilas under Kurigram district located near the left bank of the Brahmaputra-Jamuna River. These upazilas are suffering from severe flood of this river every year. Therefore, a study was undertaken by River Research Institute (RRI) to manage the Brahmaputra-Jamuna River in terms of bank protection works and dredging using physical modelling. The study provides support to the design of protective work and dredging required for the erosion prone areas. A stretch of about 26 km of the Brahmaputra-Jamuna River and part width of around 6 km have been reproduced in the model study. The model is distorted having horizontal scale 1:600 and vertical scale 1:80. The study was conducted with 2.33 and 100 year return period using three different options for the protection of erosion prone areas. In Option-1, a total of 11.59 km protective work is required to protect the erosion prone areas. In this case, maximum velocity and scour around the proposed protective work are found as 1.75 ms^{-1} and 6.88 m (18.32 mPWD) respectively. In Option-2, the proposed dredging through the Brahmaputra-Jamuna River would ensure the stability of the bank protection work by reducing the flow attack near the left bank and thereby, reducing the near bank flow velocity. But the dredged channel is found to be mostly silted up. The model results indicate that the average percentage of filling up of the dredged channel is about 46.72% in one year. For Dighla Para Char stabilization (Option-3), the length of the proposed bank protective work surrounding the char is 21.654 km which may not be economically feasible as it involves huge cost and environmental & other issues. But under this option a huge area of land (around 33 sq.km) will be reclaimed due to char stabilization.

Keywords: *Bank protective work, Brahmaputra-Jamuna River, Discharge, Dredging, Reclamation, Scour, Stabilization, and Velocity.*

Introduction

Originating from the Manas Sarovar Lake region of the Himalayas in Tibet, the river enters into Bangladesh at Rowmari upazila. Rowmari and Rajibpur upazilas are situated adjacent to the left bank of the Brahmaputra-Jamuna River and these upazilas are suffering from devastating flood of this river every year. Therefore, a study is required along the left bank of the Brahmaputra-Jamuna River at Rowmari and Rajibpur upazila for the protection of these areas. The satellite image at and around the study area is shown in **Fig. 1.** The objectives of the study are to identify the erosion prone areas within the study reach; to develop options of erosion management measures; to assess the efficacy of the developed options in arresting erosion; to assess the effects of the developed options on river hydraulics and morphology in the upstream and downstream of the same and to determine the hydraulic design parameters of the suitable bank protection works. Bank failure, characterized by erosion and collapse of riverbanks, is a prevalent issue along the Brahmaputra River in Bangladesh. It can be attributed to a combination of natural and human factors. Researchers have identified several causes of bank erosion, including high water velocity, sediment transport, riverbed changes, rainfall patterns, and human interventions. Rahman *et al.* (2009) conducted a study on the causes of riverbank erosion, emphasizing the role of channel migration and sediment dynamics in bank failure processes. They also highlighted the impact of climate change on the instability of riverbanks.

The consequences of bank failure along the Brahmaputra River have far-reaching effects on both human settlements and natural ecosystems. Scholars have examined the social, economic, and environmental impacts of bank erosion. They assessed the socio-economic consequences of riverbank erosion on affected communities, highlighting the loss of land, displacement, and disruptions to livelihoods. Destruction of agricultural fields, infrastructure, and housing has also been identified as significant consequence of bank failure (Hassan *et al.*, 2021). Efforts to mitigate and adapt to bank failure along the Brahmaputra River have been explored in research studies. Researchers have proposed various strategies to manage erosion and reduce its impacts. Islam *et al.* (2023) conducted a study on the effectiveness of river training works in mitigating bank erosion, analysing the roles of embankments, spurs, and groynes. They emphasized the need for integrated approaches, incorporating both structural and non-structural measures, to achieve effective erosion control.

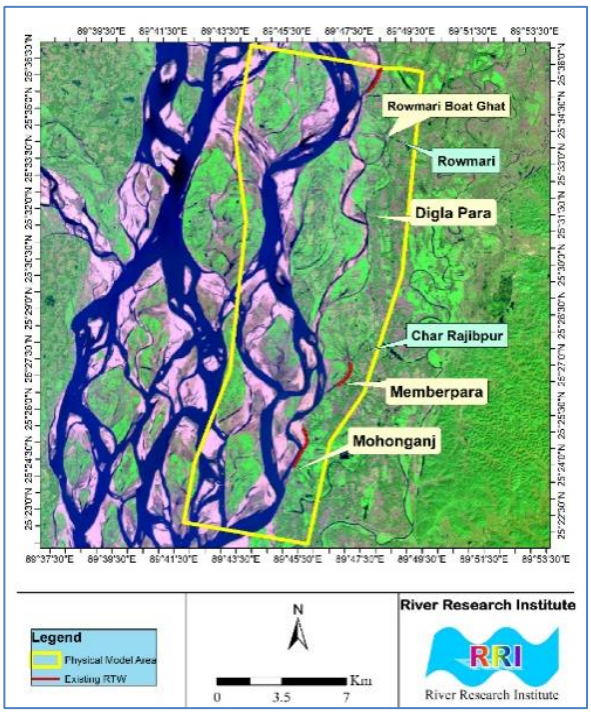

Fig. 1. Satellite image around the study area.

[1] Hydraulic Research Directorate, River Research Institute, Faridpur-7800, Bangladesh.
[*] Corresponding Author: (E-mail: ashrafcebuet89@gmail.com)
[2] Office of the Director General, River Research Institute, Faridpur-7800, Bangladesh.
[3] Geotechnical Research Directorate, River Research Institute, Faridpur-7800, Bangladesh.

The main causes of the Brahmaputra-Jamuna River's bank line change in Bangladesh will be examined in this study along with any ramifications. Rahman *et al.* (2022) used remote sensing and GIS tools in research to examine the Brahmaputra-Jamuna River's bank line dynamics. The river's bank lines have moved noticeably throughout this time, according to the researchers' analysis of satellite imagery from 1973 to 2019. The researchers ascribed this change to processes including sedimentation, erosion, and human activities like sand mining and embankment construction. Additionally, they looked at the effects of climate change on the Brahmaputra-Jamuna River's bank line displacement. In order to replicate future events, the researchers used hydrological modelling techniques while taking into consideration anticipated changes in temperature and precipitation. According to the findings, future bank line movements might be caused by climate change-related erosion and increasing river discharge. Concern has also been expressed about the socioeconomic effects of the Brahmaputra-Jamuna River's bank shift. In their study, Kundu *et al.* (2019) investigated the effects of bank erosion on the lives and agricultural production of farmers in riverine areas. They emphasized how regular riverbank erosion destroys fertile land, uproots communities, and has a negative impact on local businesses, especially those related to agriculture and fishing.

Several strategies have been put up to lessen the negative impacts of bank line shifts. The usefulness of bioengineering methods, such as the usage of vegetative bio-bunds, in preventing bank erosion along the Brahmaputra-Jamuna River was studied by Islam *et al.* (2003). According to their research, these methods can considerably lower erosion rates and stabilize the riverbank, providing a long-term fix. Sedimentation, erosion, climate change, and human activity are a few of the causes that affect the Brahmaputra-Jamuna River's bank line movement in Bangladesh. The socioeconomic and biological processes in the riverine zones are severely hampered by it. To solve the complex difficulties related to the bank line shift and guarantee sustainable development along the Brahmaputra-Jamuna River, further study and comprehensive management measures are needed. The vulnerable area along the left bank of Brahmaputra-Jamuna River is identified by IWM and is shown in **Fig. 2.** It is noticed from this figure that the left bank is subjected to erosion at various amount at different places. There are various places near the left bank of Brahmaputra-Jamuna River which are susceptible to river bank erosion is listed below (IWM, 2022).

- Shaheber Alga BGB Camp to Bolodmari Ghat (13 km) (starting Ch-0 KM).
- Rowmari Boat Ghat to West Baghmara (1.7 KM) (starting Ch-19.85 KM 24.94 KM).
- Dighlapara Kheyaghat to Dhonar Char (2.32 KM) (starting Ch- 24.94 KM).
- Rajibpur Boat Ghat to Hazipara (3.10 KM) (starting Ch-35 KM).
- Nayachar to Sanandabari (3.10 KM) (starting Ch- 41 KM).
- Bir Muktijoddha Ajharul Islam House to Babul Market (2.7 KM) (starting Ch- 45.63 KM).
- Algar Char to Old Brahmaputra Offtake (5.65 KM) (starting Ch- 52 KM).

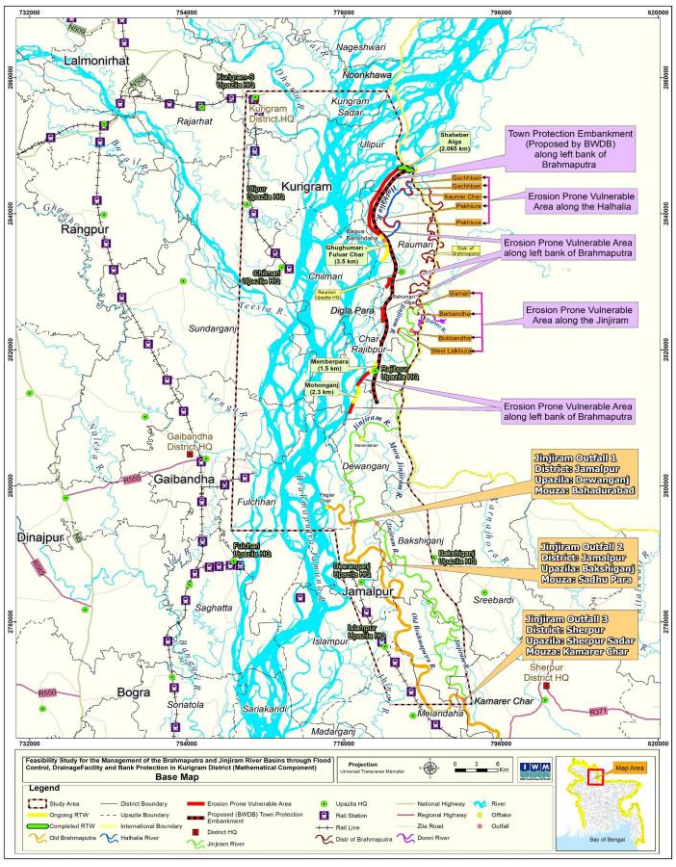

Fig. 2. Identified vulnerable area (IWM, 2022).

Bank Shifting

The satellite imageries of 1984 and 2023 of the Brahmaputra-Jamuna River in the study area are superimposed as shown in **Fig. 3.** It is noticeable from the figure that the left bank of Brahmaputra-Jamuna River is susceptible to erosion. Lateral migration of the left bank varies up to 5.3 km since 1984. More than 100 sq. Km of land have eroded since 1984 in Rowmari and Char Rajibpur upazila of Kurigram District. Thousands of people losing their lands and become homeless (RRI, 2023).

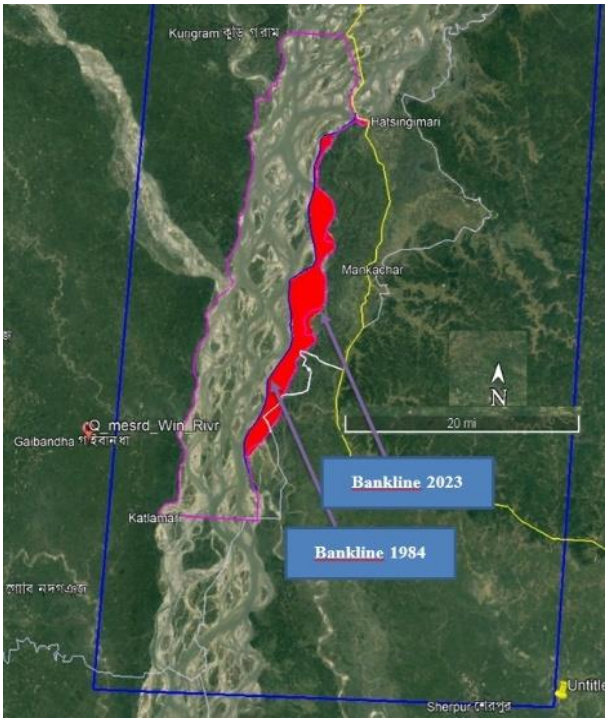

Fig. 3. Superimposed satellite imageries of 1984 and 2023 of the Brahmaputra River (RRI, 2023).

Methodology

An overall distorted morphological model was constructed which includes a river stretch covering around 26 km of Brahmaputra-Jamuna River. In order to meet the scale conditions for reproducing the flow and sediment transport processes simultaneously as well as to meet the roughness condition of the model, a distorted model with suitable geometric scales had been planned. The model was constructed having horizontal scale 1:600 and vertical scale 1:80. This model had part width of the river from the left bank so that at least 30% of the total discharge was passing within the lateral boundary. The model had been planned to come up with the hydraulic design parameters of the interventions and to assess the impacts of the same qualitatively. The main purpose of this model was to provide decision support for determining of suitable and optimal design of bank protection work as well as dredging alignment if necessary and also to investigate the efficacy of the alternative measures to ensure a stable river course.

One of the important considerations in scale modelling is the selection of bed material size to have roughly similar hydraulic and morphological condition both in model and prototype. To this end, a number of sediment samples had been collected from the river bed and bank of the Brahmaputra River. These samples were analysed to determine bed load, suspended load, wash load and soil properties in the sediment laboratory of RRI. Latest maps and satellite imageries covering the study reach had been collected from different sources including USGS. Historical satellite imageries of study area had also been collected for different periods. These satellite imageries had been super-imposed to have an understanding of the changes in the channel pattern with the passage of time due to morphological developments.

Dredging has been proven as an effective process to control the deposited sediment to prevent flooding and make a pathway for the main channel flow (Gob *et al.*, 2005; Zinger *et al.*, 2011). The process also allows us to further solve engineering problems related to sedimentation and erosion in rivers, estuaries, and coastal seas (Van Rijn, 2005). A better prediction of erosion-sedimentation scenarios is inevitable to justify the long-term effectiveness of dredging, which could further promote the design strategies based on qualitative and quantitative analysis. Prediction of accurate scour depth and deposition of the braided river is methodologically very challenging because of the variation in simple path-length distribution resulting in over-scouring (Kasprak *et al.*, 2019).

Sediment was fed into the model manually. Generally, the rate of sediment feeding for a particular model discharge was determined first by using sediment transport formulae /relation proposed by different researchers. For this model the sediment transport formulae proposed by Engelund and Hansen (1967) had been used to determine the initial sediment feeding rate. The sediment feeding rate, however, had been calibrated. The calibration of sediment feeding rate had been done by taking measurements of bed levels along a few cross-sections located at different parts of the model at a regular interval of time. Calibration of sediment feeding rate

involves a condition where bed level remains more or less unchanged. It means whatever sediment is fed into the model is transported out of the model.

The initial bathymetry of the model was reproduced based on the field survey data collected under the framework of this study. The model was designed as a fine sand bed morphological model. Since it was a distorted model, the model had been constructed based on selected geometric scales. The initial bathymetry of the model is shown in **Fig. 4**. The construction of model involves a series of tasks. Besides selection of geometric scale ratios, the model bed had been prepared by uprooting the grass, dismantling of the previous works in the selected model bed and disposal of debris, removing the old sand from the model bed and filling the same with new fine sand having required median size, procurement of model construction materials, collection of bathymetric and bank line data etc. The model layout is shown in **Fig. 5**.

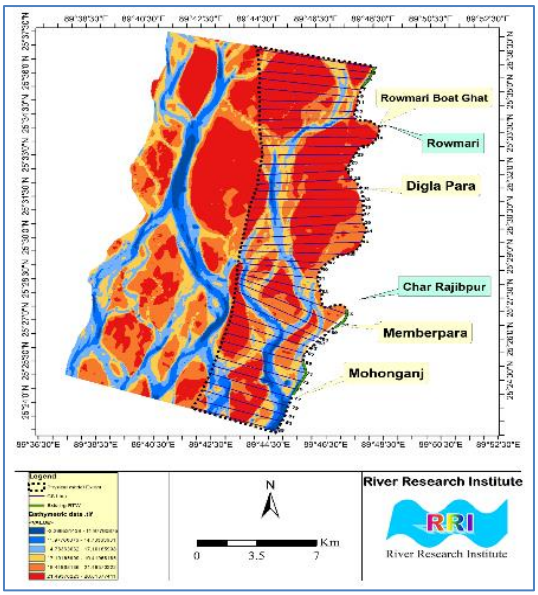

Fig. 4: Initial bathymetry of Brahmaputra River.

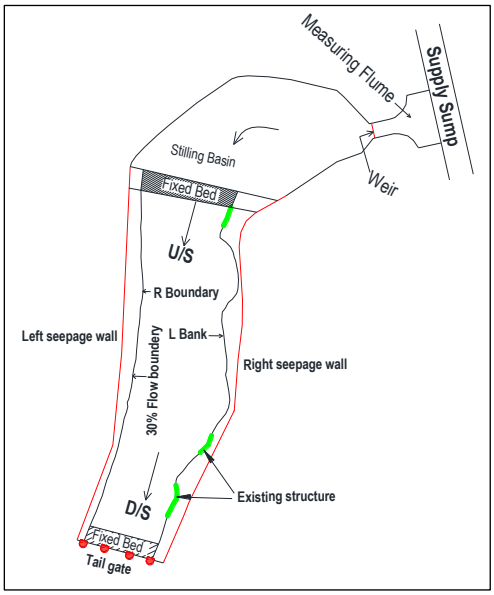

Fig. 5: Layout of the Model.

Test Scenarios

In this model, calibration test (T0) & base test (T1) in existing condition and five application test runs (T2-T4) with proposed interventions (bank protection & dredged channel) in place have been conducted. The proposed test scenarios of the model along with various test & flow conditions are mentioned in **Table 1**.

Table 1. Test Scenarios of the model.

Tests	Test Conditions	Flow Conditions
T0 (Calibration)	Existing (without project) condition and surveyed bathymetry as initial bed of the model	2.33 year return period discharge and corresponding water level at preselected location
T1 (Base run)	Existing (without project) condition and calibrated bathymetry as initial bed of the model	2.33 year return period discharge as well as 100 year return period discharge with corresponding water level
T2 (Option-1)	Existing (without project) condition + Proposed Bank Protection Works	-Do-
T3 (Option-2)	Existing (without project) condition + Proposed Bank Protection Works + Dredging at 1 location of Brahmaputra-Jamuna River (Rowmari)	-Do-
T4 (Option-3)	Existing (without project) condition + Proposed Bank Protection Works + Dighlapara Char Stabilization	-Do-

Model Calibration

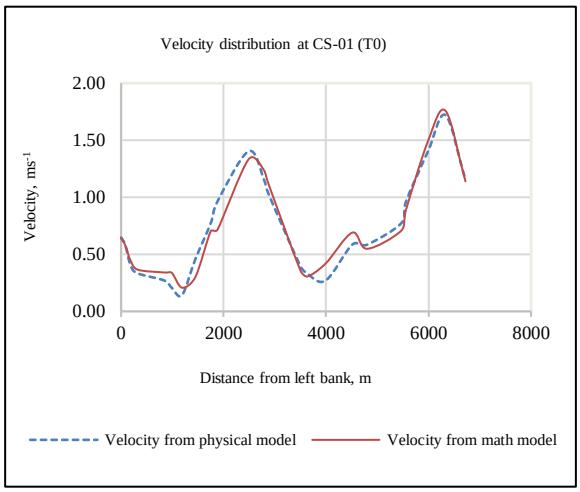

Fig. 6. Comparison of velocity distribution at CS-01 for 2.33 year return period discharge.

Model calibration is done to ensure that the model is able to reproduce the flow condition, morphological behaviour and sediment transport in the field. The calibration of the model primarily aims to see whether the model is able to reproduce a more or less similar bathymetry as is measured during field survey under imposed conditions to bring about similarity between model and prototype in terms of flow and sediment transport simultaneously. The measurements during the calibration include water levels, bed levels, point velocities, float tracks, discharge etc. The model bathymetry obtained after calibration of the model has been considered as initial bathymetry for subsequent application tests in base and intervention conditions. Calibration test was done using 2.33 year return period discharge (Q= 20,452 cumec) and corresponding water level (24.68 mPWD). This test was carried out with existing condition. The model bed was prepared according to the bathymetric survey of October, 2022**.** Flow velocity was measured in the model and is compared with the prototype measurement (mathematical model). A comparison between prototype and model velocity is made as shown in **Fig. 6.** From this figure it is evident that the velocities observed in the model are close to the prototype values.

Results and Discussion

In test results, the findings of base run (T1) and 3 (three) application tests (T2, T3 & T3) have been presented. In base run, there are three existing protective structures to protect the left bank of Brahmaputra-Jamuna River within the model boundary. These places are Godabari, Char Khonjonmara (U/S of Rowmari Boat Ghat), Kodalkati Boat Ghat, Munshipara (Memberpara) and Nayar Char Launch Ghat, Mohangonj Union and the length of the existing structures is 1428m, 1498m & 2364m respectively (**Fig. 7**). Bank erosion at the left bank of Brahmaputra-Jamuna model is shown in **Fig. 8**. In test T2 (Option-2), there are three proposed structures to protect the left bank of Brahmaputra-Jamuna River in addition to the existing structures. The places of proposed structures are Baghmara /Rowmari Boat Ghat, Dighlapara/Dhonar Char under Jadurchar Union and Rajibpur Boat Ghat. The length of the proposed structures is 1766m, 2338m & 3063m respectively. In the design of protective structures, the length of launching apron is 45 m, assorted CC blocks to be dumped below LWL (Low Water Level) @ 35 $m^3.m^{-1}$ (500X500X500 - 60%, 400X400X400 - 40%, 250 kg geobag to be dumped below LWL @ 33.75 $m^3.m^{-1}$. The proposed protective work is constructed in the model as per design. There are three places where bank erosion is observed at left bank during test T2 in addition to the proposed bank protection work. These places are downstream of existing protective work (Faluar Char Nouka Ghat), downstream of proposed protective work at Rowmari Boat Ghat (Chaktabari, Jadurchar Union) and Char Rajibpur (Char Velamari). These areas require bank protection work. The location of existing, proposed & erosion prone areas are shown in **Fig. 9**. Proposed and existing protective work around Char Rajibpur is shown in **Fig. 10**. Erosion prone area upstream of Rowmari Boat Ghat is shown in **Fig. 11**.

Fig. 7. Placement of existing bank protection works at Memberpara and Mohonganj ($T1_{2.33yr}$).

Fig. 8. Bank erosion occurred at the left bank of Brahmaputra model under base condition ($T1_{100yr}$).

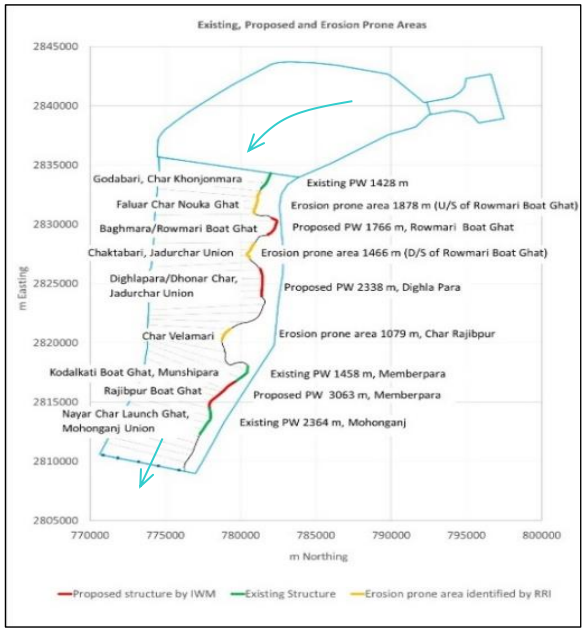

Fig. 9. Layout of model for test T2 including location of existing, proposed & erosion prone areas (T2).

Fig. 10. Proposed and existing protective work around Char Rajibpur.

Fig. 11. Erosion prone area upstream of Rowmari Boat Ghat ($T2_{100yr}$).

In test T3 (Option-2), a proposed dredged channel is reproduced **(Fig. 12 & 13)** in the model at Rowmari in addition to the existing & proposed protective works. The length of the dredged channel **(Fig. 14)** is 13.2 km. The bottom level of dredged channel is 11 mPWD, side slope 1:3, average top level 17 mPWD, longitudinal slope 5cm.km^{-1}, average height of the dredged channel is 6m. **Fig. 15** shows the longitudinal section through the proposed dredged channel. The amount of dredged volume, which is measured around 2,72,17,863 m^3 in the model. The average thickness of dredging is about 5.55m.

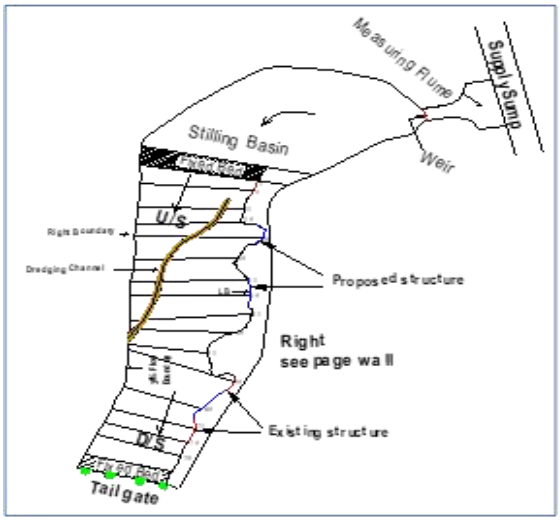

Fig.12: Layout of model for test

Fig.13: Initial alignment of dredged channel in the model (T3)

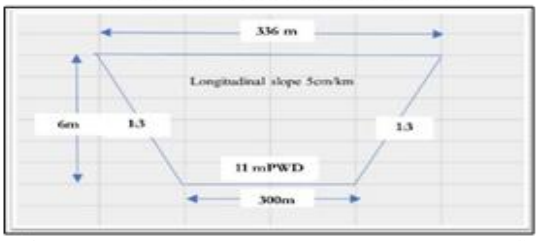

Fig.14: Section of the dredged channel

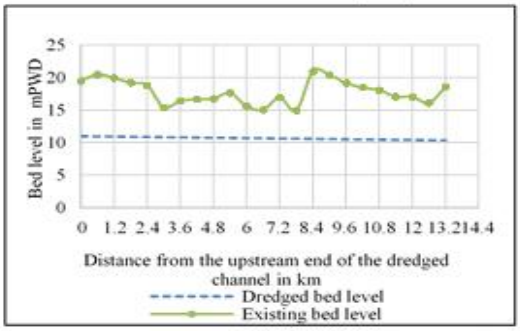

Fig.15: Longitudinal section through the proposed dredged channel ($T3_{100yr}$)

The volume of filling up of the dredged channel is found about 1,27,15,570 m^3. The average filling depth is 3.39 m. The dredged channel is mostly found to be silted up. The model results indicate that the average percentage of filling up of the dredged channel is about 46.72%. **Fig. 16-18** shows the initial & final bed level through dredged channel ($T3_{100yr}$). **Fig. 19** shows the alignment of silted dredged channel in test $T3_{100yr}$.

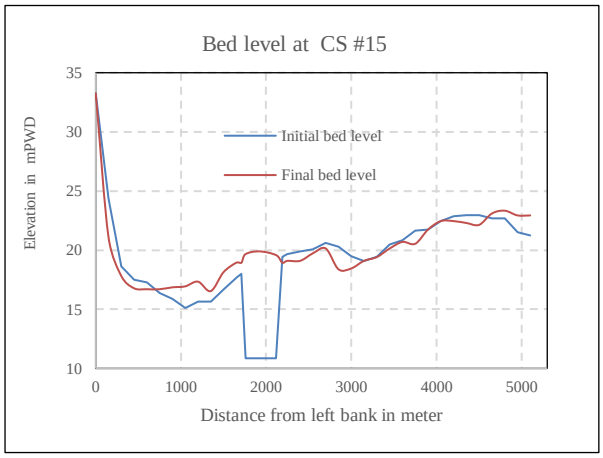

Fig. 16. Initial & final bed level through dredged channel in test T3 (U/S part).

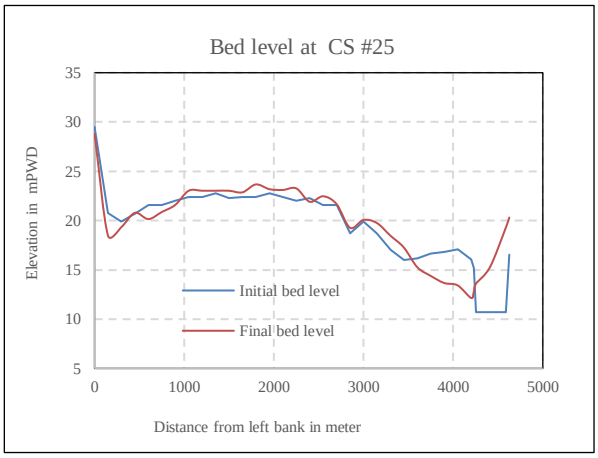

Fig. 17. Initial & final bed level through dredged channel in test T3 (middle part).

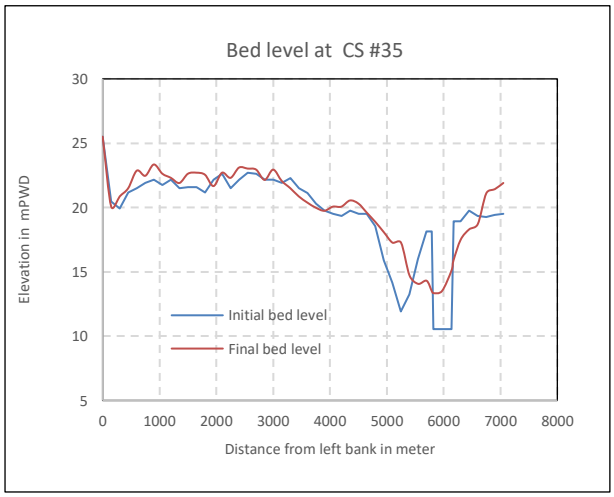

Fig. 18. Initial & final bed level through dredged channel in test T3 (D/S part).

Fig. 19. Alignment of silted dredged channel.

Test T4 (Option-3) is the third application test conducted for char stabilization (Connecting Char Dighla Para with the main-land including river bank protection) in place. The advantage of interventions considered under this option is that a huge area of land (around 33 sq.km) will be reclaimed due to char stabilization. Moreover, the reclaimed area may be developed rapidly immediately after char stabilization due to the construction of different infrastructures such as schools, colleges, offices, industries, factories etc. Due to these, the socio-economic condition of that area will be improved a lot. At present, the char land is separated from the main land by a secondary channel of the Brahmaputra-Jamuna River. The proposed design of bank protective work for Dighla Para Char Stabilisation is verified by physical modelling. The model layout for test T4 is shown in **Fig. 20.** Here the length of the proposed protective work (as shown in **Fig. 21)** surrounding the Dighla Para Char is 21.654 km. The launching of protective work is shown in **Fig. 22-23.**

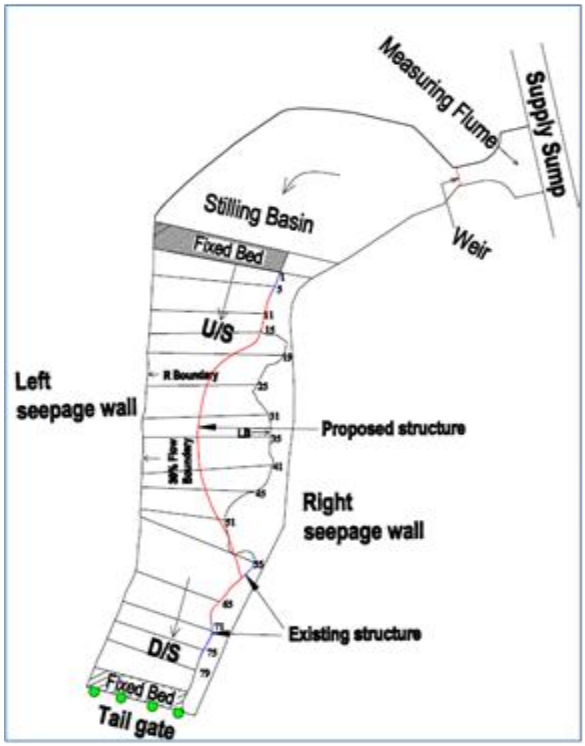

Fig.20: Layout of model for test T4

Fig.21: Proposed protective works surrounding Dighla Para Char

Fig. 22. Launching behaviour of proposed protective works (T_{100yr}).

Fig. 23. Launching pattern of proposed protective works after run (T_{100yr}).

Suitable Option

The protection measures considered under Option-1 will arrest left bank erosion of the Brahmaputra-Jamuna River at the erosion prone locations where they are implemented. Erosion may still occur at some unprotected locations. Also, this option does not facilitate reclamation of any land if it does not happen naturally by abandonment of secondary channel or retreat of the river channel. If land development/reclamation occurs naturally it may again come under erosion attack at a future time given the very dynamic nature of the Brahmaputra-Jamuna River. Therefore, with interventions considered under Option-1 in place recovery of the lands that are already engulfed by the river remains uncertain.

Option-2 also does not facilitate reclamation of any lost land unless it happens naturally. Dredging at Rowmari considered under this option appears to be not feasible as the dredged channel may get largely filled up within a year. The cost of capital and maintenance dredging may not be compatible with the likely benefit from the dredging.

Bank protection and char stabilization considered under Option-3 appear to be beneficial in terms of erosion protection and land reclamation. Char stabilization in the Brahmaputra-Jamuna River may occur naturally. However,

implementation of suggested protective works (21.654km long) is likely to be a challenging task as the protective works will come under high flow attack of a major channel of the Brahmaputra-Jamuna River. In the past the river has shown a trend of increase in braiding intensity and width leading to large scale bank erosion in the project area. It is believed that this trend no more exists now. It creates an opportunity to go for narrowing the river and reclaim valuable floodplain land. However, response of the Brahmaputra-Jamuna River to human interventions still remains unpredictable.

Under this circumstance, it would be wise to implement the proposed protective works following an adaptive approach keeping scope for improving and optimizing the designs for systematic stabilization measures to be implemented. Since interventions under Option-3 provides left bank erosion protection of the Brahmaputra-Jamuna River covering a long stretch and facilitates regaining of lost land it could be a suitable option that may be considered.

Conclusion

The near left bank velocity is high enough to cause bank erosion at unprotected places when tested for flood discharge of 2.33 year and 100 years. Bank erosion may continue at these areas if appropriate bank protection measures are not taken immediately. Float tracking in the base run reveals that the left bank of the Brahmaputra-Jamuna River is under flow attack at the unprotected areas. In base condition (T1), maximum velocity around the existing protective work at the upstream of Rowmari Boat Ghat, at Memberpara and at Mohonganj is found as 1.32, 1.32 and 0.92 ms^{-1} respectively for 2.33 year discharge and as 1.34, 0.94 and 1.40 ms^{-1} respectively for 100 year discharge. In test T2 (Option-1), maximum velocity around the proposed protective work at Rowmari Boat Ghat, at Dighla Para and at Memberpara is found as 0, 1.52 and 1.17 ms^{-1} respectively for 2.33 year discharge and as 0, 1.63 and 1.75 ms^{-1} respectively for 100 year discharge. In test T3 (Option-2), maximum velocity around the proposed protective work at Rowmari Boat Ghat, at Dighla Para and at Memberpara is found as 0, 0.59 and 0.19 ms^{-1} respectively for 2.33 year discharge and as 0, 0.77 and 1.00 ms^{-1} respectively for 100 year discharge. In test T4 (Option-3), maximum velocity along the proposed protective work placed around Dighla Para Char is found as 1.78 ms^{-1} for 2.33 year discharge, 4.5 km downstream from the upstream end of the proposed protective work and as 2.81 ms^{-1} for 100 year discharge, 5.1 km downstream from the same.

In base condition (T1), with respect to initial bed level maximum scour depth around the existing protective work at upstream of Rowmari Boat Ghat, at Memberpara and at Mohonganj is found as 3.52 m (17.84 mPWD), 2.32 m (19.84 mPWD) and 1.36 m (20.43 mPWD) respectively for 100 year flood discharge. In test T2 (Option-1), with respect to initial bed level maximum scour depth around the proposed protective work at Rowmari Boat Ghat, at Dighla Para and at Memberpara is found as 0.96 m (20.85 mPWD), 0.96 m (18.73 mPWD) and 6.88m (18.32 mPWD) respectively for 100 year flood discharge; In test T3 (Option-2), with respect to initial bed level maximum scour depth around the proposed protective work at Rowmari Boat Ghat, at Dighla Para and at Memberpara is found as 1.12 m (20.69 mPWD), 4.72 m (25.06 mPWD) and 6.88 m (11.43 mPWD) respectively for 100 year flood discharge. In test T4 (Option-3), with respect to initial bed level maximum scour depth along the proposed protective work placed around Dighla Para Char is found as 12.72 m. The corresponding minimum scour level is 8.88 mPWD. It has happened at around 5.7 km downstream from the upstream end of the proposed protective work for 100 year flood discharge. The maximum scour depths and corresponding minimum scour levels obtained from different options are qualitative due to presence of scale effects in reproduction of scour holes.

The proposed bank protection works proposed by IWM and introduced along the left bank at their appropriate positions is found to be working well as noticed from the model study. However, still there are three places along the left bank where bank erosion may occur as revealed from the physical model investigation (Test T2, Option-1) in addition to the bank protection work proposed by IWM**.** The location of these erosion prone places is in the downstream of the existing protective works (Faluar Char Nouka Ghat), in the downstream of the protective work proposed by IWM at Rowmari Boat Ghat (Chaktabari, Jadurchar Union) and at Char Rajibpur (Char Velamari). Protection against bank erosion is also needed at these places. In Option-2, the flow velocity along the dredged channel in the beginning of the test varies from 0.42 ms^{-1} to 1.63 ms^{-1} and from 0.94 ms^{-1} to 2.04 ms^{-1} for 2.33yr and 100yr discharge respectively. With the passage of time flow velocity along the dredged channel is found to have decreased due to progressive filling up of the dredged channel. The upstream portion of dredged channel gets silted up earlier than the downstream portion. For the considered dredge plan and design under Option-2, the total volume of material to be dredged is 27217863 m^3. The likely volume of material that may get deposited in the dredged channel within a year for an extreme event (100 year discharge) is 12715570 m^3. The dredged channel is found to have gotten mostly silted up in the upstream part of the channel and the average percentage of filling up of the dredged channel is about 46.72% in one year. The average dredging area and dredging depth is 49,04,119 m^2 and 5.55 m respectively. The near bank velocity along the left bank of the river within the study reach is reduced to some extent due to the introduction of dredged channel. However, this positive effect of the dredging may diminish with time due to progressive filling up of the dredged channel. It appears from the model results that maintenance dredging is needed once in a year and may be carried out for two to three years following the capital dredging. If the proposed capital and maintenance dredging is accomplished it will ensure the stability of the bank protection works by reducing the flow attack near the left bank and thereby, reducing the near bank flow velocity. However, proposed dredging involves economic, management, availability of dredger, environmental and other issues to be considered for implementation. Monitoring of the developments in the dredged channel will be needed for taking decision as to maintenance dredging. Cross-section survey along the dredged channel at some preselected locations before dredging, after dredging and during post monsoon period is needed for this purpose.

For char stabilization, the length of the protective work around Dighla Para Char proposed by IWM is 21.654 km. The proposed protective work may come under high flow attack during flood period and consequently large scour hole may develop near the protection works. Char stabilization may be implemented following an adaptive approach i.e., systematic construction of the protective works together with monitoring and assessment of morphological developments allowing for improvement and optimization in the design of

protective works. Char stabilization around Dighla Para Char under Option-3 (T4) will be helpful for massive land reclamation. However, this option involves cost, environmental and other issues and in the present physical model, a 26 km stretch of the Brahmaputra-Jamuna River covering part width has been reproduced. Therefore, morphological developments beyond the study reach under different discharge conditions remain unknown. Also, the rate of bank erosion varies spatially and temporarily and depends on several factors. The model is able to reproduce bank erosion qualitatively. Therefore, it is not possible to predict the rate of bank or char erosion quantitatively.

Recommendation

It is revealed from the examination of historical satellite images that over the last four decades the Brahmaputra River has shown an overall widening trend due to increase in the braiding intensity leading to widespread bank erosion in the project area and elsewhere. Due to left bank erosion of the Brahmaputra River in the project area numerous people have lost their homesteads and valuable lands. Many infrastructures are also swallowed up by the river. At present the widening trend of the Brahmaputra River is reversing. Therefore, emphasis should be put on reclamation of lost land in all river stabilization projects concerning the Brahmaputra River.

Interventions considered under Option-3 may be implemented in the field in order to meet the project objectives despite the fact that it entails massive construction and huge cost. The implementation of the proposed protective works should be adaptive. Monitoring and assessing the river behaviour in response to phased construction should form the basis for improving and optimizing the design of proposed protective works and there should be a concrete plan for beneficial use of the reclaimed land including resettlement of displaced people.

References

Engelund, F. and Hansen, E. (1967). A Monograph on Sediment Transport in Alluvial Streams. Teknish Forlag, Copenhagen, p. 62.

Gob, F., Houbrechts, G., Hiver, J. and Petit, F. (2005). River Dredging, Channel Dynamics and Bedload Transport in an Incised Meandering River (the River Semois, Belgium). *River Research and Applications*. 21: 791-804. https://doi.org/10.1002/rra.883

Hassan *et al*. (2021). Morphological changes in the hazardous zones of the Ganga and the Brahmaputra Rivers in East and Northeast India. DOI: 10.1007/s12518-021-00395-y, 2021.

Islam *et al.* (2003). Quantification of erosion patterns in the Brahmaputra–Jamuna River using geographical information system and remote sensing techniques. Hydrological Processes, vol-17, 2003.

IWM (2022). Consultancy Services in connection with the Mathematical Modelling Component of the Project "Feasibility Study for the Management of the Brahmaputra and Jinjiram River Basins through Flood Control, Drainage Facility and Bank Protection in Kurigram District, Inception Report (Revised), October, 2022.

Kasprak, A., Brasington, J., Hafen, K., Williams, R. D. and Wheaton, J. M. (2019). Modelling Braided River Morphodynamics Using a Particle Travel Length Framework. *Earth Surface Dynamics*. 7: 247-274. https://doi.org/10.5194/esurf-7-247-2019.

Kundu *et al.* (2019). DNA barcoding of freshwater fishes from Brahmaputra River in Eastern Himalaya biodiversity hotspot, Resources, Volume 4, Issue 2, 2019.

Rahman, H., Yesmin, N., Ahmed, J., Banik, B., Alam, J., Misbah, U., Islam, J. Study of the morphological change of the River Old Brahmaputra and its impacts. *Asian Journal of Water, Environment and Pollution*. vol-6, 2009.

Rahman *et al.* (2022). A geospatial analysis of Jamuna (Brahmaputra) River in Bangladesh during 1973–2019 using Landsat satellite remote sensing data and GIS, Environmental Monitoring and Assessment. 195(1) DOI:10.1007/s10661-022-10638-z, 2022.

RRI (2023). Physical Modelling Component for Feasibility Study for the Management of the Brahmaputra River Basin through Flood Control, Drainage Facility and Bank Protection in Kurigram District, Final Report, June, 2023.

Van Rijn, L. C. (2005). Principles of Sedimentation and Erosion Engineering in Rivers, Estuaries and Coastal Seas Including Mathematical Modelling Package (Toolkit on CD-ROM). Aqua Publications.

Technical Journal
River Research Institute ISSN: 1606-9277

ASSESSMENT OF THE PHYSICOCHEMICAL PARAMETERS AND THE WATER QUALITY INDEX AT THE UPSTREAM PART OF THE SANGU AND MATAMUHURI RIVERS OF BANGLADESH

N. C. Ghosh[1,2,3*], K. B. Anwar[3]

Abstract

This study assessed 16 water quality parameters in situ at 4 locations in the upstream valley of each Sangu and Matamuhuri Rivers. Water Temperature (WT), pH, Electrical Conductivity (EC), Total Dissolved Solids (TDS), and Dissolved Oxygen (DO) were measured by direct probe method. Total Alkalinity (TA), Chloride (Cl^-), Total Hardness (TH), and Carbon-di-oxide (CO_2) were measured by titration method, and Turbidity, Total Suspended Solids (TSS), Ammonia (NH_3), Nitrite (NO^-_2), Nitrate (NO^-_3), Sulfate (SO^{2-}_4), and Orthophosphate (PO^{3-}_4) were measured by colorimetric method. The Canadian Council of Ministers of the Environment Water Quality Index (CCMEWQI) was used to calculate the water quality index (WQI). Water quality parameters pH, EC, TDS, DO, TA, Cl^-, TH, CO_2, NO^-_2, NH_3, NO^-_3, and SO^{2-}_4 were found within the range of standard values for drinking water in all the points of both the rivers, whereas, the WT was found slightly low (19.9°C) from the standard values (20-30°C) at one point of the Matamuhuri River. CO_2 and PO^{3-}_4 were higher than the standard values at all sampling points of both rivers, with a mean value of 26.15 mgL^{-1} having a standard deviation (SD) of 1.61 and 0.19 mgL^{-1} (SD 0.05) for Sangu River and 24.15 mgL^{-1} (SD 4.49) and 0.21 mgL^{-1} (SD 0.03) for Matamuhuri River respectively. The turbidity was higher at all the points of the Sangu River, whereas at two points of the Matamuhuri River. TSS was higher at two and one points of the Sangu and Matamuhuri Rivers, respectively. The CCMEWQI of the Sangu and Matamuhuri Rivers was calculated at 82.95 and 81.08, respectively. The water quality, according to the CCMEWQI for both the Sangu and Matamuhuri Rivers, was in the "good" category of the index.

Keywords: *Sangu, Matamuhuri, Physicochemical, Water Quality Index, WQI, CCMEWQI.*

Introduction

The water quality parameters control the quality of the ecosystem and biodiversity of any aquatic environment (Mukherjee, *et al.*, 2023). The traditional approach of reporting the water quality of a point or a water body parameter by parameter in compliance with the guideline provides a wealth of information but has its complexity of understanding by general peoples and somewhat policymakers. A WQI reduces the multivariate nature of the data, combines all the parameters mathematically, compares them with their guideline values, and provides a readily understandable form of value with insight into water quality and human influences. WQI is a helpful tool to state the suitability of the water for humans, aquatic life, and wildlife (CCME, 2017).

Bangladesh, a land of rivers having about 700 rivers (Hossen, *et al.*, 2019), is divided into four major river networks such as i) the Brahmaputra-Jamuna River system, ii) the Ganges-Padma River system, iii) the Surma-Meghna River system, and iv) the Chittagong region hilly river system. The first three systems are interconnected, but the Chittagong hilly river system is completely separate and disconnected from the other systems and has a flow direction from south to north to fall into the Bay of Bengal (Rahman, *et al.*, 1990).

The total area of 13295 km^2 of the Chittagong Hill Tracts (CHTs) is comprised of seven valleys formed by the rivers Feni, Karnafuli, Chengi, Maini, Kassalong, Sangu, and Matamuhuri and their tributaries (Gain, 2000; Khan and Haque, 2003). Sangu and Matamuhuri are the two main rivers of the Bandarban districts, flowing parallel through the Sangu-Matamuhuri wildlife sanctuary, separated by the Chimbuk range. Sangu River is named after the Sangu chara, the largest one of the three charas which combined near the 62 and 63 nos. pillars of the Bangladesh-Myanmar border. These three charas formed the Sangu River, which flows through Thanchi and Bandarban Sadar upazilas and falls to the Bay of Bengal at Juidondi, Dohajari union of Chandanaish upazila of Chittagong district (Charlie, 1945). Matamuhuri is a transboundary river that originates in the north Arakan hills of Myanmar, enters Bangladesh at the Poyamuhuri union of Alikadam upazila, and falls to the Bay of Bengal near the Matarbari of Cox's Bazar district.

The annual runoff discharge of the Sangu and Matamuhuri watersheds is about 2167.77 and 1490.61 million cubic meters, respectively, of which 84% and 79% discharge are in the wet season (Rudra and Alam, 2023). These rivers and their streams are the only water sources in the valleys' upland. These once-vibrant rivers are facing unusual siltation, navigability crisis, excess water in monsoon, and water scarcity in the dry season, which leads to drinking water, irrigation, and fishing crisis due to deforestation, stone extraction, changing cropping practices, and climate change (Rudra and Alam, 2023; Islam, *et al.*, 2017). These hilly rivers are dependent on the forest for their survival, and deforestation can degrade the rivers to a great extent (Shachi, 2018).

CCMEWQI has been adopted by the United Nations Environment Programme in various forms and used to rate water quality worldwide. The Egyptian WQI is based on the CCMEWQI (Khan *et al.*, 2008), New Zealand used this for marine water quality assessment (Walker and Vaughan, 2013), Brazil used it for shrimp culture (Ferreira *et al.*, 2011), USA used it in several states (Bya.org, 2003; IDNR, 2011), India and Vietnam used it for surface water monitoring (Darapu *et al.*, 2011; Hanh *et al.*, 2011).

Several studies have been conducted in the downstream reaches of the Sangu and Matamuhuri Rivers. Haque *et al.* (2020) investigated the relationship between WT and macrobenthos at the estuary of the Sangu River. Perkins (1976) showed the dependence of the benthic community on the salinity, DO, WT, etc. Other physical and nutrient parameters also determine the quality of the aquatic

[1] Dhaka Laboratory, River Research Institute, Dhaka-1205, Bangladesh.
[2] Department of Physics, Bangladesh University of Engineering and Technology, Dhaka-1000, Bangladesh.
[3] Isabela Foundation, Dhaka-1209, Bangladesh.
[*] Corresponding Author: (E-mail: nayan.ghs@gmail.com)

environments (Blaber and Blabar, 1980; Cyprus and Blaber, 1992; Jones, *et al.*, 1996; Fraser, 1997; Young, *et al.*, 1997; Akin, *et al.*, 2005; Jaureguizar, *et al.*, 2003; Simier, *et al.*, 2004; Vivier, *et al.*, 2010; Nabi, *et al.*, 2011). Nabi *et al.* (2015) showed that DO and salinity are the most important parameters for the aquatic environment at the estuary of the Matamuhuri River. Knowing the water quality at the upstream of the rivers is crucial as these are the only water sources. So far, research has yet to be conducted on the water quality at the upstream valleys of the Sangu and Matamuhuri Rivers. This study aims to determine the physicochemical and nutrient parameters of the upstream part of the Sangu and Matamuhuri Rivers within the range of the Santu-Matamuhuri Wildlife Sanctuary and calculate the WQI of each sampling point and the overall study reach of the rivers by CCMEWQI.

Methodology

Sampling parameters

Sampling was done at 4 points of each of the Sangu and Matamuhuri rivers. Sampling started from downstream and completed upstream. The names of the sampling points and the coordinates are shown in **Table 1**. All the sampling points are shown in **Fig. 1**. Samples were collected 6 cm below the water surface.

Water quality parameters

All the water quality parameters were measured in situ at the sampling site. WT, pH, EC, TDS, and DO were measured using a portable HACH HQ30d multi-parameter meter. TA, Cl^-, TH, and CO_2 were measured by titration method using a digital titrator associated with the HACH ff2 aquaculture kit. Turbidity, TSS, NO^-_2, NH_3, NO^-_3, PO^{3-}_4, and SO^{2-}_4 were measured by using a portable HACH DR900 colorimeter. In all the cases, appropriate reagents listed in the manufacturer's (HACH) method were used and the methods were followed accordingly. The details of the methods are given in **Table 2**.

Table 1. Location and Coordinates of the Sampling points.

River	Location	Longitude	Latitude
Sangu	Ma Lung Gya	21°24.26′	92°36.23′
	Licri	21°24.44′	92°35.20′
	Choto Yang Bong	21°26.20′	92°34.51′
	Mo Reng Yang	21°32.13′	92°33.16′
Matamuhuri	Machkum	21°24.53′	92°29.19′
	Chaillatoli	21°24.95′	92°28.36′
	Sindumukh	21°25.79′	92°28.34′
	Indumukh	21°26.13′	92°28.42′

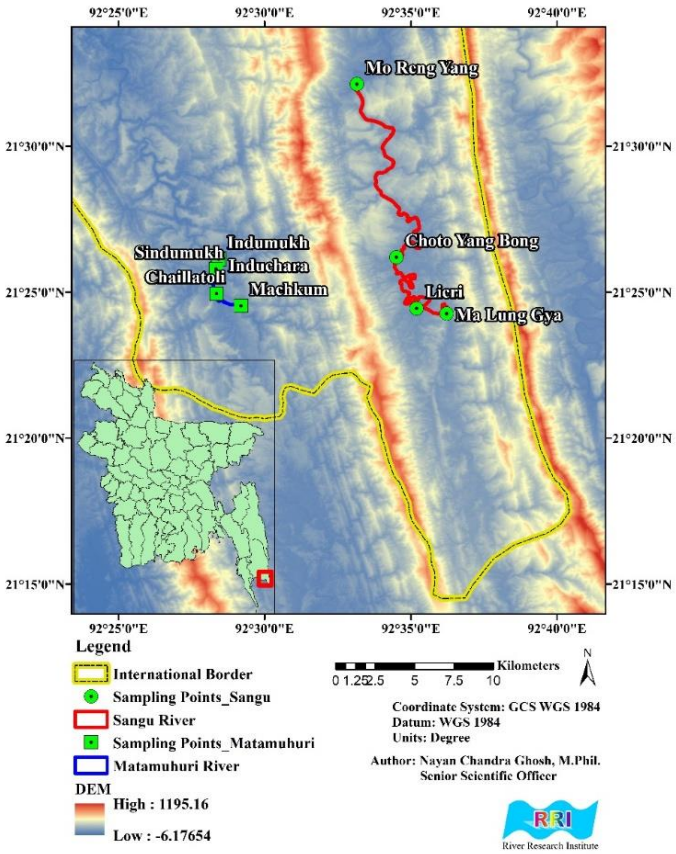

Fig. 1. Sampling points of Sangu and Matamuhuri Rivers.

Water Quality Index (WQI)

We used CCMEWQI (CCME, 2017) to calculate the water quality index of the Sangu and Matamuhuri rivers. The calculation of CCMEWQI is based on three factors, the number of parameters whose guidelines are not met (scope), the frequency with which the guidelines are not met (frequency), and the deviation of each parameter from the standard guideline (amplitude). These three factors are combined as the summation of three vectors to obtain a single water quality value of 0 – 100, where 0 – 44 is considered poor, 45 – 64 is considered marginal, 65 – 79 is considered fair, 80 – 94 is considered good, and 95 – 100 is considered excellent (CCME, 2017).

The "scope" is the percentage of parameters that do not meet the guidelines at least once during the considered period and is calculated by Eq. (1)

$$F_1 = \left(\frac{Number\ of\ failed\ parameters}{Total\ number\ of\ parameters}\right) \times 100 \qquad \text{Eq. (1)}$$

The "frequency" is the percentage of individual tests that do not meet the guidelines and is calculated by Eq. (2)

$$F_2 = \left(\frac{Number\ of\ failed\ tests}{Total\ number\ of\ tests}\right) \times 100 \qquad \text{Eq. (2)}$$

The "amplitude" is the amount by which the failed test values deviate from the standard guideline and is calculated by three different steps.

The first step is called "excursion", which is the number of times by which an individual concentration is greater than (or less than, if the guideline is a minimum) the guideline. For the cases where the concentration must not exceed the guideline, it is calculated by Eq. (3a)

$$excursion_i = \left(\frac{FailedTestValue_i}{Objective_i}\right) - 1 \qquad \text{Eq. } (3a)$$

For the cases where the concentration must not fall below the guideline, it is calculated by Eq. (3b)

$$excursion_i = \left(\frac{Objective_i}{FailedTestValue_i}\right) - 1 \qquad \text{Eq. } (3b)$$

The collective amount by which individual tests are out of compliance is called the "normalized sum of excursions or nse" and is calculated by Eq. (4)

$$nse = \frac{\sum_{i=1}^{n} excursion_i}{Number\ of\ tests} \qquad \text{Eq. (4)}$$

where "Number of tests" represents the tests meeting and not meeting guidelines.

The "amplitude" is then calculated by an asymptotic function that scales the normalized sum "nse" to yield a range between 0 – 100 and is given by Eq. (5)

$$F_3 = \left(\frac{nse}{0.01nse + 0.01}\right) \qquad \text{Eq. (5)}$$

Once all three factors are calculated from Eq. (1), (2), and (5), the CCMEWQI is calculated by Eq. (6)

$$CCMEWQI = 100 - \left(\frac{\sqrt{F_1^2 + F_2^2 + F_3^2}}{1.732}\right) \qquad \text{Eq. (6)}$$

The divisor 1.723 normalizes the resultant values to a range between 0 – 100 (CCME 2017).

The standard guidelines used for calculating the CCMEWQI are the DoE standard (ECR, 2023) for drinking water for the parameters WT, pH, DO, TDS, TH, Cl^-, Turbidity, TSS, NH_3, NO^-_2, NO^-_3, SO^{2-}_4, and PO^{3-}_4; DoE standard (ECR, 1997) for drinking water for EC; Arthur (2022) for alkalinity and Advanced BioTech (2023) for CO_2.

Table 2. Details of the Water Quality Measurement Methods.

Parameter	Method	Range	Source
WT	USEPA Electrode Method	-10-110°C	HACH 8156, (2021)
pH	USEPA Electrode Method	0-14	HACH 8156, (2021)
EC	USEPA Direct Measurement Method	0.01– 200,000 µS/cm	HACH 8160, (2021)
TDS	USEPA Direct Measurement Method	0-50,000 mgL-1	HACH 8160, (2021)
DO	Direct Measurement Method	0.1-20.0 mgL^{-1}	HACH 10360, (2021)
TA	Titration Method	10-400 mgL^{-1}	HACH 8203, (2018)
Cl^-	Titration Method	10-100 mgL^{-1}	HACH 8207, (2015)
TH	Titration Method	10-4000 mgL^{-1}	HACH 8213, (2015)
CO_2	Titration Method	0-100 mgL^{-1}	HACH 8205, (2015)
Turbidity	Absorptometric Method	21-1000 FAU	HACH 8237, (2013)
TSS	Photometric Method	5-750 mgL^{-1}	HACH 8006, (2014)
NO^-_2	USEPA Diazotization Method	0.005 - 0.350 mgL^{-1}	HACH 8507, (2019)
NH_3	Salicylate Method	0.01 - 0.80 mgL^{-1}	HACH 8155, (2018)
NO^-_3	Cadmium Reduction Method	0.3 - 30.0 mgL^{-1}	HACH 8039, (2019)
PO^{3-}_4	USEPA PhosVer 3 (Ascorbic Acid) Method	0.02 - 2.50 mgL^{-1}	HACH 8048, (2017)
SO^{2-}_4	USEPA SulfaVer 4 Method	2 - 70 mgL^{-1}	HACH 8051, (2013)

Results and Discussions

The spatial variation of all the water quality parameters of the Sangu and Matamuhuri Rivers are shown in **Fig. 2** and **Fig. 3** respectively. The Numerical values of the water quality parameters along with the mean, SD, and drinking water standard are shown in **Table 3**.

The mean WT of the Sangu River was determined at 24.05°C (SD 0.93), whereas the Matamuhuri River's mean WT was 21.4°C (SD 1.38). Both the rivers' values are within the DoE standard range of 20-30°C (ECR, 2023) except the Machkum Point of Matamuhuri River. The Machkum point of the river is a very narrow strip (about 6m in width) of the Matamuhuri River, with a right-angled, very high sedimentary rocky riverbank. It is also a point of comparatively high depth of

around 6-8m, whereas the other points are about 1-2m deep. The banks are covered with tall trees, rarely allowing sunlight onto the river. The low sunlight exposure along with high water depth increases the water heating time, making the water relatively cooler than the other points.

The mean DO concentrations of the Sangu and Matamuhuri rivers are 7.89 mgL^{-1} (SD 0.46) and 9.36 mgL^{-1} (SD 0.17), respectively. Both rivers' points have a value of DO concentrations above the DoE standard >6mgL^{-1} for drinking water and aquaculture (ECR, 2023). The higher average DO level of the Matamuhuri River indicates that it possesses more healthier ecology than the Sangu River. The higher SD of the Sangu River suggested that the distribution of DO among the sampling points is more varying than in the Matamuhuri River. Both rivers have an increasing trend as the river progresses, but Sangu has a higher increasing slope than Matamuhuri, as shown in **Fig. 2** and **Fig. 3**. This may be because the measuring points of the Sangu River were nearer the origin of the river than the Matamuhuri River. As the rivers progress, more and more interventions and human and natural influences come into play in the DO concentration variation.

The pH value also shows a similar trend to the DO concentrations and can be incorporated into the same facts. The mean pH of the Sangu River was 7.89 (SD 0.20); in the Matamuhuri River, it was 8.34 (SD 0.11). Both rivers possess pH values within the DoE standard range of 6.5-8.5 (ECR, 2023). A higher pH of Matamuhuri River indicates that it is more suitable for aquatic life.

Although the pH of the Matamuhuri River was higher than the Sangu River, the acid-neutralizing capacity, i.e., TA of the Sangu River, is higher than the Matamuhuri River. This usually happens when water has a high concentration of dissolved acid-neutralizing (alkali) substances such as carbonate, bicarbonate, and hydroxide ions (Arthur, 2022). The mean TA concentrations of the Sangu River were found to be 119 mgL^{-1} (SD 15.03), whereas the Matamuhuri River was 101 mgL^{-1} (SD 4.64). The higher SD of the Sangu River shows variability among points, whereas the Matamuhuri River shows a more consistent distribution of alkalinity. Both rivers have alkalinity within the standard range of 20-250 mgL^{-1} (Arthur, 2022).

The distribution of EC and TDS concentrations in the Sangu and Matamuhuri Rivers has a similar trend. EC and TDS of the Sangu River have a nearby value for the Ma Lung Gya, Licri, and Choto Yang Bong points but have a higher value in the Mo Reng Yang point. The upstream of Mo Reng Yang has a deep and wide portion of the Sangu River called Andharmanik, named after the word “Andhar”, which means darkness. This is a section of high ecological health and geological formation of sedimentary rocky steep bank, which may have influenced the EC and TDS values of these points. The mean EC value for the Sangu River was 168.78 µS/cm (SD 15.15), whereas for the Matamuhuri River was 203.73 µS/cm (SD 5.72). On the other hand, the mean TDS value for the Sangu River was 79.68 mgL^{-1} (SD 6.59), whereas for the Matamuhuri River was 96.90 mgL^{-1} (SD 2.85). The higher SD of the Sangu River is due to the high value of the Mo Reng Yang point. Both rivers have the EC and TDS values within the standard range of 1200 µS/cm (ECR, 1997) and 1000 mgL^{-1} (ECR, 2023), respectively.

The Cl^- concentration of both rivers shows a varying type of spatial distribution. In the Sangu River, the mean value of Cl^- concentration was 10 mgL^{-1} (SD 3.32), while the Matamuhuri River had 13.25 (SD 2.86). Both rivers have chloride values within the DoE standard of 250 mgL^{-1} (ECR, 2023) and have an increasing trend with the rivers’ progress. Both rivers have a nearby value and low concentrations compared to the standard value. Maintaining low chloride concentration is very important for various freshwater fishes, aquatic microorganisms, aquatic plants, etc.

The mean TH concentration in the Sangu River was 70.25 mgL^{-1} (SD 6.06), and in the Matamuhuri River was 81.0 mgL^{-1} (SD 3.54), well within the DoE standard 500 mgL^{-1} (ECR, 2023). Sangu River shows a high value of TH at the Mo Reng Yang point whereas, the Matamuhuri River shows a lower concentration at the Machkum point. The deviation of TH content in both these points can be explained by the unique nature of the sampling points described in the previous sections. The low value in the Machkum might facilitate the high fish yield in that area. According to the locals, the Machkum word came from two different words, “Mach” means fish, and “Kum” means home.

The distribution of CO_2 in the Sangu River is reasonably consistent, whereas it varies in the Matamuhuri River. The mean CO_2 concentration in the Sangu River was 26.15 mgL^{-1} (SD 1.61), whereas, in the Matamuhuri River, it was 24.15 mgL^{-1} (SD 4.49). In both cases, the values exceed the standard limit of 10 mgL^{-1} (Advanced BioTech, 2023). As the rivers are in the hilly regions and lie in the Sangu-Matamuhuri wildlife sanctuary, the aquatic life is somewhat preserved. Hence, CO_2 concentration may possess a higher value due to the influence of organic matter and aquatic respiration.

Turbidity is a parameter dependent on that point's natural and human events. The Sangu River has high but relatively consistent turbidity within the measuring reach, having a mean value of 12 FAU (SD 2.35). The Matamuhuri River has low but widespread turbidity with a mean value of 7.5 FAU (SD 6.87). The very low turbidity at the Machkum point of the Matamuhuri River may be due to the unique characteristics of that point described previously. At the same time, zero turbidity at the Indumukh point may be because the measuring point and it's upstream up to about a kilometer extent has a gravel riverbed that inhibits the sand and silt from mixing with the water and also filters the sediments coming from upstream. On the other hand, in Chaillatoli Point, the riverbed is made of fine sand and silt, and there were numerous human activities on the measuring instance, which led the water to be highly turbid. All the points of the Sangu River exceed the DoE standard 5 mgL^{-1} (ECR, 2023), while for Matamuhuri River, Chaillatoli and Sindumukh points the value exceeds the standard. Although the colorimeter gives turbidity values, these values are lower than the measuring range of the method used in this study and hence cannot be used to calculate the WQI. The mean TSS concentration of the Sangu River was 10.75 mgL^{-1} (SD 1.48), which is much more consistent among the points. TSS concentration of the Matamuhuri River showed a similar trend as turbidity with a mean concentration of 9.50 mgL^{-1} (SD 6.87). The Ma Lung Gya and Mo Reng Yang points of the Sangu River and the Chaillatoli point of the Matamuhuri River exceed the DoE standard of 10 mgL^{-1} of TSS for drinking water (ECR, 2023).

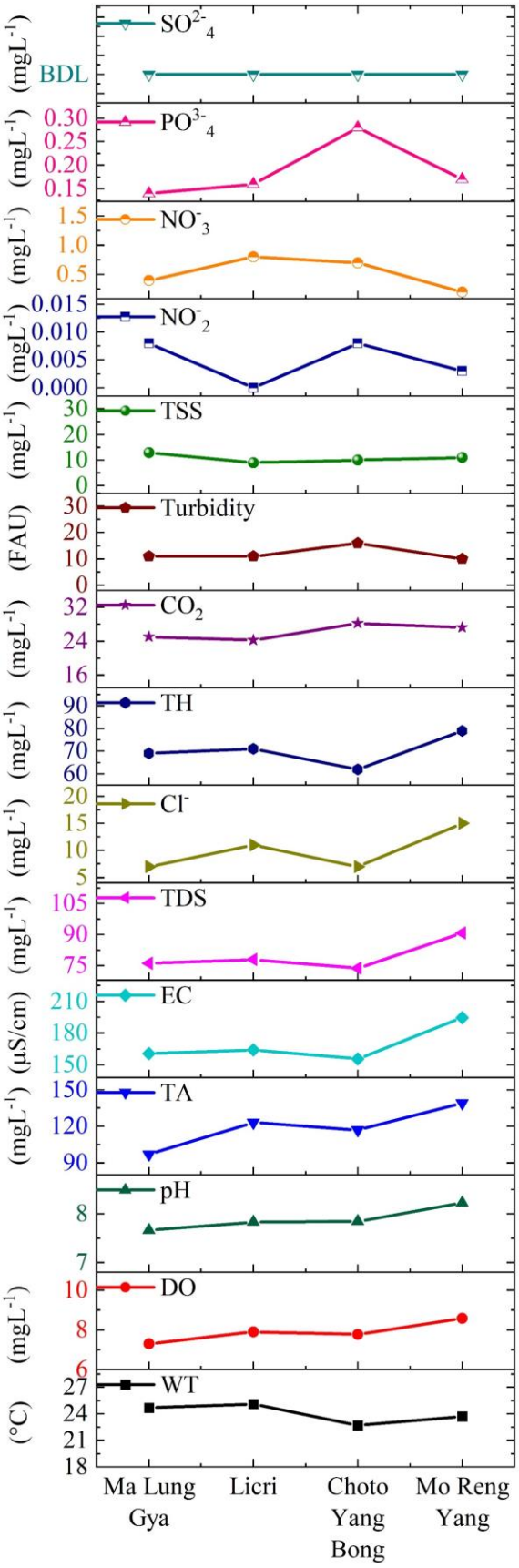

Fig. 2. Spatial variation of water quality parameters of the Sangu River.

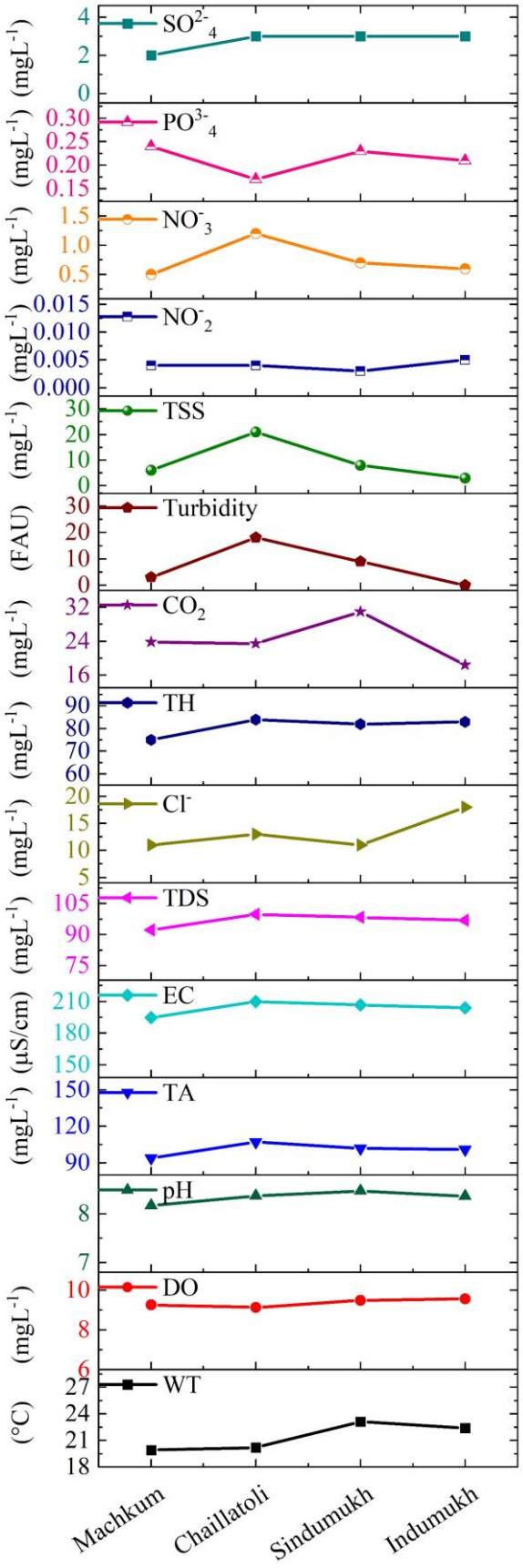

Fig. 3. Spatial variation of water quality parameters of the Matamuhuri River.

Table 3. Water quality parameters of the Sangu and Matamuhuri Rivers.

River	Location	WT (°C)	DO (mgL^{-1})	pH	TA (mgL^{-1})	EC µS/cm	TDS (mgL^{-1})	Cl^{-} (mgL^{-1})	TH (mgL^{-1})	CO_2 (mgL^{-1})	Turbidity (mgL^{-1})	TSS (mgL^{-1})	NO^{-}_{2} (mgL^{-1})	NH_3 (mgL^{-1})	NO^{-}_{3} (mgL^{-1})	PO^{3-}_{4} (mgL^{-1})	SO^{2-}_{4} (mgL^{-1})
Sangu	Ma Lung Gya	24.7	7.3	7.66	97	160.6	76.2	7	69	25	11	13	0.008	BDL*	0.4	0.14	BDL*
	Licri	25.1	7.9	7.83	123	164.2	77.9	11	71	24.2	11	9	0	BDL*	0.8	0.16	BDL*
	Choto Yang Bong	22.7	7.78	7.85	117	155.8	73.8	7	62	28.2	16	10	0.008	BDL*	0.7	0.28	BDL*
	Mo Reng Yang	23.7	8.59	8.22	139	194.5	90.8	15	79	27.2	10	11	0.003	BDL*	0.2	0.17	BDL*
	Average	24.05	7.89	7.89	119	168.78	79.68	10.00	70.25	26.15	12.00	10.75	0.005	--	0.53	0.19	--
	Standard Deviation	0.93	0.46	0.20	15.03	15.15	6.59	3.32	6.06	1.61	2.35	1.48	0.003	--	0.24	0.05	--
Matamuhuri	Machkum	19.9	9.26	8.17	94	194.5	92.3	11	75	23.8	3	6	0.004	BDL*	0.5	0.24	2
	Chaillatoli	20.2	9.13	8.37	107	209.8	99.9	13	84	23.4	18	21	0.004	BDL*	1.2	0.17	3
	Sindumukh	23.1	9.48	8.47	102	206.7	98.4	11	82	31	9	8	0.003	BDL*	0.7	0.23	3
	Indumukh	22.4	9.57	8.36	101	203.9	97	18	83	18.4	0	3	0.005	BDL*	0.6	0.21	3
	Average	21.40	9.36	8.34	101	203.73	96.90	13.25	81.00	24.15	7.50	9.50	0.004	--	0.75	0.21	2.75
	Standard Deviation	1.38	0.17	0.11	4.64	5.72	2.85	2.86	3.54	4.49	6.87	6.87	0.001	--	0.27	0.03	0.43
Standard for Drinking Water		20-30	>6	6.5-8.5	20-250	1200	1000	250	500	10	5	10	10		45	0.1	250

(Note: *BDL → Below Detection Limit.)

The NO^{-}_{2} concentration of both rivers is within the DoE standard 10 mgL^{-1} (ECR, 2023) and found in very low concentrations. The mean NO^{-}_{2} concentration of the Sangu River is 0.005 mgL^{-1} (SD 0.003), while in the Matamuhuri River, the concentration is 0.004 mgL^{-1} (SD 0.001). The SD value shows that the nitrite distribution is more widespread in the Sangu River than in the Matamuhuri River. Still, the concentrations are very low than the standard, so it does not affect the water. The NH_3 concentration of both rivers was measured and found to be Below the Detection Limit (BDL) of the method (<0.01 mgL^{-1}) at all the points of both rivers.

The NO^{-}_{3} concentration has also shown a very low value compared to the DoE standard 45 mgL^{-1} (ECR, 2023) in both rivers. The Sangu River has a lower mean concentration of 0.53 mgL^{-1} (SD 0.24) than the Matamuhuri River of 0.75 mgL^{-1} (SD 0.27). Still, the distribution is very similar in both rivers, as the SD values indicate. The very low presence of NO^{-}_{2}, NH_3, and NO^{-}_{3} indicates no nitrogen contamination in both rivers.

While there was no contamination by nitrogen, the PO^{3-}_{4} concentration, as an indicator of contamination from agriculture and livestock, was higher at all the points of both rivers than the DoE standard of 0.1 mgL^{-1} (ECR, 2023). The mean PO^{3-}_{4} concentration of the Sangu and Matamuhuri rivers was measured at 0.19 mgL^{-1} (SD 0.05) and 0.21 mgL^{-1} (SD 0.03), respectively. The distributions of the PO^{3-}_{4} are reasonably consistent in both rivers. Both rivers flow through hilly areas where indigenous people cultivate their ways at hills, and livestock is essential to their livelihood. This leads to the washout of agriculture and livestock contaminants to the river by rain and other measures, which may explain the high PO^{3-}_{4} concentration of these rivers.

The SO^{2-}_{4} concentration of the Sangu River was BDL (<2 mgL^{-1}) at all the points and a mean concentration of 2.75 mgL^{-1} (SD 0.43) was found at the Matamuhuri River which is within the DoE standard of 250 mgL^{-1} for drinking water (ECR, 2023). The distribution of SO^{2-}_{4} is reasonably consistent in the Matamuhuri River.

The CCMEWQI was measured based on 15 parameters out of 16 measured parameters, leaving turbidity out of the calculation due to the non-reliability of the method. The WQI of the Sangu River is calculated to be a "good" category at all points throughout the reach studied as shown in **Fig. 4**. The highest WQI in the Licri point is 87.33, while the lowest in the Mo Reng Yang point is 81.88. The overall WQI upstream of the Sangu River is calculated to be 82.95. The deviation of the WQI from the excellent criterion is due to the high value of CO_2, TSS, and PO^{3-}_{4}.

The CCMEWQI of the Matamuhuri River also shows a "good" category of water in all the measured points. The highest WQI found at the Indumukh point is 87.45, while the lowest at the Machkum point is 81.56. The overall WQI of the study reach of the Matamuhuri River is calculated to be 81.08 as shown in **Fig. 5**. The WQI of the Matamuhuri River deviated from the excellent criterion due to the deviation of the WT, CO_2, TSS, and PO^{3-}_{4} parameters from the standard value. Among them, TSS was measured very high at Chaillatoli Point due to human interference.

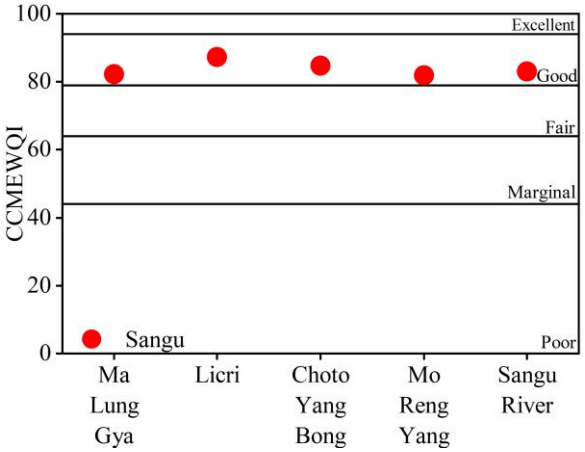

Fig. 4. CCMEWQI of Sangu Rivers.

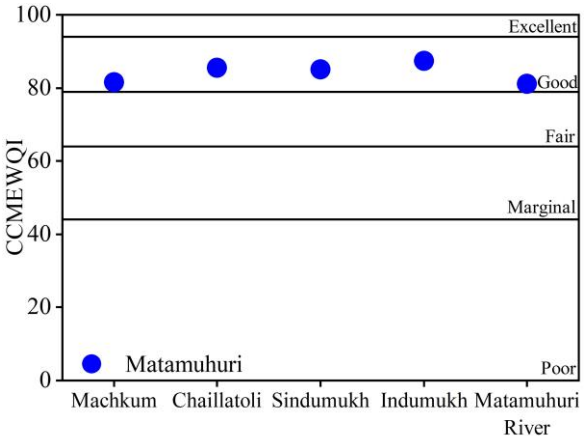

Fig. 5. CCMEWQI of Matamuhuri Rivers.

Conclusions

Sixteen water quality parameters have been measured in this study at 4 points of both rivers, and 15 parameters were used to calculate the CCMEWQI. Among them, at the Sangu River, three parameters, CO_2, TSS, and PO^{3-}_{4}, were found higher than the standard guideline, while at the Matamuhuri River, four parameters, WT, CO_2, TSS, and PO^{3-}_{4}, were found to deviate than the standard guideline. WQI was calculated by the CCMEWQI method and found to be "good" category in both rivers, with a value of 82.95 and 81.08 for the Sangu and Matamuhuri, respectively.

Recommendations

The study was at a very remote location where resources are hard to find and access to various points is also very limited. A more comprehensive study of seasonal water quality assessment, along with more parameters, including biological pollutants and heavy metal determination, would give a better estimation of the WQI of these rivers.

Acknowledgment

The authors acknowledge Isabela Foundation for conducting this study at very remote and inaccessible locations with their funding and utmost logistic support, and River Research Institute, Bangladesh, for their instrumental and testing support.

References

Advanced BioTech. (2023). Water Analysis – Dissolved Carbon Dioxide. [online] https://www.adbio.com/water-analysis-dissolved-carbon-dioxide/#:~:text=Surface%20waters%20normally%20contain%20less%20than%2010%20ppm,solubility%20is%20about%20200%20times%20that%20of%20oxygen, (Accessed on July 31 2023).

Akin, S., Buhan, E., Winemiller, K. O. and Yilmaz, H. (2005). Fish assemblage structure of Koycegiz Lagoon–Estuary, Turkey: Spatial and temporal distribution patterns in relation to environmental variation. *Estuar. Coast Shelf Sci.* 64(4): 671-684, https://doi.org/10.1016/j.ecss.2005.03.019.

Arthur, D. (January 24, 2022). What is Alkalinity of Water. [online] https://watertreatmentbasics.com/alkalinity-of-water/ (Accessed on July 31 2023).

Bay.org. (2003). The Bay Institute Ecological Scorecard. San Francisco Bay Water Quality Index Indicator analysis and evaluation. http://thebayinstitute.blob.core.windows.net/assets/Scorecard_4page.pdf

Blaber, S.J.M. and Blaber, T.G. (1980). Factors affecting the distribution of juvenile estuarine and inshore fish. *J. Fish Biol.* 17(2): 143-162. https://doi.org/10.1111/j.1095-8649.1980.tb02749.x

CCME (2017). Canadian water quality guidelines for the protection of aquatic life, CCME Water Quality Index User's Manual 2017 Update. *Canadian Council of Ministers of the Environment (CCME).* Winnipeg, Canada.

Charlie, S. (1945). The Sangu River, 1943. *RUSI Journal.* 90(559): 313-322. https://doi.org/10.1080/03071844509423960

Cyprus, D.P. and Blaber, S.J.M. (1992). Turbidity and salinity in a tropical northern Australian estuary and their influence on fish distribution. *Estuar. Coast Shelf Sci.* 35(6): 545-563. https://doi.org/10.1016/S0272-7714(05)80038-1.

Darapu, S.S.K., Sudhakar, B., Krishna, K.S.R., Rao, P.V. and Sekhar, M.C. (2011). Determining water quality index for the evaluation of water quality of River Godavari. *Int. J. Eng. Res. App.* 1(2): 174-182.

ECR (1997). Environmental Conservation Rule, 1997. Depart of Environment, Government of the People's Republic of Bangladesh.

ECR (2023). Environmental Conservation Rule, 2023. Depart of Environment, Government of the People's Republic of Bangladesh.

Ferreira, N.C., Bonetti, C. and Seiffert, W.Q. (2011). Hydrological and water quality indices as management tools in marine shrimp culture. *Aquaculture.* 318(3): 425-433, https://doi.org/10.1016/j.aquaculture.2011.05.045.

Fraser, T.H. (1997). Abundance, Seasonality, Community Indices, Trends and Relationships with Physicochemical Factors of Trawled Fish in Upper Charlotte Harbor, Florida. *Bull. Mar. Sci.* 60(3): 739-763.

Gain, P. (2000). The Chittagong Hill Tracts: Life and Nature at Risk. Society for Environment and Human Development. University Press Limited, Dhaka.

HACH 8006. (2014). Suspended Solids, Photometric Method. Edition 9. DOC316.53.01139.

HACH 8039. (2019). Nitrogen-Nitrate, Cadmium Reduction Method. Edition 10. DOC316.53.01066.

HACH 8048. (2017). Phosphorus, Reactive (Orthophosphate), USEPA PhosVer 3 (Ascorbic Acid) Method. Edition 10. DOC316.53.01119.

HACH 8051. (2013). Sulfate, USEPA SulfaVer 4 Method. Edition 8. DOC316.53.01135.

HACH 8155. (2018). Nitrogen, Ammonia, Salicylate Method. Edition 3. DOC316.53.01466.

HACH 8156. (2021). pH, USEPA Electrode Method. Edition 9. DOC316.53.01245.

HACH 8160. (2021). Conductivity, USEPA Direct Measurement Method. Edition 10. DOC316.53.01199.

HACH 8203. (2018). Alkalinity, Phenolphthalein and Total Alkalinity. Edition 9. DOC316.53.01166.

HACH 8205. (2015). Carbon Dioxide, Sodium Hydroxide Method. Edition 8. DOC316.53.01167.

HACH 8207. (2015). Chloride, Silver Nitrate Method. Edition 8. DOC316.53.01171.

HACH 8213. (2015). Hardness, Total, Titration Method with EDTA. Edition 8. DOC316.53.01176.

HACH 8237. (2013). Turbidity, Absorptometric Method. Edition 8. DOC316.53.01332.

HACH 8507. (2019). Nitrite, USEPA Diazotization Method. Edition 11. DOC316.53.01074.

HACH 10360. (2021). Oxygen, Dissolved, Direct Measurement Method. Edition 9. DOC316.53.01243.

Hanh, P.T.M., Sthiannopkao, S., Ba, D.T. and Kim, K.W. (2011). Development of water quality indexes to identify pollutants in Vietnam's surface water. *J. Environ. Eng.* 137(4): 273 https://doi:10.1061/(ASCE)EE.1943-7870.0000314.

Haque, M. M., Sharif, A. S. M., Ahmed, M. K., Anwar, F., Rani, S., Molla, M. H. R. and Khan, M. I. (2020). Distribution and Diversity of Macrobenthos in Sangu River, Bangladesh. *Dhaka Uni. Jour. Ear. Env. Sci.* 9(2): 27-33.

Hossen, M. S., Hossain, M. S. and Rahaman, M. M. (2019). Sangu River's Contribution to the Livelihood of local People. River: A Living Being, 4th International Water Conference 2019 - January 29 - 30, 2019, Kuakata, Potuakhali, Bangladesh.

Indiana Department of Natural Resources (IDNR). (2011). Hoosier Riverwatch Datawatch. http://www.hoosierriverwatch.com [Accessed 31 July 2023]

Islam, M.T., Ullah, M.M., Amin, M.G.M. and Hossain, S. (2017). Rainwater harvesting potential for farming system development in a hilly watershed of Bangladesh. *Appl. Water Sci.* 7(5): 2523–2532. https://doi.org/10.1007/s13201-016-0444-x.

Jaureguizar, A.J., Menni, R., Bremec, C., Miaizan, H. and Lasta, C. (2003). Fish assemblage and environmental patterns in the Río de la Plata estuary. *Estuar. Coast Shelf Sci.* 56 (5–6): 921-933. https://doi.org/10.1016/S0272-7714(02)00288-3.

Jones, G.K., Baker, J.L., Edyvane, K. and Wright, G.J. (1996). Nearshore fish community of the Port River-Barker Inlet Estuary, South Australia. I. Effect of thermal effluent on the fish community structure, and distribution and growth of economically important fish species. *Mar. Freshwater Res.* 47(6): 785-799. https://doi.org/10.1071/MF9960785.

Khan, A.A., Abdel-Gawad, S. and Khan, H. (2008). A Real Time Water Quality Monitoring Network and Water Quality Indices for River Nile. Proceedings of the XIIIth International Water Resources Association (IWRA) World Water Congress, Montpellier, France, September 1 - 4, 2008, http://www.iwra.org/congress/2008/resource/authors/abs894_article.pdf

Khan, M.A.A. and Haque, S.M.S. (2003). Features and Characteristics of Bangladesh Watershed. B. Sc. (Hons) Project Paper, Institute of Forestry and Environmental Sciences, University of Chittagong, Bangladesh.

Mukherjee, P., Mishra, S. N., Kumar, P., Kumar, S., Singh, K. P. and Kumar, R. (2023). Water Quality: An Ecological Indicator for Aquatic Biodiversity Survival and Ecorestoration. *Indian For.* 149(5): 533-542. https://doi.org/10.36808/if/2023/v149i5/168052

Nabi, M.R., A1-Mamun, M.A., Ullah, M.H. and Mustafa, M.G. (2011) Temporal and spatial distribution of fish and shrimp assemblage in the Bakkhali river estuary of Bangladesh in relation to some water quality parameters. *Mar. Biol. Res.* 7(5): 436-452, https://doi.org/10.1080/17451000.2010.527988.

Nabi, M.R.U., Mallick, M., Chowdhury, M.A.U., Haque, M.A. and Shamsuzzaman, M.M. (2015). Effects of Water Quality on Spatiotemporal Variation in Fish Assemblage in Matamuhuri River Estuary, Cox's Bazar, Bangladesh. *Chiltagong Univ. J. Sci.* 37:31-61.

Perkins, E. J. (1976). The biology of estuaries and coastal waters. *Academic Press, London and New York.* ix + 678.

Rahman, A.A., Huq, S. and Conway, G. (1990). Environmental Aspects of Surface Water Systems of Bangladesh. *University Press Limited*. 52.

Rudra, A. K. and Alam, A.K.M.R. (2023). Streamflow characteristics of Sangu-Matamuhuri watershed in the southeastern part of Bangladesh. *Heliyon*. 9(3): e14559. https://doi.org/10.1016/j.heliyon.2023.e14559.

Shachi, M. (2018). The Sangu, a dying transboundary river. Retrieved July 31, 2023, from thethirdpole.net: https://www.thethirdpole.net/en/2018/02/12/sohara-mehroze-shachi/

Simier, M., Blanc, L., Aliaume, C., Dioul P.S. and Albaret, J.J. (2004). Spatial and temporal structure of fish assemblages in an “inverse estuary”, the Sine Saloum system (Senegal). *Estuar. Coast Shelf Sci.* 59(1): 69-86. https://doi.org/10.1016/j.ecss.2003.08.002.

Vivier, L., Cyrus, D.P., Owen, R.K. and Jerling, H.L. (2010). Fish assemblages in the Mfolozi–Msunduzi estuarine system, KwaZulu-Natal, South Africa, when not linked to the St Lucia mouth. *Afr. J. Aquat. Sci.* 35(2): 141-l54. https://doi.org/10.2989/16085914.2010.490984.

Walker, J. and Vaughan, M. (2013). Marine water quality annual report: 2010. Auckland Council technical report, TR2013/030, https://knowledgeauckland.org.nz/media/1646/tr2013-030-marine-water-quality-annual-report-2010.pdf

Young, G. C., Potter, I. C., Hyndes, G. A. and Lestang, S.D. (1997). The Ichthyofauna of an Intermittently Open Estuary: Implications of Bar Breaching and Low Salinities on Faunal Composition. *Estuar. Coast Shelf Sci.* 45(1): 53-68, https://doi.org/10.1006/ecss.1996.0165.

Technical Journal
River Research Institute ISSN: 1606-9277

HUMAN HEALTH RISK ASSESSMENT FROM THE CONTAMINANTS OF MAHANANDA RIVER WATER AND ITS ADJACENT GROUNDWATER IN BANGLADESH

N. C. Ghosh[1,2*], M. Moniruzzaman[3,4], M. M. R. Mondol[3,5]

Abstract

This study aims to assess the physicochemical parameters of the surface water of the Mahananda River and the concentration of the nutrients of the Mahananda River water and the adjacent groundwater. Among physicochemical parameters, pH, Dissolved Oxygen (DO), and Total Dissolved Solids (TDS) were measured on 18 sampling sites of the river, while Sulfate (SO_4^{2-}), Orthophosphate (PO_4^{3-}), Arsenic (As), and Manganese (Mn) concentrations were measured on 17 equidistant sampling sites of the river and the adjacent groundwater. The mean pH value was 8.50 with a standard deviation (SD) of 0.30. DO and TDS were 9.56 mgL^{-1} (SD 1.67) and 127.62 mgL^{-1} (SD 24.76), respectively. The mean SO_4^{2-} concentration was found to be 5.38 mgL^{-1} (SD 12.00) for groundwater and 2.29 mgL^{-1} (SD 1.96) for surface water, while the mean PO_4^{3-} concentration was 1.17 mgL^{-1} (SD 0.78) and 0.63 mgL^{-1} (SD 0.15) for groundwater and surface water respectively. The contamination of As was found to be as high as 100 μgL^{-1} in the groundwater while within 25 μgL^{-1} in the surface water. Mn concentration was high at almost all the points, with a mean value of 1.64 mgL^{-1} (SD 0.90) and 0.54 mgL^{-1} (SD 0.23) for the groundwater and surface water, respectively. The carcinogenic risk from As and non-carcinogenic risk from both As and Mn was estimated for adults and children. The carcinogenic risks were found to be high for both surface water and groundwater, while non-carcinogenic risks were found high for surface water and very high for groundwater. In both cases, children were found more vulnerable than adults.

Keywords: *Arsenic, Carcinogenic Risk, Groundwater, Mahananda River, Manganese, Non-Carcinogenic Risk.*

Introduction

Mahananda is one of the major transboundary rivers between Bangladesh and India. It originates from the Himalayas. Several hilly streams meet at Gyan Sangam and form the Mahananda River. From the origin, it flows about 31 km to reach to Bangladesh and India border adjacent to the Banglabandha-Fulbari land port. About 1.5 km up from this point, the river experienced a major diversion by the Fulbari barrage, where the river meets the Teesta irrigation canal of India and flows further downstream with the same canal name up to Nitaiganj. The mainstream of the river with the remaining streamflow flows as the border river for about 20 km. It then flows through India for 225 km and finally falls on the Ganges near the Farakka barrage. Prior to the falls on the Ganges, a part of the river bifurcated and flowed about 71 km to reach the Bholahat upazila of Chapainawabganj district of Bangladesh. The following 16 km river flow from Bholahat upazila sadar to Baruipara of Gomostapur upazila is again a border river and finally enters Bangladesh at this point. Mahananda River travels about 76 km and falls to the Padma River at Sultanganj of the Godagari upazila of Rajshahi. The total catchment area of the river from its origin to Sultanganj is 20600 km^2, where 11530 km^2 is in India, and 9070 km^2 is in Bangladesh (Ghosh *et al.*, 2022).

The Mahananda River in Bangladesh, crosses Gomastapur, Shibganj, and Chapainawabganj Sadar upazilas. The river has two tributaries in Bangladesh, one on the left bank at Gomostapur, Punarbhaba River, and the other on the right bank at Chapainawabganj Sadar, Pagla River. According to the Bangladesh Water Development Board (BWDB) data, the river's minimum water level declined from 1977 to 2017. BWDB data also suggest that the adjacent groundwater level follows the same trend, and the southern part has a lower groundwater level than the northern part (RRI, 2019). The river contributes to the irrigation of above 10000 hectares of cropland. People near the river use its water for bathing, washing, and household work. According to the Bangladesh Population and Housing Census 2011, about 8.3% of the district's population uses tap water for drinking purposes, while 88.2% uses groundwater and 3.5% other water sources, including surface water (BBS, 2014). They also use this water for cooking.

As is found on Earth naturally. There are both organic and inorganic forms of As in the environment. The organic form is much less harmful than the inorganic form. Inorganic As is highly toxic and found at high levels in the groundwater of many countries, including Bangladesh. Ingestion of As-rich groundwater poses the greatest threat to human health. Inorganic As is a significant contaminant in drinking water and is a confirmed carcinogen (Farzan *et al.*, 2013). Long-term exposure to a high level of inorganic As causes skin, lung, and bladder cancer, pigmentation changes, skin lesions, and hard patches on the palms and soles. In addition to skin cancer, long-term exposure to As may also cause cancers of the bladder and lungs (Tolins *et al.*, 2014). The other effects of As on human health include developmental effects, diabetes, pulmonary disease, and cardiovascular disease (Ravenscroft *et al.*, 2009).

Mn is an essential element for humans. Both under and over-exposure to Mn can cause adverse health effects. Although Mn deficiency is rare, overexposure to Mn is very common globally since it is found in various foods and natural water (USEPA, 1984; Hurley and Keen, 1987). Chronic inhalation of high Mn has been found to have adverse neurological effects on humans. It can cause weakness, anorexia, muscle pain, apathy, slow speech, monotonous tone of voice, emotionless masklike facial expression, and slow, clumsy movement of the limbs (Canavan *et al.*, 1934; Cook *et al.*, 1974; Roels *et al.*, 1999; ATSDR, 2012). Long-term high intake of Mn from drinking water also causes neurotoxicity, and the concentration of Mn is proportional to neurotoxicity (Kondakis *et al.*, 1989).

Both oral and dermal contact with these metals can cause health risks. Thus, it is important to determine the health risk

[1] Dhaka Laboratory, River Research Institute, Dhaka-1205, Bangladesh.
[2] Department of Physics, Bangladesh University of Engineering and Technology, Dhaka-1000, Bangladesh.
[*] Corresponding Author: (E-mail: nayan.ghs@gmail.com)
[3] Geotechnical Research Directorate, River Research Institute, Faridpur-7800, Bangladesh.
[4] Institute of Water and Flood Management, Bangladesh University of Engineering and Technology, Dhaka-1000, Bangladesh.
[5] Department of Civil Engineering, Bangladesh University of Engineering and Technology, Dhaka-1000, Bangladesh.

of both carcinogenic and non-carcinogenic manner of these contaminants to estimate the health hazard. Assessing the health risk of environmental pollutants is known as human health risk assessment (Momot and Synzynys, 2005). The assessment's main component includes identifying hazards, dose-response relationships, exposure assessment, and risk characterization (Wu *et al*., 2010). It is a useful way to show the degree of health risk caused by various contaminants (Bortey-Sam *et al*., 2015).

Tuinhof and Kemper (2011) studied "Mitigation of As Contamination in Drinking Water Supplies of Bangladesh." They studied the severity of As contamination in groundwater at Chapai Nawabganj town was investigated thoroughly, and a scheme was designed to supply As-free water to the townspeople. Islam *et al.* (2014) studied the accumulation of heavy metals in two urban rivers and found a high concentration of accumulation in all the fish species. Akter *et al.* (2021) Conducted a study on the human health risk assessment of groundwater As, Fe, and Mn contamination at the Dhamrai upazila of Bangladesh. Ali *et al.* (2022) studied the heavy metal toxicity of the Bhairab river and reported various heavy metals exceed the permissible limit. Kubra *et al.* (2022) reported the high carcinogenic risks from the sediments of Rupsa River. Several other studies have been conducted to assess human health risks through oral and dermal routes by heavy metals in water (Zhang *et al.*, 2019; Ramazanova *et al.*, 2022). Kormoker *et al.* (2023) studied the physicochemical and heavy metal concentrations of the Buriganga River and reported high carcinogenic and non-carcinogenic risks for both children and adults with a higher vulnerability of children. There has been no report on the human health risk analysis of the Mahananda River. Hence, this study aims to assess the human health risk from the Mahananda River water and its adjacent groundwater.

Methodology

Study Area

The whole reach of the Mahananda River in the Chapainawabganj district of Bangladesh was considered the study area as this is the only part of the river where it flows completely through Bangladesh. The extent of the studying of physicochemical parameters was 86 km, from Bazratek (24°57.025'N, 88°13.953'E), Bholahat, the furthest a civilian can go to the Bangladesh-India border to Sultanganj Ghat (24°29.663'N, 88°18.381'E), Godagari, Rajshahi, where it falls to the Padma River. The extent of the studying of nutrients and elements was 76 km, the total reach of the Mahananda River through Bangladesh, from Baruipara (24°52.639'N, 88°15.490'N), Gomostapur, Chapainawabganj, where the river ultimately enters the Bangladesh territory to Sultanganj (24°29.598'N, 88°18.384'N), where it falls to Padma River.

Sampling Points

Physicochemical parameters were analyzed at 18 points of the Mahananda River, whereas, nutrient and elemental analysis was done at 17 equidistant points of the Mahananda River and adjacent groundwater samples. The groundwater samples were analyzed at the nearest available tube well of the river sampling points. The surface water sampling points for physicochemical parameters are shown in **Fig. 1** and **Table 1**, while nutrients and elemental analysis points are shown in **Fig. 2** and **Table 2**.

Water Quality

All the parameters were determined in situ at the sampling site. The physicochemical parameters such as pH, DO, and TDS were measured only for river water by direct probe method using a portable HACH hq30d multiparameter meter. The Analysis of As was carried out by using a HACH low-range As testing kit method. Mn, SO_4^{2-}, and PO_4^{3-} were determined by the HACH DR 900 portable colorimeter. USEPA Periodate Oxidation Method was used for the determination of Mn concentrations (USEPA, 1979) with a detection limit of 0.1 to 20.0 mgL^{-1}, USEPA SulfaVer 4 Method was used for the determination of SO_4^{2-} concentrations (USEPA a) with a detection limit of 2.0 to 70.0 mgL^{-1}. USEPA PhosVer 3 (Ascorbic Acid) Method was used to determine PO_4^{3-} concentrations (USEPA b) with a detection limit of 0.02 to 2.5 mgL^{-1}.

Health Risk Assessment

Ingestion of water for drinking and cooking purposes and dermal contact during bathing and washing were taken as the intake routes for human health risk assessment. The intake rate of metal through the ingestion route (I_o) was calculated by Eq. (1) (USEPA, 1989):

$$I_o = \frac{C_w \times IR \times EF \times ED}{BW \times AT} \quad \text{Eq. (1)}$$

where C_w is the metal concentration at the exposure site (mgL^{-1}); IR is the ingestion rate (L/day); EF is the exposure frequency (day/ year); ED is the exposure duration (years); BW is the average body weight (kg); AT is the averaging time (day). The intake rate of metal through dermal contact (I_d) was calculated by Eq. (2) (USEPA, 1989):

$$I_d = \frac{C_w \times SSA \times k_p \times CF \times ET \times EF \times ED}{BW \times AT} \quad \text{Eq. (2)}$$

where SSA is the skin surface area (cm^2); k_p is the permeability coefficient specific for each metal ($cm.h^{-1}$); CF is the respective conversion factor ($L.cm^{-3}$); ET is the exposure time (h/event); Oral and dermal intakes are expressed as $mg.kg^{-1}$ of body weight/day.

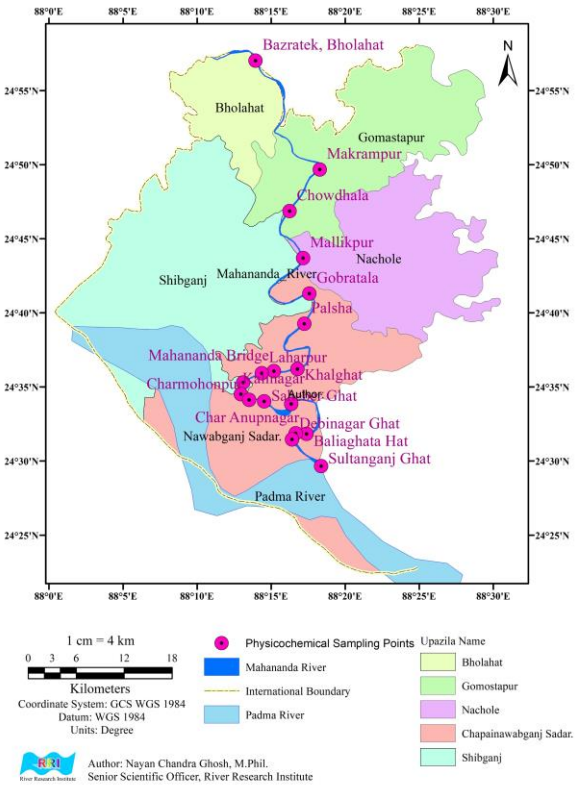

Fig. 1. Surface water sampling points for the analysis of physicochemical parameters.

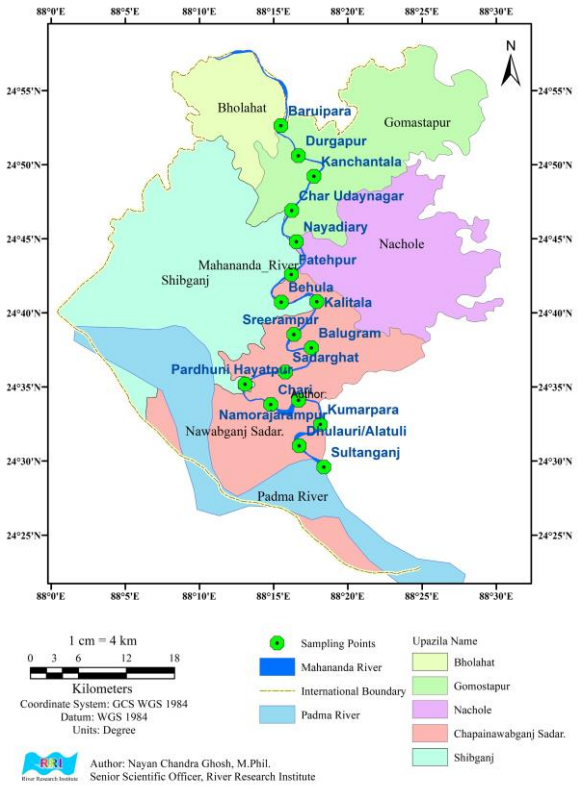

Fig. 2. Surface water sampling points for the analysis of nutrients and elements.

Table 1. Coordinates of the surface water sampling points for the analysis of physicochemical parameters.

Name	Latitude	Longitude
Bazratek, Volahat	24°57.025'N	88°13.953'E
Makrampur	24°49.673'N	88°18.295'E
Chowdhala	24°46.869'N	88°16.257'E
Mallikpur	24°43.700'N	88°17.171'E
Gobratala	24°41.304'N	88°17.593'E
Palsha	24°39.265'N	88°17.247'E
Khalghat	24°36.217'N	88°16.785'E
Mahananda Bridge	24°36.067'N	88°15.196'E
Laharpur	24°35.937'N	88°14.377'E
Ansarer Ghat	24°35.301'N	88°13.119'E
Kalinagar	24°34.514'N	88°12.967'E
Charmohonpur	24°34.137'N	88°13.526'E
Saheber Ghat	24°34.034'N	88°14.538'E
Rajarampur Ghat	24°33.858'N	88°16.361'E
Baliaghata Hat	24°31.836'N	88°17.397'E
Char Anupnagar	24°31.878'N	88°16.668'E
Debinagar Ghat	24°31.466'N	88°16.422'E
Sultanganj Ghat	24°29.663'N	88°18.381'E

Table 2. Coordinates of the surface water sampling points for the analysis of nutrients and elements.

Name	Latitude	Longitude
Baruipara	24°52.639'N	88°15.490'E
Durgapur	24°50.615'N	88°16.673'E
Kanchantala	24°49.218'N	88°17.724'E
Char Udaynagar	24°46.906'N	88°16.219'E
Nayadiary	24°44.809'N	88°16.532'E
Fatehpur	24°42.595'N	88°16.192'E
Behula	24°40.735'N	88°15.515'E
Kalitala	24°40.760'N	88°17.911'E
Sreerampur	24°38.547'N	88°16.366'E
Balugram	24°37.642'N	88°17.547'E
Sadarghat	24°36.008'N	88°15.792'E
Pardhuni Hayatpur	24°35.191'N	88°13.076'E
Chari	24°33.817'N	88°14.809'E
Namorajarampur	24°34.105'N	88°16.680'E
Kumarpara	24°32.479'N	88°18.151'E
Dhulauri/Alatuli	24°31.032'N	88°16.721'E
Sultanganj	24°29.598'N	88°18.384'E

Risk assessment: carcinogenic risk

The carcinogenic risk caused by a specific heavy metal was estimated by Eq. (3) (USEPA, 1989):

$$Risk = I \times SF \quad \text{Eq. (3)}$$

where SF is the slope factor of the carcinogenic heavy metal (kg. day/mg).

Since two exposure routes were considered in this study, the total cancer risk caused by As through oral and dermal exposures was estimated using Eq. (4) (USEPA, 1989):

$$Risk = \sum_{i=1}^{n}\sum_{j=1}^{m} I \times SF \quad \text{Eq. (4)}$$

The threshold range for carcinogenic risk was taken as 10^{-6} as it was determined for a single carcinogenic element (Tepanosyan *et al.*, 2017).

Risk assessment: non-carcinogenic risk

The non-carcinogenic risk was characterized by the hazard quotient (HQ) and estimated by Eq. (5) (USEPA, 1989):

$$HQ = I/RfD \quad \text{Eq. (5)}$$

where RfD is the respective metal's reference dose ($mg.kg^{-1}.Day^{-1}$).

The total non-carcinogenic risk caused by both metals through both exposure routes was characterized as the hazard index (HI) and estimated as the sum of obtained hazard quotients (USEPA, 1989) by Eq. (6):

$$HI = \sum_{i=1}^{n}\sum_{j=1}^{m} HQ \quad \text{Eq. (6)}$$

The threshold value for non-carcinogenic risk was taken as 1.00 (LaGrega *et al.*, 2010).

The parameters used to assess the carcinogenic and non-carcinogenic risk assessment for both adults and children are presented in **Table 3**.

Table 3. Risk assessment parameters.

Parameters	Value (Adult)	Value (Child)	
IR	2	1	(Akter *et al.*, 2021)
EF	365	365	(USEPA, 1989)
ED	74.3	10	(BBS, 2014; Akter *et al.*, 2021)
BW	70	25	(Akter *et al.*, 2021)
AT	27120	3650	(USEPA, 2011)
SSA	18000	13000	(USEPA, 2011)
k_p	0.001	0.001	(USEPA, 2004)
CF	0.001	0.001	(Turdiyeva and Lee, 2023)
ET	0.58	1.00	(USEPA, 2004
SF oral	1.5	1.5	(USEPA IRIS, 2019; RAIS, 2022; OEHHA, 2018)
SF dermal	1.58	1.58	(USEPA, 2004)
RfD oral (As)	0.0003	0.0003	(USEPA IRIS, 2019; RAIS, 2022)
RfD dermal (As)	0.000285	0.000285	(USEPA, 2004)
RfD oral (Mn)	0.024	0.024	(USEPA, 2004; USEPA IRIS, 2019; RAIS, 2022)
RfD dermal (Mn)	0.00096	0.00096	(USEPA, 2004)

Results and Discussions

The pH value of the Mahananda River was in the standard range (6.5-8.5) of the DoE (ECR, 2023) in most places, but at the river's entrance to Bangladesh has a slight overvalue. The mean pH value was 8.50 (SD 0.30), while the maximum value was 9.39. A similar value was reported on the Bangladesh part of the Mahananda River (Anonna *et al.*, 2022), but a less value was reported on the Indian territory of the Mahananda River (Rangarajan *et al.*, 2019).

The DO and TDS values were found in good complement to the DoE standards (≥6 mgL^{-1} and 1000 mgL^{-1} respectively) (ECR, 2023) throughout the reach of the river. The mean DO was found to be 9.56 mgL^{-1} (SD 1.67) with a maximum value of 11.71 mgL^{-1} at the Chowdhala point. A DO value of less than 7 mgL^{-1} was reported at the Indian part of the Mahananda River (Rangarajan *et al.*, 2019). The TDS value was found to be 127.62 mgL^{-1} (SD 24.76), with an increasing trend as the river flows downstream. Similar data values on the Bangladesh part of the Mahananda River were reported (Anonna *et al.*, 2022). The rising trend of TDS can be attributed to the influence of the Punarbhaba and Pagla rivers and the urbanization on the banks of the river. The graphical representation of pH, DO, and TDS is shown in **Fig. 3.**

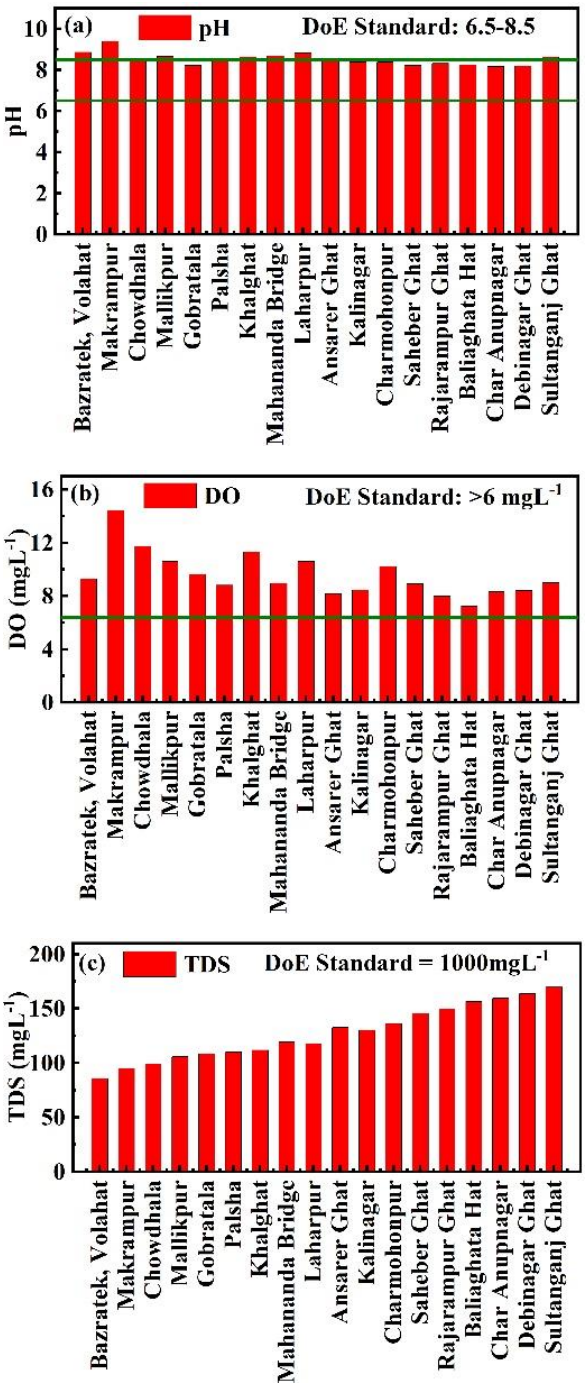

Fig. 3. Distribution of (a) pH, (b) DO, and (c) TDS through the reach of the Mahananda River.

The SO_4^{2-} concentration of both surface water and groundwater of total reach of the Mahananda River is within the standard concentration <250 mgL^{-1} for drinking water by DoE (ECR, 2023), as shown in **Fig. 4.** The maximum concentration of 49 mgL^{-1} of SO_4^{2-} was found in the groundwater of Chari point, and the minimum concentration <2 mgL^{-1}, the lowest measuring range of the testing method, was found in the sampling points of 1-7, 9, 10, and 14. On the other hand, in the surface water, only points 4 and 6 have the Below Measuring Range (BMR) of SO_4^{2-} concentration. The mean SO_4^{2-} concentration in the groundwater was found to be 5.38 mgL^{-1} (SD 12.00), while for surface water, it was 2.29 mgL^{-1} (SD 1.96). The deviation of data shows that the distribution of SO_4^{2-} concentration in groundwater is more scattered than the surface water. A higher SO_4^{2-} concentration in the surface water was reported in (Anonna *et al*., 2022).

Phosphorous in the form of PO_4^{3-} has been found in all the points of sampling points of the Mahananda River and its adjacent groundwater, as shown in **Fig. 5.** The maximum concentration of 2.7 mgL^{-1} PO_4^{3-} was found in the groundwater of the Durgapur point, and the minimum concentration was 0.27 mgL^{-1} at the Fatehpur point. For surface water, it was 0.91 mgL^{-1} at Kalitala point and 0.23 mgL^{-1} at Sultanganj for maximum and minimum concentration, respectively. The mean PO_4^{3-} concentration of the groundwater was 1.17 mgL^{-1} (SD 0.78), while for surface water, it was 0.63 mgL^{-1} (SD 0.15). The recorded data was within the safety limit of ECR 1997 of <6 mgL^{-1} for drinking water (ECR, 1997).

Mn was found high in concentration than the DoE standard of 0.1 mgL^{-1} (ECR, 2023) in all the ground and surface water samples except the samples of the Sadarghat surface water. The maximum concentration of 3.5 mgL^{-1} of Mn was found in the groundwater of Char Udaynagar, while the lowest of 0.4 mgL^{-1} was found at Kanchantala. The lowest concentration of Mn in the groundwater was four times the DoE standard of Mn for drinking water.

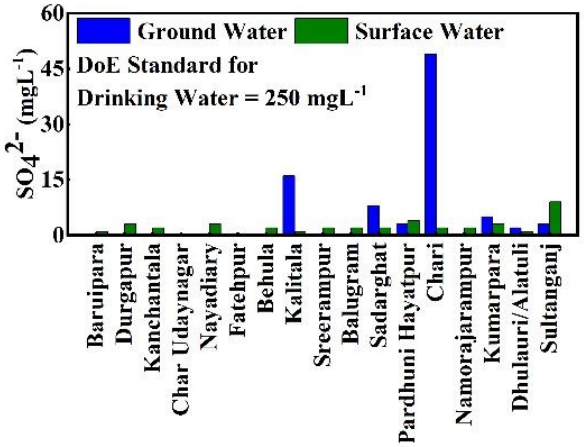

Fig. 4. Distribution of SO_4^{2-} concentration on Groundwater and surface water of Mahananda River.

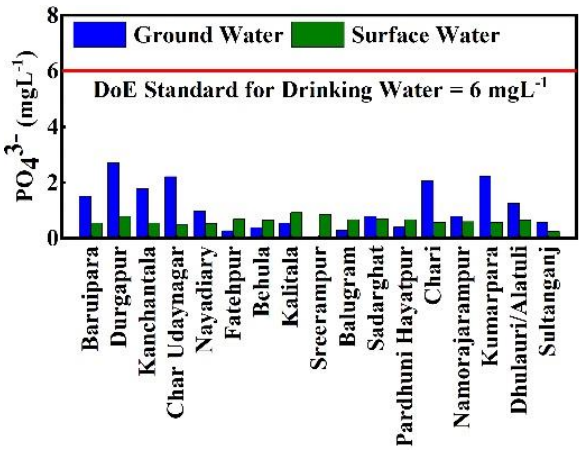

Fig. 5. Distribution of PO_4^{3-} concentration on Groundwater and surface water of Mahananda River.

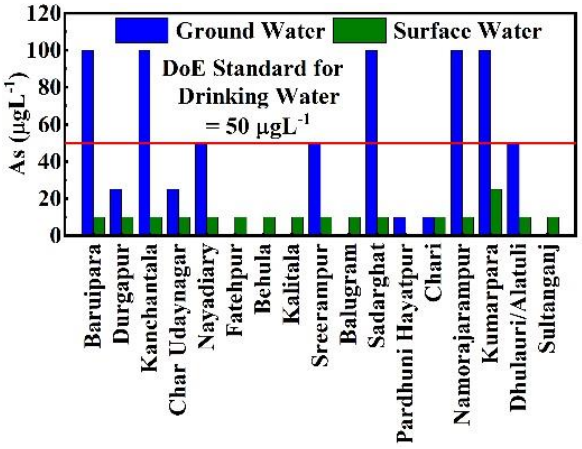

Fig. 6. The As concentration of groundwater and surface water of the reach of Mahananda River.

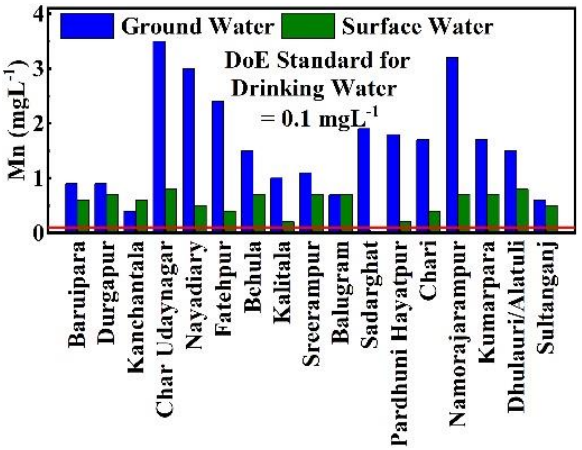

Fig. 7. The Mn concentration of groundwater and surface water in the reach of Mahananda River.

The surface water of the Mahananda River holds a maximum of 0.8 mgL^{-1} of Mn and a minimum of 0.2 mgL^{-1} except at one point. The mean concentration of Mn in groundwater and surface water of the Mahananda River is 1.64 mgL^{-1} (SD 0.90) and 0.54 mgL^{-1} (SD 0.23), respectively. The mean concentration of Mn in groundwater and surface water is higher than the allowable limit of DoE by about 16 and 5 times respectively. This phenomenon may also be attributed to the increasing withdrawal rate of groundwater.

Since As and Mn are higher in concentration than the DoE standard, both carcinogenic and non-carcinogenic health risks were determined from these contaminants and shown in **Table 4** and **Table 5**, respectively. The carcinogenic risk was determined for only As, and the non-carcinogenic risk was determined for both As and Mn. The risk was determined for both adults and children. And also for both maximum and mean concentrations of As and Mn.

The carcinogenic risk from the river water was estimated at 4.44×10^{-04} and 1.08×10^{-03} for mean and maximum concentration of As, respectively, for adults, while 6.26×10^{-04} and 1.52×10^{-03} for children. For groundwater, the value for adults are 1.83×10^{-03} and 4.31×10^{-03} and for children are 2.58×10^{-03} and 6.08×10^{-03} for mean and maximum concentration, respectively. From the result, it is evident that both the surface and groundwater possess high carcinogenic risks. Groundwater poses more risk than surface water; in both cases, children are more vulnerable than adults. A high carcinogenic risk from As was also reported in the groundwater of other parts of Bangladesh (Akter *et al.*, 2021).

The non-carcinogenic risks from surface water at mean concentration is 1.72 for adults and 2.59 for children, while at maximum concentration are 3.47 and 5.15 for adults and children, respectively. Thus, the non-carcinogenic risks are high for both adults and children. For groundwater, the risks are 6.25 and 9.33 for adults and children, respectively, at the mean concentration, while 14.29 and 21.25 are at the maximum concentration. The results show that at mean concentration, the risks are high for adults and children, while the risks are very high at the maximum concentrations of As and Mn in the groundwater. In all the cases, children possess more risks than adults. A similar assessment of risks has been reported in (Akter *et al.*, 2021; Turdiyeva and Lee, 2023; Mohammadi *et al.*, 2019).

Table 4. Carcinogenic risk of As from Mahananda River water and its adjacent groundwater.

Source of Water	Adult			Children		
	Oral	Dermal	Sum	Oral	Dermal	Sum
Surface Water (Mean Concentration)	4.41×10^{-04}	2.43×10^{-06}	**4.44×10^{-04}**	6.18×10^{-04}	8.46×10^{-06}	**6.26×10^{-04}**
Surface Water (Max. Concentration)	1.07×10^{-03}	5.89×10^{-06}	**1.08×10^{-03}**	1.50×10^{-03}	2.05×10^{-05}	**1.52×10^{-03}**
Groundwater (Mean Concentration)	1.82×10^{-03}	9.98×10^{-06}	**1.83×10^{-03}**	2.54×10^{-03}	3.48×10^{-05}	**2.58×10^{-03}**
Groundwater (Max. Concentration)	4.29×10^{-03}	2.36×10^{-05}	**4.31×10^{-03}**	6.00×10^{-03}	8.22×10^{-05}	**6.08×10^{-03}**

Table 5. Non-carcinogenic risk of As in Mahananda River water and its adjacent groundwater.

Source of Water	Metal	Adult			Children		
		Oral	Dermal	HQ Sum	Oral	Dermal	HQ Sum
Surface Water (Mean Concentration)	As	0.98	0.01	0.99	1.37	0.02	1.39
	Mn	0.65	0.08	0.73	0.91	0.29	1.20
	HI			**1.72**			**2.59**
Surface Water (Max. Concentration)	As	2.38	0.01	2.39	3.33	0.05	3.38
	Mn	0.95	0.12	1.08	1.33	0.43	1.77
	HI			**3.47**			**5.15**
Groundwater (Mean Concentration)	As	4.03	0.02	4.05	5.64	0.08	5.72
	Mn	1.95	0.25	2.20	2.73	0.88	3.61
	HI			**6.25**			**9.33**
Groundwater (Max. Concentration)	As	9.52	0.05	9.58	13.33	0.18	13.52
	Mn	4.17	0.54	4.71	5.83	1.90	7.73
	HI			**14.29**			**21.25**

Conclusions

The physicochemical parameters of the surface water were found within the allowable range of the DoE standard. SO_4^{2-} and PO_4^{3-} were also in the permissible range for surface water and groundwater. The As concentration of surface water was found within the allowable range, but it has been found high at several points for groundwater. Mn concentration was high at all the surface water and groundwater points except for one moment. The carcinogenic risk from As and non-carcinogenic risk from both As and Mn was estimated for adults and children. The estimation shows a high carcinogenic risk from surface water and groundwater, while non-carcinogenic risks were assessed as high from surface water and very high from groundwater. In both cases, children were found at more risk than adults. To alleviate the risks, this water should be filtered through an appropriate filter that can remove As and Mn for drinking. For other uses, surface water should give preference over groundwater as long as there is no treated water supply from authorities.

Recommendations

The study was limited by the availability and resources, both equipment and funds. A more comprehensive study with more contaminants, including heavy metal determination, would better estimate carcinogenic and non-carcinogenic human health risks.

Acknowledgment

The authors acknowledge the Government of the People's Republic of Bangladesh and the River Research Institute, Bangladesh, for funding the study.

References

Akter, S., Brahma, P. P., Tasneem, A. and Uddin, M. K. (2021). Probabilistic Human Health Risk Assessment of Fe, As and Mn in the Groundwater of Dhamrai Upazila, Dhaka, Bangladesh. *Journal of Scientific Research & Reports*. 27(4): 1-11. https://doi.org/10.9734/jsrr/2021/v27i430374

Ali, M. M., Rahman, S., Islam, M. S., Rakib, M. R. J., Hossen, S., Rahman, M. Z., Kormoker, T., Idris, A. M. and Phoungthong, K. (2022). Distribution of heavy metals in water and sediment of an urban river in a developing country: A probabilistic risk assessment. *Int. J. Sediment Res.* 37(2): 173–187. https://doi.org/10.1016/j.ijsrc.2021.09.002

Anonna, T.A., Ahmed, Z., Alam, R., Karim, M.M., Xie, Z., Kumar, P., Zhang, F. and Simal-Gandara, J. (2022). Water Quality Assessment for Drinking and Irrigation Purposes in Mahananda River Basin of Bangladesh. *Earth Syst. Environ.* 6: 87–98. https://doi.org/10.1007/s41748-021-00274-x

ATSDR (2012). Toxicological profile for manganese. Atlanta, GA, US Department of Health and Human Services, Public Health Service, Agency for Toxic Substances and Disease Registry.

BBS (2014). Bangladesh Bureau of Statistics Community Report, Bangladesh population and housing census 2011, Zila: Chapainawabganj, pp-501.

Bortey-Sam, N., Nakayama, S. M. M., Ikenaka, Y., Akoto, O., Baidoo, E., Mizukawa, H. and Ishizuka, M. (2015). Health risk assessment of heavy metals and metalloid in drinking water from communities near gold mines in Tarkwa, Ghana. *Environ. Monit. Assess.* 187(7): 397. https://doi.org/10.1007/s10661-015-4630-3

Canavan, M. M., Cobb, S. and Drinker, C. K. (1934). Chronic manganese poisoning: report of a case, with autopsy. *J. Nerv. Ment.* 32(3): 501. https://doi.org/10.1001/archneurpsyc.1934.02250090036003

Cook, D.G., Fahn, S. and Brait, K.A. (1974). Chronic manganese intoxication. *Arch Neurol*. 30(1): 59–64. https://doi.org/10.1001/archneur.1974.00490310061010

ECR (1997). Environmental Conservation Rule, 1997. Department of Environment, Ministry of Environment, Forest and Climate Change, Government of the People's Republic of Bangladesh.

ECR (2023). Environmental Conservation Rule, 2023. Department of Environment, Ministry of Environment, Forest and Climate Change, Government of the People's Republic of Bangladesh.

Farzan, S. F., Karagas, M. R. and Chen, Y. (2013). In utero and early life Arsenicas exposure in relation to long-term health and disease. *Toxicol Appl Pharmacol*. 272(2): 384-390. https://doi.org/10.1016/j.taap.2013.06.030

Ghosh, A., Roy, M. B. and Roy, P. K. (2022). Flood Susceptibility Mapping Using the Frequency Ratio (FR) Model in the Mahananda River Basin, West Bengal, India. In: Islam, M.N., Amstel, A.v. (eds) India II: Climate Change Impacts, Mitigation and Adaptation in Developing Countries. *Springer Climate. Springer, Cham.* 73-96. https://doi.org/10.1007/978-3-030-94395-0_3.

Hurley, L. S. and Keen, C. L. (1987). Manganese, Editor(s): WALTER MERTZ, Trace Elements in Human and Animal Nutrition. (Fifth Edition). *Academic Press.* 185-223. https://doi.org/10.1016/B978-0-08-092468-7.50010-7

Islam, M. M., Rahman, S. L., Ahmed, S. U. and Haque, M. K. I. (2014). Biochemical characteristics and accumulation of heavy metals in fishes, water and sediments of the river Buriganga and Shitalakhya of Bangladesh. *J. Asian Sci. Res.* 4(6): 270.

Kondakis, X. G., Makris, N., Leotsinidis, M., Prinou, M. and Papapetropoulos, T. (1989). Possible health effects of high manganese concentration in drinking water. *Archives of Environmental Health.* 44(3):175–178. https://doi.org/10.1080/00039896.1989.9935883

Kormoker, T., Islam, M. S., Siddique, M. A. B., Kumar, S., Phoungthong, K., Kabir, M. H., Iqubal, K. F., Kumar, R., Ali, M. M. and Islam, A. R. M. T. (2023). Layer-wise physicochemical and elemental distribution in an urban river water, Bangladesh: potential pollution, sources, and human health risk assessment. *Environ. Sci. Adv.* 2: 1382–1398. https://doi.org/10.1039/D3VA00094J

Kubra, K., Mondol, A. H., Ali, M. M., Palash, M. A. U., Islam, M. S., Ahmed, A. S. S., Masuda, M. A., Islam, A. R. M. T., Bhuyan, M. S., Rahman, M. Z. and Rahman, M. M. (2022). Pollution level of trace metals (As, Pb, Cr and Cd) in the sediment of Rupsha River, Bangladesh: Assessment of ecological and human health risks. *Front. Environ. Sci.* 10:778544. https://doi.org/10.3389/fenvs.2022.778544

LaGrega, M. D., Buckingham, P. L. and Evans, J.C. (2010). Hazardous Waste Management. (Reissue). *Waveland Pr Inc.* 865–907.

Mohammadi, A. A., Zarei, A., Majidi, S., Ghaderpoury, A., Hashempour, Y., Saghi, M. H., Alinejad, A., Yousefi, M., Hosseingholizadeh, N. and Ghaderpoori, M. (2019). Carcinogenic and non-carcinogenic health risk assessment of heavy metals in drinking water of Khorramabad, Iran. *MethodsX.* 19(6): 1642-1651. https://doi.org/10.1016/j.mex.2019.07.017

Momot, O. and Synzynys, B. (2005). Toxic aluminium and heavy metals in groundwater of middle Russia: Health risk assessment. *Int. J. Environ. Res. Public Health.* 2(2): 214–218. https://doi.org/10.3390/ijerph2005020003

OEHHA (2018). Lead and Lead Compounds. Toxicity Criteria, California Office of Environmental Health Hazard Assessment, https://oehha.ca.gov/chemicals/lead-and-lead-compounds [accessed July 2023].

RAIS (2022). The Risk Assessment Information System. https://rais.ornl.gov/cgi-bin/tools/TOX_search [accessed July 2023].

Ramazanova, E., Bahetnur, Y., Yessenbayeva, K., Lee, S. H. and Lee, W. (2022). Spatiotemporal evaluation of water quality and risk assessment of heavy metals in the northern Caspian Sea bounded by Kazakhstan. *Mar. Pollut. Bull.* 181:113879. https://doi.org/10.1016/j.marpolbul.2022.113879

Rangarajan, S., Thattai, D. V., Kumar, H., Nagalapalli, S., Yadav, R. and Rustagi, P. (2019). Evaluation of Water Quality Index for River Mahananda West Bengal India. *IJITEE.* 8(6): 1307-1309.

Ravenscroft, P., Brammer, H. and Richards, K. (2009). Arsenic Pollution: A Global Synthesis. Wiley-Blackwell.

Roels, H. A., Eslava, M. I. O., Ceulemans, E., Robert, A. and Lison, D. (1999). Prospective study on the reversibility of neurobehavioral effects in workers exposed to manganese dioxide. *Neurotoxicology.* 20(2-3): 255–271. PMID: 10385889

RRI (2019). Technical report on Research on hydro-morphological study of the Mahananda River in Bangladesh with focus on problems and probable solutions of dry season flow scarcity. River Research Institute. June 2019.

Tepanosyan, G., Maghakyan, N., Sahakyan, L. and Saghatelyan, A. (2017). Heavy metals pollution levels and children health risk assessment of Yerevan kindergartens soils. *Ecotoxicol. Environ. Saf.* 142: 257–265. https://doi.org/10.1016/j.ecoenv.2017.04.013

Tolins, M., Ruchirawat, M. and Landrigan, P. (2014). The developmental neurotoxicity of arsenic: cognitive and behavioral consequences of early life exposure. *Ann Glob Health.* 80(4): 303-314. https://doi.org/10.1016/j.aogh.2014.09.005

Tuinhof, A. and Kemper, K. (2011). Mitigation of Arsenic Contamination in Drinking Water Supplies of Bangladesh-the case of Chapai Nawabganj. Published by Ground Water Management Advisory Team (GW-MATE), World Bank, U.S.A.

Turdiyeva, K. and Lee, W. (2023). Comparative analysis and human health risk assessment of contamination with heavy metals of Central Asian rivers. *Heliyon.* 9(6): e17112. https://doi.org/10.1016/j.heliyon.2023.e17112

USEPA a, Accepted for reporting wastewater analyses. Procedure is equivalent to USEPA method 375.4 for wastewater, US Environmental Protection Agency, Washington, DC.

USEPA b, Accepted for reporting for drinking water analysis. Procedure is an acceptable version of EPA Method 365.1, approved at 40 CFR part 141 NPDWR compliance monitoring. US Environmental Protection Agency, Washington, DC.

USEPA (1979). Approved for reporting wastewater analyses (digestion required). Federal Register. 44(116): 34-193. US Environmental Protection Agency, Washington, DC.

USEPA (1984). Health assessment document for manganese. Cincinnati, OH, US Environmental Protection Agency, Environmental Criteria and Assessment Office (EPA-600/8-83-013F). Washington, DC.

USEPA (1989). Risk Assessment Guidance for Superfund Volume 1: Human Health Evaluation Manual (Part A), US Environmental Protection Agency, Washington, DC.

USEPA (2004). Risk Assessment Guidance for Superfund Volume I: Human Health Evaluation Manual (Part E, Supplemental Guidance for Dermal Risk Assessment) Final. US Environmental Protection Agency. EPA/540/R/99/005.

USEPA (2011). Exposure Factors Handbook. (EPA/600/R-09/052F). US Environmental Protection Agency, Washington, DC.

USEPA IRIS (2019). US Environmental Protection Agency)'s Integrated Risk Information System Environmental Protection Agency Region I," Washington DC 20460, http://www.epa.gov/iris/ [accessed July 2023].

Wu, B., Zhang, Y., Zhang, X. and Cheng, S. (2010). Health risk from exposure of organic pollutants through drinking water consumption in Nanjing, China. *Bull Environ Contam Toxicol.* 84(1): 46–50. https://doi.org/10.1007/s00128-009-9900-8

Zhang, W., Ma, L., Abuduwaili, J., Ge, Y., Issanova, G. and Saparov, G. (2019). Distribution characteristics and assessment of heavy metals in the surface water of the Syr Darya River, Kazakhstan. *Pol. J. Environ. Stud.* 29: 979–988. https://doi.org/10.15244/pjoes/104357

Technical Journal
River Research Institute ISSN: 1606-9277

ASSESSMENT OF EROSION-ACCRETION AND IDENTIFICATION OF THE CHANGE IN BANK LINE OF THE PADMA RIVER IN BANGLADESH USING GIS AND RS APPROACH

M. E. A. Mondal[1*], A. A. Imran[2] , M. Shahabuddin[2] and B. Roy[2]

Abstract

The Ganges-Padma is an important river system in South Asia which supports the life and livelihoods of millions of people both in India and Bangladesh. Bangladesh is a riverine country. Every year the country faces many natural hazards due to the natural dynamic behavior of these rivers. These dynamic actions motivate massive migration of banks, producing thousands of homeless families and enormous land losses each year. This study has analyzed the severity of erosion, accretion and bank shifting of the Padma River at Bagha-Rajshahi, Lalpur-Natore, Ishwardi-Pabna and Bheramara, Daulatpur-Kushtia district. Remote Sensing (RS) and Geographic Information Systems (GIS) techniques were applied to calculate erosion, accretion and bank shifting. This study has been carried out to evaluate the river shifting and assessment of related effects on the land-use/land cover using geographic information system (GIS) and remote sensing (RS) techniques between 1972 and 2023 for Padma River in Bangladesh. Only secondary data has been applied for obtaining the research goal. Several computer software such as ArcGIS, Google Earth etc. have been applied to examine raw data. Seven USGS Landsat, MSS, ETM, OLI_TRIS, sensor, and data images between 1972 and 2023 were used in this study. Padma's riverbank shifting designs and changing land cover resulting from 51 years of erosion and accretion methods have been practical. These river shifting rates are based on the difference between 1972 to 1980, 1980 to 1990, 1990 to 2000, 2000 to 2010, 2010 to 2020 and 2020 to 2023. The average rates of erosion and accretion are 506.41 hectares/year and 468.70 hectares/year individually. This study shows that the river bank line shifted significantly between 1972 and 2023 and this triggered massive bank erosion and accretion.

Keywords: *Accretion, ArcGIS, Bank Shifting, Erosion, Khulna, Rajshahi, River Dynamics.*

Introduction

A river flows from upstream to downstream across the landscape and is an important part of the water cycle. Rainfall, surface runoff, groundwater flow and relief of huge volumes of water which is deposited in normal glacier basins can feed the rivers (Sinha and Ghosh, 2012). River channel migration frequently takes place in the river in the floodplain zones. The morphological dynamics of rivers in the floodplain zones act as an important ecological indicator of its profound effect on both ecological and human existence (Ritu *et al*.,2023). Still, natural hazards, such as bank erosion, flooding and sideways change also occur with this river. The rivers have been an important part of Bangladesh's history and culture. Rivers are particularly environmentally sensitive and deposited channels can reactivate or respond to varying levels activated by water, sedimentation, tectonic activity and human activity on a diversity of time and time scales (Ophra *et al*., 2018). Any natural or anthropogenic alterations can lead to a deviation from a state of dynamic stability. In addition, this can cause channel variability, leading to channel and design changes (Midha and Mathur, 2014). The rivers have changed their courses often and therefore there is no actual permanent map of bank lines (Mithun *et al*., 2012).

The hydraulic and deltaic deltas of Bangladesh are unique in this country which is established by the accumulation of the Padma, Meghna and Jamuna Rivers (Islam *et al*., 2010). These river progressions and their dynamics over time have been an interesting subject of study in geomorphology (Petts, 1995). Bangladesh is intersected by more than 600 rivers, which makes this country fertile land (Khan and Islam, 2015). The Padma, the Meghna, and the Jamuna are the three main rivers in Bangladesh. These rivers and their distributaries & tributaries regulate their hydrological and fluvial-morphological activities. The Rivers vary from each other in their physical characteristics and the construction of the channels. The Padma River plays an important role in changing morphological activities than any other river (Hassan and Akhtaruzzaman, 2010). The river's dynamic occupation of the river causes erosion of riverbanks in Bangladesh that causes huge suffering every year to thousands of homeless and landless people (Elahi, 1991).

The Ganges river system is one of the biggest river systems in the world and covers an area of 1.09 million kilometres, Inventing on the Himalayan Gangotri Glacier. In its 2526-kilometer-long journey through China, Nepal, India and Bangladesh to reach the confluence with the Meghna, making it a famous international river. India's largest share of the entire catchment (79.1%) is, however, just 4.3% (equivalent to 32% of that country's area) located in Bangladesh (Dewan *et al*., 2017). The data from the social survey showed that 95% of people living along the riverbank had lost most of their land. (Eshita *et al*., 2023). Bank erosion is a regulated process which is mostly controlled by river dynamics. More than 230 rivers including Padma flow into the Bay of Bengal through Bangladesh, which drains 2.4 billion tons of sediment. This influences most of the country (Hussain *et al*., 2021). Riverbank erosion usually occurs on the edges of bordered meandering channels and the erosion rate depends largely on the characteristics and bank materials of rivers. Bangladesh is possibly the world's most vulnerable to flooding, and some researchers claim that it is the world's most prone to disasters (Zaman, 2019). The Padma is one of Bangladesh's three largest rivers and one of the longest rivers in the sub-landmass. Two hundred and fifty million people of India and Nepal live in its catchment area. More than 20 million people of Bangladesh also live in the catchment area of this river (Kalam and Jabbar, 1991). The Remote Sensing technique is useful to inspect river channel vibrations across a wide range. It has been normally used to track the movement of river channels and identify polio-enlarged terrace surface channels. Several studies inspected the fundamental shift of channels using geospatial methods, such as overlaying a series of historical channel maps. For the checking of river channel changes, anthropogenic moves and movements of land use-related actions in Bangladesh remote sensing data is used (Islam *et al*., 2014).The study Area Satellite images direct that the rivers consume approximately 8500 hectares of arable land yearly. The event affects around 1368459 people. At present, the study area is vital as it has

[1] Administration and Finance Directorate, River Research Institute, Faridpur-7800, Bangladesh.
[*] Corresponding Author: (E-Mail: emranhossainduet@gmail.com)
[2] Hydraulic Research Directorate, River Research Institute, Faridpur-7800, Bangladesh.

significant installations by the Bangladesh Government like the Ruppur Nuclear Power Plant, Ishwardi EPZ, Bangladesh-India Friendship Power Transmission Station, the Bheramara Thermal Power Station, the Hardinge Bridge, the Lalon Shah Bridge, and the G.K Project, etc. This district is on the bank of the Padma River; shifting and meandering in this area is very rapid, and lastly, most parts have been eroded and deposited recently. The main objective of this study was to investigate the morphological dynamics as well as the effects of erosion and accretion in the study area of the Padma River.

Methodology

Study Area

The study area Bagha-Rajshahi, Lalpur-Natore, Ishwardi-Pabna, and Bheramara-Daulatpur, Kushtia is positioned in the north-western part of Bangladesh and this area is 45km long and its width varies from 4-14 Km. It is a part of the Rajshahi and Khulna divisions. It is situated between the latitudes 20'12.17 to 24'2.24 and longitude 88'44.96 to 89'2.37. In specific, no study of this place calculated the severe erosion, accretion, and rapid bankline movement of the Padma River at the micro-level. A specific emphasis of this research was on investigating morphological dynamics as well as the effects of erosion and accretion in the study area (**Fig. 1**).

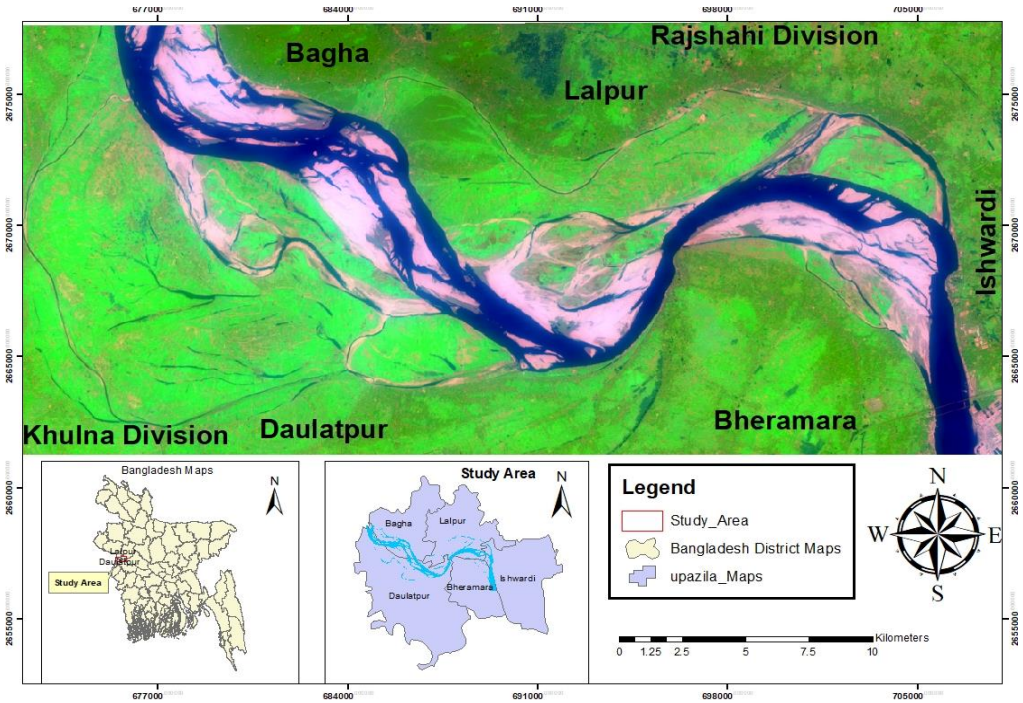

Fig. 1. Details Study Area.

RS and GIS methods

The Remote Sensing (RS) and Geographic Information System (GIS) methods and other statistical data techniques have been used for the assessment of river bank erosion-accretion and identification of the bank line shifting design of the Padma River. At first, the essential data were mainly collected from satellite image analysis to complete this research work. Such satellite images were taken from the United States Geological Survey (earthexplorer.usgs.gov) website, Google Earth Pro, and other maps from LGED. To investigate 51 years of river bank shifting; erosion and Accretion 7 satellite images of 1972, 1980, 1990, 2000, 2010, 2020, and 2023 have been collected. The time intervals are not the same because of maintaining the equivalent (i.e., quality; cloud coverage) between the images. ArcGIS 10.3 is used to envision; correct (Geometric Modification; Radiometric Correction; Atmospheric Correction); Sub setting layer; and Study area's image preparation of Landsat images. Then Landsat images were used for supervised classification. The images are disconnected into two large classifications, namely water and land. After that, the classified image was transferred into ArcGIS 10.3 to attempt a reclassifying process. Then 11 Section/Reference lines for considering the migration of river channels are identified. These 11 Segment/Reference lines are accepted provisional on where the highest rate of erosions occurred. Finally, ArcGIS' standard measurement tool is used to assess the movement of river channels based on two sequential years, i.e., 1972 to 1980; 1980 to 1990; 1990 to 2000; 2000 to 2010; 2010 to 2020; 2020 to 2023 and lastly 1972 to 2023. **Table 1** shows the description of Landsat Select imageries. The Landsat 5 MSS, TM and OLI & TIRS were taken to keep the spatial resolution and maximum band configuration comparable among all images. Some essential articles from the RRI library were accessed. Other minor data sources include Wikipedia, published works and various online sources. Software and Tools used to shape the work were—ArcGIS; Version: 10.3, ArcMap; Version: 10.3, Microsoft Office 2010: Word, and Excel.

Table 1. Description of Landsat Select imageries.

Image No	Acquisition Date	Satellite ID	Sensor ID	Path/Row	Spatial Resolution	Quality	Cloud Coverage
1	23/11/1972	Landset5	MSS	148/043	30 Meter	4	10
2	16/01/1980	Landset5	MSS	148/043	30 Meter	7	10
3	30/01/1990	Landset5	TM	148/043	30 Meter	7	10
4	26/01/2000	Landset5	TM	148/043	30 Meter	7	10
5	21/01/2010	Landset8	OLI &TIRS	148/043	30 Meter	7	10
6	01/01/2020	Landset8	OLI &TIRS	148/043	30 Meter	11	10
7	25/01/2023	Landset8	OLI &TIRS	148/043	30 Meter	11	10

Result and discussion

River bank Erosion trend in the study area

River bank erosion drive in the study area Bagha-Rajshahi, Lalpur-Natore, Ishwardi-Pabna and Bheramara-Daulatpur, Kushtia is the most vulnerable district to the river bank erosion in Padma River. From 1972 to 2023, a 51-year period the erosion was measured. There are seven satellite images reserved to calculate the area of the worn land. Six intermission periods take place for measurement. The interval is 1972-1980, 1980-1990, 1990-2000, 2000-2010, 2010-2020 & 2020- 2023. In 2020-2023 it was made that the erosion rate was highest with 952.98 hectares/year, 2858.94 hectares land was eroded in these 3 years. The erosion rate was also higher in the 1972- 1980 years period with 682.56 hectares/year, 5460.48 hectares land eroded in these 8 years. In 1980-1990 time periods the average erosion rate decreased from 682.56 to 558.32 hectares/year. In the period of 1990-2000, the erosion rate progressively reduced to 349.77 hectares/year and in 2000-2010 the erosion rate increased to 541.69 hectares/year. In 2010-2020 the erosion rate was somewhat reduced to 300.99 hectares/year from the past 10-year time period of 2010-2020. Finally, the average erosion rate was 506.41 hectares/year with a total 25827.03 hectares of land eroded in these 51 years. This high rate of erosion caused unbelievable land loss. **Table 2** describes the detailed result of the river bank erosion charge in this study area.

Table 2. Details Bank erosion in Padma River.

SL No	Period	Duration (Year)	Total Erosion (hectares)	Average Erosion (hectares/year)
1	1972-1980	8	5460.48	682.56
2	1980-1990	10	5583. 15	558.32
3	1990-2000	10	3497.67	349.77
4	2000-2010	10	5416.92	541.69
5	2010-2020	10	3009.87	300.99
6	2020-2023	3	2858.94	952.98
Grand Total		51	25827.03	506.41

River bank Accretion trend in the study area

Erosion and accretion are instantaneous processes of a river basin. In these 51 years from 1972-2023 the accretion rate is significant in Bagha-Rajshahi, Lalpur-Natore, Ishwardi-Pabna and Bheramara-Daulatpur, Kushtia districts. Maximum accretion rate found in 2020-2023 period with 1077.45 hectares/year, and total of 3232.35-hectares land was increased in this frame. And the lowest Accretion rate in 2000-2010 and 2010-2020 with 288.54 hectares/year and 355.28 hectares/year respectively. From 1972 to 1980, the accretion rate was 541.94 hectares/year with a total of 4335.48 hectares of accretion land. From 1990 to 2000, the accretion rate was very close to 1980-1990 which was 484.00 hectares/year. The average accretion rate was measured as 468.70 hectares/year through a total accretion of 23903.73-hectares from 1972-2023 in this study area. The detailed result of river bank accretion is shown in **Fig. 2** and **Table 3**.

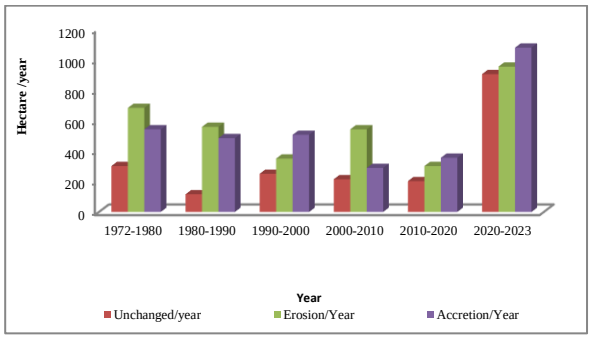

Fig. 2. A chart plot for Erosion and accretion.

Table 3. Details Bank accretions in Padma River.

SL No	Period	Duration (Year)	Total Accretion (hectares)	Average Accretion (hectares/year)
1	1972-1980	8	4335.48	541.94
2	1980-1990	10	4840.02	484.00
3	1990-2000	10	5057.64	505.76
4	2000-2010	10	2885.4	288.54
5	2010-2020	10	3552.84	355.28
6	2020-2023	3	3232.35	1077.45
Grand Total		51	23903.73	468.70

Land area of the study area

The Bagha-Rajshahi, Lalpur-Natore Ishwardi-Pabna and Bheramara-Daulatpur, Kushtia districts land area has changed over time as an outcome of erosion and accretion of the active Padma river. The area of the land falls in the periods 1972–1980, 1980–1990 and 2000–2010, since it was above the accretion level and the inverse cycle was accompanied by a rise in the area between 1990–2000, 2010–2020, and 2020–2023. The most serious period was between 2000 and 2010 across ten-time intermissions; at that time 5416.92 hectares of land were lost. In the period 1990-2000, the largest land accretion happened; there was an increase of 5057.64 hectares of land. During the period from 2000 to 2010, the accretion rate was the lowest, with only 288.54 hectares increased. The specifics are presented in **Table 4** and **Table 5** the study region covered a total of 25827.03 hectares of land eroded between 1972 and 2023, with a cumulative deposit of 23903.73 hectares. Over the 51 years, total land loss was calculated to be 1923.30 hectares with a rate of 37.71 hectares per year.

Table 4. Details Land Area Change by Erosion and Accretion.

SL No	Period	Total Accretion (hectares)	Total Erosion (hectares)	Duration (year)	Unchanged (hectares)	Change Land area (hectares)
1	1972-1980	4335.48	5460.48	8	2406.6	-1125.00
2	1980-1990	4840.02	5583.15	10	1158.93	-743.13
3	1990-2000	5057.64	3497.67	10	2501.28	1559.97
4	2000-2010	2885.4	5416.92	10	2142.00	-2531.52
5	2010-2020	3552.84	3009.87	10	2017.53	542.97
6	2020-2023	3232.35	2858.94	3	2711.43	373.41
Grand Total		23903.73	25827.03	51	12937.77	-1923.30

Table 5. Details Land Area of the study area.

SL No	Year	Total Land (hectares)	Duration (year)	Total Land Loss (hectares)	Land Loss Rate (he/year)
1	1972	128646	8		
2	1980	129771	10		
3	1990	130514	10		
4	2000	128955	10	1923.30	37.71
5	2010	131486	10		
6	2020	130943	3		
7	2023	130570	51		

River bank shifting

Most rivers complete their courses in the wet and sub-humid areas in three phases – young, mature and old. In the old period, during these three stages, the river flowed due to a gentle slope. This causes a side erosion and channel shift in the river valley. A common singularity is bank failure (separation and confinement of bank materials by fluvial,

sub-aerial and geotectonic methods in the forms of scraps, aggregates or blocks) downstream of each channel. Padma changes its direction quite frequently. In this analysis, the dynamic change of the Padma River was established over the past few years (**Fig. 3**).

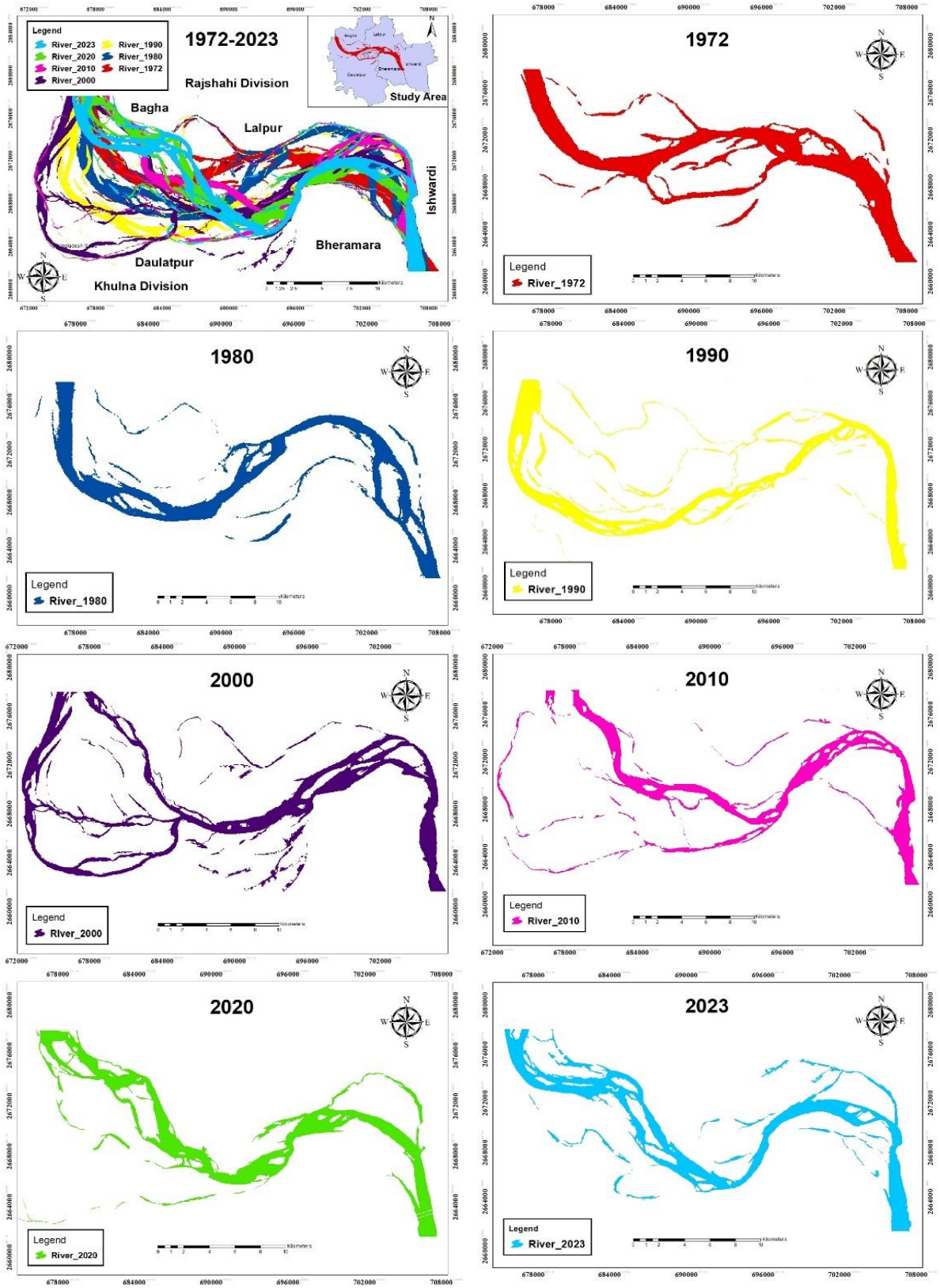

Fig. 3. Position of the river in different years.

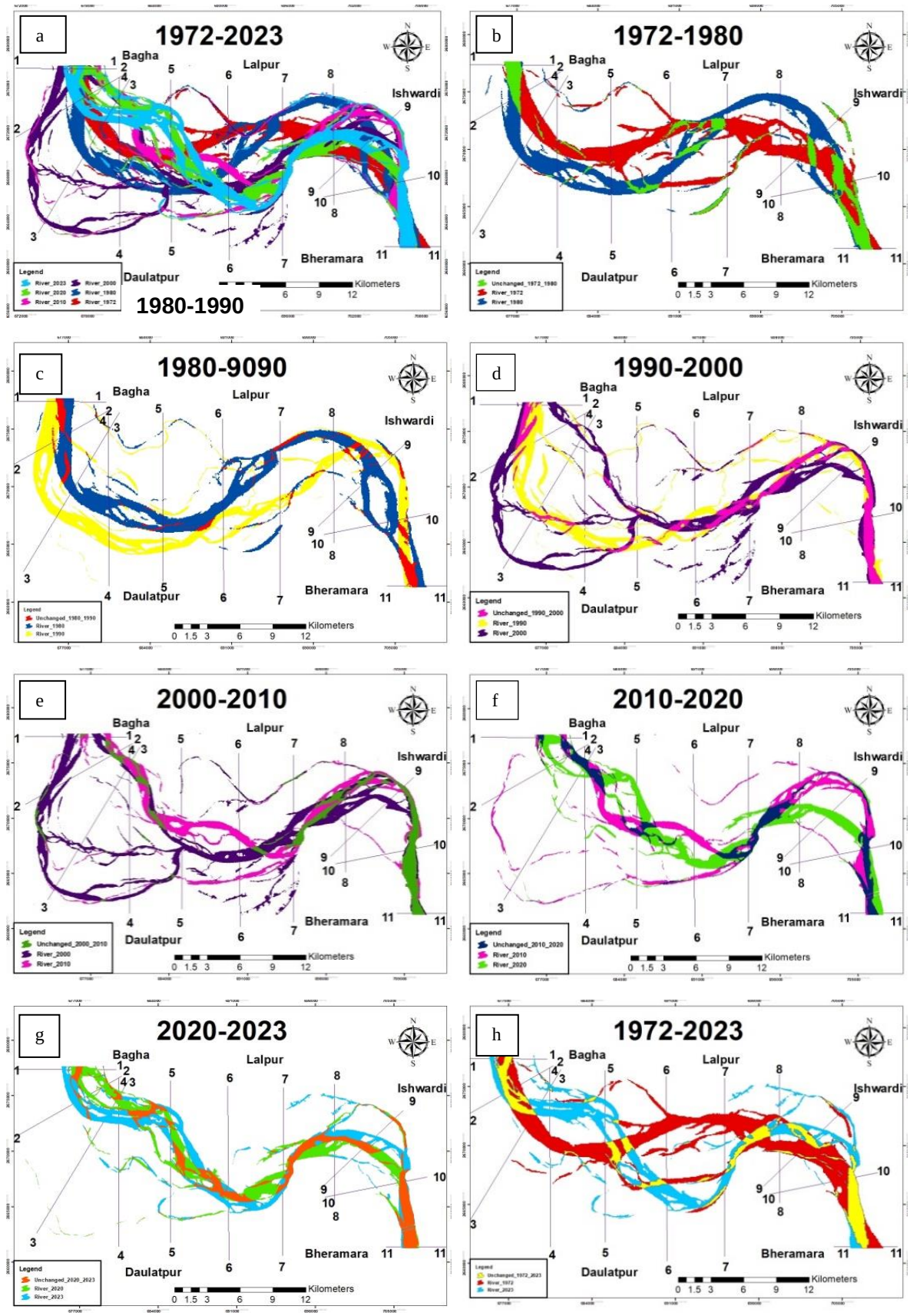

Fig. 4. Sequential change of Padma River Bank shifting, a(1972–1980), b(1972–1980), c(1980–1990), d (1990–2000), e(2000–2010), f(2010–2020), g(2020–2023) and h(1972–2023).

Table 6. Net migration Direction Left to Left Bank (in meters) of Padma River at 11 different locations in different periods.

Section/ Reference line	Net Migration and Direction Left to Left Bank (Meter)						
	1972-1980	1980-1990	1990-2000	2000-2010	2010-2020	2020-2023	1972-2023
1-1	147 W	877 W	1600 E 352 W	673 E 3104 E	200 W	0	114 W
2-2	882 SW	1420 SW	3565 NE 2739 SW	0 6825 NE	0	2690 SW	0
3-3	3358 SW	2441 SW	8458 NE 4876 SW	0 13300 NE	0	1760 SW	1188 NE
4-4	1446 S	3100 S	9370 N 3006 S	0 12360 N	0	1850 S	2877 N
5-5	2744 S	1963 S	2716 N	2013 N	3223 N	768 N	3621 N
6-6	4025 S	1087 S	715 S	1754 N	2500 S	450 N	6110 S
7-7	1000 N	4453 S	1361 N 2545 S	2153 N	210 N	0	4778 S
8-8	2314 N	1964 S	250 N	596 N	2010 S	574 N	1373 S
9-9	1617 NE	1409 NE	271 NE 1363 SW	1680 NE	3185 SW	981 N	1145 NE
10-10	0	832 NE	0	0	0	0	0
11-11	777 W	780 W	0	0	480 E	200 W	1368 E

Shifting nature of Padma river channel

In our study area, the shifting nature of the Padma River is a typical fluvial geomorphic phenomenon that can occur anywhere on rivers. The centrifugal force prevents the river's topmost water surface movement. Moreover, towards the river bottom, the velocities are much less than towards the river top. Enough centrifugal force is not available to counteract the tendency of water at the river top to move inwards. These rotary currents cause the erosion of the concave edge and accretion on the convex side. This shifting nature is like a swing along the river's left and right banks. We consider here only one side of the Padma River. The maps of 1972, 1980, 1990, 2000, 2010, 2020, and 2023 of the Padma Rivers were ready here to show the changing nature of the channel.

Fig. 4-a (1972-2023) shows the maps of all the rivers together, showing that the rivers were spread over an area of 4 to 14 km at different times. The section-wise description of the different two-year rivers of the mentioned rivers is as follows-

Fig. 4-b (1972–1988) of the study area shows that the river was stationary in the tributaries and lowlands. But the 1980 image shows that the main river has eroded and traversed the Daulatpur section to the south. It is also seen that the river crossed in the middle, and in the north, the Lalpur part was much eroded. There was a large char in the middle of the river, but it is not visible in the 1980 photo. In the eastern part of Ishwardi-Pabna, the river was in its original state; no river course had changed.

In **Fig. 4-c** (1980–1990), it is seen that the main river has eroded further to the south, towards the Daulatpur and Veramara sections. The main river moved slightly upstream and downstream to the west. Here it can also be seen that in 1980 the main river was very wide, but in 1990 the river was very thin, and many tributaries and small ones were formed. The 1990 image also shows the river to the northeast By crossing the section, Ishwardi-Pabna moved towards the section.

Fig. 4-d (1990-2000), it is seen that the main river underwent major changes in upstream. The 2000 photograph shows that the river separates to form a narrow channel in the north and another narrow channel in the southwest. The two rivers joined in the middle to form a wide channel in 1990. The figure of 2000 can be seen at that time; many large channels and small channels were created in the river. No significant change was observed on the downstream side of the river, but a little upstream, the river shifted towards the south-Veramara section.

Fig. 4–e (2000–2010) shows that the river has shifted upstream to the northeast, towards the Bagha area. The 2000 image shows three channels upstream, but the 2010 image shows one channel as before. In 2010, the river appeared much narrower, and a branch of the river was seen downstream. A little upstream and downstream, the river moved somewhat towards the northeast towards the Lalpur-Ishwardi section.

Fig. 4-f (2010-2020) shows that in 2020, the river moved upstream to the southwest. Compared to 2010, the river in 2020 was much wider and produced more forage. In 2020, the river moved south towards the Veramara section along the middle. Here it can also be seen that the downstream part of the river has not changed much, but a little upstream, it moved from the northeast to the southwest part of Veramara.

Fig. 4-g (2020-2023) shows that in 2023, the river has moved slightly upstream in the southwest. Compared to 2020, the river in 2023 was much wider, and more char was produced. The river in 2020 did not change much along the middle of the river. Here it can also be seen that the downstream part of the river has not changed much, but a little upstream has moved northeast towards the Lalpur-Ishwardi section.

Fig. 4-h (1972-2023) shows that the upstream has moved upwards in Bagha, and the Daulatpur and Veramara middle positions have shifted far south to form a U shape. There was no change downstream of the river. Analyzing the pictures of 1972 and 2023, it can be seen that the river is returning to its previous state. From the mentioned picture, it is also observed that the river of 2023 is thinner and more formed than the river of 1972.

Table 6 shows the net migration of the Padma River (in meters) at 11 different locations during various periods. Where N, S, E, W, NE, NW, SE, and SW symbolize north, south, east, west, northeast, northwest, southeast, and southwest.

Conclusion

The River shifted between 1972- 2023, a total area casing 25827.03 hectares was eroded and 23903.73 hectares were accretion in the study area. In the period 1972 and 2023, the average erosion rate was 506.41 hectares/year and the accretion rate was 468.70 hectares/year during this 51-year. The highest erosion rate 952.98 hectares/year happened in the period 2020-2023 and the lowest was 300.99 hectares/year in 2010-2020. The highest accretion rate was measured at 1077.45 hectares/year and the lowest was found at 288.54 hectares/year in the 2020-2023 and 2000-2010 periods respectively. In these 51 years from 1972 to 2023, land loss was estimated at 1923.30 hectares with a rate of 37.71 hectares per year. In 1972 the Padma River was almost straight or small in curve, and in 1980 the river gradually thickened and highest in 2000. In 2000 the progression was highly meandered. In these 51 years compared to 1972 and 2023, the river went winding and massive stretches in the Upper and Middle portions which shifted towards north-south in the mid portion and the lower portion shifted Ishwardi north-east, the upper and lower portion remaining almost in the past course. The river moved several times between 1972 and 2023 and this activated erosion and land deposition in this period. In addition to settlement, structural, and economic loss, both physical and mental health of the riverbank people is affected due to frequent migration. Immediate steps through effective river management policy guidelines and implementation are required to adopt a permanent solution.

Acknowledgement

For this paper, at first, I want to thank Almighty Allah, the most gracious and merciful who gave me the strength to finish this paper. I want to give special thanks to S M Abu Horayra, Honorable DG Sir, River Research Institute for his continuous support, guidance, help and instructions.

Reference

Dewan, A., Corner, R., Saleem, A., Rahman, M. M., Haider, M. R., Rahman, M. M. and Sarker, M. H. (2017). Assessing channel changes of the Ganges-Padma River system in Bangladesh using Landsat and hydrological data. *Geomorphology*, 276: 257–279.

Elahi, K. M. (1991). Riverbank erosion, flood and population displacement in Bangladesh. *Riverbank Impact Study*, 14.

Hassan, S. and Akhtaruzzaman, A. (2010). Environmental change detection of the Padma River in the North-Western part of Bangladesh using multi-date landsat data. Proc. of International Conference on Environmental Aspects of Bangladesh (ICEAB10), Japan.

Hussain, T., Uddin, M., Munna, G., Sanzidah, R. and Choudhury, T. P. (2021). Assessment of bank erosion-deposition and bankline shifting of Padma River at Chapainawabgonj district in Bangladesh using RS and GIS technique. *International Journal of Scientific and Technology Research*, *10*(04): 376–381.

Islam, M. S., Han, S., AHMED, M. K. and Masunaga, S. (2014). Assessment of trace metal contamination in water and sediment of some rivers in Bangladesh. *Journal of Water and Environment Technology*, *12*(2): 109–121.

Islam, S. N., Singh, S., Shaheed, H. and Wei, S. (2010). Settlement relocations in the char-lands of Padma River basin in Ganges delta, Bangladesh. *Frontiers of Earth Science in China*, 4: 393–402.

Kalam, M. and Jabbar, M. (1991). River course monitoring of the Ganges at Godagari, Rajshahi using remote sensing techniques. Riverbank Erosion, Flood and Population Displacement in Bangladesh. REIS-JU, Dhaka, 73–85.

Khan, M. S. and Islam, A. (2015). Anthropogenic impact on morphology of Teesta River in Northern Bangladesh: An exploratory study. *Journal of Geosciences and Geomatics*, *3*(3): 50–55.

Eshita, N. R., Bhuiyan, M. A. H. and Saadat, A. H. M. (2023) Recent morphological shifting of Padma River: geoenvironmental and socioeconomic implications. *Natural Hazards. 117: 447–472.*

Midha, N. and Mathur, P. K. (2014). Channel characteristics and planform dynamics in the Indian Terai, Sharda River. *Environmental Management. 53*: 120–134.

Mithun, D., Dabojani, D. and Misbah, U. (2012). Evaluation of meandering characteristics using RS & GIS of Manu River. *Journal of Water Resource and Protection*, *2012*.

Ophra, S. J., Begum, S., Islam, R. and Islam, M. N. (2018). Assessment of bank erosion and channel shifting of Padma River in Bangladesh using RS and GIS techniques. *Spatial Information Research*. *26*: 599–605.

Petts, G. E. (1995). *Changing river channels: The geographical tradition*. Wiley.

Ritu, S. M., Sarkar, S. K. and Zonaed, H. (2023). Prediction of Padma river bank shifting and its consequences on LULC changes. *Ecological Indicators*. 156: 111104.

Sinha, R. and Ghosh, S. (2012). Understanding dynamics of large rivers aided by satellite remote sensing: A case study from Lower Ganga plains, India. *Geocarto International*. *27*(3): 207–219.

Zaman, M. Q. (2019). Vulnerability, Disaster, and Survival in Bangladesh: Three Case Studies 1. *The angry earth*. 162–177. Routledge.

GENERAL INFORMATION

The Technical Journal of River Research Institute is published yearly. The journal publishes Scientific Research Papers in the fields of:

Hydraulics, Hydrology, River Morphology, Sediment Management, Geotechnical Engineering, Sediment Technology, Water Quality, Concrete and Building Materials, Physical and Numerical Modeling, Groundwater Utilization, Environmental Science & Engineering, Hydraulic structures, Water Management or any other Water Resources Engineering.

The Editorial Board, Technical Journal of River Research Institute is responsible for the final acceptance of any paper and the Board's decision is final in case of any controversy.

The following guidelines should be followed strictly by the authors in submitting the manuscript of paper:

❖ The authors should be submitted their papers in three hard copies along with the soft copy through e-mail: tech.jour@rri.gov.bd

❖ All words of the manuscript must be written in UK English and SI unit should be used throughout the paper.

❖ The manuscript should be single spaced and double column computer typed using Microsoft Word (.doc or docx and pdf.) Times New Roman 9 font size for text and MS- Excel for graphs. The paper size should be A4 with page margin of the top, bottom, left, right 1 inch (25mm) and header, footer 0.5 inch respectively. The font sizes for all headings and sub-headings should be 10 Times New Roman (bold) and italic font 9 pt. respectively.

❖ The manuscript of a full paper must not exceed 10 Journal pages including tables, graphs, figures etc.

❖ The paper should contain minimum number of editable tables, graphs and figures. Each figure and table must be clearly referenced in the text. The font size of table and figure captions should be 9 Times New Roman throughout and not bold. The word "Figure" should be abbreviated as "Fig.", while "Table" is not abbreviated (e.g. Fig. 4, Table 5). All illustrations should be in ".jpg" format using a resolution of at least 300 dpi.

❖ The manuscript of the paper should contain the Title of the paper, Abstract, Key words, Introduction, Methodology, Results and discussion, Conclusion, Acknowledgement (if any) and References.

❖ The Title of the paper should not exceed 90 characters (capital) without spaces and font size should be Times New Roman 11 (Upper case, bold). The name of the author(s) should appear just below the title of the paper in the centre position with font size 9. Affiliations, postal and e-mail address should appear as the foot note at the bottom of the 1st page of the paper with font size 8 (Times New Roman).

❖ References should be listed at the end of the manuscript according to the alphabetical order of the author's surname followed by the year, title of the paper, abbreviated name of the journal, volume number and after colon, page number for example:

- In case of scientific journal:

Hasanuzzaman, A. K. M and Mehedi H. M. (2016). Numerical modelling using MIKE 21C for the proposed bridge on Kalni river under Habiganj road division. *Tech. J. River Res. Inst.*13 (1): 76-86.

- In case of Book example:

The title should be *italic* and the name of publisher should be given with total pagenumber. e.g.

Guy H.P. (1999). *Laboratory Methods for Sediment Analysis*. Adelaide Univ. PressAustralia P.500.

- In case of thesis:

Mehedi, H.M. (2005). *Determination of friction angle of soil by Double-Punch Test.* Unpublished B.Sc. Dissertation, Bangladesh Agricultural University, Mymensingh.

- Web site reference example:

RRI (2016). *History of RRI. River Research Institute, Faridpur* [online]. http://www.rri.gov.bd/history-rri-0 (Accessed 22 March 2017).

❖ In the text, the citation of the references should be given by the last name of the author with year of publication. e.g. Mehedi (2018)/Mehedi *et al.* (2018) and (Mehedi, 2018; Mehedi *et al.*, 2018)

The paper will be selected on the basis of the following criteria:

1. Theme of the manuscript
2. Problem formulation
3. Authenticity of the database
4. Way of approach- materials and methods/methodology
5. Supporting literature/Document
6. Analysis-Presentation
7. Standard with respect to Scientific and Technical field
8. National Importance/Socio-economic importance
9. Relation to RRI activities
10. Linguistic soundness
11. Findings/Conclusion

The Technical Journal is published by the Editorial Board of River Research Institute, Faridpur. All editorial correspondence should be addressed to the Executive Editor, Editorial Board, Technical Journal of RRI, Bangladesh. RRI Editorial Board reserves all rights to accept, reject and publish the manuscript.

SUBSCRIPTION RATE 2023-2024

Subscription for each copy: Tk. 500/-
$ 30 (for Foreigner)

The Payment should be made in the form of Pay Order/ Demand Draft in favour of the Director General, River Research Institute.

The Editorial Board, Technical Journal of RRI as a body, is not responsible for any statement made or opinion expressed by the author in the publication.

Contact Address

Head Office: Harukandi, Faridpur-7800. Phone: +8802478803007, Fax: +8802478863065

Dhaka Office: 4th Floor, WARPO Bhaban, 72, Green Road, Dhaka-1205. Phone: +8802-58155538

Email: tech.jour@rri.gov.bd; dg@rri.gov.bd, **Website:** https://rri.gov.bd